UNIVERSITY OF OKLAHOMA

GRADUATE COLLEGE

A LABORATORY INVESTIGATION AND MODELING OF DYNAMIC MODULUS OF ASPHALT MIXES FOR PAVEMENT APPLICATIONS

A DISSERTATION

SUBMITTED TO THE GRADUATE FACULTY

in partial fulfillment of the requirements for the

Degree of

DOCTOR OF PHILOSOPHY

By

DHARAMVEER SINGH
Norman, Oklahoma
2011

A LABORATORY INVESTIGATION AND MODELING OF DYNAMIC MODULUS OF ASPHALT MIXES FOR PAVEMENT APPLICATIONS

A DISSERTATION APPROVED FOR THE
SCHOOL OF CIVIL ENGINEERING AND ENVIRONMENTAL SCIENCE

BY

Dr. Musharraf Zaman

Dr. Sesh Commuri

Dr. Douglas D. Gransberg

Dr. Gerald A. Miller

Dr. Kianoosh Hatami

DEDICATION

"It is my pleasure to dedicate this dissertation to my teachers, my parents, my sisters, and my wife for their support throughout the course of my studies."

ACKNOWLEDGEMENTS

First and foremost I would like to thank God, for His blessings on me with the opportunity and ability to complete this work. I could never have done this without the faith, I have in you, the Almighty.

I would like to express my deepest appreciation and gratitude, and heartiest thanks to the Chair of my doctoral committee, Professor Musharraf Zaman, for his thoughtful guidance, constant support, encouragement, and considerable patience throughout my doctoral studies. I appreciate all his contributions to ideas and funding to make my Ph.D. experience productive and stimulating. His remarkable insights and valuable suggestions have contributed greatly to the completion of this study. Apart from the subject of my research, I learnt a lot from him, which I am sure will be useful in different stages of my life. He provided me the opportunity to peer-review several international journal and conference papers. I appreciate Dr. Zaman for setting a high standard for each student. He never accepts less than the best efforts. He believes that his students should get diversified experience during their stay at OU. He has tremendous trust and confidence on his students. I know how much energy and resources you have invested in your students, I hope you get a payback you deserve. Without his critical comments and patient instructions the completion of the present dissertation would have been impossible.

I solemnly submit my honest and humble thanks to the Co-Chair of my doctoral committee, Professor Sesh Commuri, for his creative suggestions, motivation, encouragement, and exemplary guidance throughout the course of my doctoral research. I would like to thank him from the bottom of my heart for providing funding during my

stay. He has been so kind in supporting me throughout my studies. In spite of his busy schedule, he always provided me time to discuss research findings and results. I always found him full of energy and confidence. Without his enlightening suggestions and great encouragement, it would have not been possible for this dissertation to achieve its goal. I remember that I had tough times during the course of this study, and Dr. Zaman and Dr. Commuri guided me through and infused in me a lot of confidence so that I could again able to believe in myself and pursue my dreams. Throughout the years to follow, you have been an exemplary guide, a motivator, and a mentor. So, "Thanks to Both of You," for all your steadfast support and help throughout this journey.

I would like thank Dr. Gerald A. Miller for serving on my doctoral committee. It was Dr. Miller's "Foundation Engineering" class that I took first when I came to OU. It was a great learning experience to attend Dr. Miller's lecture. I would like to thank him for sharing his practical and theoretical experience during the class lecture. I very much appreciated his enthusiasm, intensity, willingness to help students. I greatly thank him for sharing his knowledge and ideas with me.

I gratefully thank Dr. Douglas D. Gransberg for being always supportive and for sharing his experience with field construction projects from time to time. I found Dr. Gransberg a source of encouragement and motivation. I am also thankful for the excellent example he provided as a successful researcher and professor. I found him very cordial, generous, and soft spoken. I am especially grateful to him for his gracious and earnest assistance and guidance throughout my studies. It has been a pleasure to have him on my dissertation committee.

I would like to express my heart-felt gratitude to Dr. Kianoosh Hatami for his unfailing support and guidance during my doctoral program. I found him to be very friendly, cooperative, approachable, and helpful. I appreciate your help and time spent in serving on my doctoral committee.

I must thank Dr. Luther White from Mathematics Department for sharing his wealth of knowledge in the field of neural network modeling. Also, thanks are due to Dr. Joakim G. Laguros for his help and guidance. Also, I would like to extend special thanks to Mr. Danny Gierhart from Asphalt Institute (AI) and Mr. Kenneth Hobson from the Oklahoma Department of Transportation (ODOT) for their technical advice throughout this study. I would also like to thank other faculty members in geotechnical engineering at the University of Oklahoma for teaching me some of the basics in geotechnical engineering. Their lectures were of great help and value in making progress during this study.

I am indebted to many of my colleagues who supported me in the laboratory testing. I would like to appreciate Mr. Imran Asif for his help in preparation and testing of aggregates samples. Also, thanks are due to Mr. Beainy Fares, Mr. Anh Mai, and Mr. Harish Gadigota, for helping me in collection of materials from the plants and the field. I would also like to extend my sincere thanks to Dr. Zahid Hossain, Dr. Pranshoo Solanki, Dr. Quingyan Tian, Mr. Rouzbeh Ghabchi, Mr. Ashish Gupta, Mr. Caleb Riemer, Mrs. Dominique Pittenger, Mr. Nur Hossain, Mr. Marc Breidy, Mr. David Adje, Mr. Moeen Nazari, Mr. Jackson Autrey, Mr. Curtis Doiron, Mr. Roy Khalife, Mr. Rami Akkari, Mr. Hasan Kazmee, and Ms. Tahsina Mahmood, for being valuable colleagues in the class and in the laboratories. The group has been a source of friendship as well as good advice

and collaboration. I cannot forget to thank some of my friends in the U.S.A and in India, Mr. Sidhartha Mitra, Mr. Laxmikant Yadu, Mr. Yogesh Varma, Dr. Subrat Roy, Dr. Ravi Kumar, Mr. Anurag Srivastava, Mr. Akash Rao, Mr. Kanwardeep Bhachu, and Mrs. Sarab Bhachu for their encouragement and support during this study.

I take this opportunity to thank all of the academic and administrative staff for the wonderful cooperation and support to get this study completed. I sincerely thank Mrs. Susan Williams and Mrs. Lindsey Johnston for providing necessary guidelines and information throughout this study. They kept me organized and were always ready to help. Special thanks to Mrs. Karen Horne, who was always very kind and helpful for anything we would need at any time. Also, thanks are due to Mrs. Holly Chronister, Mrs. Katie Hargrove, Mrs. Molly Smith, Mrs. Audre Carter, Mrs. Karen Kelly, Mrs. Brenda Clouse, Mrs. Shauna Signleton, Mrs. Andrea Flores, Mrs. Suzanne Hodgson, Mrs. Sonya Grant, Mr. T. Mike Shaw, and Mr. Joshua Gibson. My heartiest thanks are also extended to Mr. Michael Schmitz (Mike) for his technical support in the laboratories. Without Mike's help it would have not been possible to finish successful testing in the laboratory. I owe my deepest gratitude to Mr. James E. Bierman from Engineering Library for assisting me in getting journal papers and books needed during the course of this study.

I would like to express my sincere appreciation to the Federal Highway Administration (FHWA), Volvo Construction Equipment Company, the Oklahoma Department of Transportation (ODOT), the Oklahoma Transportation Center (OTC), and the University of Oklahoma for providing fund for this study. Special thanks go to suppliers of asphalt mixes and asphalt binders used in this study, namely, Haskell Lemon Construction Company in Oklahoma City and Valero in Ardmore. Furthermore, I would

like to thank Mr. Brian Wolfe, Mrs. Connie Dolph both from Haskell Lemon Construction Company for providing necessary information used throughout this study.

I would like to express my heartfelt thanks to my master thesis advisors Dr. K. S. Reddy, Dr. B.B. Pandey, and Dr. B. Maitra from Indian Institute of Technology, Kharagpur for teaching me several pavement materials and design related subjects. They all motivated me to pursue higher studies. I would like to thank Dr. A.K. Sarkar and Dr. A. P. Singh both from Birla Institute of Technology and Science, Pilani (BITS-Pilani) for their suggestions and guidance during my stay at BITS-Pilani.

Finally, I would like to acknowledge all the unconditional love, encouragement, sacrifice, and support given to me for that I am eternally grateful to my father (Mr. Mahipal Singh) and mother (Mrs. Urmila Kanwar), my sisters (Mrs. Anita Kanwar, Mrs. Anjana Kanwar, Mrs. Archana Kanwar, Mrs. Laxmi Kanwar, and Mrs. Arti Kanwar), my cousins (Mr. Shakti Singh, Mr. Ravinder Singh, Ms. Rajni Kanwar, Mr. Shiva Singh, and Ms. Anjali Kanwar), my in-laws (Mr. Chander Singh, Mrs. Bhanwar Kanwar, Mr. Kamal Singh, and Mrs. Sunita Kanwar) and my extended family members. They have been selfless in giving me the best of everything and I express my deep gratitude for their love, without which this work would not have been completed. I take this moment to express my never ending love and respect towards my wife (Mrs. Kiran Chauhan) for her endless support, inspiration, and motivation during this journey. She was always there cheering me up and stood by me through the good times and bad. Without her, I would be a very different person today, and it would have been certainly much harder to finish a Ph.D.

Lastly, I offer my regards to all of those who supported me in any respect during the completion of this study.

TABLE OF CONTENTS

LIST OF TABLES

LIST OF FIGURES

ABSTRACT

The performance of asphalt mixes is largely determined by the characteristics of its constituents: aggregates, asphalt binder, and additives. Traditionally, stiffness of asphalt mix has been used as a measure of the pavement's ability to carry vehicular traffic loads without undergoing excessive deformation. Early deterioration of pavements due to rutting, fatigue cracking, and other types of distresses may be attributed to inadequate stiffness. Therefore, pavement design and evaluation require a careful evaluation of a number of factors such as material properties, traffic characteristics, and environmental conditions. In recent times, several researchers and state Departments of Transportations (DOTs) have worked to replace the empirical mix designs with mechanistic-empirical design techniques. The mechanistic empirical pavement design guide (MEPDG) emphasizes the use of dynamic modulus of asphalt mixes at all three different levels of design (i.e., Level 1, Level 2, and Level 3) for predicting the performance (fatigue, rutting, and low temperature cracking) of flexible pavements. Several studies have shown that dynamic modulus correlates better with the performance of pavements. The present study characterized the asphalt mixes and aggregates that are commonly used in Oklahoma for the construction of flexible pavements. Five different mixes and aggregates were collected from the production plant. Samples were prepared using a Superpave gyratory compactor (SGC) at four different levels of air voids (i.e., 6%, 8%, 10%, and 12%). It is expected that the selection of this wide range of air voids would cover the practical range of the compaction density achieved in the field (i.e., 88% to 94% of maximum theoretical density). The dynamic modulus values for each mix were measured in the laboratory at selected combinations of temperatures and frequencies. The

relationship between the loading frequency and modulus measured at a specified test temperature can be represented in a graphical form using the master curve, which is a critical input parameter for the design of flexible pavements. The database of dynamic modulus and master curves is developed for the mixes used in this study, which is expected to be useful in the implementation the MEPDG for the design and analysis of flexible pavements.

Aggregates contribute approximately 95% of the total weight of asphalt mix. The shape characteristics of aggregates, namely angularity, texture, two-dimensional form, and sphericity are considered to have a direct influence on the performance and serviceability of asphalt mix. Several researchers have reported that a change in the aggregate shape parameters can alter the volumetric properties of asphalt mixes. A change in aggregate shape parameters can occur either at a plant site during the production of a mix or in the laboratory while preparing compacted asphalt mix samples. In the present study, the effect of plant production and sample preparation methods on different shape parameters was evaluated. Six different types of aggregates: original aggregates (OA), plant mix aggregates (PM), and aggregates compacted at different levels of air voids (AV) were used for this purpose. An automated aggregate image measurement system (AIMS) is used to measure the shape properties of the different types of aggregates. It was observed that the texture of original coarse aggregates (i.e., OA aggregates) was higher compared to that of the plant mix coarse aggregates (i.e., PM aggregates), indicating that the plant production process lowers the texture of coarse aggregates. Similarly, aggregate compacted at different levels of air voids (i.e., AV aggregates) were found to have more texture compared to the PM aggregates. For fine

aggregates, angularity and texture were found to be very similar for all six types of aggregates, indicating that the plant production process and sample preparation method did not influence the shape properties of these particles significantly.

An accurate measurement of the shape properties is important for developing specifications for quality control and quality assurance of aggregates. Currently, the Superpave mix design system is used to ensure the quality of aggregates. The Superpave method is subjective, time-consuming, and labor intensive, and may not reflect the overall quality of the aggregates. The current study compared the shape properties of three different types of aggregates (i.e., granite, rhyolite, and limestone) and sizes of coarse aggregates. Each type of coarse aggregate was divided into three different sizes (i.e., CA1, CA2, and CA3), with CA1 having the largest size, followed by CA2 and CA3. The shape parameters for each type and size of aggregate were measured using the AIMS. It was observed that there is no significant difference in angularity between the different sizes of aggregates. The larger size aggregates were found to be rougher and more cubical compared to the smaller size aggregates (i.e., high texture, low form, and high sphericity), indicating that aggregate particles become smoother and elongated with a reduction in size. Furthermore, the ranking of the aggregates was conducted based on the composite shape index factor (CI). The overall rank sequence for the aggregates was found to be as follows: granite>rhyolite>limestone, indicating that the performance of granite aggregates in asphalt mix is expected to be better compared to the other two aggregates.

The MEPDG offers three levels of input: Level 1, Level 2, and Level 3. Dynamic modulus values at Level 1 are measured in the laboratory at combinations of frequency

and temperature for the samples compacted at a wide range of air voids. On the other hand, dynamic modulus for Level 2 and Level 3 are estimated based on the asphalt binder and volumetric properties of the compacted samples. It was found that the percent difference between the measured and the predicted dynamic modulus increases with the type of asphalt binders. For the modified mix, Level 2 resulted in a higher error compared to Level 3, which is contrary to the expectation that Levels 1, 2, and 3 are in decreasing order of accuracy. For the unmodified mix, Level 2 resulted in less error compared to Level 3, which indicates that assuming default viscosity values from the MEPDG would work well for the unmodified mix used in the present study.

Although the measurement of dynamic modulus in the laboratory is highly desirable, it is not always feasible to conduct this test because it is tedious and time consuming. Therefore, empirical models such as Witczak 1999, Witczak 2006, Hirsch, and Al-Khateeb have been used to estimate dynamic modulus of asphalt mixes. While predictive models are convenient, their performance varies with the type of mixes and volumetric properties. The Hirsch and the Al-Khateeb models were found to perform with good accuracy at low temperatures. The Witczak 1999 and the Witczak 2006 models performed well at high temperatures. None of these models performed well at low temperatures and high air voids. Calibration factors were developed at individual air voids levels to account for the inaccuracies in the model.

Since the volumetric properties of the mix depend on the shape parameters of the aggregates, it is expected that these shape parameters would directly influence dynamic modulus values. In the present study, statistical and neural network (NN) models were developed to estimate dynamic modulus using aggregate shape parameters. Results show

that dynamic modulus of the mix increases with an increase in the angularity and texture of aggregates and that the inclusion of shape parameters can enhance the predictive capability of a model. The results from this study are expected to be helpful in characterizing asphalt mixes using micro levels properties of aggregates.

Recent use of reclaimed asphalt pavement (RAP) in asphalt mix has been favored over the use of virgin materials due to the increasing cost of raw materials and to reduce environmental impacts. The current study investigated the effect of long-term oven (LTO) aging on dynamic modulus of two mixes including RAP. It was found that the LTO-aging resulted in approximately a 42% to 60% increase in dynamic modulus, depending upon the amount of RAP in the mix and air voids. It is seen that the degree of compaction (amount of air voids), temperature, and frequency have a significant impact on dynamic modulus. A proper selection of these parameters is important in estimating dynamic modulus of asphalt mixes containing RAP.

In conclusion, the current study characterizes selected asphalt mixes for pavement applications using dynamic modulus as a performance indicator. The shape parameters of the aggregates are measured using the AIMS. The measured shape parameters are used to rank different types of aggregates. In addition, dynamic modulus values of modified and unmodified mixes are compared at three different design levels of the MEPDG. The predictive capacity of different models is evaluated and correction factors are developed. The aggregate shape based statistical and NN models are developed, and are expected to help in accurately characterizing a mix. Finally, the effect of LTO aging on RAP mixes is studied. Overall, enhanced characterization of aggregates and asphalt mixes is found to be extremely important for pavement design applications.

CHAPTER 1 : INTRODUCTION

1.1 Background and Needs

Over 90 percent of pavements in the U.S. are paved with asphalt binder (NECEPT, 2010). Nationwide, over 550 million tons of asphalt mixes are produced each year for the construction of flexible pavements. Pavement design and evaluation for construction and rehabilitation purposes requires a careful evaluation of important factors such as material properties, traffic characteristics, and environmental conditions.

To ensure good quality, the Superpave mix design and analysis method was developed in 1990's to establish criteria for selecting high quality aggregates and asphalt binders (Cominsky et al., 1994). Since then, many agencies in North America have adopted different parts of that method, including the performance-grade (PG) binder specification and the volumetric mixture design method (Witczak et al., 2002a). The Superpave design method for asphalt mixtures consists of three phases: (1) materials selection for the asphalt binder and aggregate, (2) aggregate blending, and (3) volumetric analysis of specimens compacted using the Superpave gyratory compactor (SGC). It was hypothesized that the selection of good quality aggregate and asphalt binder would be sufficient for better performance of pavements in the field under real life traffic and climatic conditions. However, it was later realized that some performance tests must be established to evaluate the performance of pavements in the field. Subsequently, simple performance tests (SPTs) were developed under the national cooperative highway research program **(**NCHRP**)** 9-19 project (Witczak, 2005; Witczak et al., 2002b) titled "Superpave support and performance models management." The following three performance tests were recommended: dynamic modulus (|E*|), flow number, and flow

time. These tests measure a mixture's response characteristics that are highly correlated to the pavement distresses over a diverse range of traffic and climatic conditions (Witczak et al., 2002b). Out of the three tests, dynamic modulus tests have been widely used to characterize a mix under different temperature and loading frequencies. Specifically, the mechanistic empirical pavement design guide (AASHTO, 2004) considered dynamic modulus as an important parameter to predict the performance (rutting, fatigue, and low temperature cracking) of flexible pavements (Far et al., 2009; Zeghal and Mohamed, 2008; Loulizi et al., 2007; Bari et al., 2006; Obulareddy, 2006; Birgisson et al., 2005; Dongre et al., 2005; Tran and Hall, 2005; AASHTO, 2004; Ayres and Witczak, 1998). Dynamic modulus tests are conducted in accordance with AASHTO TP62 (AASHTO, 2006), at combinations of temperatures and frequencies. The relationship between the loading frequency and the modulus measured at a specified test temperature can be represented in a graphical form using the master curve (Cline, 2003; Medani and Huurman, 2003; DiBenedetto et al., 2001). The master curve for a mix is a critical input for the flexible pavement design (AASHTO, 2004). In recent years, several researchers and state Departments of Transportations (DOTs) have worked to develop a database for dynamic modulus and master curves for the asphalt mixes used in a given state. To that end, one of the objectives of the present study is to evaluate dynamic modulus from the laboratory tests and develop master curves for asphalt mixes that are commonly used in Oklahoma.

The performance of asphalt mixes is largely determined by the characteristics of its constituents: aggregates, asphalt binders, and additives. Mineral aggregates make up between 80% and 90% of the total volume or 94% to 95% of the mass of asphalt mix

(Prowell et al., 2005). Because of the significant amount of aggregates, their shape characteristics, namely angularity, texture, two-dimensional form, and sphericity are considered to have a direct influence on the mix performance and serviceability (Liu and You, 2011; Wang et al., 2008; Anthony, 2007; Lynn et al., 2007; Masad et al., 2007a, 2007b; Alvarado et al., 2006; Pan et al., 2006; Fletcher et al., 2002; Kuo, 2002; Masad et al., 2001a, 2001b; Coree and Hislop, 2000; Huber et al., 1998, Abdul-Malak et al., 1996; Barksdale et al., 1992). Rough and angular particles are desired for providing a better aggregate interlock, thus increasing the rut resistance (Kandhal and Mallick, 2001; Sousa et al., 1991; Brown and Bassett, 1990; Button et al., 1990). On the other hand, smooth and circular particles have a tendency to roll over each other and result in a poor performance of the associated mix. Several researchers have reported that a change in the aggregate shape parameters can alter the volumetric properties of a mix (Johnson et al., 2007; Masad et al., 2001b; Chadbourn et al., 1999). A change in aggregate shape parameters can occur either at the plant site during the production of a mix or in the laboratory while preparing the compacted asphalt mix samples. Such changes in aggregate shape parameters can lead to different mix performance (i.e., field vs. laboratory). The current study aims to evaluate the change in aggregate shape parameters of a selected aggregate due to production and sample preparation methods. An automated aggregate image measurement system (AIMS) is used to measure the shape properties of different types of aggregates. The AIMS is a promising instrument to evaluate the effects of different processes, such as crushing and blending, on the aggregate shape distribution (Masad et al., 2007a, 2007b; Gatchalian et al., 2006; Al-Rousan et al., 2005; Fletcher et al., 2003). Furthermore, it provides a simple, unbiased, and quantitative measure of the

morphological characteristics of aggregates (Al-Rousan et al., 2005; Masad et al., 2005; Rao et al., 2002).

Another important concern is the selection of aggregates for developing quality control and quality assurance specifications for construction of pavements. Currently, the Superpave mix design system is used to ensure the quality of aggregates by determining their consensus and source properties (Cominsky, 1994). The source properties of aggregates include toughness, durability, and amount of deleterious materials; consensus properties consist of the following: coarse aggregate angularity, fine aggregate angularity (FAA), flat and elongated (F&E) particles, and amount of clay content in aggregates (Cominsky, 1994). Several researchers have reported that Superpave tests may not yield the overall quality of the aggregates (Bennert et al., 2011; Wang et al., 2009; Bhasin et al., 2006; Hand et al., 2000). This method does not provide a direct measure of the texture of the particles. The lack of a direct measurement of the texture might cause some aggregate sources to be discarded based on the angularity of aggregates. This method is subjective and provides limited information on producing a statistically valid sample. Furthermore, the method cannot distinguish between the shape properties of different sources, types, and sizes of aggregates. Recently digital image-based techniques have been widely used for developing quality control and quality assurance specifications of aggregates based on the shape parameters of the aggregates (Wang et al., 2009). The present study focuses on the comparison of shape parameters of different types of aggregates. The AIMS is used to measure the shape parameters of the aggregates.

The MEPDG uses three different levels (i.e., Level 1, Level 2, and Level 3) for design and analysis of flexible pavements. The use of a particular hierarchal input level

of analysis depends on the amount of information available to the designer and the criticality of the project. The dynamic modulus of asphalt mix is used for all three levels of design. At Level 1, asphalt binder and asphalt mixes are tested in the laboratory at different frequency and temperature combinations to measure dynamic modulus. On the other hand, Level 2 and Level 3 designs use the Witczak 1999 model (Andrei et al., 1999) to estimate dynamic modulus without conducting actual modulus tests in the laboratory. Measurement of dynamic modulus requires costly equipment and trained personnel for specimen preparation, testing, and data analysis (Azari et al., 2007*)*. Therefore, the use of Level 2 and Level 3 seems to be a reasonable approach for design and analysis of pavements. However, caution should be taken while using the Level 2 and Level 3 for modified mixes (Bennert, 2009; Dongre et al., 2005). Bennert (2009) reported that the percent difference between the modulus used at Level 1 and at Level 2 and at Level 3 increases with modified asphalt binders. Therefore, it is important to develop a relationship between different design levels of the MEPDG for modified and unmodified mixes separately. The current study aims to compare dynamic modulus of selected modified and unmodified mixes at three different levels of the MEPDG.

Although the measurement of dynamic modulus in the laboratory is highly desirable, it is not always feasible to conduct this test because of its tedious and time consuming nature (Gopalakrishnan and Kim, 2011; Azari et al., 2007; Tran and Hall, 2005). Therefore, several regression-based and neural network (NN)-based models are used to predict dynamic modulus. In recent years, the Witczak 1999 (Andrei et al., 1999), Witczak 2006 (Bari and Witczak, 2006), Hirsch (Christensen et al., 2003), and Al-Khateeb (Al-Khateeb et al., 2006) models have been increasingly used to estimate

dynamic modulus of asphalt mixes. These models use aggregate gradation (i.e., percentage passed and retained on selected sieve sizes), viscosity of asphalt binder, shear modulus of asphalt binder, and volumetric properties of the mix (i.e., air voids, effective binder) as input variables to the model. While predictive models are convenient, their performance varies with the type of mixes and volumetric properties (Azari et al., 2007; Bari and Witczak, 2006; Obulareddy, 2006; Birgisson et al., 2005; Dongre et al., 2005; Kim et al., 2005; Schwartz, 2005; Tran and Hall, 2005; Pellinen and Witczak, 2002). The use of these predictive models without taking account the variability in estimation might result in inaccurate design and performance of pavements. To account for such variability, calibration factors need to be developed for each model. The present study evaluates the strengths and weaknesses of four predictive models (i.e., Witczak 1999, Witczak 2006, Hirsch, and Al-Khateeb) for estimation of dynamic modulus of selected asphalt mixes that are commonly used in Oklahoma.

Since the volumetric properties of a mix depend on the shape parameters of the aggregates (Aschenbrener and MacKean, 1994), it is expected that these shape parameters would directly influence the dynamic modulus values as well. However, none of the empirical models (i.e., Witczak 1999, Witczak 2006, Hirsch, and Al-Khateeb) utilize aggregate shape parameters (i.e., angularity, texture, form, and sphericity) in the development of the model. It is expected that at high temperatures, asphalt mixes behave like a granular non-linear elastic materials; therefore, aggregate gradation and shape parameters play an important role (Bari and Witczak, 2006). Recognizing the importance of aggregate morphological properties, it is necessary to consider aggregate shape parameters in the estimation of dynamic modulus. The present study aims to develop

statistical and NN models using aggregate shape parameters. It is expected that these models would be helpful in characterizing asphalt mixes using micro levels properties of aggregates.

In recent years, the use of reclaimed asphalt pavement (RAP) in a asphalt mix has been favored over the use of virgin materials due to the increased cost of raw materials and reduced environmental impacts (FHWA, 2010a; Al-Qadi et al., 2007; Kennedy et al., 1998; Page and Murphy, 1987). The addition of RAP is beneficial to resisting permanent deformation at high temperature (Huang et al., 2004; Li et al., 2004; Kandhal et al., 1989; Brown, 1984; Meyers et al., 1983; Little et al., 1981; Little and Epps, 1980). On the other hand, excessive RAP content may reduce the resistance to cracking at low temperatures (Li et al., 2008). So far, limited studies have been conducted to investigate the effect of long-term oven (LTO)-aging on plant produced asphalt mixes containing RAP. Aging of asphalt mixes can lead to the development of distresses such as fatigue and thermal cracking (Woo et al., 2008; NCHRP, 2007; Chen et al., 2000). The hardening of original asphalt binder due to plant mixing and lay-down operation (short-term aging) and in-situ aging (long-term aging) are complex phenomena because of numerous factors influencing the rate of aging. The present study evaluates the effect of LTO-aging on the dynamic modulus of modified and unmodified mixes containing RAP.

1.2 Objectives of the Research

The main goal of this research work is to characterize selected asphalt mixes for pavement applications using dynamic modulus as a performance indicator. The specific objectives of this study are listed below:

(1) Develop dynamic modulus master curves and shift factors of selected asphalt mixes that are commonly used in Oklahoma.

(2) Evaluate the effect of production and sample preparation methods on shape parameters of coarse and fine aggregates.

(3) Compare the shape parameters for different types of aggregates and develop a methodology to rank aggregates based on these parameters.

(4) Evaluate dynamic modulus of modified and unmodified asphalt mixes for different input levels (i.e., Level 1, Level 2, and Level 3) of the MEPDG for design and analysis of pavements.

(5) Evaluate the strengths and weaknesses of selected predictive models (i.e., Witczak 1999, Witczak 2006, Hirsch, and Al-Khateeb) for estimating dynamic modulus of commonly used asphalt mixes in Oklahoma.

(6) Develop statistical and neural network (NN)-based models considering aggregate shape parameters (i.e., angularity, form, texture, and sphericity) for estimating dynamic modulus of asphalt mixes.

(7) Evaluate the effect of long-term oven (LTO) aging on dynamic modulus of asphalt mixes containing reclaimed asphalt pavements (RAP), and evaluate the effect of air voids, temperature, and frequency on dynamic modulus.

1.3 Organization of the Dissertation

This study is focused on characterizing asphalt mixes using dynamic modulus as a performance indicator. Dynamic modulus and |E*| are used interchangeably in this dissertation.

This dissertation is composed of nine chapters. Following the introduction presented in Chapter 1, Chapter 2 entitled "*Dynamic Modulus Master Curves for Asphalt Mixes,"* presents the introduction to dynamic modulus and a methodology to construct the master curves and shift factor. Three surface mixes with nominal maximum aggregate

size (NMAS) of 12.5 mm, and two base mixes with NMAS of 25 mm were collected from the production plant. These mixes included different types of aggregates, namely limestone, granite, and rhyolite, as well as different types of performance grade (PG) asphalt binders: PG 64-22, PG 70-28, and PG 76-28. For each mix, samples were compacted using a Superpave gyratory compactor (SGC) at four different levels of air voids (i.e., 6%, 8%, 10%, and 12%). Dynamic modulus tests were conducted at four different temperatures (i.e., 4, 21, 40, and 55^{o}C) and six different frequencies (i.e., 25, 10, 5, 1, 0.5, and 0.1 Hz). The viscosities of each asphalt binder were measured in the laboratory at four different temperatures (i.e., 135, 150, 165, and 180^{o}C). A (intercept) and VTS (slope) pertaining to the temperature and viscosity relationship of asphalt binder was determined. The master curves and shift factors for each mix are developed.

Chapter 3 entitled *"Effect of Production and Sample Preparation Methods on Aggregate Shape Parameters,"* includes a study on the effects of degradation on aggregate shape parameters (Singh et al., 2011a). The effects of plant production and laboratory sample preparation methods are evaluated on a mix that is commonly used for paving in Oklahoma. The original aggregates (OA) from the stockpile and loose asphalt mix were collected from the production plant. A majority of the aggregates were limestone. The loose mix was divided into five different groups. One group was left un-compacted, and was called 'plant mix' (PM), while the other four groups were used to compact samples in a SGC at four different air voids: 6%, 8%, 10%, and 12%. These groups were named as AV6, AV8, AV10, and AV12, respectively. Aggregates from the PM and compacted samples (i.e., AV6, AV8, AV10, and AV12) were retrieved after burning them in a National Center for Asphalt Technology (NCAT) ignition oven. All six

types of aggregates were divided into coarse and fine aggregates. The shape parameters of each type of aggregate are measured using the AIMS. Statistical analyses are conducted to identify the change in aggregate shape parameters. Furthermore, change in shape parameters with aggregate size is also investigated.

Chapter 4 entitled *"Shape Parameters for Different Types of Coarse Aggregates,"* compares the shape parameters (i.e., angularity, texture, form, and sphericity) of different types and sizes of coarse aggregates (Singh et al., 2011b). Three different types of aggregates (granite, rhyolite, and limestone) that are commonly used in Oklahoma are collected from stockpiles. Aggregates are washed and separated into three different sizes (i.e., CA1, CA2, and CA3). The shape parameters of the aggregates are measured using the AIMS, and a ranking of the aggregates is done based on the composite index (CI).

Chapter 5 entitled *"Evaluation of Dynamic Moduli for Different MEPDG Levels,"* examines dynamic modulus of modified and unmodified mixes at three different input levels (i.e., Level 1, Level 2, and Level 3) of the MEPDG (Singh et al., 2011c). Two Superpave asphalt mixes, one containing a modified PG 70-28 binder and the other containing an unmodified PG 64-22 binder, are used for this purpose. Dynamic modulus and master curves for these mixes are compared. Furthermore, development of correction factor is discussed in this chapter.

Chapter 6 entitled *"Evaluation of Predictive Models for Estimating Dynamic Modulus,"* is devoted to examining the strengths and weaknesses of the four predictive models (i.e., Witczak 1999, Witczak 2006, Hirsch, and Al-Khateeb) for estimating dynamic modulus (Singh et al., 2011d). A combined dataset of five mixes is used for this purpose. Dynamic modulus values of a mix are estimated using each predictive model. A

comparison of the measured and the predicted modulus values is made at different air voids and temperature levels. The predictive capability of each model is discussed with changes in air voids and temperature. Furthermore, this chapter presents the development of correction factors for each model.

Chapter 7 entitled *"Statistical and Neural Network Modeling of Dynamic Modulus,"* is related to statistical and neural network modeling for the estimation of dynamic modulus using aggregate shape parameters (Singh et al., 2011e, 2011f). Dynamic modulus tests on several mixes were conducted. The aggregate shape properties of different coarse and fine aggregates were measured using the AIMS. The models are developed considering various independent parameters: viscosity (η), frequency (f), air voids (V_a) (%), and effective asphalt binder (% volume) (V_{beff}), as well as shape parameters of the aggregates. Also, the effect of aggregate shape parameter on dynamic modulus is investigated in this chapter.

The study presented in Chapter 8, *"Effect of Aging on Dynamic Modulus,"* was undertaken to evaluate the effect of long term oven-aging (LTO) on dynamic modulus of two reclaimed asphalt mixes (RAP) (Singh et al., 2011g). Furthermore, the effect of air voids, temperature, and frequency are investigated.

Finally, in Chapter 9 the summary and conclusions of this dissertation as well as recommendations for future studies are presented.

CHAPTER 2 : DYNAMIC MODULUS MASTER CURVES FOR ASPHALT MIXES

2.1 Introduction

Pavement design and evaluation for construction and rehabilitation purposes requires a careful evaluation of factors such as material properties, traffic characteristics, and environmental conditions. Traditionally, stiffness of asphalt mix is used as a measure of the pavement's ability to withstand traffic loads without undergoing excessive deformation. Early deterioration of pavements due to rutting, fatigue cracking, and other types of distresses may be attributed to inadequate stiffness (Zeghal and Mohamed, 2008; Azari et al., 2007; Pellinen and Witczak, 2002). The stiffness of a pavement is typically expressed in terms of its modulus (i.e., the relationship between the applied stress and the resulting deformation) (Medani and Huurman, 2003; DiBenedetto et al., 2001). Existing pavement design procedures, namely AASHTO (1993) and the Asphalt Institute (AI) (AI, 1991), recognize the resilient modulus (M_r) as one of the primary mechanistic properties to evaluate the performance of pavement materials under vehicular loading and environmental conditions. Specifically, these design methods require the evaluation of M_r of asphalt mix with temperature as well as the M_r of subgrade soil with moisture.

In recent years, several researchers and state Departments of Transportation (DOT) have worked to replace the empirical mix designs with mechanistic-empirical design techniques. The focus of these approaches is to determine the fundamental engineering material properties that can be linked back to the stress-strain behavior that is needed to analyze the pavement performance. As a result, several mix design methodologies and associated measuring methods for asphalt pavements have been developed (Francken and Partle, 1996). Laboratory tests on the cyclic behavior of

compacted asphalt mix specimens show that their stress-strain relationships are temperature-dependent. Therefore, the mechanistic-empirical pavement design guide (MEPDG) recommends the use of dynamic modulus to characterize asphalt mixes (AASHTO, 2004). Dynamic modulus is the time-temperature-dependent property of asphalt materials. The master curve is constructed to estimate to dynamic modulus over a wide range of temperatures and frequencies (Medani and Huurman, 2003; DiBenedetto et al., 2001). Several studies have shown that dynamic modulus of asphalt mixes is a key design factor that directly impacts the load bearing capacity of roadway pavements (Commuri et al., 2011; Singh et al., 2011h; Far et al., 2009; Loulizi et al., 2007; Bari et al., 2006; Obulareddy, 2006; Birgisson et al., 2005; Dongre et al., 2005; Tran and Hall, 2005; AASHTO, 2004). Furthermore, several researchers reported that dynamic modulus of asphalt mix is highly correlated to pavement distresses (i.e., rutting, fatigue, and low temperature cracking) over a wide range of traffic and climatic conditions (Goh et al., 2011; Loulizi et al., 2006; Bonaquist and Christensen, 2005; Pellinen and Witczak, 2003; Shenoy and Romero, 2002; Witczak et al., 2002b; Cominsky et al., 1998). Therefore, it is necessary to accurately determine the dynamic modulus of asphalt mixes over a wide range of temperatures and frequencies.

2.2 Background

2.2.1 Dynamic Modulus

For linear visco-elastic materials such as asphalt mixes, the stress-strain relationship under a continuous sinusoidal loading is defined by its complex dynamic modulus (E*). The complex modulus is defined as the ratio of the amplitude of the sinusoidal stress at any given time, t, and the angular load frequency (ω), $\sigma = \sigma_o \sin(\omega t)$ (i.e., $\sigma_o e^{i\omega t}$) and the amplitude of the sinusoidal strain $\varepsilon = \varepsilon_o \sin(\omega t - \phi)$ (i.e., $\varepsilon_o e^{i\,(\omega t - \phi)}$), at

the same time and frequency, that results in a steady state response (Figure 2.1). Mathematically, E* is defined as shown in Equations (2.1) through (2.3) (Witczak et al., 2002).

$$E^* = \frac{\sigma_o e^{i\omega t}}{\varepsilon_o e^{i(\omega t - \phi)}} \tag{2.1}$$

$$E^* = \frac{\sigma_o \cos\phi}{\varepsilon_o} + i\frac{\sigma_o \sin\phi}{\varepsilon_o} \tag{2.2}$$

$$E^* = E_1 + iE_2 \tag{2.3}$$

where,

σ_o = applied stress amplitude,

ε_o = measured strain amplitude,

ϕ = the phase angle,

ω = angular velocity,

t = loading time in seconds,

E_1 = storage or elastic modulus,

E_2 = loss or viscous modulus, and

E^* = complex modulus.

For elastic material ϕ = 0, so E_2 = 0, and for viscous materials ϕ = 90^o, so E_1 = 0. The absolute value of the complex modulus (Equation (2.3)) is calculated using Equation (2.4). The ratio of stress and strain amplitudes is called dynamic modulus ($|E^*|$), as shown in Equation (2.5).

$$|E^*| = \sqrt{(E_1)^2 + (E_2)^2} \tag{2.4}$$

$$|E^*| = \frac{\sigma_o}{\varepsilon_o} \tag{2.5}$$

2.2.2 Methodology to Generate Master Curves

The master curves are constructed using the principle of time-temperature superposition. First, a standard reference temperature is selected (i.e., 21°C), and then data at various temperatures are shifted with respect to time until the curves merge into a single smooth function. The master curve of dynamic modulus as a function of time formed in this manner describes the time dependency of the material. The amount of shifting at each temperature required to form the master curve describes the temperature dependency of the material. Thus, both the master curve and the shift factors are needed for a complete description of the rate and temperature effects.

AASHTO TP62 (2006) recommends the testing of |E*| on five different temperatures ranging from -10^{o}C to 54^{o}C, and six different frequencies: 25, 10, 5, 1, 0.5, 0.1 Hz. The Equation (2.6) is a sigmoidal function, which is used in fitting the master curve. A typical master curve is shown in Figure 2.2.

$$Log\,|E^{*}| = \delta + \frac{\alpha}{1+\exp(\beta+\gamma(\log f_r))} \tag{2.6}$$

where,

f_r = reduced frequency at reference temperature,

δ = minimum value of |E*|,

$\delta+\alpha$ = maximum value of |E*|, and

β, γ = parameters describing the shape of the sigmoidal function.

The fitting parameters δ and α depend on aggregate gradation, binder content, and air void content. The fitting parameters β and γ depend on the characteristics of the

asphalt binder and the magnitude of δ and α. Equations (2.7) and (2.8) provide the general form of the shift factor.

$$a(T) = \frac{f_r}{f} \tag{2.7}$$

$$\log(f_r) = \log(a(T)) + \log(f) \tag{2.8}$$

where,

$a(T)$ = shift factor as a function of temperature,

f_r = reduced frequency at reference temperature, and

f = frequency at a particular temperature.

It is evident from Equations (2.7) and (2.8) that the shift factor is a function of temperature, which implies that it is a function of viscosity of the asphalt binder. The shift factor can be expressed in the following form (Equation (2.9)).

$$\log(a(T)) = c(\log\eta - \log\eta_{t=r}) \tag{2.9}$$

To estimate the shift factor, the viscosity of the asphalt binder at the temperature of interest can be determined from the ASTM viscosity-temperature relationship (ASTM, 2009), defined by Equations (2.10) and (2.11).

$$\log\log\eta = A + VTS\log(T_R) \tag{2.10}$$

$$\log\eta = 10^{(A+VTS\log(T_R))} \tag{2.11}$$

where,

T_R = temperature in Rankine,

η = viscosity of asphalt binder in Centipoise (cP),

$\eta_{t=r}$ = viscosity of asphalt binder at reference temperature in Centipoise (cP),

c = coefficient of shift factor, and

A and VTS = regression parameters pertaining to temperature-viscosity relationship of the associated asphalt binder.

Generally, there are two methods used for estimating A and VTS values: (a) using viscosity measured by a Brookfield rotational viscometer, and (b) using complex modulus and phase angle measured by a dynamic shear rheometer (DSR) (AASHTO, 2004). Birgisson et al. (2005) reported that A and VTS values estimated using a Brookfield rotational viscosity data are more accurate compared to those obtained from DSR data. Therefore, viscosity measured using the Brookfield viscometer is used in the present study. The procedure to estimate the A and VTS parameters will be explained later in this chapter.

Equation (2.12) can be obtained by substituting Equation (2.11) into Equation (2.9).

$$\log(a(T)) = c(10^{(A+VTS\log(T_R))} - \log\eta_{t=r}) \tag{2.12}$$

Once the coefficient of shift factor "c" and the viscosities are known, shift factors at various temperatures can be calculated using Equation (2.12). A nonlinear optimization program is used for solving the coefficient of the shift factors. A quadratic polynomial fit (Equation (2.13)) is used to establish the relationship between shift factor and temperature.

$$\log(a(T)) = mT^2 + nT + p \tag{2.13}$$

where,

T = temperature in ^{o}F, and

m, n, p = fitting coefficients.

Substituting Equation (2.12) into Equation (2.8), we get the following equation (Equation (2.14)).

$$\log(f_r) = c(10^{(A+VTS\log(T_R))} - \log\eta_{t=r}) + \log(f) \tag{2.14}$$

Substituting Equation (2.14) into Equation (2.6), the master curve equation can be written in the form of Equation (2.15). A nonlinear optimization program, called Solver, available in Microsoft Excel was used for solving the unknown parameters.

$$Log|E^*| = \delta + \frac{\alpha}{1+\exp(\beta+\gamma\left[\log(f) + c(10^{(A+VTS\log(T_R))} - \log\eta_{t=r})\right]} \tag{2.15}$$

To find the maximum value of dynamic modulus, Equation (2.15) requires the testing of a mix at lower temperatures (i.e., -10°C or -20°C). Testing of a mix at a lower temperature is time consuming and needs a costly environmental chamber to maintain the temperature. Moreover, it causes problems in terms of ice formation inside the environmental chamber, which hinders the testing procedure.

An approach developed by Bonaquist et al. (2005) eliminates the lower temperature requirement, so that the time required in conducting dynamic modulus testing and master curve construction can be reduced. This approach uses three temperatures between 4 and 46.6°C and four frequencies between 0.01 and 10 Hz, instead of five temperatures between (-10° and 54° C) and six loading rates between 0.1 and 25 Hz, as recommended by AASHTO TP62 (2006). The modified form of the master curve is shown in Equation (2.16). The limiting maximum modulus is estimated based on the

basis of binder stiffness and volumetric data of the mix using Equations (2.17) and (2.18) (Christensen et al., 2003). This approach is used in the present study.

$$Log\left|E^*\right| = \delta + \frac{Max - \delta}{1 + \exp(\beta + \gamma\left[\log(f) + c(10^{(A+VTS\log(T_R))} - \log\eta_{t=r})\right]} \tag{2.16}$$

$$\left|E^*\right|_m = P_c\left[4{,}200{,}000(1 - \frac{VMA}{100}) + 3\left|G^*\right|_b\left(\frac{(VMA)(VFA)}{10{,}000}\right)\right] + \frac{1 - P_c}{\left[\frac{(1 - \frac{VMA}{100})}{4{,}200{,}000} + \frac{VMA}{3\left|G^*\right|_b(VFA)}\right]} \tag{2.17}$$

$$P_c = \frac{\left(20 + \frac{3\left|G^*\right|_b(VFA)}{VMA}\right)^{0.58}}{650 + \left(\frac{3\left|G^*\right|_b(VFA)}{VMA}\right)^{0.58}} \tag{2.18}$$

where,

$|E^*|_m$ = absolute value of asphalt mixture dynamic modulus (psi) (Maximum value),

$|G^*|_b$ = absolute value of asphalt binder complex shear modulus (psi) (i.e., 145,000 psi),

VMA = voids in mineral aggregates in compacted mixture (%),

VFA = voids filled with asphalt binder in compacted mixture (%), and

Max = limiting maximum modulus of an asphalt mix.

2.3 Materials

A total of five different loose asphalt mixes (referred to as Mix-1, Mix-2, Mix-3, Mix-4, and Mix-5) that are commonly used for paving in Oklahoma were collected from the production plant of Haskell Lemon Construction Company in Norman, Oklahoma. Asphalt mixes contained three types of aggregates (limestone, granite, and rhyolite) and three different binders (PG 64-22, PG 70-28, and PG 76-28). Three of these mixes were

surface mixes with nominal maximum aggregate size (NMAS) of 12.5 mm, and the other two were base mixes with NMAS of 25 mm. Each of these mixes used Superpave aggregate gradation. The Oklahoma Department of Transportation (ODOT) gives a different designation to the Superpave mix depending on their NMAS. For example, a mix with 19 mm NMAS is called S3, while a mix with 12.5 mm NMAS is called a S4 mix. Thus, Mix-1 and Mix-2 are named as S3 mix, while Mix-3, Mix-4, and Mix-5 are called S4 mixes. The three asphalt binders used in this study were obtained from the Valero Refinery in Ardmore, Oklahoma. Table 2.1 and Table 2.2 summarize the aggregate gradation and volumetric properties of all five mixes, respectively. The details of the five mixes are summarized below.

Mix-1

The nominal maximum aggregate size was 19 mm. The mix contained approximately 20 percent 1" (25 mm) rock, 44 percent manufactured sand, 11 percent sand, 25 percent reclaimed asphalt pavements (RAP), and 4.1 percent PG 64-22 binder. This mix is generally used for the construction of the base layer. This mix is designated as a S3 64-22 mix.

Mix-2

The nominal maximum aggregate size was 19 mm. The mix contained approximately 22 percent 1" (25 mm) rock, 50 percent manufactured sand, 13 percent sand, 15 percent RAP, and 4.1 percent PG 76-28 binder. This mix is generally used for the construction of the base layer. This mix is designated as a S3 76-28 mix.

Mix-3

The nominal maximum aggregate size was 12.5 mm. The mix contained approximately 38 percent 5/8" (15.8 mm) chips, 27 percent manufactured sand, 24

percent screening, 11 percent sand, and 4.5 percent PG 70-28 binder. This mix is generally used for the construction of the surface layer. This mix is designated as a S4 70-28 mix.

Mix-4

The nominal maximum aggregate size was 12.5 mm. The mix contained approximately 25 percent 5/8" (15.8 mm) chips, 38 percent manufactured sand, 22 percent screening, 15 percent sand, and 5.1 percent PG 64-22 binder. This mix is generally used for the construction of the surface layer. This mix is designated as a S4 64-22 mix.

Mix-5

The nominal maximum aggregate size was 12.5 mm. The mix contained approximately 22 percent 5/8" (15.8 mm) chips, 23 percent manufactured sand, 20 percent screening, 10 percent screening, 10 percent sand, 15 percent RAP, and 4.2 percent PG 76-28 binder. This mix is generally used for the construction of the surface layer. This mix is designated as a S4 76-28 mix.

2.4 Sample Preparation

Since the loose mixes were collected from the production plant, no short-term aging was done in the laboratory. To prepare cylindrical samples for laboratory testing, the loose mixes were directly preheated in an oven. The mixing and compaction temperatures for the mixes were obtained from the mix design sheet. Specimens were compacted using a Superpave Gyratory Compactor (SGC). The SGC machine was operated in height mode so as to stop automatically when the desired height is reached. For each mix, three replicate specimens were compacted at 6%, 8%, 10%, and 12% ± 0.5% air voids. It is expected that specimens compacted at 6% air voids (i.e., 94% of

maximum density) represent a well compacted pavement immediately after construction, while 8% to 10% air voids indicate an intermediate compaction (i.e., 92% to 90% of maximum density). Similarly, 12% air voids simulate lay-down density (i.e., 88% density) of a mix in the field. The selection of these four levels of air voids would cover a practical range of compaction densities encountered during the construction of a flexible pavement. A trial and error process was used to achieve target air voids in the compacted specimen. First, the weight of loose asphalt mix was calculated at a selected target air void, and specimens having a size of 150 mm diameter by 167.5 mm height were prepared (Figure 2.3). The test specimens with 100 mm diameter were cored from the center of the SGC compacted specimens, and then sawed from each end to obtain the final specimens having a diameter of 100 mm and a height of 150 mm (Figure 2.3). This procedure produced specimens with consistent air void distribution in both the vertical and radial directions (Chehab et al., 2000). Moreover, these geometries are currently recommended for the simple performance test and are also used in constitutive modeling (Chehab et al., 2002; Schwartz et al., 2002; Witczak et al., 2002b; Daniel, 2001).The air voids of the final specimens were calculated in accordance with AASHTO T166 (AASHTO T166, 2006). Three samples were prepared at each level of air voids. Therefore, a total of 60 specimens (5 mixes x 4 air voids x 3 specimens) were compacted. Volumetric analyses of final compacted specimens were conducted to obtain effective binder content (V_{beff}), VMA, VFA, and air voids (V_a). Tables 2.3 through 2.7 summarize the volumetric properties of the samples compacted. These properties are used in Chapters 5 through 8.

2.5 Measurement of Dynamic Modulus

Dynamic modulus values were measured in the laboratory in accordance with AASHTO TP62 specifications (AASHTO, 2006). Tests were performed using a mechanical testing system (MTS) equipped with a servo-hydraulic testing system (MTS, 2011). The test specimen was placed in an environmental chamber and allowed to reach equilibrium to the specified testing temperature ±0.5^{o}C. The specimen temperature was monitored using a dummy specimen with a thermocouple mounted at the center. Two linear variable differential transducers (LVDTs) were mounted on the specimen at 100 mm gauge length. A device was manufactured to mark the LVDT point exactly at 100 mm gauge length. To hold the LVDT onto the position, brass rods were attached to these points. Figures 2.4 and 2.5 show the process of marking the LVDT and attaching the LVDTs with the specimen, respectively. The accuracy of measuring dynamic modulus with three specimens, with two LVDTs on each specimen, is expected to range within ±15.0% (AASHTO, 2006). The variability in the measurement of dynamic modulus can be reduced by increasing the number of replicates samples and LVDT. Two friction reducing end treatment or teflon papers were placed between the specimen and loading platens. A sinusoidal axial compressive load was applied to the specimen without impact in a cyclic manner. The test was conducted on each specimen at four different temperatures: 4, 21, 40, and 55^{o}C, starting from the lowest temperature and going to the highest temperature. For each temperature level, the test was conducted at different loading frequencies from the highest to the lowest: 25, 10, 5, 1, 0.5, and 0.1 Hz. Prior to testing, the specimen was conditioned by applying 200 cycles of load at a frequency of 25 Hz. The loading sequence used for conducting dynamic modulus test is given in Table 2.8. The load magnitude was adjusted based on the material stiffness, air voids content,

temperature, and frequency to keep the strain response within 50-150 micro-strains (Tran and Hall, 2006). The data was recorded for the last 5 cycles of each sequence. Dynamic modulus was calculated using Equation (2.5) for combinations of temperatures and frequencies (Witczak et al., 2002b). The dynamic modulus test matrix for the mixes is given in Table 2.9. Figure 2.6 shows the set up for dynamic modulus testing. Table 2.10 shows the measured dynamic modulus for Mix-1 for sample compacted at 6% air voids. A total of 1440 |E*| values (5 mixes x 4 air voids x 3 specimens x 4 temperatures x 6 frequencies) were measured in the laboratory. These measured dynamic modulus values are used in Chapters 5 through 8.

2.6 Testing on Asphalt Binders

Viscosity values of the three asphalt binders (i.e., PG 64-22, PG 70-28, and PG 76-28) were determined using a Brookfield rotational viscometer (Figure 2.7), in accordance with AASHTO T316 (AASHTO, 2002). Prior to measuring the viscosity, the binders were subjected to short-term aging in a rolling thin film oven (RTFO), in accordance with AASHTO T240 (AASHTO, 2003). The viscosity was measured at four temperatures (i.e., 135, 150, 165, and 180^{o}C). Table 2.11 lists the results of the Brookfield rotational viscometer test. The viscosity and temperature plot for all three binders is shown in Figure 2.8. The corresponding A and VTS values for the selected asphalt binders (PG 64-22, PG 70-28, and PG 76-28) are found to be 10.59, -3.537; 9.780, -3.233; and 9.254, -3.037; respectively (Table 2.11). Viscosity of asphalt binders at four test temperatures (i.e., 4, 21, 40, and 55^{o}C) can be calculated using Equations (2.10) and (2.11) (ASTM, 2009). Table 2.12 summarizes the calculated viscosities for all three binders. These measured viscosity and A and VTS values are used in Chapters 5 through 8.

2.7 Developed Master Curve

The approach discussed in Section 2.2.2 is used to develop the master curves for all the mixes. Figure 2.9 shows an example of the master curve and shift factor developed for Mix-1 for samples compacted at 6% air voids. The parameters for this master curve and shift factors are listed in Table 2.13. Similar plots are constructed for all five mixes for samples compacted at different levels of air voids. Appendix A summarizes the master curve and shift factor for the selected mixes. Appendix B lists the parameters for master curves and shift factors.

2.8 Effect of Various Factors on Dynamic Modulus

Various factors can affect dynamic modulus of an asphalt mix. These factors include air voids, temperature, frequency, aggregate shape parameters (i.e., angularity, texture, and sphericity), and aging. Chapter 7 discusses the affect of aggregate shape parameters, while Chapter 8 covers the effect of air voids, frequency, and temperature.

Table 2.1 Aggregate Gradation for all Mixes

(%Passing)	Mix Types				
Sieve size (mm)	Mix-1	Mix-2	Mix-3	Mix-4	Mix-5
25	100	100			
19	98	98	100	100	100
12.5	87	87	97	98	98
9.5	80	80	89	87	87
4.75	58	62	69	62	62
2.36	37	40	49	40	40
1.18	25	27	35	28	28
0.6	19	20	25	21	21
0.3	12	12	15	13	13
0.15	4	5	7	5	5
0.075	2.9	2.8	2.5	3.2	3.2
ODOT Designation S: Superpave	S3	S3	S4	S4	S4

Table 2.2 Details of All Mixes

Volumetric Properties	Mix Types				
	Mix-1	Mix-2	Mix-3	Mix-4	Mix-5
G_{mm}	2.505	2.523	2.463	2.477	2.508
G_{se}	2.671	2.677	2.658	2.681	2.688
G_{sb}	2.645	2.657	2.634	2.669	2.652
G_b	1.01	1.01	1.01	1.02	1.01
Binder Type	PG 64-22	PG 76-28	PG 70-28	PG 64-22	PG 76-28
P_b (%)	4.1	4.1	4.5	5.1	4.2
Aggregate Type	Limestone	Limestone	Granite	Rhyolite	Limestone
Mix Type	Recycled	Recycled	Virgin	Virgin	Recycled

G_{mm} = Max.Theo. Sp. Gr. Mix G_{se} = Effective Sp.Gr. of Agg.

G_{sb} = Bulk Sp. Gr. of Agg. G_b = Sp. Gr. of Binder

V_a = Air Voids P_b = Binder Content

Table 2.3 Volumetric Properties for Mix-1

Volumetric Properties (%): Mix-1 (S3 64-22)					
Target Air Voids (%)	Samples	V_a	VMA	VFA	V_{beff}
6	Sample 1	5.4	14.1	62.2	8.78
	Sample 2	5.6	14.3	61.4	8.76
	Sample 3	5.6	14.3	61.5	8.77
8	Sample 1	7.3	15.8	54.5	8.61
	Sample 2	7.2	15.7	54.7	8.61
	Sample 3	7.2	15.7	54.9	8.62
10	Sample 1	9.3	17.7	47.7	8.42
	Sample 2	9.6	17.9	46.9	8.39
	Sample 3	9.1	17.5	48.3	8.44
12	Sample 1	11.5	19.7	41.8	8.21
	Sample 2	12.4	20.4	39.9	8.14
	Sample 3	12.4	20.4	39.9	8.14

V_a = Air Voids; VMA = Voids in Mineral Aggregates
VFA = Voids Filled with Asphalt; V_{beff} = Effective Asphalt (% Volume)

Table 2.4 Volumetric Properties for Mix-2

Volumetric Properties (%): Mix-2 (S3 76-28)					
Target Air Voids (%)	Samples	V_a	VMA	VFA	V_{beff}
6	Sample 1	6.5	14.9	60.1	8.9
	Sample 2	6.4	14.8	60.4	8.9
	Sample 3	6.4	14.7	60.8	9.0
8	Sample 1	8.3	16.5	53.3	8.8
	Sample 2	8.1	16.3	53.9	8.8
	Sample 3	7.9	16.1	54.6	8.8
10	Sample 1	9.6	17.7	48.9	8.6
	Sample 2	10.2	18.3	47.0	8.6
	Sample 3	9.8	17.9	48.3	8.6
12	Sample 1	12.2	20.0	41.9	8.4
	Sample 2	11.7	19.6	43.2	8.4
	Sample 3	12.0	19.9	42.3	8.4

V_a = Air Voids; VMA = Voids in Mineral Aggregates
VFA = Voids Filled with Asphalt; V_{beff} = Effective Asphalt (% Volume)

Table 2.5 Volumetric Properties for Mix-3

Volumetric Properties (%): Mix-3 (S4 70-28)					
Target Air Voids (%)	Samples	V_a	VMA	VFA	V_{beff}
6	Sample 1	6.2	16.2	58.7	9.5
	Sample 2	6.3	16.4	58.1	9.5
	Sample 3	6.2	16.2	58.8	9.5
8	Sample 1	7.9	17.7	52.8	9.4
	Sample 2	7.9	17.7	52.7	9.4
	Sample 3	8.3	18.1	51.4	9.3
10	Sample 1	10.2	19.9	45.9	9.1
	Sample 2	10.3	19.9	45.7	9.1
	Sample 3	10.2	19.8	45.9	9.1
12	Sample 1	11.9	21.4	41.8	8.9
	Sample 2	12.2	21.6	41.4	8.9
	Sample 3	12.1	21.5	41.5	8.9

V_a = Air Voids; VMA = Voids in Mineral Aggregates
VFA = Voids Filled with Asphalt; V_{beff} = Effective Asphalt (% Volume)

Table 2.6 Volumetric Properties for Mix-4

Volumetric Properties (%): Mix-4 (S4 64-22)					
Target Air Voids (%)	Samples	V_a	VMA	VFA	V_{beff}
6	Sample 1	6.1	16.8	67.3	11.28
	Sample 2	5.9	16.6	68.1	11.30
	Sample 3	6.3	16.9	66.5	11.26
8	Sample 1	8.2	18.7	59.0	11.02
	Sample 2	7.8	18.3	60.5	11.07
	Sample 3	8.2	18.6	59.3	11.03
10	Sample 1	9.9	20.2	53.7	10.82
	Sample 2	9.6	19.9	54.6	10.86
	Sample 3	9.9	20.2	53.7	10.82
12	Sample 1	12.1	22.1	47.7	10.56
	Sample 2	11.6	21.7	49.0	10.62
	Sample 3	11.7	21.7	48.9	10.61

V_a = Air Voids; VMA = Voids in Mineral Aggregates
VFA = Voids Filled with Asphalt; V_{beff} = Effective Asphalt (% Volume)

Table 2.7 Volumetric Properties for Mix-5

Volumetric Properties (%): Mix-5 (S4 76-28)					
Target Air Voids (%)	Samples	V_a	VMA	VFA	V_{beff}
6	Sample 1	6.2	15.0	57.6	8.65
	Sample 2	6.3	15.1	57.1	8.63
	Sample 3	6.1	14.9	57.9	8.65
8	Sample 1	8.2	16.8	50.2	8.46
	Sample 2	8.2	16.8	50.2	8.46
	Sample 3	8.1	16.7	50.6	8.47
10	Sample 1	9.7	18.2	45.7	8.32
	Sample 2	9.7	18.2	45.6	8.32
	Sample 3	9.2	17.7	47.2	8.37
12	Sample 1	12.3	20.6	39.2	8.08
	Sample 2	12.0	20.2	40.1	8.11
	Sample 3	11.9	20.2	40.3	8.12

V_a = Air Voids; VMA = Voids in Mineral Aggregates
VFA = Voids Filled with Asphalt; V_{beff} = Effective Asphalt (% Volume)

Table 2.8 Load Sequence for Dynamic Modulus Test

Frequency (f)	Number of Cycles
Precondition (25)	200
25	200
10	200
5	100
1	20
0.5	15
0.1	15

Table 2.9 Dynamic Modulus Test Matrix

Mix Groups	Air Voids (%)	No. of Samples	T (^{o}C)	f (Hz)	Dynamic Modulus Values
Mix-1	6	3	4, 21, 40, 55	25, 10, 5, 1, 0.5,0.1	72
	8	3			72
	10	3			72
	12	3			72
Mix-2	6	3	4, 21, 40, 55	25, 10, 5, 1, 0.5,0.1	72
	8	3			72
	10	3			72
	12	3			72
Mix-3	6	3	4, 21, 40, 55	25, 10, 5, 1, 0.5,0.1	72
	8	3			72
	10	3			72
	12	3			72
Mix-4	6	3	4, 21, 40, 55	25, 10, 5, 1, 0.5,0.1	72
	8	3			72
	10	3			72
	12	3			72
Mix-5	6	3	4, 21, 40, 55	25, 10, 5, 1, 0.5,0.1	72
	8	3			72
	10	3			72
	12	3			72
Total		60			1440

Table 2.10 Measured Dynamic Modulus Values (Mix-1: 6% Air Voids)

Mix-1 (S3:64-22):Target Air Voids = 6%							
f	T	Sample 1	Sample 2	Sample 3	Average	Stdev	COV
Hz	^{o}C	E* (MPa)					(%)
25	4	18729	17553	17623	17968	659	3.7
10		16248	17853	16908	17003	807	4.7
5		15050	16387	15618	15685	671	4.3
1		14032	13254	13446	13577	405	3.0
0.5		13040	12365	12013	12473	522	4.2
0.1		11203	9021	8982	9735	1271	13.1
25	21	7684	6557	7839	7360	700	9.5
10		6851	5949	6971	6590	559	8.5
5		6153	5414	6353	5973	494	8.3
1		4621	3937	4490	4349	363	8.3
0.5		3767	3148	3924	3613	410	11.4
0.1		2248	2789	3000	2679	388	14.5
25	40	3817	3041	3114	3324	429	12.9
10		3022	2595	2957	2858	230	8.1
5		2433	2197	2554	2395	181	7.6
1		1472	1268	1671	1470	202	13.7
0.5		1101	1047	1367	1171	171	14.6
0.1		789	613	857	753	126	16.7
25	55	1242	1439	1350	1344	99	7.3
10		943	1045	1051	1013	61	6.0
5		722	729	872	775	85	10.9
1		587	503	565	552	44	7.9
0.5		484	409	473	455	41	9.0
0.1		351	285	376	337	47	14.0

Table 2.11 Viscosity and A and VTS Parameters for Asphalt Binders

T	PG 64-22		PG 70-28		PG 76-28	
	cP					
(^{o}C)	Average	Stdev.	Average	Stdev.	Average	Stdev.
135	667	7.2	1747	19.9	3627	101.6
150	313	12.5	842	14.4	1439	40.0
165	163	12.5	415	4.8	709	19.2
180	89	2.4	204	7.2	388	12.3
A	10.590		9.780		9.254	
VTS	-3.537		-3.233		-3.037	

Table 2.12 Calculated Viscosities at Test Temperatures

T	PG 64-22	PG 70-28	PG 76-28
(^{o}C)	10^6 poise		
4	1408	2589	3070
21	11	26	39
40	0.17	0.49	0.85
55	0.01	0.04	0.08

Table 2.13 Master Curve and Shift Factor Parameters (Mix-1:6% Air Voids)

Mix-1:S3 64-22 : 6% Air Voids								
Master Curve Parameters								
Max |E*| (MPa)	α	δ	β	γ	c	R^2	S_e/S_y	Fit
23084	2.54	1.82	-1.01	-0.43	1.24	0.99	0.07	Excellent

Shift Factors Parameters		
m	n	p
0.0003	-0.1155	6.7155

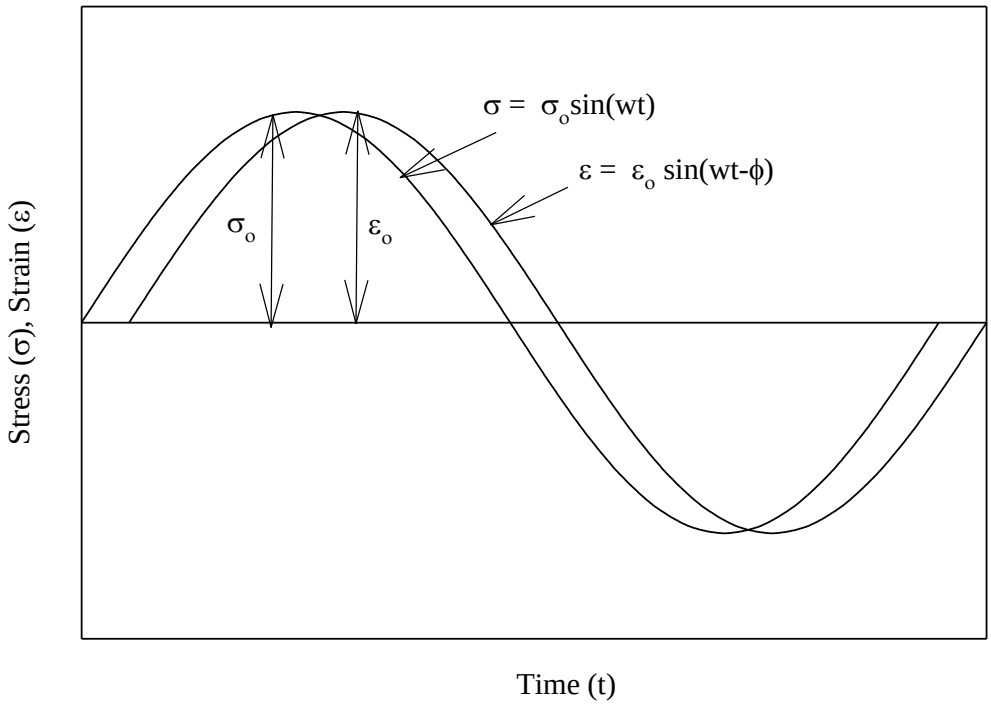

Figure 2.1 Sinusoidal Loading Pattern for Dynamic Modulus Test

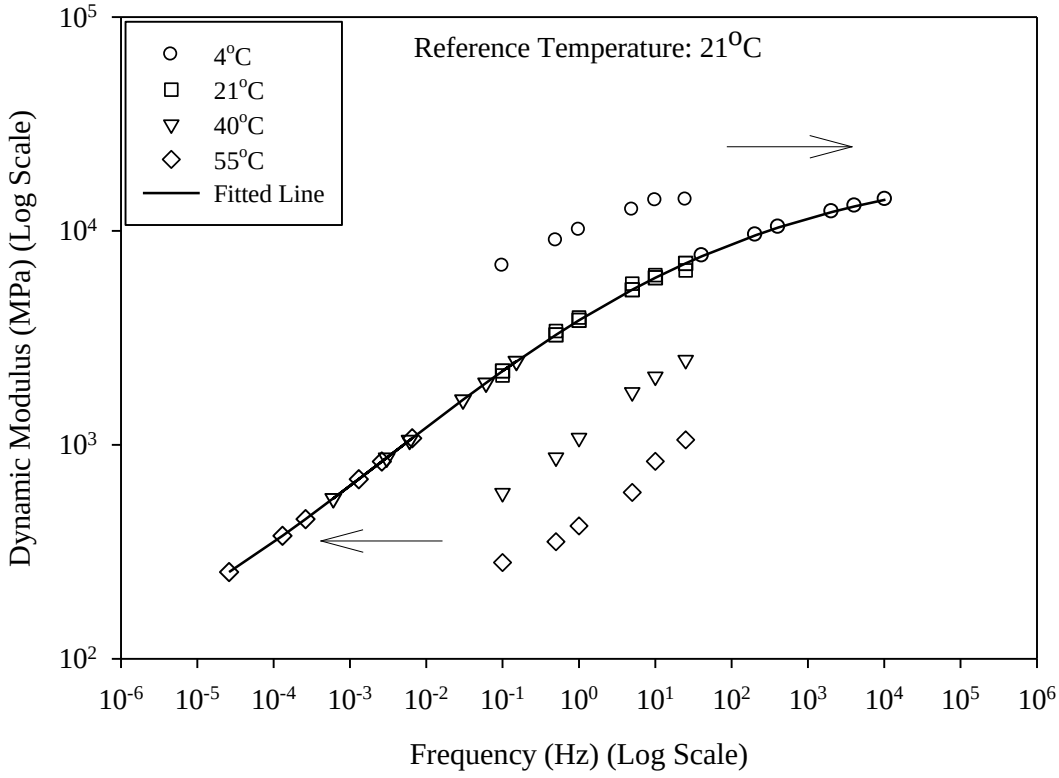

Figure 2.2 Typical Master Curve

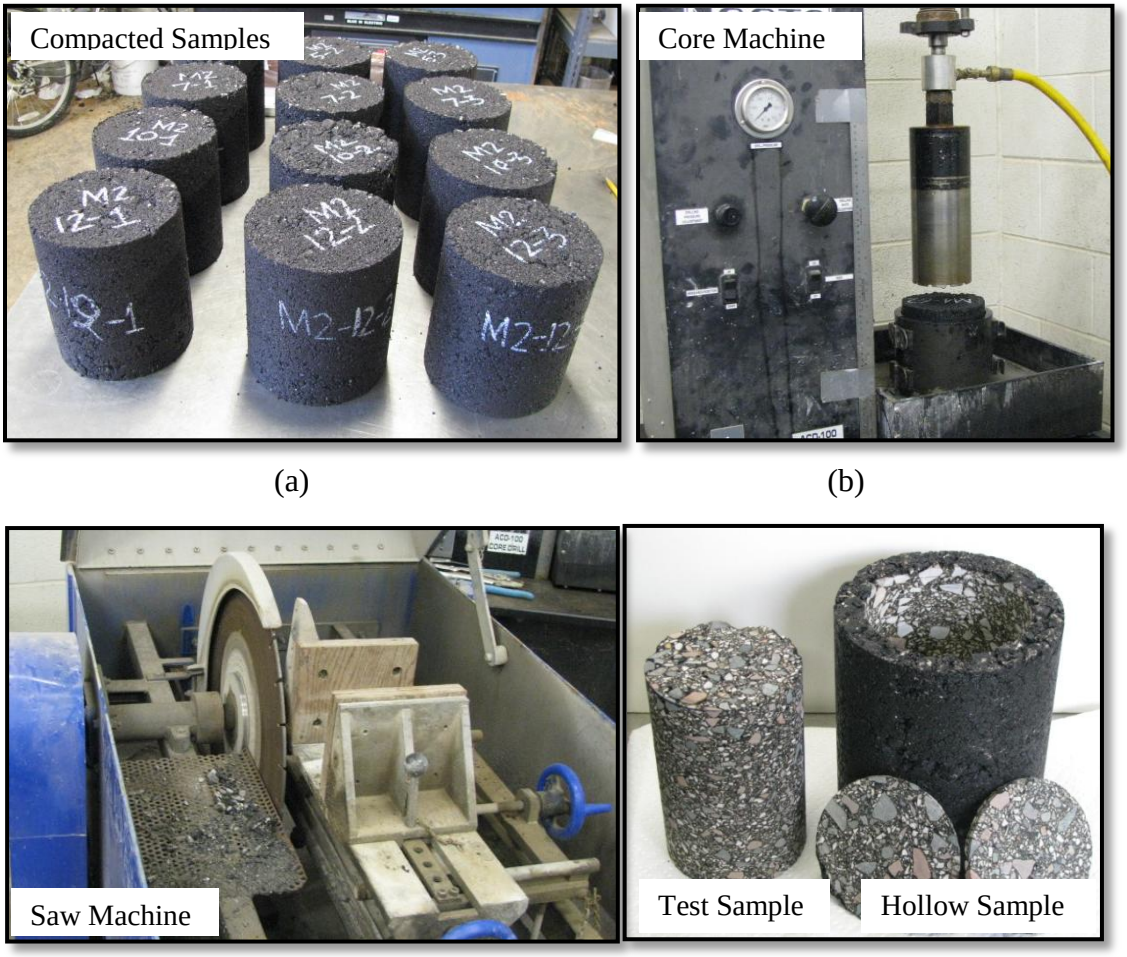

Figure 2.3 Specimen Preparation (a) SGC Compacted Specimen, (b) Core Machine, (c) Saw Machine, and (d) Final Test Sample

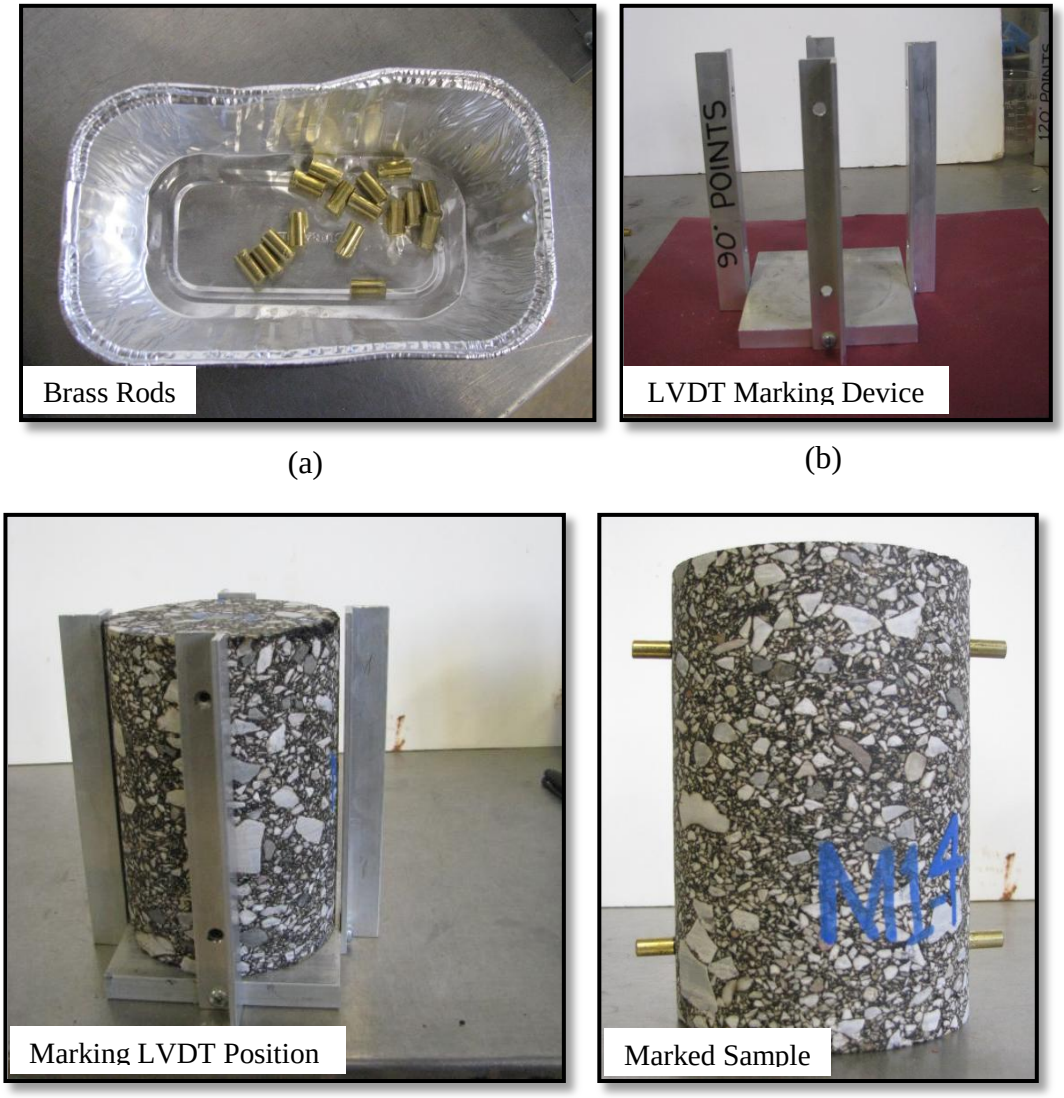

Figure 2.4 Fixing of LVDT (a) Brass Rods, (b) LVDT Marking Device, (c) Marking LVDT Position, and (d) Marked Sample

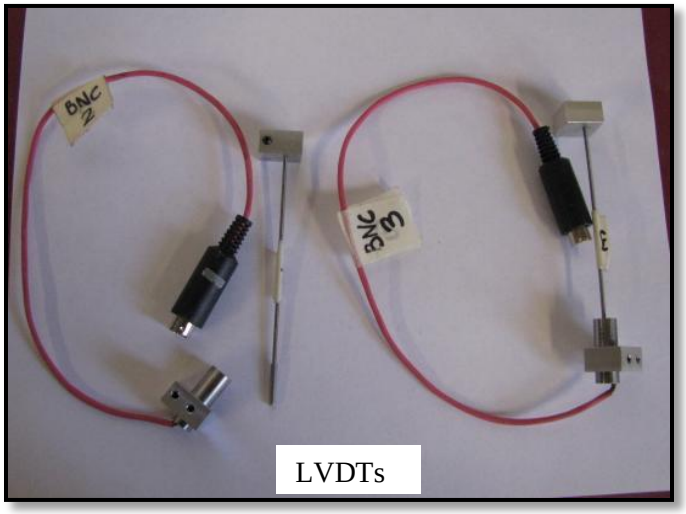

(a)

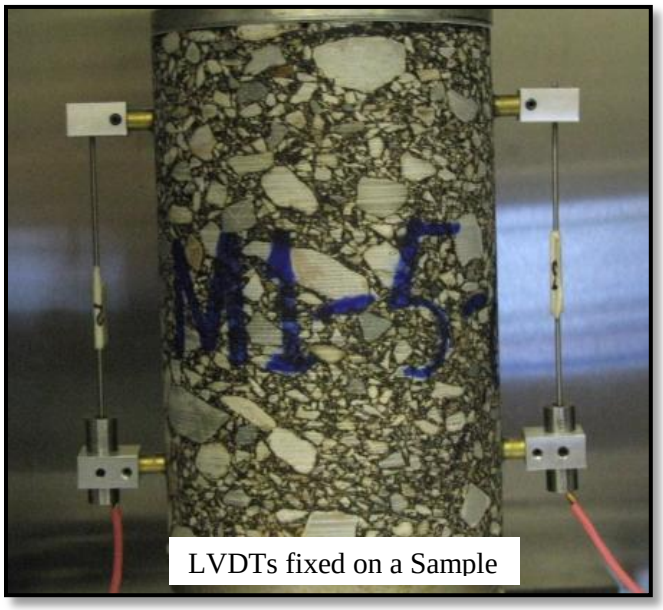

(b)

Figure 2.5 (a) LVDTs, (b) LVDTs Attached with Sample

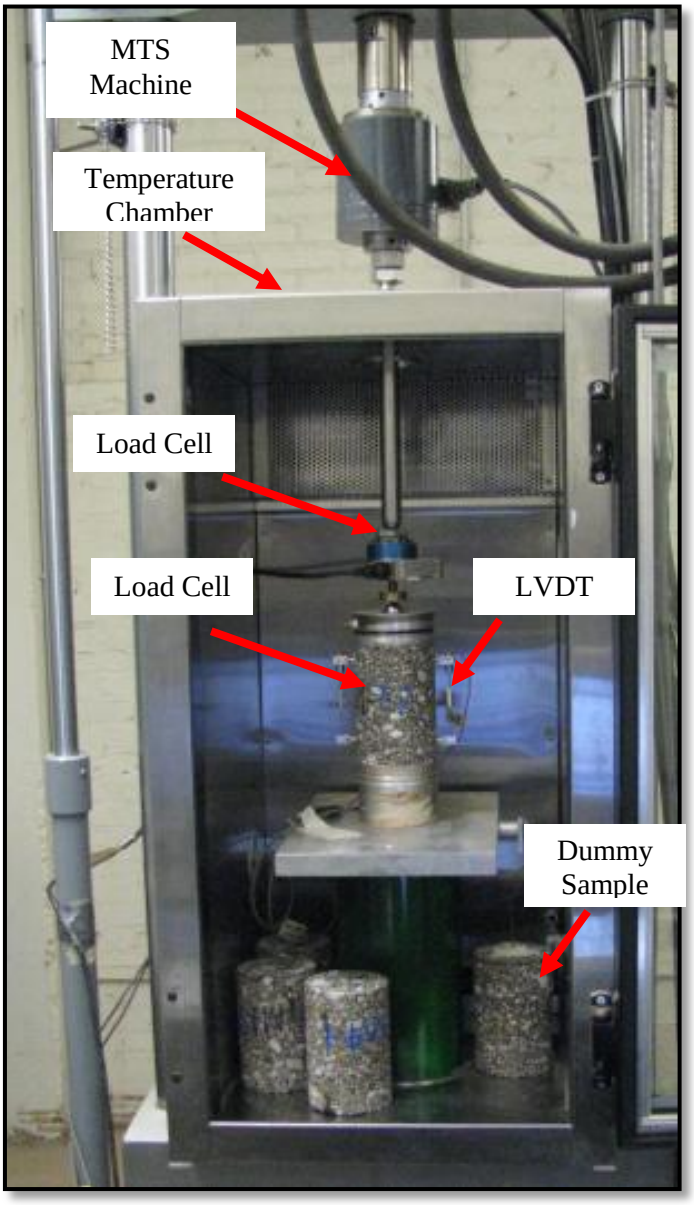

Figure 2.6 Set up of Dynamic Modulus Test

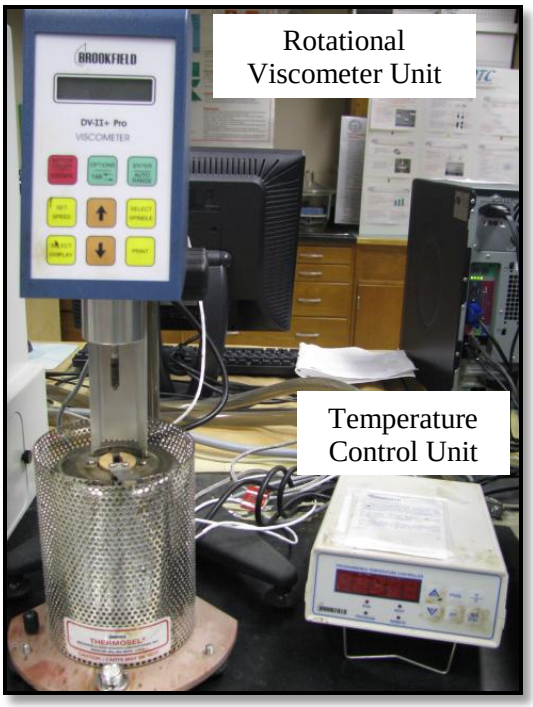

Figure 2.7 Brookfield Rotational Viscometer

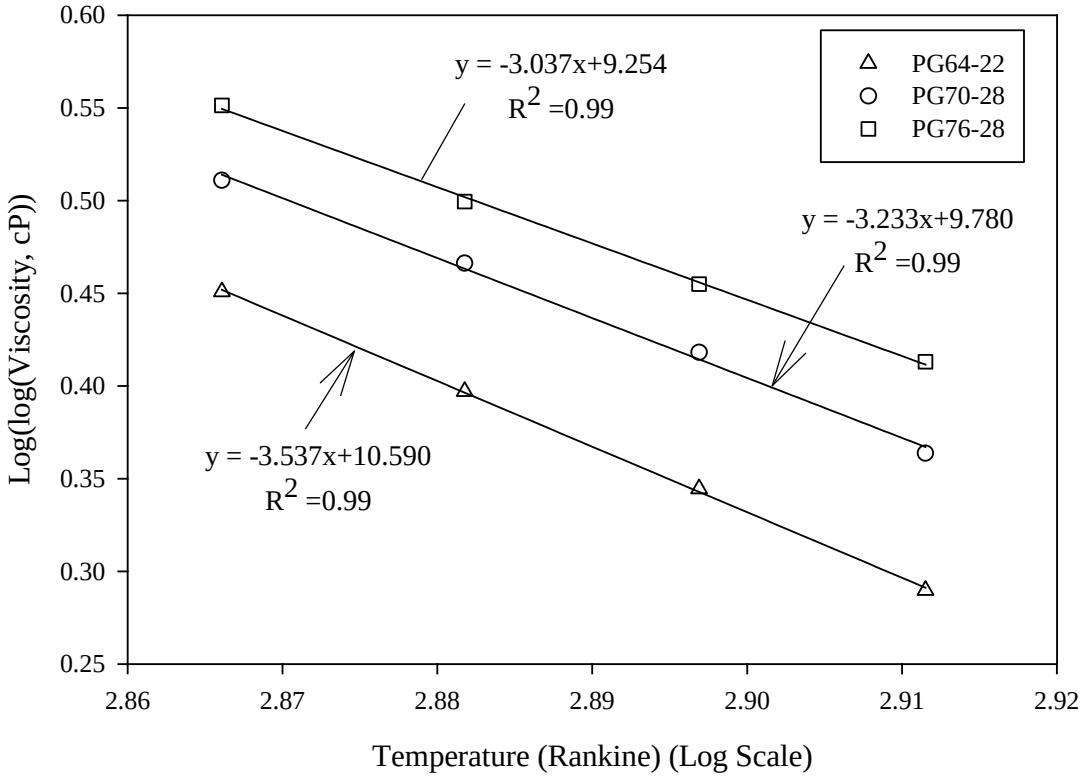

Figure 2.8 Temperature-Viscosity Graphs for Different Asphalt Binders

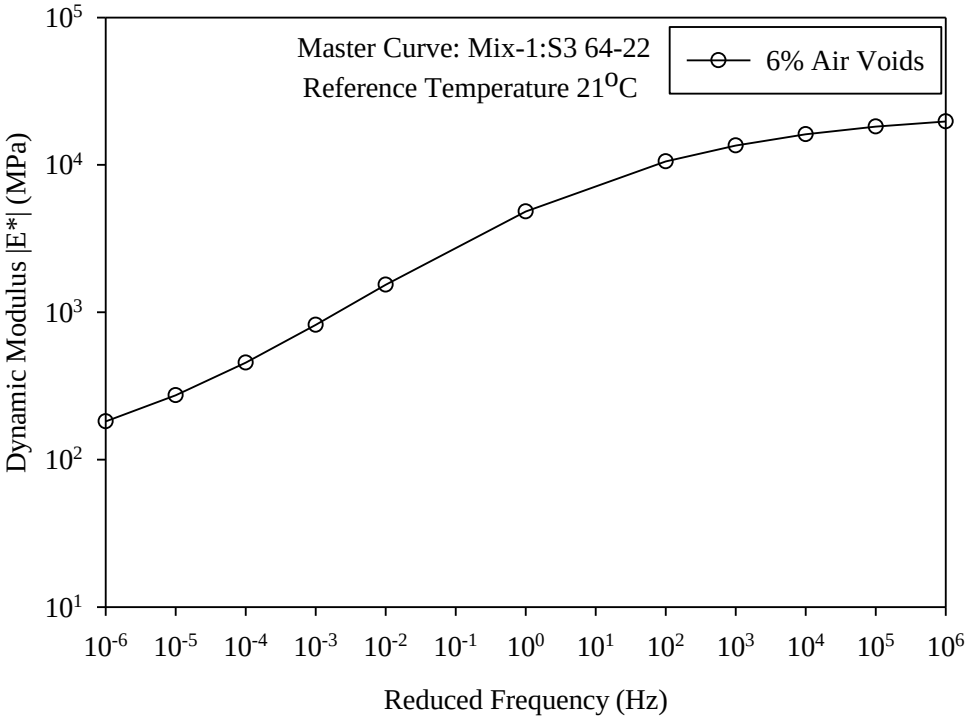

(a)

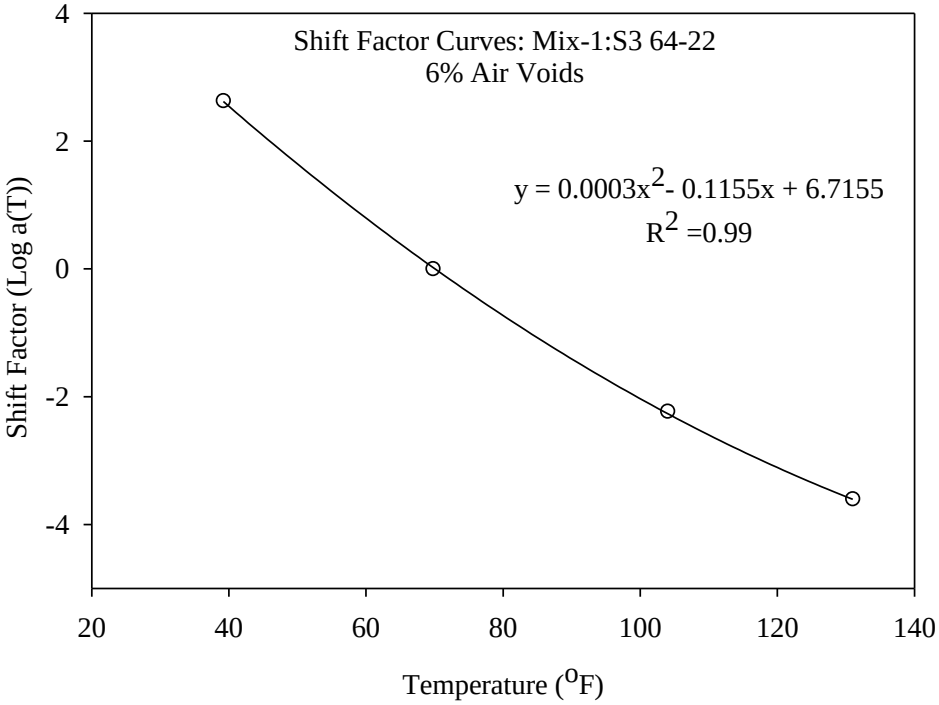

(b)

Figure 2.9 Master Curve and Shift Factor Plots for Mix-1 at 6% Air Voids (a) Master Curve, (b) Shift Factor

CHAPTER 3 : EFFECT OF PRODUCTION AND SAMPLE PREPARATION METHODS ON AGGREGATE SHAPE PARAMETERS

3.1 Introduction

Asphalt mix is a mixture of aggregates and asphalt binder, with aggregates contributing approximately 95% of the total weight. Because of the significant amount of aggregates, their shape characteristics, namely angularity, texture, two-dimensional (2D) form, and sphericity (3D form) are considered to have a direct influence on the asphalt mix performance and serviceability (Liu and You, 2011; Wang et al., 2008; Anthony, 2007; Lynn et al., 2007; Masad et al., 2007a, 2007b; Alvarado et al., 2006; Pan et al., 2006; Kuo, 2002; Fletcher et al., 2002; Masad et al., 2001a, 2001b; Coree and Hislop, 2000; Huber et al., 1998; Abdul-Malak et al., 1996; Barksdale et al., 1992). The 2D form represents the overall shape of a particle, while the 3D characteristics of a particle are captured using sphericity measurements. Generally, rough-textured surfaces result in stronger mixes by providing more friction between aggregate faces (Kandhal and Mallick, 2001; Ahlrich, 1996; Roberts et al., 1996; Sousa et al., 1991; Brown and Bassett, 1990; Button et al., 1990). Similarly, angular aggregates provide better interlock, which increases the rut resistance (Kandhal and Mallick, 2001; Sousa et al., 1991; Brown and Bassett, 1990; Button et al., 1990). Several researchers have investigated the effect of aggregate shape parameters on the performance of asphalt mix. For example, Johnson et al. (2007) conducted performance testing (i.e., dynamic modulus and rut testing) on four different types of asphalt mixes by varying the quantity of fine aggregate angularity (FAA). It was found that dynamic modulus and rut resistance are strongly related to FAA. Similarly, Masad et al. (2001b) studied the effect of the fine aggregate shape

indices on the performance of asphalt mixture and reported that the texture of fine aggregate has the strongest correlation with rutting resistance compared to other shape indices. According to these researchers, a change in the aggregate shape parameters can strongly influence the performance of a pavement.

Very few studies have been conducted to investigate the effect of aggregate degradation on the shape characteristics of the aggregate. Aggregate degradation can cause particles to lose their shape, texture, and gradation, resulting in a change in the volumetric properties of asphalt mix (Chadbourn et al., 1999). Degradation of aggregates may occur at the plant site as the aggregates are exposed to impact and abrasive forces during the production of the mix (Lynn et al., 2007; Mahmoud et al., 2007; Page et al., 1997). In addition, the compaction of asphalt mix in the field or in the laboratory can result in changes in aggregate shape parameters. Such changes in aggregate gradation and aggregate shape characteristics (i.e., angularity, shape, and texture) can result in a different structure of the aggregates (Mahmoud and Masad, 2007; Chadbourn et al., 1999; Wu et al., 1998).

Pintner et al. (1987) compared the fines produced in the laboratory and in the field, and reported that laboratory tests generally produced more fines, when compared to field. Similarly, Page et al. (1997) determined the amount of degradation for limestone aggregates and reported that the aggregates degraded significantly as they were processed through the asphalt mix plant. Recently, Lynn et al. (2007) studied 22 different mixes and found that plant mixing and field compaction activities resulted in significant degradation of aggregates. However, these studies were limited to the measurement of fines; any changes in aggregate shape characteristics due to degradation were not evaluated.

As mentioned earlier, aggregate degradation can also occur during the preparation of samples in a Superpave gyratory compactor (SGC). The weight of the loose asphalt mix to be poured in the SGC mold depends on the level of air voids required in a compacted sample. For example, for a given dimension of a sample, the weight of the loose mix increases as target air voids decrease. The gyratory compactor actuators exert forces on the specimen during compaction in order to apply vertical pressure and angle of gyration. Particles are pushed as the weight is increased, resulting in a changed gradation and shape of aggregates (Collins et al., 1997). Peterson et al. (2003) mentioned that the current gyratory protocol produces specimens with significantly different mechanical properties than those of field cores produced with the same material and compacted to the same level of air voids.

Therefore, it is important to evaluate the change in aggregate shape characteristics (i.e., angularity, texture, shape, and sphericity) due to asphalt mix production and laboratory preparation methods. The focus of the present study was to compare shape parameters for different types of aggregates collected from the plant site, and aggregates retrieved from samples compacted in the laboratory. The shape parameters of coarse and fine aggregates were measured using an automated aggregate image measurement system (AIMS).

3.2 Introduction to AIMS

The AIMS is an automated system that captures images of aggregates at different resolutions using different lighting schemes (Masad , 2005; Fletcher et al., 2003; Masad et al., 2003) (Figure 3.1). The system is designed to analyze 2D form, angularity, and texture of coarse aggregates and angularity and 2D form of fine aggregates. Aggregates with sizes ranging from 37.5 mm to 150 mm can be analyzed using this system.

Studies by Masad (2003) indicate that the particle geometry of an aggregate can be fully expressed in terms of three independent properties which can influence the performance of asphalt mixes: angularity, texture, and shape (2D form) (see Figure 3.2). Angularity indicates the sharpness of the edges of a particle, 2D form represents the two-dimensional shape of a particle, and surface texture is used to describe the surface irregularity of a particle at the micro level (see Figure 3.2) (Masad, 2005). Any of these properties can vary widely without necessarily affecting the other two properties (Masad, 2005). The AIMS provides the range and classification of the different types of shape parameters (Table 3.1). It is to be noted here that these range of the shape parameters are different than those provided in the AASHTO TP81 (AASHTO, 2010b). The AASHTO TP81 ranges are applicable to the newly developed AIMS system (FHWA, 2010a). The Binder Laboratory in the University of Oklahoma owned a research unit of the AIMS system which follows the classification of the shape parameters based on the range and sizes provided by Masad (2005); therefore, the ranges provided in Table 1 is used in the present study. Based on the shape index, the aggregates can be classified into different sub-groups. Additional information on the AIMS can be found elsewhere (Masad et al., 2007a, 2007b; Masad, 2005; Masad et al., 2003; Masad, 2003; Masad et al., 2000).

3.3 Definition of Different Shape Parameters

3.3.1 Angularity

The AIMS uses two methods to measure angularity of a particle: gradient and radius. The gradient method measures angularity by considering the sharpness of the edges of a particle, while the radius method considers the difference between the particle radius in a certain direction with respect to an equivalent ellipse (Masad et al., 2007b).

3.3.1.1 Gradient Method

The gradient-based method for measuring angularity starts by calculating the gradient vectors at each edge-point. The following equation is used for the calculation of angularity. (Equation (3.1))

$$Angularity\,Index\,(Gradient\ Method) = \frac{1}{\frac{N}{3} - 1} \sum_{i=1}^{N-3} \left| \theta_i - \theta_{i+3} \right| \tag{3.1}$$

where,

i = ith point on the edge of the particle,

N = total number of points on the edge of the particle, and

θ = angle of orientation of every third point on the boundary of the aggregate.

The aggregates can be classified into the following four groups: rounded (angularity index less than 2100), sub-rounded (angularity index between 2100 and 4000), sub-angular (angularity index between 4000 and 5400), and angular (angularity index greater than 5400) (Table 3.1).

3.3.1.2 Radius Method

Masad et al. (2001b) developed a method for the analysis of particle 2D form using black and white images. This method measures the difference between the particle radius in a certain direction and that of an equivalent ellipse (Equation (3.2)).

$$Angularity\ Index\ (Radius\ Method) = \sum_{\theta=0}^{355} \frac{\left| R_\theta - R_{EE\theta} \right|}{R_{EE\theta}} \tag{3.2}$$

where,

R_θ = radius of the particle at an angle of θ, and

REE_θ = radius of the equivalent ellipse at an angle of θ (Masad et al., 2001b).

The equivalent ellipse has the same aspect ratio of the particle but has no angularity (i.e., smooth with no sharp corners). The aggregates can be classified into following five groups: rounded (angularity index less than 5), sub-rounded (angularity index between 5 and 7), sub-angular (angularity index between 7 and 10), angular (angularity index between 10 and 16), and highly angular (angularity index greater than 16) (Table 3.1).

3.3.2 Texture Analysis

The texture analysis of a particle is done using the wavelet method. It is a powerful method for the decomposition of the different scales of texture (Mallat, 1989). The texture index at any given decomposition level is the arithmetic mean of the squared values of the detail coefficients at that level (Equation (3.3)).

$$Texture\ Index = \frac{1}{3N}\sum_{i=1}^{3}\sum_{j=1}^{N}[D_{i,j}(x, y)]^2 \tag{3.3}$$

where,

N = total number of coefficients in a detailed image of texture,

i = takes values 1, 2, or 3, for the three detailed images of texture,

j = wavelet coefficient index, and

(x, y) = location of the coefficients in the transformed domain.

Texture is classified into five groups: polished (texture index less than 165), smooth (texture index between 165 and 275), low roughness (texture index between 275

and 350), medium roughness (texture index between 350 and 460), and high roughness (texture index greater than 460) (Table 3.1).

3.3.3 2D Form Index

The 2D form index, proposed by Masad (2005), was used to quantify the shape of a particle in two dimensions. This index uses incremental change in the particle radius. The 2D form index is expressed by Equation (3.4).

$$Form\ Index = \sum_{\theta=0}^{\theta=360-\Delta\theta} \frac{\left|R_{\theta+\Delta\theta} - R_{\theta}\right|}{R_{\theta}} \tag{3.4}$$

where,

R_θ = radius of the particle at an angle of θ,

$R_{\theta+\Delta\theta}$ = radius of the particle at an angle of θ+Δθ (Masad et al., 2001b), and

$\Delta\theta$ = incremental difference in the angle, which is taken to be 4^o.

The 2D form index classifies the aggregates into four groups: circular (2D form index less than 6.5), semi-circular (2D form index between 6.5 and 8), semi-elongated (2D form index between 8 and 10.5), and elongated (2D form index greater than 10.5) (Table 3.1). A perfect circle has a 2D form value of zero (AASHTO, 2010b).

3.3.4 Sphericity

The 3D characteristics of a particle are captured using sphericity measurements, which are defined in terms of: the longest dimension, (d_L), the intermediate dimension (d_I), and the shortest dimension (d_s), and is given by Equation (3.5) (Masad, 2005).

$$Sphericity = \sqrt[3]{\frac{d_s \cdot d_I}{{d_L}^2}} \tag{3.5}$$

where,

d_L = longest dimension of the particle,

d_I = intermediate dimension of the particle, and

d_s = shortest dimension of the particle.

The shpericity index categorizes aggregates into the following four groups: flat/elongated (sphericity index less than 0.6), low sphericity (sphericity index between 0.6 and 0.7), moderate sphericity (sphericity index between 0.7 and 0.8), and high sphericity (sphericity index greater than 0.8) (Table 3.1). A sphericity value of one indicates a particle has equal dimensions (AASHTO, 2010b).

3.4 Measurement of Shape Parameters Using AIMS

The AIMS uses a simple setup that consists of one camera and two different types of lighting schemes to capture images of aggregates at different resolutions, from which aggregate shape properties are measured using image analysis techniques. The system operates based on two modules. The first module is for the analysis of coarse aggregates (larger than 4.75 mm). For coarse aggregates, the 0.25x objective lens was installed and the camera position was set to “coarse.” Fifty-six coarse aggregates particles are placed on the AIMS testing grid (Figure 3.3). The AIMS performs two passes for coarse aggregates. The first pass measures the 2D form and angularity, and uses the bottom light. The second pass uses the top light to obtain the measurements for sphericity and texture. After both of these passes are completed for a sample, the AIMS’s software then analyzes the images.

The second module is for the analysis of fine aggregates (smaller than 4.75 mm). The 0.50x objective lens was installed and the camera position was set to “fine.” Next,

about 100 grams of fine particles were spread out evenly across the grid so that they were not touching each other (Figure 3.3). For fine aggregates only one pass is performed, which uses the bottom light to measure the 2D form and angularity. After this pass was completed, the AIMS software was used to analyze the images. A study by Masad et al. (2001b) clearly shows that a high correlation exists between the angularity and texture of fine aggregates. Therefore, only texture is measured for fine aggregates.

3.5 Types of Aggregates

The original aggregates (OA) from the stockpile and loose asphalt mixes were collected from the production plant of Haskell Lemon Construction Company in Norman, Oklahoma. The majority of the aggregates were limestone. The loose mix was divided into five different groups. One group was left un-compacted, and was called 'plant mix' (PM), while the other four groups were used to compact samples in a SGC at four different air voids: 6%, 8%, 10%, and 12%. These groups were named as AV6, AV8, AV10, and AV12, respectively. Lynn et al. (2007) reported that post-compaction degradation in the SGC correlated well with degradation associated with the compaction of the asphalt mix in the field. Thus, samples compacted at the previously mentioned air voids are expected to simulate aggregates in the field for a mix compacted at different levels of density (i.e., 88% to 94% of maximum theoretical density). Three samples were compacted for each level of target air void. A trial and error process was used to adjust the weight of the loose asphalt mix to get the desired level of air voids in compacted samples. In the present study, SGC was operated in the height mode. This mode allows the machine to stop automatically when the desired height of a sample is reached. Initially, samples having a 150 mm diameter and 167.5 mm height were compacted. These samples were then cut and cored to get final samples with a diameter of 100 mm

and a height of 150 mm. This size of the sample is used for conducting the performance testing (i.e., dynamic modulus, flow number, and flow time) of the asphalt mix (AASHTO, 2006). Usually, core drill machine is used to get the full depth cores from the pavements to conduct the performance tests in the laboratory. Therefore, to simulate the field cores, the cored specimens (100 mm diameter and 150 mm height) were used to extract aggregates.

Aggregates from the loose mix (i.e., PM) and compacted samples were extracted by burning them in a National Center for Asphalt Technology (NCAT) ignition oven. Table 3.2 summarizes the gradation of all six types (OA, PM, AV6, AV8, AV10, and AV12) of aggregates. Figure 3.4 is a plot of these aggregate gradations. It can be seen from this figure that the gradation of OA aggregates was slightly different from the rest of the aggregates, indicating the effect of the production and sample preparation method. In general, the aggregates passing 4.75 mm and 0.075 mm sieves increased, resulting in more fines in the PM and AV aggregates. Although the gradation plots provide important information in terms of change in fines and aggregate size, they do not reveal the change in the shape properties of the aggregates.

3.6 Preparation and Testing of Aggregates

Aggregates were processed before conducting the AIMS testing. All six types of the aggregates were washed and allowed to dry for 24 hours at a temperature of 110°C. After drying, each type of aggregate was divided into two different sizes. For coarse aggregates (CA), these sizes include the following: passing a 19 mm sieve and retained on a 12.5 mm sieve (CA12), and passing a 9.5 mm sieve and retained on a 4.75 mm sieve (CA4). The two sizes of the fine aggregates (FA) include the following: passing a 4.75 mm (#4) sieve and retained on a 2.36 mm (#8) sieve (FA8), and passing a 2.36 mm (#8)

sieve and retained on a 1.18 mm (#16) sieve (FA16). Table 3.3 summarizes the AIMS test matrix for all the aggregates. The shape parameters of coarse and fine aggregates are measured as per the process discussed in Sections 3.3 and 3.4. The mean and standard deviation for all shape parameters for all types of coarse and fine aggregates are given in Tables 3.4 and 3.8, respectively. A detailed discussion on these shape parameters is provided in Section 3.8.

3.7 Statistical Analysis Methodology

A statistical method called analysis of variance (ANOVA) was conducted using a commercially available software package called Statistical Package for the Social Sciences (SPSS®). The null hypothesis for this analysis was that the difference in the mean of shape parameters for the six types of aggregate was equal to zero ($H_0 = \mu_{OA} = \mu_{PM} = \mu_{AV6} = \mu_{AV8} = \mu_{AV10} = \mu_{AV12}$), and an alternative hypothesis (H_a) was that the mean of shape parameters were not equal. The test was conducted at a significance level of 0.05. A p-value of <0.05 indicates rejection of the null hypothesis.

Prior to the statistical analyses, any outliers from the data were removed. A data point was considered to be an outlier if it falls outside a range of mean±3σ (standard deviation) (Tarefder, 2005a). Furthermore, the data was screened to ensure that it satisfies ANOVA's assumptions (i.e., normality and equality of variance). The normality of each set of aggregates and shape parameters was checked by conducting skewness and kurtosis tests (Statsoft, 2011; Uddin et al., 2011; Alam et al., 2007; Jiang et al., 2003; Ramsey and Schafer, 2002; Lindman, 1974). Therefore, the standard error of skewness (SES), standard error of kurtosis (SEK), skewness, and kurtosis values for each shape parameters pertaining to different types of aggregates were estimated. The data was considered normally distributed if the skewness and kurtosis values fall within ±2SES and ±2SEK,

respectively (Alam et al., 2007). The skewness and kurtosis tests showed that the data was approximately normally distributed.

Similarly, Levene's test was used to verify if samples would have equal variances (homogeneity of variance) (Hughes et al., 1998). This test was conducted at a significance level of 0.05. The H_o for the test matrix was that the variances of all the types of aggregates were not statistically different, and the H_a was that the variances were not equal. Depending upon the equal or unequal variances, two different ANOVA tests were conducted. In the case of equal variance, the ANOVA F-statistics was used, while in the case of inequality of variance, the robust Welch one-way ANOVA statistics was used. It was found that both methods provided the same results. This might be due to that fact that the ANOVA test is fairly robust against the inequality of variances and normality assumption (Prophet Statguide, 2011; Statsoft, 2011; Lindman, 1974).

Furthermore, a multi-comparison post-hoc test was used to evaluate whether the groups within the factor are significantly different or not (Kutner et al., 2004). Again, depending upon the equality and inequality of variance, two different types of tests were conducted. In the case of equality variance, the Tukey's honestly significant difference (HSD) was used, while in the case of inequality of variance, the Games-Howell test was used. A confidence level of 0.05 was used for this purpose.

3.8 Results and Discussion

3.8.1 Coarse Aggregates

3.8.1.1 Angularity

Angularity creates greater interlock and internal friction between particles, therefore resulting in greater mechanical stability than can be achieved with rounded particles**.** The mean of radius angularity for both CA12 and CA4 aggregates ranged from

10.1 to 11.4, indicating that all coarse aggregates were in angular range (Table 3.1 and Table 3.4). Figures 3.5(a) and 3.6(a) show the plot of percentage cumulative aggregates and angularity index for CA12 and CA4 aggregates, respectively. It can be seen from these figures that the distribution of particles seems approximately the same for all types of aggregates. An ANOVA test was conducted to check if the difference in the angularity of different types of aggregate was statistically significant or not. Table 3.5 shows the results of the ANOVA test. The p-value for the angularity for both CA12 and CA4 aggregates was more than 0.05, indicating that no statistically significant difference existed among the angularity of different types of aggregates.

3.8.1.2 Texture

Texture is important for developing a strong friction surface and stable structure of aggregates. The mean of the texture for CA12 and CA4 aggregates ranged from 149 to 200 and 89 to 132, respectively (Table 3.4). Figures 3.7(a) and 3.8(a) show the plot of percentage cumulative aggregates and texture index for CA12 and CA4 aggregates, respectively. It can be seen from these figures that the distribution of the particles was different for OA and PM aggregates. PM aggregates were found to have a lower texture index compared to OA aggregates, indicating that the plant production process may reduce the texture of aggregates (Table 3.4). Similarly, AV aggregates were found to have the highest texture index, indicating that the laboratory sample preparation method resulted in an increase in the texture of aggregates. It is expected that an increase in texture for AV aggregates (i.e., aggregates compacted at different compaction levels) might be due to the fracture of particles during compaction of samples in the SGC. The SGC exerts forces on the specimen during compaction (Collins et al., 1997). Figure 3.4 is a plot of aggregate gradation for six different types of aggregates (i.e., OA, PM, AV6,

AV8, AV10, and AV12). It can be seen from this figure that AV aggregates had higher percentage of fines compared to OA aggregates, which indicates that AV aggregates might have been crushed during the compaction process in the SGC. Furthermore, mixes with higher percentages of flat and elongated particles are likely to break during compaction, resulting in increased fractured faces of particles and consequently a higher texture.

To further understand the reason for the increase in texture for laboratory processed aggregates, graphs were plotted for different types of the textured particles (i.e., polished, smooth, low, moderate, and high roughness) (Figures 3.7(b) and 3.8(b)). It can be seen from these figures that the percentages of polished and smooth particles were found to be slightly higher in the PM aggregates resulting in a reduction in the texture index. All AV aggregates were observed to have less polished particles than OA and PM aggregates.

Statistical Analysis

The ANOVA statistics indicate that the texture is significantly different for all types of aggregates (p-value = 0.000) (Table 3.5). To further check the difference in texture among a group of aggregates, a multi-comparison post-hoc test was conducted using the Games Howell method (Table 3.6). The results indicate that a statistically significant difference existed in texture between OA and AV aggregates. A similar trend was observed for PM and AV aggregates (Table 3.6). With the increased texture of AV aggregates, the performance of laboratory compacted samples can be significantly different from plant produced mix. For example, aggregates with rough surface textures have a high level of internal friction, higher air void contents, and higher voids in mineral

aggregates (VMA). In addition, rougher aggregates also have the potential for improved adhesion of the asphalt binder to the aggregate due to the jagged surface texture. On the other hand, rounded aggregate particles contribute to a lack of internal friction, the ability to compact in a dense arrangement, and a decrease in void space and VMA. Therefore, it is recommended that a proper care should be taken while comparing the laboratory and field sample performance. The OA and PM aggregates did not show any significant difference. Similarly, no significant difference was observed among the aggregates compacted at different levels of air voids (AV aggregates).

3.8.1.3 Two Dimensional (2D) Form

2D form index is a unique parameter because it accounts for the change in a particle dimension in all directions (Masad et al., 2001b). The mean of the 2D form index for OA and PM aggregates were found to be approximately 8.0 and 7.0, respectively (Table 3.4), indicating that OA aggregates were more elongated compared to PM aggregates (Table 3.4). Figures 3.9(a) and 3.10(a) show a plot of cumulative percentage of particles and 2D form index for all types of aggregates. Similarly, Figures 3.9(b) and 3.10(b) show a distribution of various form particles (i.e., circular, semi-circular, semi-elongated, and elongated). It is seen that PM aggregates had a higher percentage of circular particles compared to OA aggregates, which might cause a reduction in the 2D form of the PM aggregates. It is expected that change in shape of aggregates would occur at the plant site as they are subjected to impact and abrasive forces during the production of the mix (Lynn et al., 2007; Mahmoud et al., 2007; Page et al., 1997). Furthermore, particles may undergo rolling and degradation during the production process which result in a higher percentage of circular particles (Chadbourn et al., 1999), and consequently a lower 2D form index. It is expected that round particles have the potential to fit very

densely together because of the smoothness of the surface and the lack of angular edges, which together reduce the internal friction. A reduction in internal friction and the ability of uncrushed aggregates to compact more easily into a dense arrangement reduces void space, which ultimately leads to a reduction in the VMA. Therefore, a change in 2D form index would result in different structure of asphalt mix, as expected.

Statistical Analysis

There was significant difference (p-value = 0.000) in the 2D form of the different types of aggregates (Table 3.5). To further evaluate the difference in 2D form among a group of aggregates, a multi-comparison test was conducted using the Games Howell Method (Table 3.7). A statistically significant difference was observed between OA and PM aggregates. Similarly, the 2D form of PM aggregates was found to be significantly different than AV aggregates. No statistically significant difference was observed among aggregates compacted at various levels of air voids (AV6, AV8, AV10, and AV12) (Table 3.7).

3.8.1.4 Sphericity

The sphericity gives a good indication of the proportions of a particle's dimensions. Figures 3.11(a) and 3.12(a) show the cumulative percentage of particles and the sphericity index, respectively. Similarly, Figures 3.11(b) and 3.12(b) show the distribution of various spherical aggregates (i.e., flat/elongated, low, moderate, and high sphericity). The sphericity index was found to be very similar for all the aggregates. It may be because sphericity is a function of three different dimensions (thickness, length, and width) of particles, which change proportionally. The ANOVA test indicates that no statistically significant differences existed among the sphericity of different types of

aggregates ($p>0.05$, Table 3.5). Therefore, the production and sample preparation methods do not seem to significantly influence the sphericity of aggregates.

3.8.1.5 Distribution of Flat and Elongated Particles

To further understand, Figures 3.13(a) and 3.13(b) were plotted to distinguish among flat, elongated, and flat and elongated particles for CA12 and CA4 aggregates, respectively. Superimposed on this chart are the 3:1 and 5:1 limits for the ratio of the longest dimension to the shortest dimension. The Superpave recommends no more than 10% by weight of the particles have an aspect ratio greater than 5:1 (Maerz, 2004). It can be seen from the plot that all the aggregates pass the 5:1 Superpave requirement (both had less than 10% of particles with a dimensional ratio less than 5:1), but they had different distributions in terms of flat and elongated particles (Figures 3.13(a) and 3.13(b)). This type of analysis reveals valuable information about the distribution that would not have been obtained if the aggregates were classified based on the 5:1 ratio only.

3.8.1.6 Comparison of CA12 and CA4 Aggregates

The angularity and 2D form of both sizes of coarse aggregates (i.e., CA12 and CA4) were found to be very similar (i.e., angularity = 10.2 and 2D form = 7), while there was a significant difference between the texture of both sizes of aggregates (Table 3.4). The texture index of CA12 was found to be higher (i.e., 149) compared to the texture index of CA4 aggregates (i.e., 89), indicating that the larger sizes of aggregates are more textured compared to the smaller sizes of aggregates. Similarly, the CA12 aggregates were found more spherical compared to CA4 aggregates (Table 3.4).

3.8.2 Fine Aggregates

3.8.2.1 Angularity

The mean of radius angularity for FA8 and FA16 aggregates ranged from 10.7 to 11.3, and 9.8 to 10.4, respectively (Table 3.8), indicating that all fine aggregates were in angular range (Table 3.1 and Table 3.8). Figures 3.14 and 3.15 show the percentage cumulative aggregates and angularity index for FA8 and FA16 aggregates, respectively. It can be seen from these figures that the distribution of particles is very similar for all types of aggregates. FA8 aggregates were found to be slightly more angular compared to FA16 aggregates (Table 3.8).

Statistical Analysis

Table 3.9 shows the results of the ANOVA test. The p-values for angularity of FA8 and FA16 aggregates were higher than 0.05, indicating that no statistically significant differences existed among the angularity of different types of fine aggregates.

Statistical analyses indicate that the production and sample preparation method do not affect the angularity of either coarse or fine aggregates used in the present study. However, precaution should be taken before generalizing these results. The present study focuses on change in the shape parameters for limestone aggregates only. Future study may be needed covering a broad range of aggregates including granite, gravel, sandstone, and rhyolite.

3.8.2.2 Two Dimensional (2D) Form

The mean of 2D form for FA8 and FA16 aggregates was found to be approximately 7.5 and 6.8, respectively, indicating that FA16 aggregates are more circular (less elongated) compared to FA8 aggregates (Table 3.8). Figures 3.16 and 3.17 show the percentage cumulative aggregates and 2D form index for FA8 and FA16

aggregates, respectively. It can be seen that the distribution of particles are very similar for all types of aggregates. Similar results were reported by Masad (2005). They found that crushing and aggregate size had a very minor effect on the resulting values of the 2D form index.

Statistical Analysis

Table 3.9 shows the results of the ANOVA test. The p-value for 2D form for FA8 and FA16 aggregates was found to be more than 0.05, indicating that no statistically significant differences existed among the 2D form of different types of aggregates.

3.8.3 Comparison of Shape Parameters for Coarse and Fine Aggregates

A comparison of the shape parameters (angularity and 2D form) for coarse and fine aggregates was conducted for OA aggregates. The OA aggregates were chosen for this purpose because the shape properties of these aggregates are not affected by plant and laboratory production methods. The results indicate that coarse aggregates were found to be more angular compared to fine aggregates (Table 3.4 and Table 3.8). Similarly, the 2D form of coarse aggregates was found to be higher than fine aggregates, indicating that fine aggregates are more circular compared to the coarse aggregates (Table 3.4 and Table 3.8).

3.9 Summary of Results

This chapter presents the effects of the production and laboratory preparation methods on the shape parameters (i.e., angularity, texture, 2D from, and sphericity) of coarse and fine aggregates. Six different types of coarse and fine aggregates were tested, including original aggregates (OA) collected from the stockpile, plant mix (PM) aggregates extracted from the loose asphalt mix, and aggregates retrieved from the sample compacted at different density levels, called AV aggregates. A statistical analysis,

called analysis of variance (ANOVA), was conducted to check the statistical validity of the results. The following conclusions and recommendations can be drawn from the results and discussion presented in this chapter.

(1) The angularity and sphericity of coarse aggregates were found to be very similar for all six types of aggregates. All aggregates passed the 5:1 Superpave requirement, but they had different distributions of flat and elongated particles.

(2) The texture of OA aggregates was found to be higher than the PM aggregates, indicating that the plant production process does affect the texture of the aggregates, consequently resulting in lower texture. Similarly, AV aggregates were found to have more texture compared to PM aggregates. It might be possible that texture is altered during the process of sample preparation, coring, and sawing.

(3) 2D form was another shape property that was affected significantly. For coarse aggregate (CA12 and CA4), 2D form of OA was found to be higher than PM aggregates. PM aggregates were found to have the lowest value of 2D form. Furthermore, no significant difference was observed among the aggregates compacted at different density levels (AV aggregates).

(4) The angularity and 2D form of fine aggregates were found to be very similar for all six types of aggregates, indicating that the plant production process and sample preparation method did not influence the shape properties of these particles significantly.

(5) Coarse aggregates were found to be more angular and elongated compared to the fine aggregates, indicating that particles become rounded and circular as its size decreases.

(6) The texture and sphericity index of larger size of coarse aggregates (CA12) were found to be higher than the smaller size of coarse aggregates (CA4).

(7) Smaller sizes of fine aggregates (FA16) were found to be more circular compared to larger sizes of fine aggregates (FA8).

The present study provides useful information on change of shape parameters of aggregates during plant production and sample preparation methods in the laboratory. It is expected that the characterization of aggregates based on the shape properties would help to develop a better understanding of the performance of asphalt and aggregates base layers. The present study was limited to only one type of aggregate (i.e., limestone). Similar approach may be used to conduct the studies on other types of aggregates (i.e., granite, sandstone, rhyolite, and gravel etc.). Furthermore, the present study is limited on using four sizes of aggregates (CA12, CA4, FA8, and FA16). It is recommended similar study be conducted using the other sieves of coarse and fine aggregates. The present study uses NCAT ignition oven to extract the aggregates from a mix. It is recommended that solvent based methods be used to extract the aggregates from the mix. Furthermore, it is recommended that aggregates be extracted without coring the samples to evaluate the effect of SGC compaction on the shape parameters.

Table 3.1 Classification of Aggregates in AIMS (Reproduced from Masad, 2005)

Aggregate Physical Property	Range and Description				
Texture	High Roughness	Moderate Roughness	Low Roughness	Smooth	Polished
	>460	350-460	275-350	165-275	<165
Angularity-Gradient Method	Angular	Sub-Angular	Sub-Rounded	Rounded	
	>5400	4000-5400	2100-4000	<2100	
Angularity-Radius Method	High Angularity	Angular	Sub-Angular	Sub-Rounded	Rounded
	>16	10-16	7-10	5-7	0-5
Sphericity	High Sphericity	Moderate Sphericity	Low Sphericity	Flat/Elongated	
	>0.8	0.7-0.8	0.6-0.7	<0.6	
2D Form	Elongated	Semi-Elongated	Semi-Circular	Circular	
	>10.5	8-10.5	6.5-8	<6.5	

Table 3.2 Gradation of Aggregates

Sieve	Aggregate Types (% Passing)					
Size (mm)	OA	PM	AV6	AV8	AV10	AV12
25	100	100	100	100	100	100
19	98	97	97	98	98	99
12.5	87	89	90	90	91	90
9.5	80	82	85	86	86	85
4.75	58	67	72	74	72	71
2.36	37	44	48	50	49	48
1.18	25	31	33	34	33	32
0.6	19	23	24	25	24	23
0.3	12	15	16	17	16	15
0.15	4	8	9	9	8	8
0.075	3	6	6	6	6	5

Table 3.3 AIMS Test Matrix

Aggregate Type	Coarse Aggregates		Fine Aggregates	
	CA12	CA4	FA8	FA16
OA	x	x	x	x
PM	x	x	x	x
AV6	x	x	x	x
AV6	x	x	x	x
AV10	x	x	x	x
AV12	x	x	x	x

CA12: Aggregate passed 3/4" (19 mm) and retained 1/2" (12.5 mm)
CA4 : Aggregate passed 3/8" (9.5 mm) and retained #4 (4.75 mm)
FA8 : Aggregate passed #4 (4.75 mm) and retained #8 (2.36 mm)
FA16 : Aggregate passed #8 (2.36 mm) and retained #16 (1.18 mm)

Table 3.4 AIMS Results for Coarse Aggregates

Aggregate Type	Radius Angularity Index				Texture			
	CA12		CA4		CA12		CA4	
	Mean	Stdev	Mean	Stdev	Mean	Stdev	Mean	Stdev
OA	11.1	3.69	11.4	3.33	158.8	67.1	102.8	46.1
PM	10.2	3.34	10.1	3.03	149.3	48.5	89.0	45.1
AV6	10.9	3.36	11.0	3.75	178.3	66.8	124.2	57.0
AV8	10.5	3.70	10.7	3.36	198.6	73.8	126.3	64.6
AV10	10.5	3.58	11.1	3.71	190.6	61.3	132.0	70.2
AV12	10.4	3.53	11.2	3.58	184.3	71.0	122.8	58.8

Aggregate Type	2D Form				Sphericity			
	CA12		CA4		CA12		CA4	
	Mean	Stdev	Mean	Stdev	Mean	Stdev	Mean	Stdev
OA	7.7	2.31	8.0	1.81	0.72	0.11	0.66	0.09
PM	7.0	1.56	7.0	1.48	0.72	0.08	0.68	0.11
AV6	7.5	2.10	7.8	2.37	0.72	0.11	0.68	0.11
AV8	7.4	2.09	8.1	2.19	0.71	0.09	0.68	0.11
AV10	7.4	2.25	8.1	2.20	0.73	0.10	0.66	0.13
AV12	7.4	1.88	8.2	2.62	0.71	0.10	0.68	0.11

Table 3.5 ANOVA Statistics for Coarse Aggregates

Coarse Aggregates						
Shape	CA12			CA4		
Parameter	F-value	p-value	Significant	F-value	p-value	Significant
Radius Angularity	0.819	0.536	No	1.826	0.106	No
Texture	8.312	0.000	Yes*	12.464	0.000	Yes*
2D Form	3.092	0.009	Yes*	7.423	0.000	Yes*
Sphericity	1.674	0.139	No	1.305	0.260	No

Yes: Significant difference exists; No: Significant difference does not exist; *Post-hoc test was conducted

Table 3.6 Results of Post Hoc Test (ANOVA) for Texture of Coarse Aggregates

Aggregate Type	Coarse Aggregate: Texture					
	CA12					
	OA	PM	AV6	AV8	AV10	AV12
OA	-	No	No	**Yes**	**Yes**	No
PM	No	-	**Yes**	**Yes**	**Yes**	**Yes**
AV6	No	**Yes**	-	No	No	No
AV8	Yes	**Yes**	No	-	No	No
AV10	Yes	**Yes**	No	No	-	No
AV12	No	**Yes**	No	No	No	-

Aggregate Type	CA4					
	OA	PM	AV6	AV8	AV10	AV12
OA	-	No	**Yes**	**Yes**	**Yes**	**Yes**
PM	No	-	**Yes**	**Yes**	**Yes**	**Yes**
AV6	**Yes**	**Yes**	-	No	No	No
AV8	**Yes**	**Yes**	No	-	No	No
AV10	**Yes**	**Yes**	No	No	-	No
AV12	**Yes**	**Yes**	No	No	No	-

Yes: Significant difference exists; No: Significant difference does not exist

Table 3.7 Results of Post Hoc Test (ANOVA) for 2D Form of Coarse Aggregates

Aggregate Type	Coarse Aggregate: 2D Form					
	CA12					
	OA	PM	AV6	AV8	AV10	AV12
OA	-	**Yes**	No	No	No	No
PM	**Yes**		No	No	No	No
AV6	No	No		No	No	No
AV8	No	No	No		No	No
AV10	No	No	No	No		No
AV12	No	No	No	No	No	

Aggregate Type	CA4					
	OA	PM	AV6	AV8	AV10	AV12
OA	-	**Yes**	No	No	No	No
PM	**Yes**		**Yes**	**Yes**	**Yes**	**Yes**
AV6	No	**Yes**	-	No	No	No
AV8	No	**Yes**	No		No	No
AV10	No	**Yes**	No	No		No
AV12	No	**Yes**	No	No	No	

Yes: Significant difference exists; No: Significant difference does not exist

Table 3.8 AIMS Results for Fine Aggregates

Aggregate Type	Radius Angularity Index				2D Form			
	FA8		FA16		FA8		FA16	
	Mean	Stdev	Mean	Stdev	Mean	Stdev	Mean	Stdev
OA	10.8	3.47	9.9	3.72	7.5	1.78	6.8	1.90
PM	11.0	3.59	10.3	3.80	7.4	1.70	6.8	1.69
AV6	10.7	3.74	9.8	3.71	7.3	1.70	6.7	1.98
AV8	10.9	3.68	9.9	3.75	7.3	1.73	6.8	1.77
AV10	11.3	3.62	9.8	3.45	7.4	1.60	6.7	1.67
AV12	11.0	3.68	10.4	3.74	7.5	1.73	7.0	2.26

Table 3.9 ANOVA Statistics for Fine Aggregates

Fine Aggregates						
Shape	FA8			FA16		
Parameter	F-value	p-value	Significant	F-value	p-value	Significant
Radius Angularity	1.783	0.113	No	1.738	0.113	No
2D Form	1.307	0.258	No	1.456	0.202	No

Yes: Significant difference exists; No: Significant difference does not exist

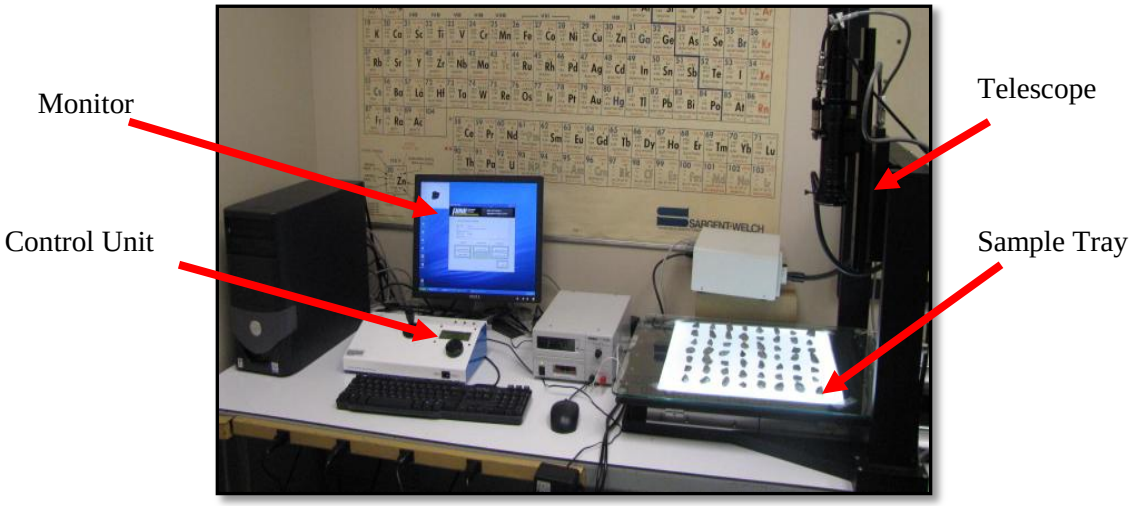

Figure 3.1 Set up of Aggregate Image Measurement System (AIMS)

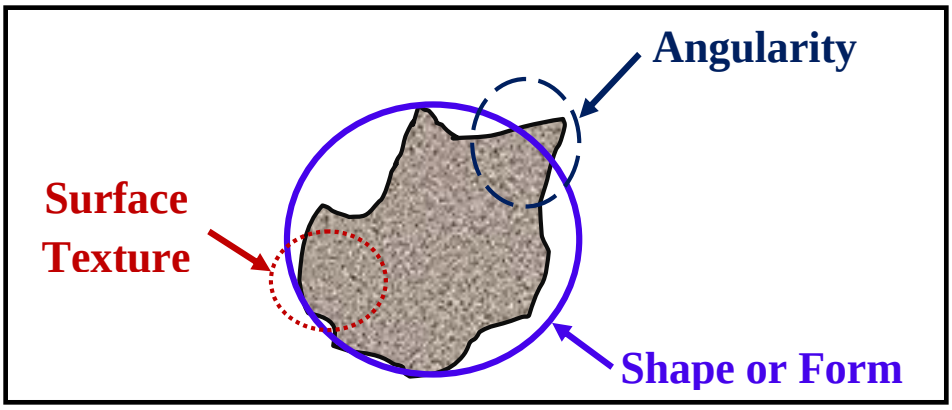

Figure 3.2 Components of an Aggregate Shape: Shape, Angularity, and Texture (Reproduced from Masad, 2005)

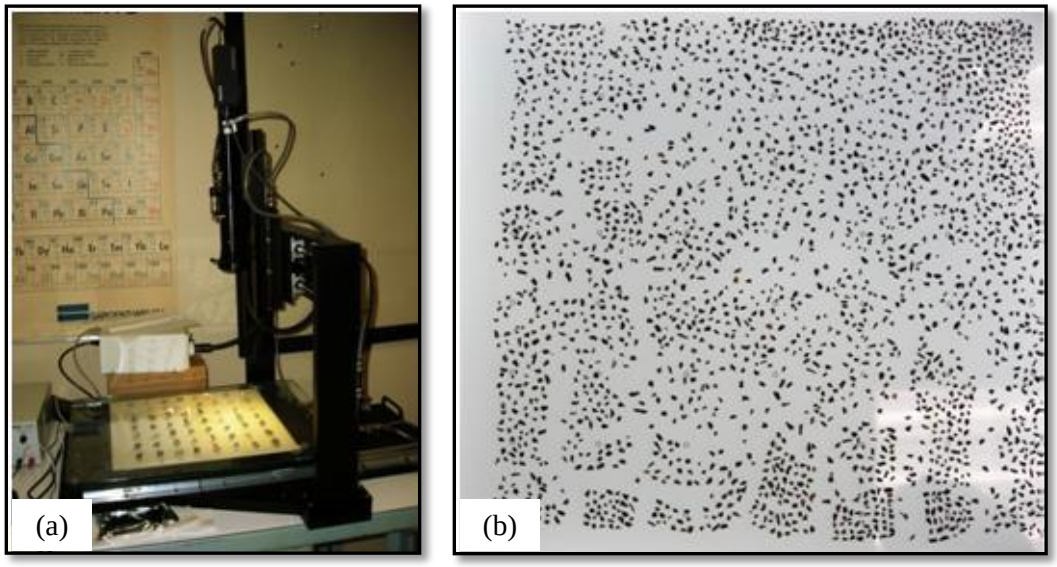

Figure 3.3 AIMS Test layout for: (a) Coarse aggregates; (b) Fine aggregates.

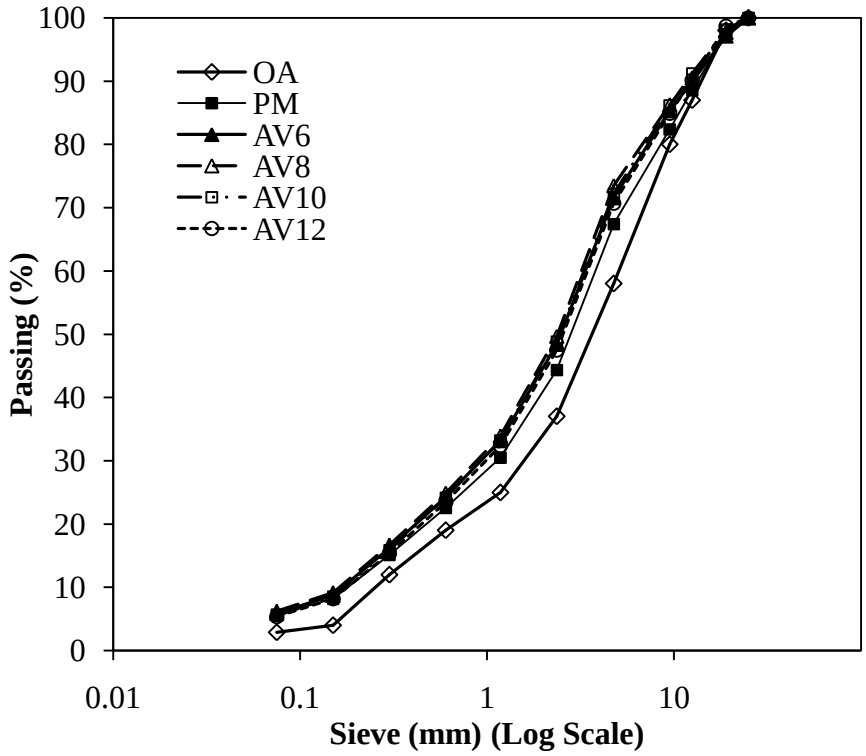

Figure 3.4 Plot of Aggregate Gradations

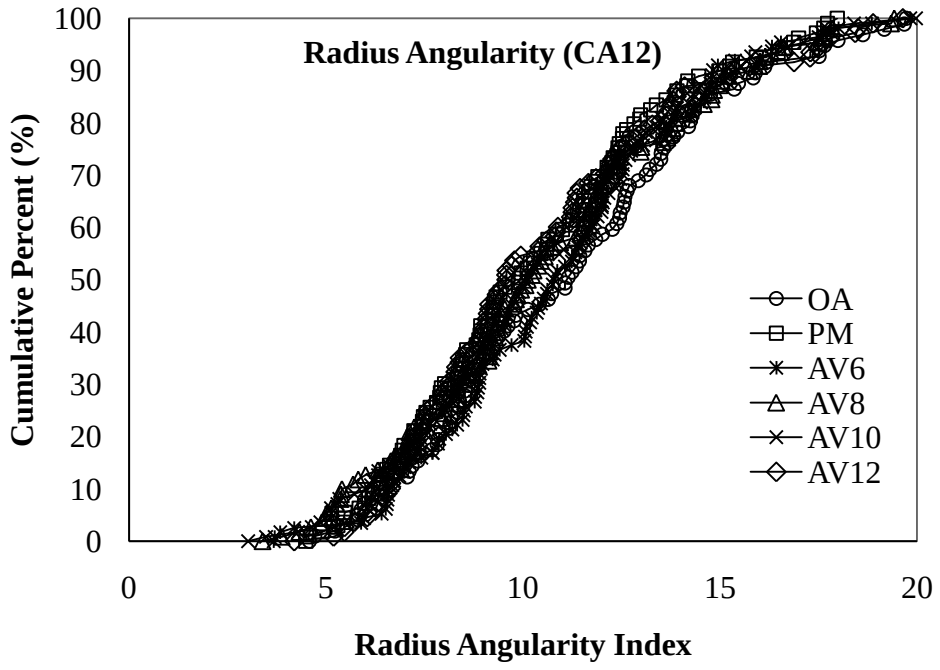

(a)

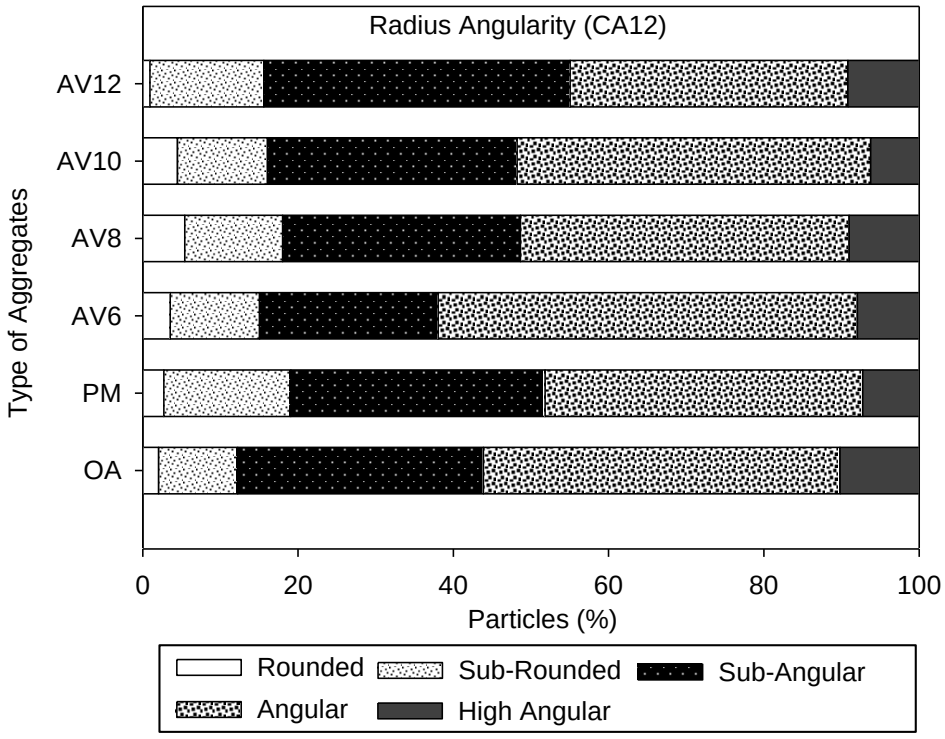

(b)

Figure 3.5 Angularity of Coarse Aggregates (CA12) (a) AIMS Plot, (b) Distribution of Different Angular Aggregates

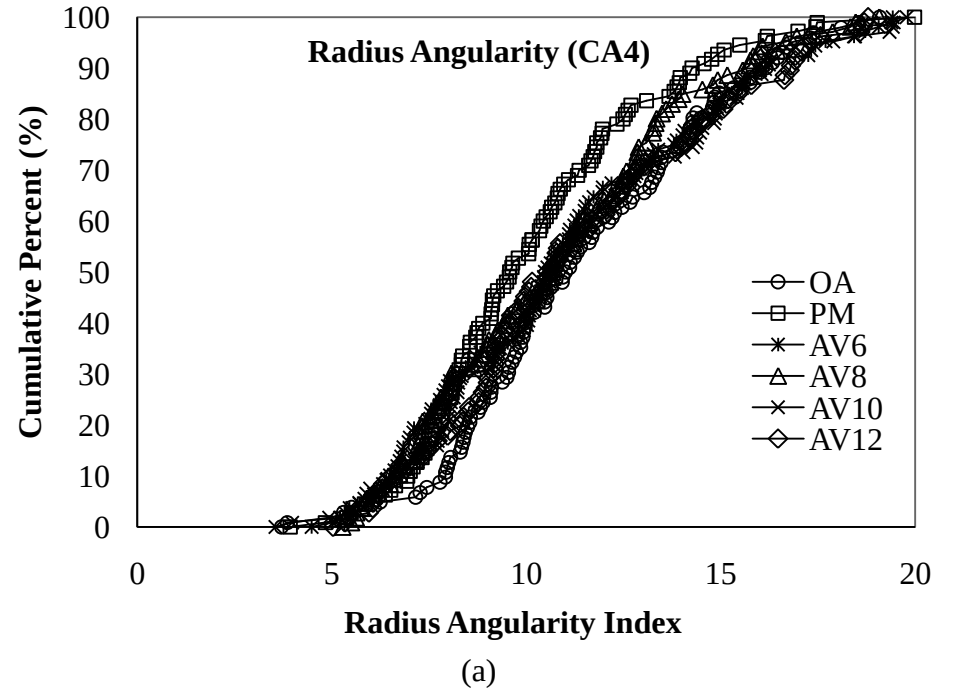

(a)

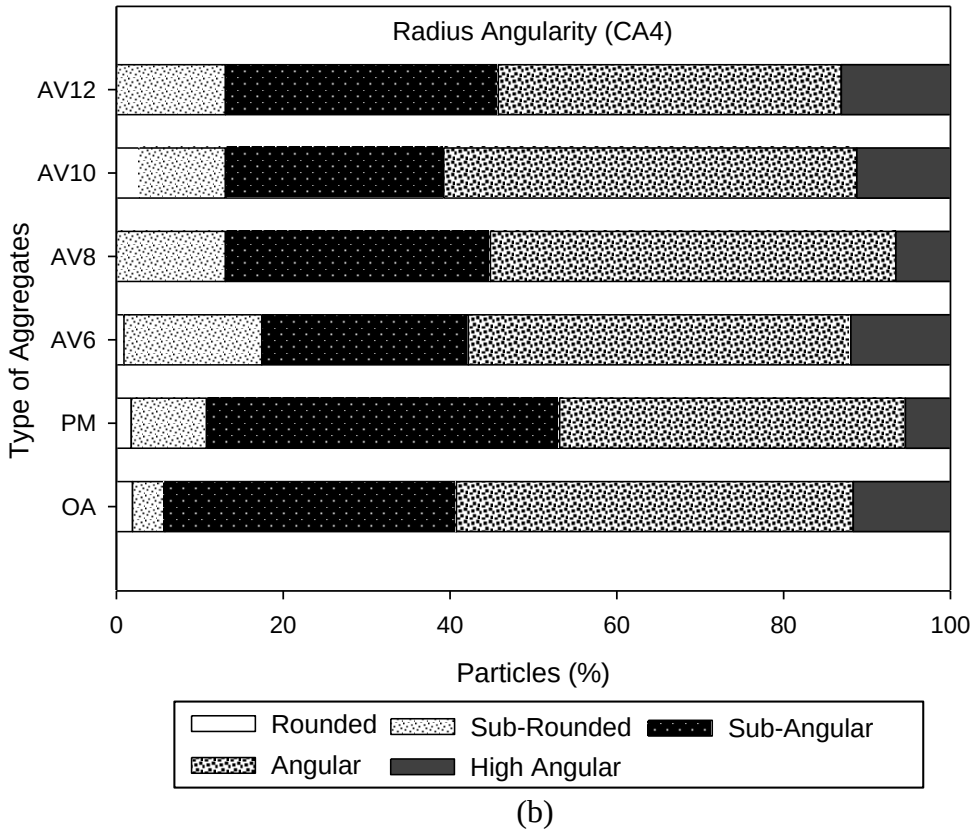

(b)

Figure 3.6 Angularity of Coarse Aggregates (CA4) (a) AIMS Plot, (b) Distribution of Different Angular Aggregates

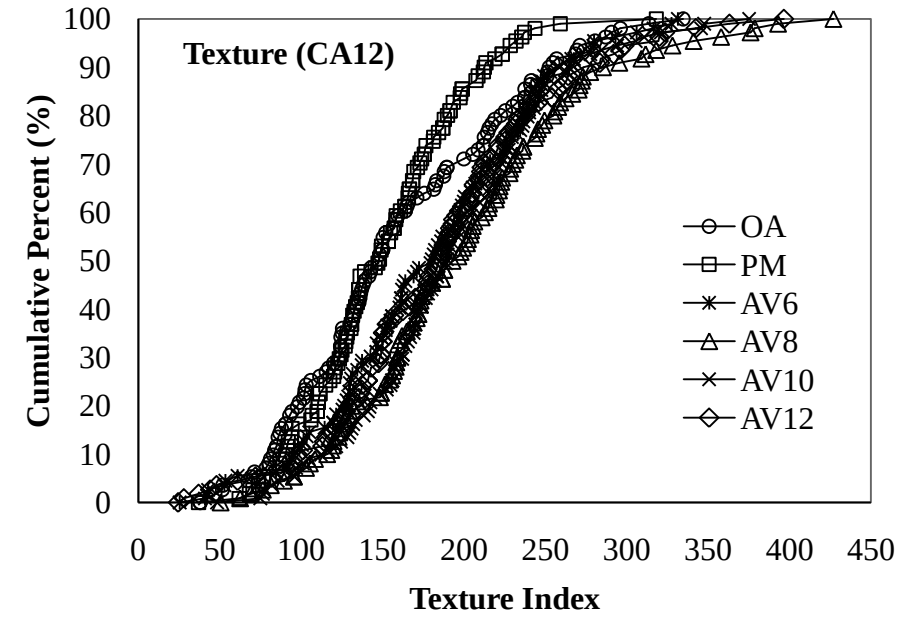

(a)

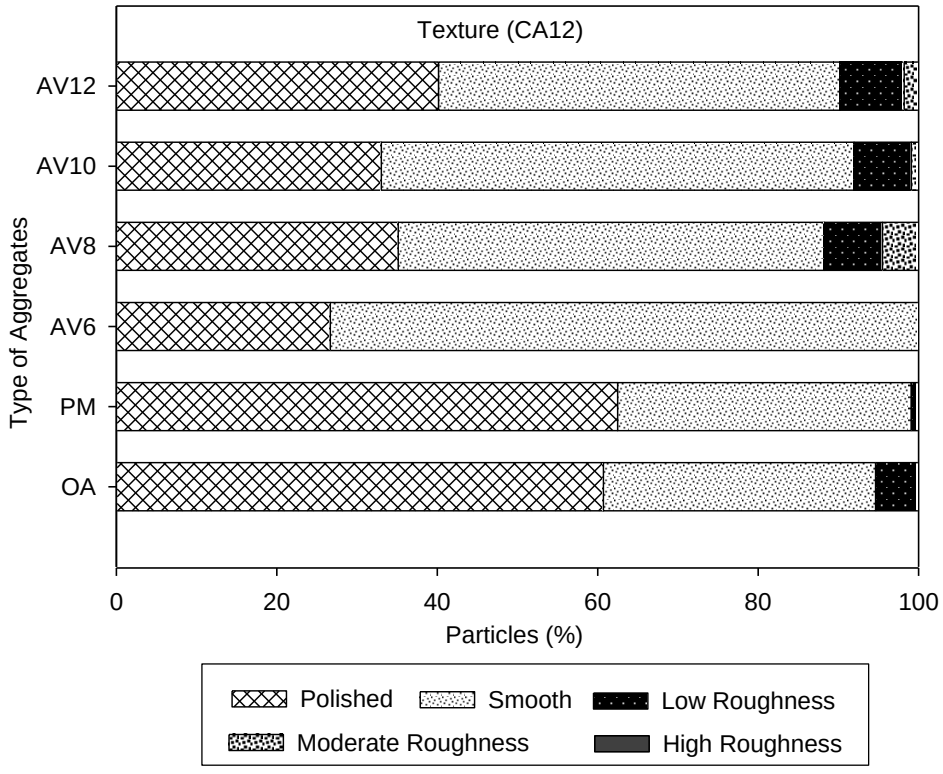

(b)

Figure 3.7 Texture of Coarse Aggregates (CA12) (a) AIMS Plot, (b) Distribution of Different Textured Aggregates

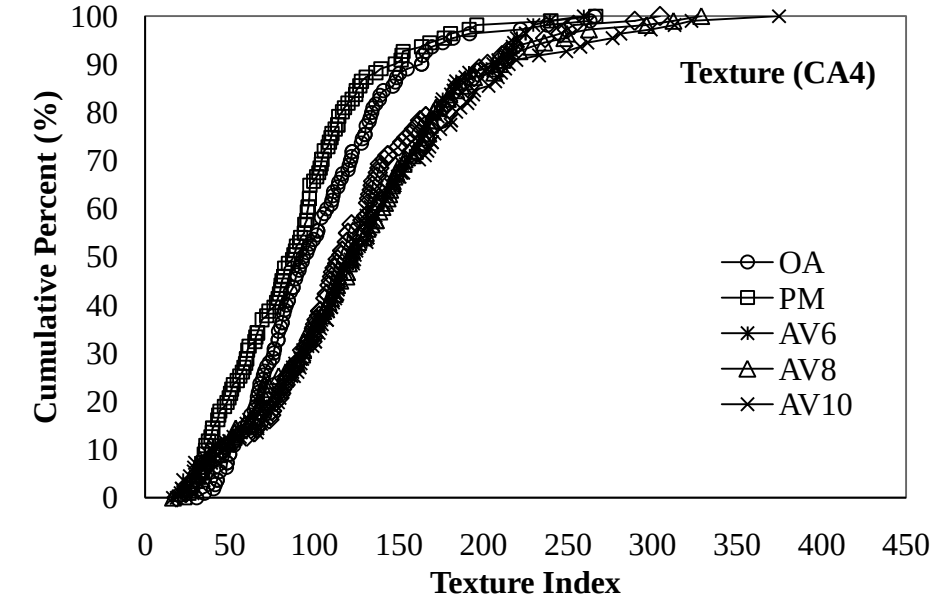

(a)

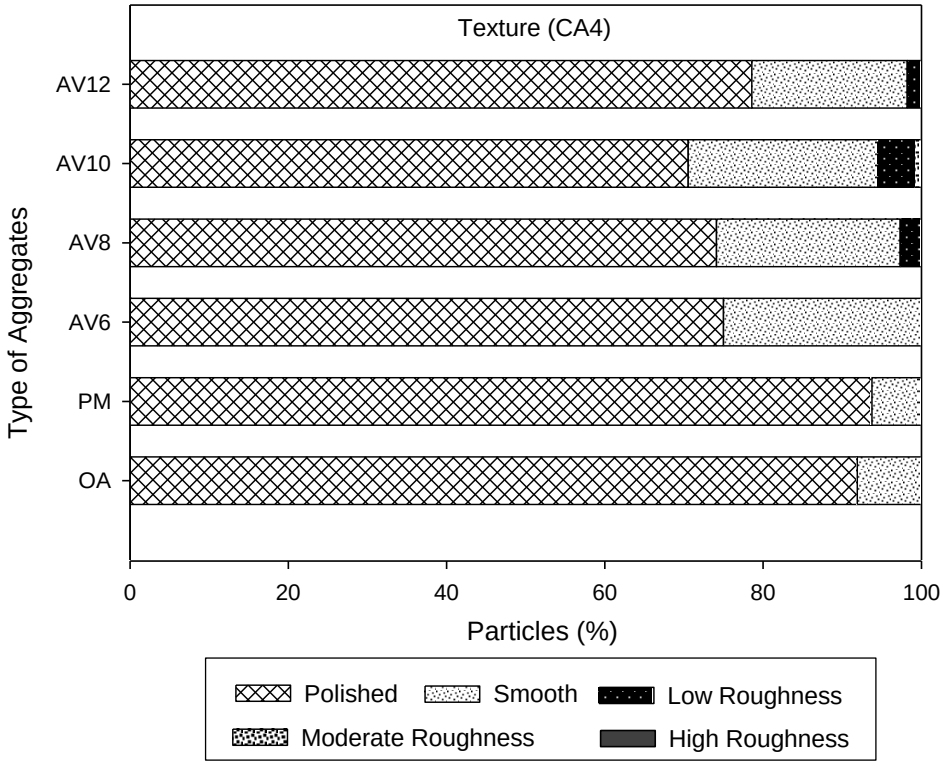

(b)

Figure 3.8 Texture of Coarse Aggregates (CA4) (a) AIMS Plot, (b) Distribution of Different Textured Aggregates

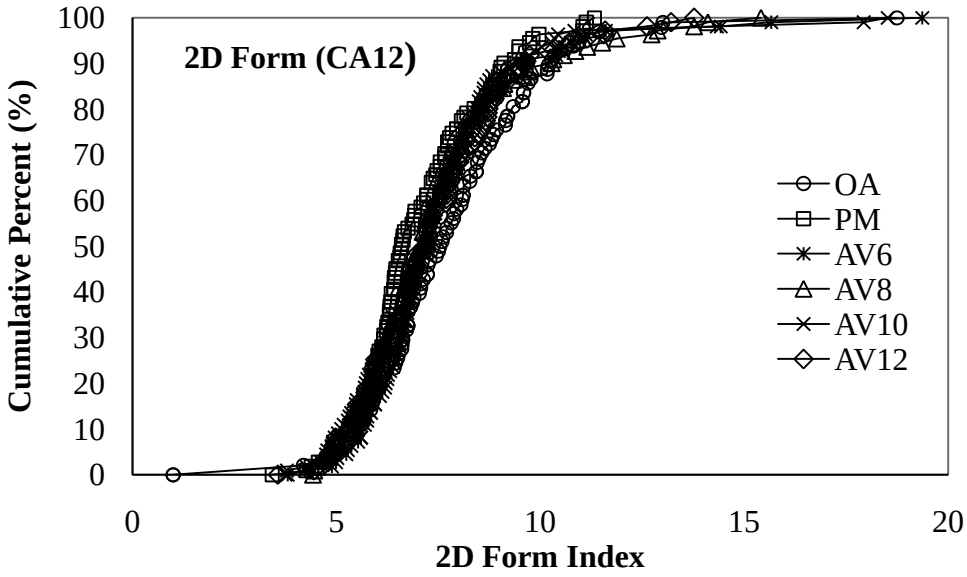

(a)

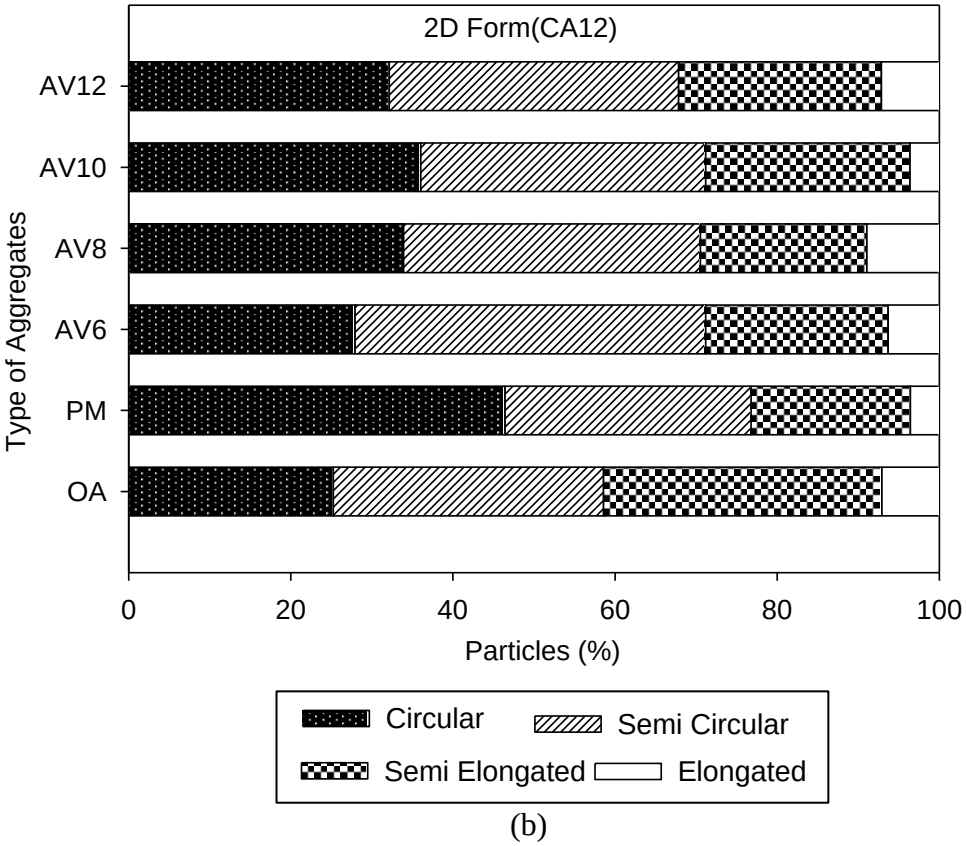

(b)

Figure 3.9 2D Form of Coarse Aggregates (CA12) (a) AIMS Plot, (b) Distribution of Different Shape of Aggregates

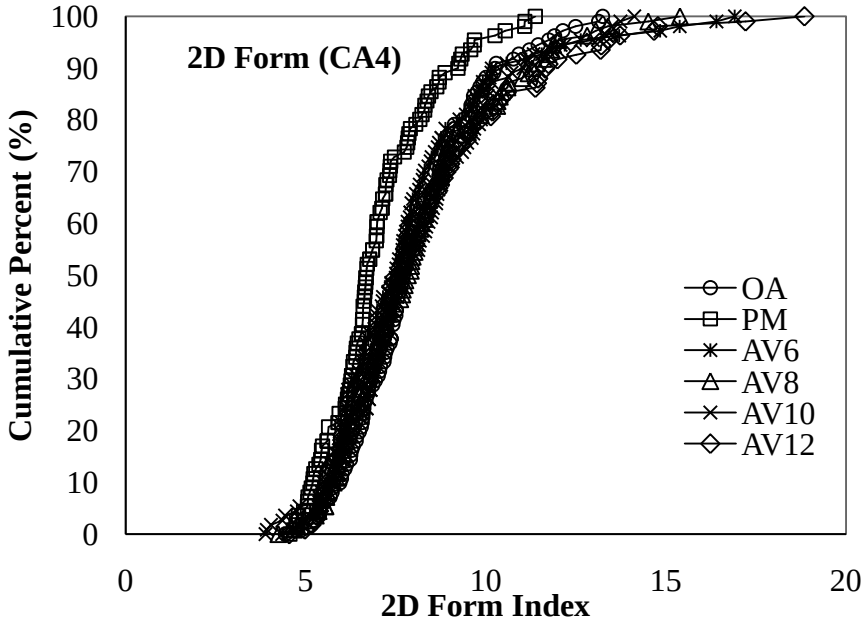

(a)

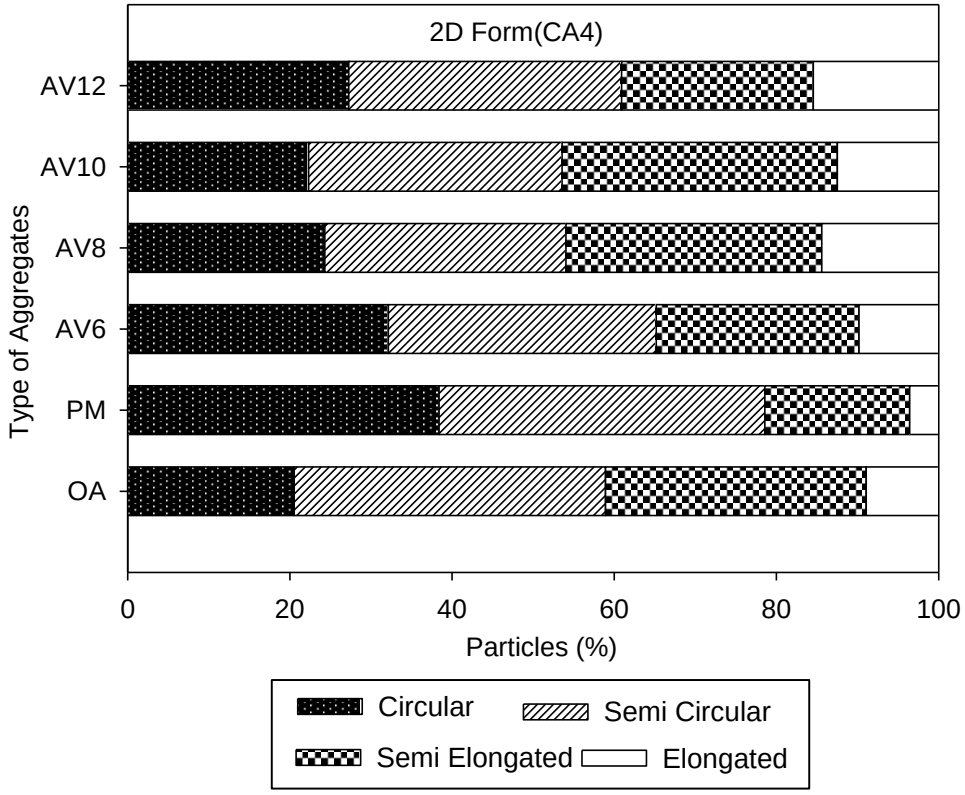

(b)

Figure 3.10 2D Form of Coarse Aggregates (CA4) (a) AIMS Plot, (b) Distribution of Different Shape of Aggregates

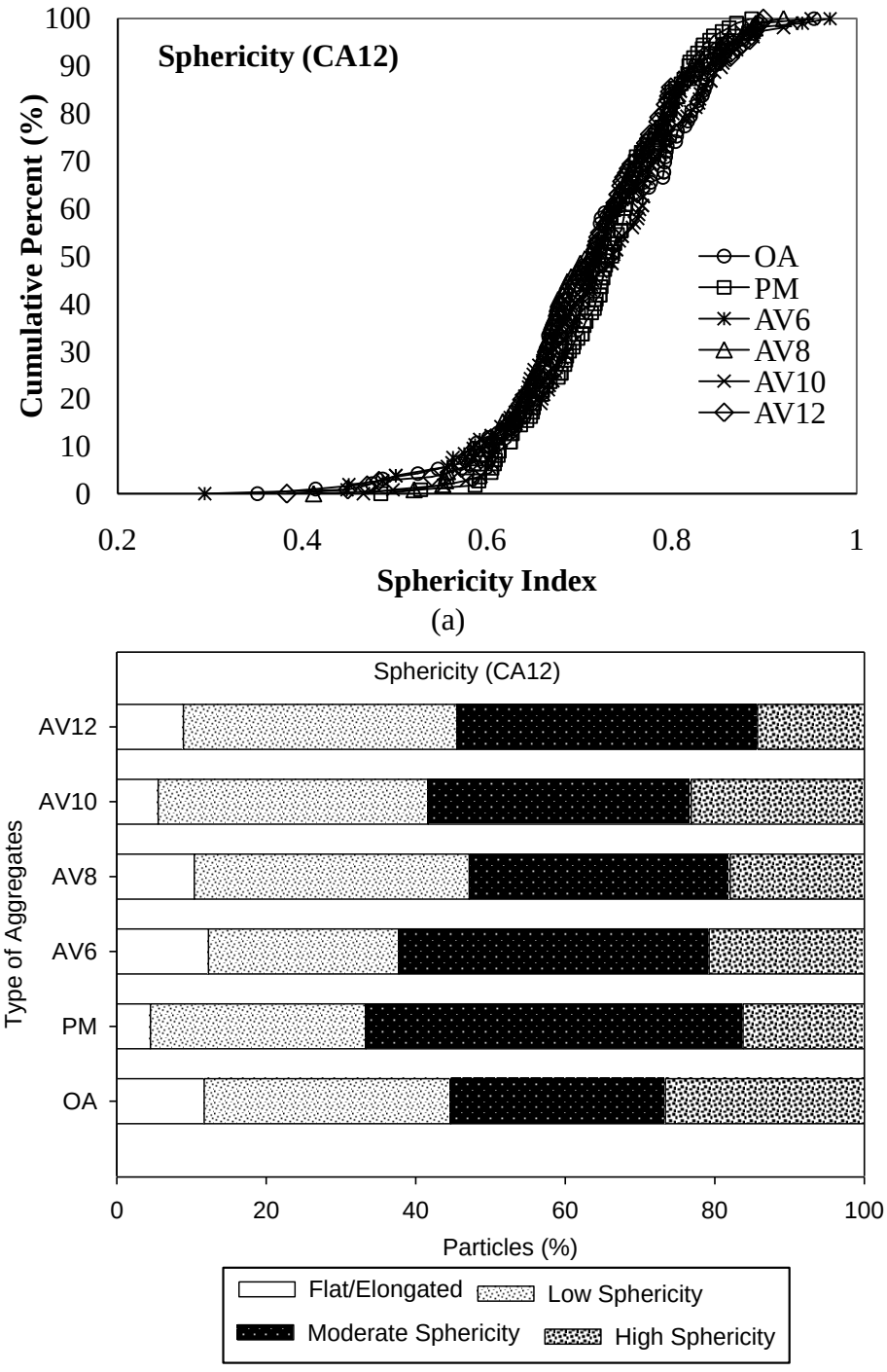

Figure 3.11 Sphericity of Coarse Aggregates (CA12) (a) AIMS Plot, (b) Distribution of Different Spherical Aggregates

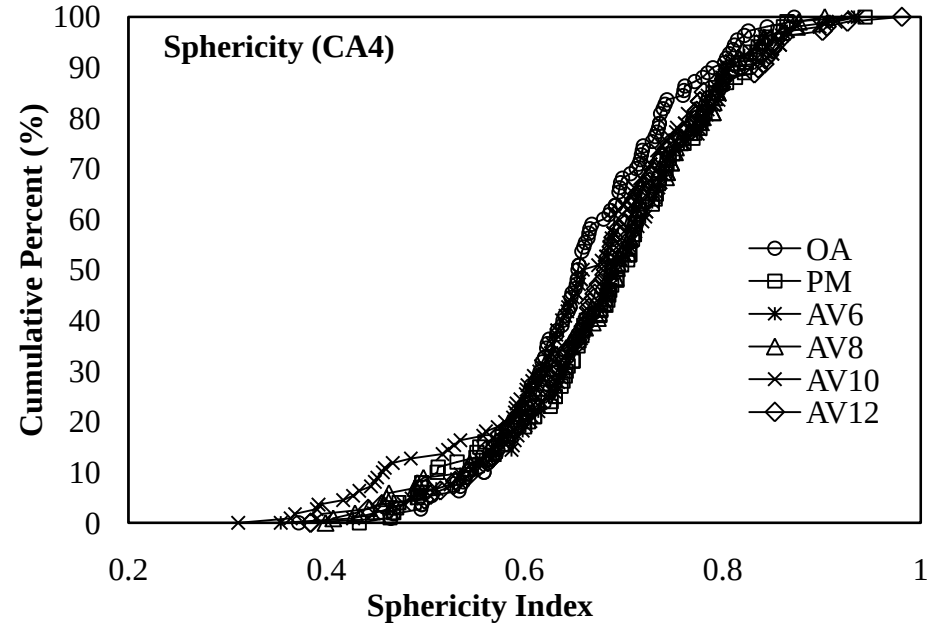

(a)

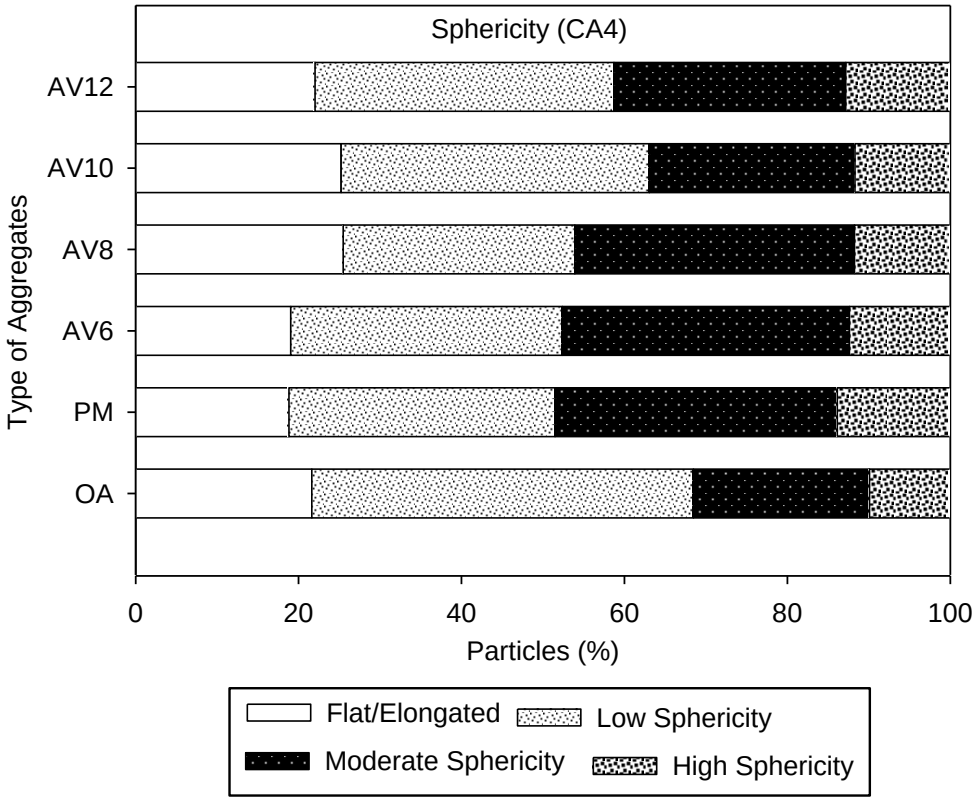

(b)

Figure 3.12 Sphericity of Coarse Aggregates (CA4) (a) AIMS Plot, (b) Distribution of Different Spherical Aggregates

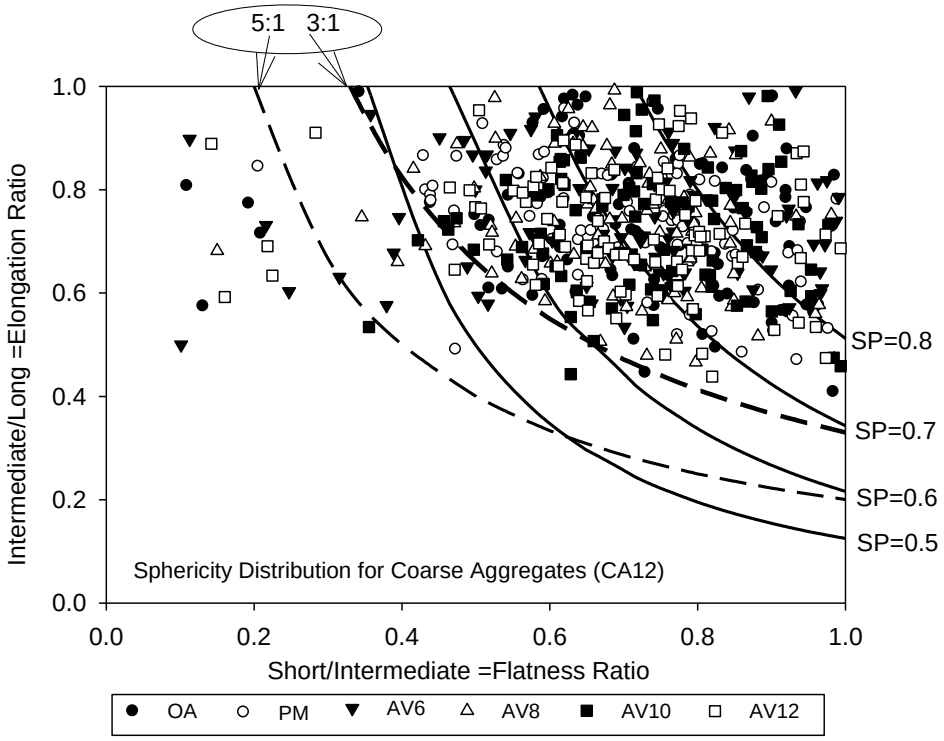

(a)

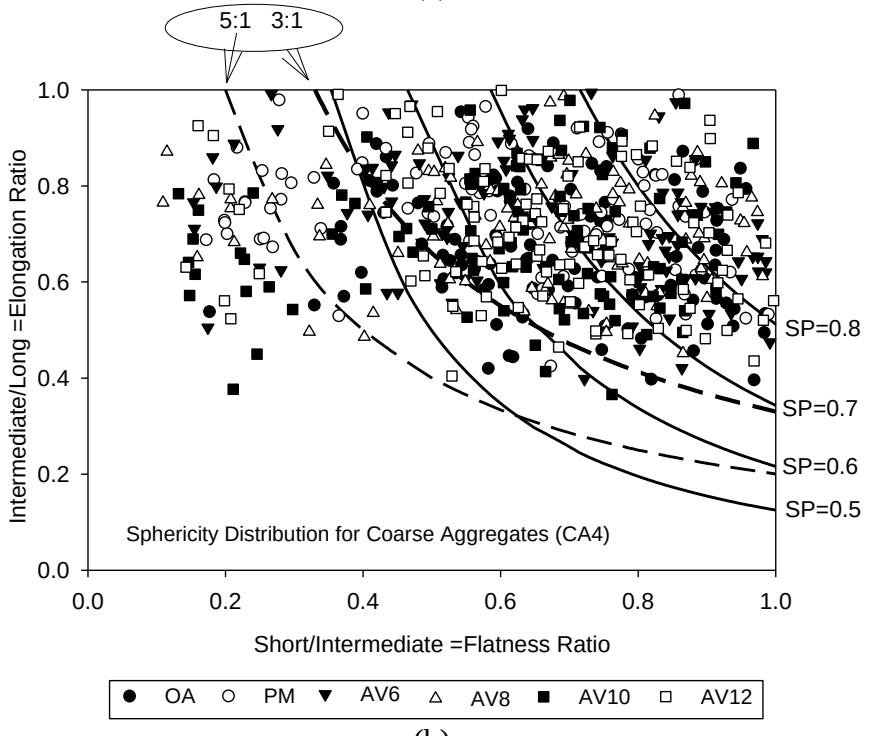

(b)

Figure 3.13 Distribution of Flat and Elongated Aggregates For (a) CA12, (b) CA4

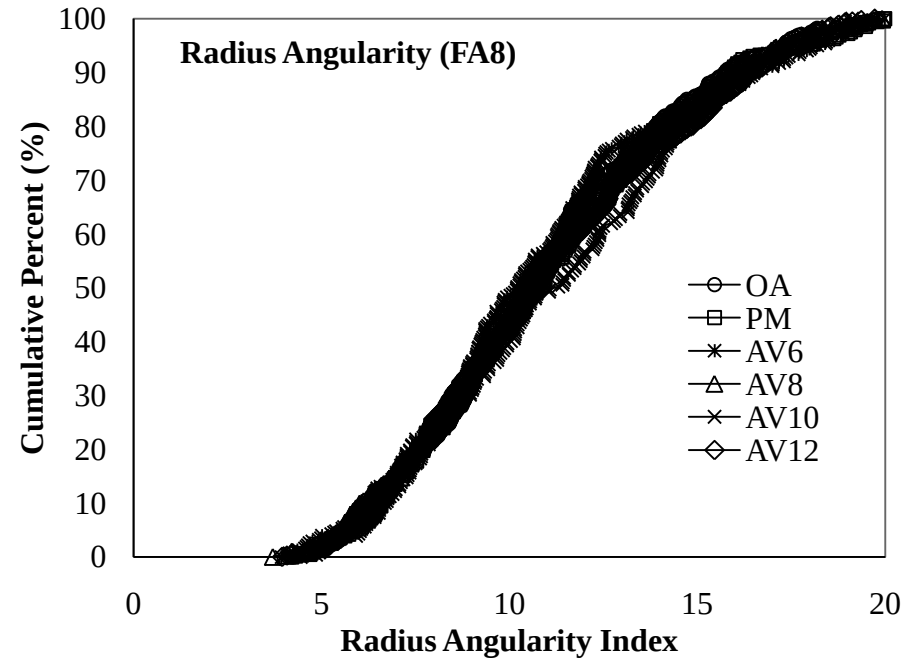

(a)

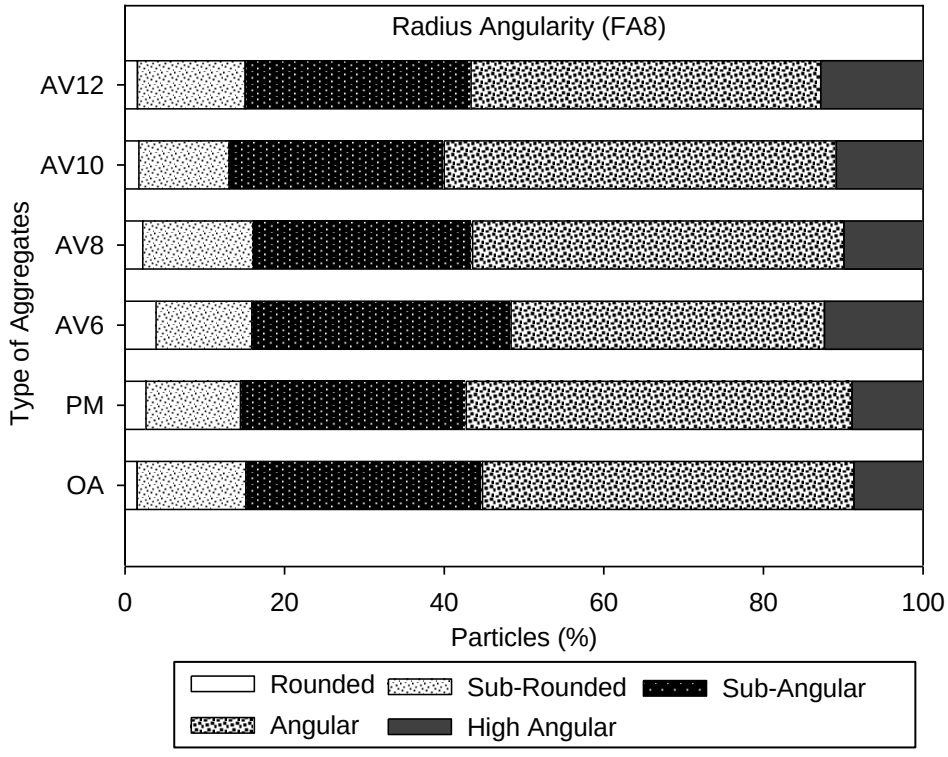

(b)

Figure 3.14 Angularity of Fine Aggregates (FA8) (a) AIMS Plot, (b) Distribution of Different Angular Aggregates

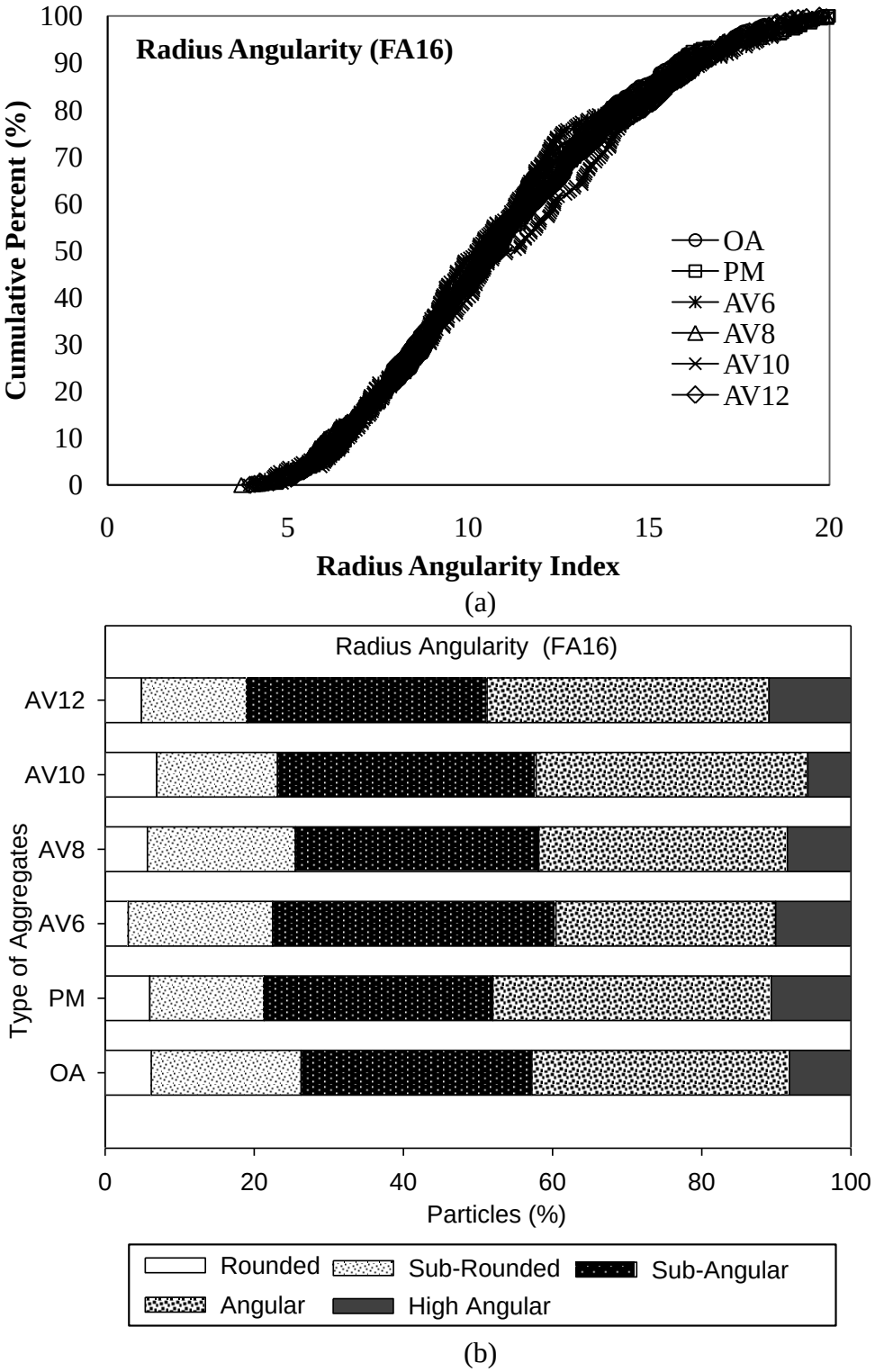

Figure 3.15 Angularity of Fine Aggregates (FA16) (a) AIMS Plot, (b) Distribution of Different Angular Aggregates

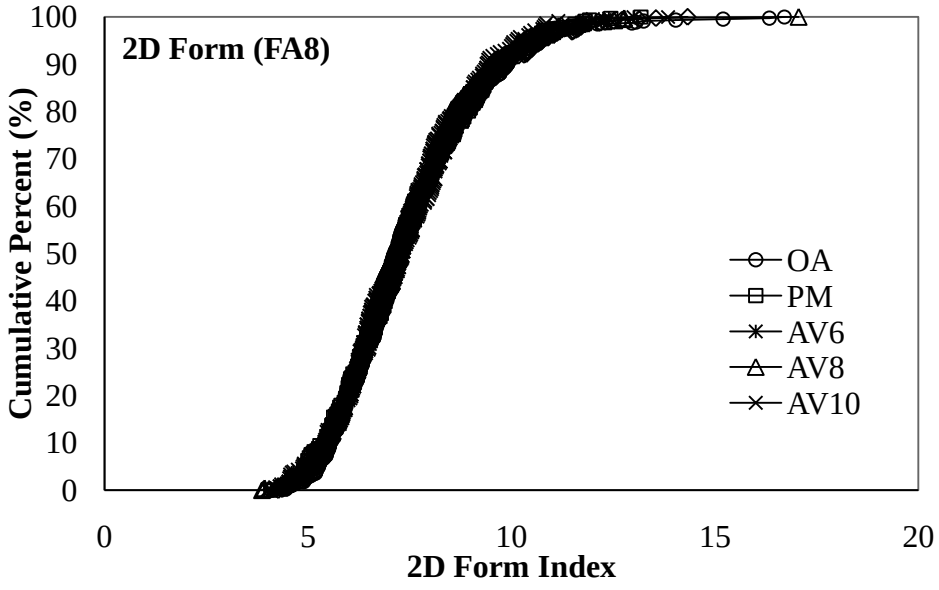

(a)

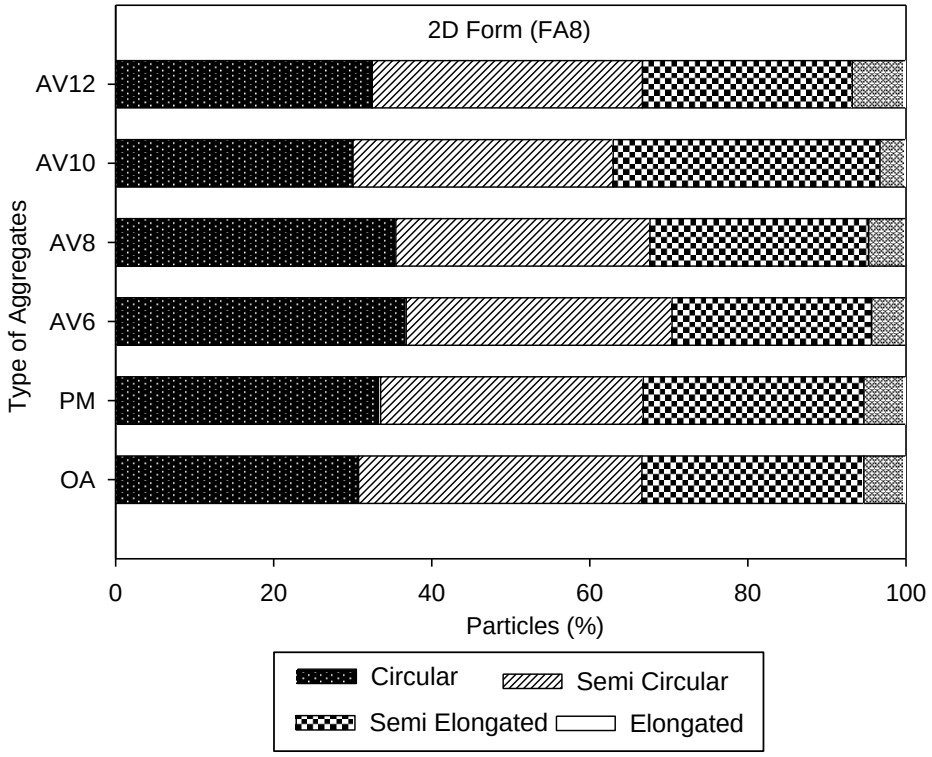

(b)

Figure 3.16 2D Form of Fine Aggregates (FA8) (a) AIMS Plot, (b) Distribution of Different Shape of Aggregates

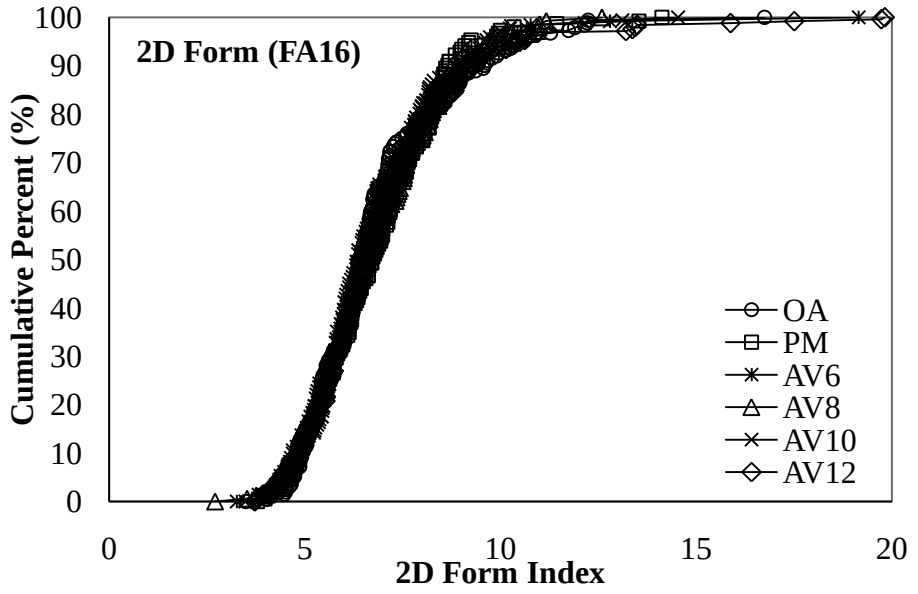

(a)

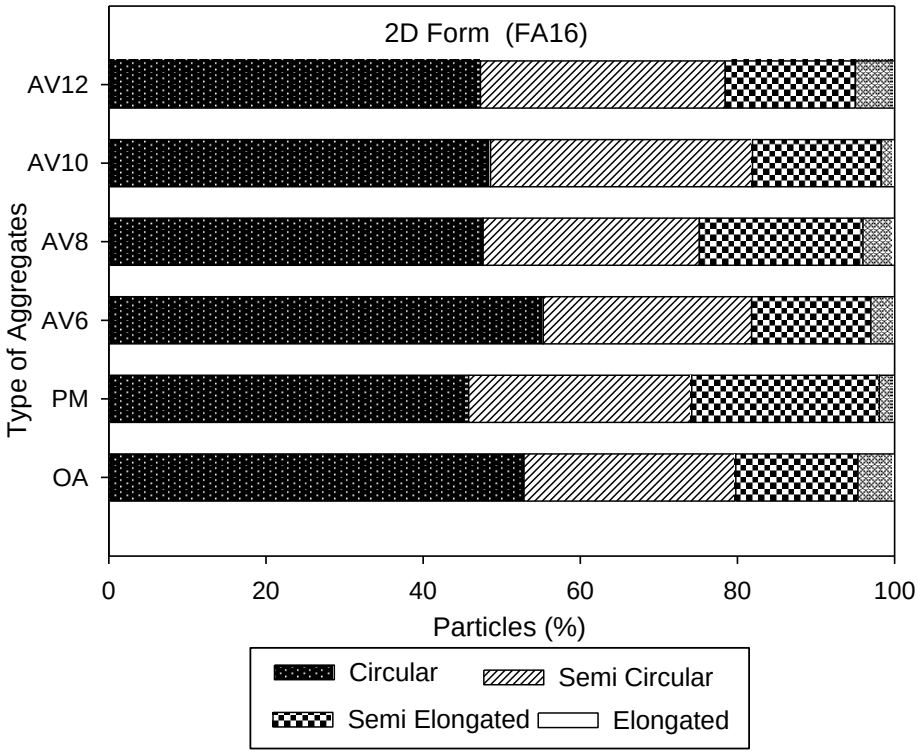

(b)

Figure 3.17 2D Form of Fine Aggregates (FA16) (a) AIMS Plot, (b) Distribution of Different Shape of Aggregates

CHAPTER 4 : SHAPE PARAMETERS FOR DIFFERENT TYPES OF COARSE AGGREGATES

4.1 Introduction

The performance of pavements can be significantly influenced by the gradation and shape parameters of aggregates (i.e., angularity, texture, form, and sphericity) (Pan et al., 2006). An accurate measurement of these properties is important for developing specifications for quality control and quality assurance of aggregates. Currently, the Superpave mix design system is used to ensure quality of aggregates by determining their consensus and source properties (Cominsky, 1994). The source properties of aggregates include: toughness, durability, and amount of deleterious materials; consensus properties consist of the following: coarse aggregate angularity (percent of fractured faces), fine aggregate angularity (FAA) (percent uncompacted voids), flat and elongated (F&E) particles, and amount of clay content in aggregates (Cominsky, 1994). Both toughness and durability tests are routinely used by state departments of transportation as an indicator of aggregate quality. However, issues are continually raised about their ability to predict the actual performance of the aggregates in service (Hossain et al., 2008; Kandhal and Frazier, 1998). Similarly, the methods of estimating angularity of aggregates and F&E particles are very subjective, time-consuming, and labor intensive (Gudimettla et al., 2006; Al-Rousan et al., 2005; Rao et al., 2002).

Several researchers have reported that Superpave tests may not reflect the overall quality of the aggregates and consequently, contradictory results have been reported in the literature (Bennert et al., 2011; Wang et al., 2009; Bhasin et al., 2006; Hand et al., 2000). For example, Bennert et al. (2011) and Hand et al. (2000) reported that the ranking of aggregates as determined by the fractured face count method did not match the general

rutting performance of the asphalt mix. Similarly, Bhasin et al. (2006) found that the fractured face count method cannot distinguish between gravel aggregates. Prowell and Weingart (1999) reported that the Superpave method of measuring F&E particles is not enough to produce a statistically valid sample. Furthermore, Superpave does not provide any direct method to measure the texture of aggregates; it assumes that crushed faces have more texture than uncrushed faces. However, crushing will not always increase texture, as some aggregates fracture with very smooth faces (D'Angelo, 1998). Al-Rousan et al. (2005) mentioned that aggregates could have the same angularity but they might differ significantly in texture. Therefore, the lack of a direct measurement of the texture might cause some aggregate sources to be discarded based on the angularity of aggregates. Also, the Superpave methods cannot distinguish between the shape properties of different sources, types, and sizes of aggregates.

Recently digital image-based techniques have been widely used for developing quality control and quality assurance specifications of aggregates based on the shape parameters of the aggregates (Wang et al., 2009). This technology provides a simple, unbiased, and quantitative measure of aggregate morphological characteristics (Al-Rousan et al., 2005; Masad, 2005; Rao et al., 2002). Researchers have observed that a good correlation exists between the digital-based shape indices and the performance of asphalt pavements (Mishra et al., 2010; Rao et al., 2002). Recognizing the importance of the digital image method, the FWHA granted Pine Instrument Company a project to design, develop, and fabricate an instrument to analyze aggregate properties using digital imaging technology (FHWA, 2010a). The outcome of the project is the development of two AASHTO provisional standards to be used to measure aggregate shape properties.

These standards are: AASHTO PP64 (AASHTO, 2010a) “calculating aggregate stockpile shape characteristics values from digital image analysis shape properties” and AASHTO TP81 (AASHTO, 2010b) “determining aggregate shape properties by means of digital image analysis.” It is expected that in coming years, the digital-based methods will be utilized for quality control and quality assurance of aggregates (Wang et al., 2009; Gudimettla et al., 2006).

The present study was undertaken to compare shape parameters (i.e., angularity, texture, form, and sphericity) of different types and sizes of coarse aggregates. The ranking of the aggregates is done based on the composite shape index factor (CI). CI is calculated using gradation and shape parameters of the associated aggregates. Three different types of aggregates (i.e., granite, rhyolite, and limestone) were collected from the stockpiles. These are common types of aggregates used for the production of asphalt mixes in Oklahoma. Each type of aggregate was divided into three different sizes of coarse aggregates (i.e., CA1, CA2, and CA3).

4.2 Properties of Aggregates

Three different types of aggregates (granite, rhyolite, and limestone) were collected from stockpiles. Both granite and rhyolite are classified as igneous rocks, while limestone is a sedimentary rock. The granite and limestone aggregates were collected from Martin Marietta quarry, Pit No. 3802 and 5005, respectively. The rhyolite aggregates were collected from Hanson quarry, Pit No. 5008. The sources of the aggregates are certified by the Oklahoma Department of Transportation (ODOT) for use in asphalt mix production (ODOT, 2011). The aggregate properties and the gradation of the aggregates are presented in Table 4.1.

The source properties for the aggregates were obtained from ODOT's material database (ODOT, 2011). The LA abrasion values for granite, rhyolite, and limestone aggregates were found to be 20%, 15%, and 24%, respectively, indicating that rhyolite aggregates were the toughest, followed by granite and limestone. The Micro-Deval wear values for granite aggregates were found to be the lowest (2.7%), followed by rhyolite and limestone. The limestone aggregates showed the highest abrasion in both LA and Micro-deval tests. The durability index for rhyolite aggregates was observed to be the lowest (80%), followed by limestone and granite. The aggregates pass the minimum ODOT requirement (ODOT, 2011) for LA abrasion (i.e., <40%), Micro-Deval wear (i.e. <25%), and durability index (i.e., >40%). F&E particles for the three aggregates were estimated as zero percent, indicating that the aggregates pass the Superpave requirement (i.e., F&E<10%). Similarly, the percentage of fracture faces for all the aggregates was found to be 100/100, showing that the aggregates were highly angular.

4.3 Preparation and Testing on Aggregates

Each type of aggregate was divided into three different sizes of coarse aggregates. These sizes include: passing a 19 mm sieve and retained on a 12.5 mm sieve (CA1), passing a 12.5 mm sieve and retained on a 9.5 mm sieve (CA2), and passing a 9.5 mm sieve and retained on a 4.75 mm sieve (CA3). Thus, CA1 type of aggregates had the largest size, followed by CA2 and CA3. The AIMS was used to measure the shape parameters of these aggregates. A summary of shape parameters for all types and sizes of aggregates is given in Table 4.2.

4.4 Results and Discussion

4.4.1 Comparison of Shape Parameters for Different Sizes of Aggregates

Three different sizes of aggregates (i.e., CA1, CA2, and CA3) were compared to evaluate the effect of particle size on the shape parameters. A statistical method, called analysis of variance (ANOVA), was conducted using commercially available software called Statistical Package for the Social Sciences (SPSS®). The null hypothesis for this analysis was that the difference in the mean of the shape parameters for the three sizes of aggregate was equal to zero ($H_0 = \mu_{CA1} = \mu_{CA2} = \mu_{CA3}$), and an alternative hypothesis (H_a) was that the mean of the shape parameters was not equal. Furthermore, a post-hoc test was conducted to evaluate whether the groups within the factor are significantly different or not. The tests were conducted at a significance level of 0.05. A p-value of <0.05 indicates rejection of the null hypothesis.

4.4.1.1 Angularity

Figures 4.1 through 4.3 show the distribution of the particles based on the angularity index. The ANOVA statistics revealed that no statistically significant difference exists in the angularity of the different sizes (i.e., CA1, CA2, and CA3) of granite and limestone aggregates ($p>0.05$) (Table 4.3). However, for rhyolite aggregates, larger sizes of aggregate were found to be less angular compared to smaller sizes of aggregate (i.e., angularity of CA1<CA2) (Figure 4.2, Table 4.3). It can be seen from the figure that rhyolite CA1 aggregates had a high percentage of sub-rounded particles, therefore resulting in low angularity values (Figure 4.2).

4.4.1.2 Texture

The distribution of particles based on texture index is shown in Figures 4.4 through 4.6. Statistical analyses show that significant differences exist in the texture of

the different sizes of aggregates ($p<0.05$) (Table 4.3). A multi-comparison test shows that, in general, the larger sizes of aggregates were found to have a higher texture index (high roughness) compared to the smaller sizes of aggregates (Figures 4.4 through 4.6, Table 4.3). The order of texture for granite aggregates was found to be CA1>CA2>CA3. Likewise, for rhyolite and limestone aggregates, the order of texture was found to be CA1>CA3 and CA2>CA3, respectively. Both rhyolite and limestone aggregates did not show any significant difference between the texture of CA1 and CA2 sizes of aggregates (Figures 4.4 and 4.5, and Table 4.3). It can be observed that the effect of the size of the particles is significantly different on angularity and texture of the aggregates. In general, angularity did not change significantly with the size of an aggregate, whereas texture was found to decrease as the size of an aggregate decreased.

4.4.1.3 Form

Figures 4.7 through 4.9 show the distribution of particles based on the form index. Statistical analyses show that significant differences exist in the form of the different sizes of granite and rhyolite aggregates ($p<0.05$) (Table 4.3). A multi-comparison test identifies that smaller sizes of aggregates have a higher form index (i.e., elongated) compared to the larger sizes of aggregates (i.e., CA1<CA3; CA2<CA3) (Table 4.3). It can be observed from the figures that smaller sizes of aggregates have a higher percentage of semi-elongated and elongated particles, thus the higher form index (Figures 4.7 and 4.8). No significant difference was observed between CA1 and CA2 aggregates (Table 4.3). Limestone aggregates did not show any significant difference in form between the different sizes of aggregates ($p>0.05$) (Table 4.3 and Figure 4.9). The results show that any change in form with size depends upon type of aggregate.

4.4.1.4 Sphericity

The distribution of particles based on the sphericity index is shown in Figures 4.10 through 4.12.Statistical analyses show that significant differences exist in the sphericity of different sizes of aggregate ($p<0.05$) (Table 4.3). A multi-comparison test indicates that, in general, the larger size aggregates are found to be more cubical compared to the smaller size aggregates (Figures 4.10 through 4.12). The order of sphericity for granite, rhyolite, and limestone aggregates was observed to be CA1>CA2>CA3, CA1>CA2; and CA1>CA3, and CA1>CA3, respectively (Table 4.3).

4.4.2 Comparison of Granite, Rhyolite, and Limestone Aggregates

The shape parameters of granite, rhyolite, and limestone aggregates were compared. The null hypothesis was that the difference in the mean of the shape parameters for the three types of aggregate was equal to zero ($H_0 = \mu_{granite} = \mu_{rhyolite} = \mu_{limestone}$), and an alternative hypothesis (H_a) was that mean of shape parameters was not equal. The test was conducted at a significance level of 0.05.

4.4.2.1 Angularity

Figures 4.13 through 4.15 show the distribution of particles based on angularity index for CA1, CA2, and CA3 sizes of aggregates, respectively. The ANOVA results revealed that significant differences exist in the angularity of the different types of aggregates ($p<0.05$) (Table 4.4). A multi-comparison test identifies that rhyolite and limestone aggregates were more angular compared to granite aggregates (Figures 4.13 through 4.15, Table 4.4), contrary to what was expected. It is believed that the aggregate production process might have altered the angularity of the granite aggregates. No significant difference was found between the angularity of limestone and rhyolite aggregates (Figures 4.13 through 4.15, Table 4.4). It is important to note that the

Superpave angularity method (i.e., percentage fracture faces) measures the angularity of three aggregates as 100/100, indicating the all the aggregates are equally angular; however, the AIMS data identifies that subtle differences exist in the angularity of the aggregates.

4.4.2.2 Texture

Figures 4.16 through 4.18 show the distribution of the particles based on the texture index. Statistical analyses show that significant differences exist in the texture of the different types of aggregates ($p<0.05$) (Figures 4.16 through 4.18, Table 4.4). For all sizes (i.e., CA1, CA2, CA3), granite aggregates were found to have the highest texture index compared to rhyolite and limestone aggregates. On the other hand, no significant difference was found between the texture of rhyolite and limestone aggregates, except for CA1 size, where the limestone aggregates showed more texture when compared to the rhyolite aggregates (Figures 4.16 through 4.18, Table 4.4). Although the granite aggregates had the lowest angularity index, their texture is significantly higher than the rhyolite and limestone aggregates. Therefore, the selection of aggregates merely based on angularity may not be appropriate for quality control and quality assurance purposes.

4.4.2.3 Form

Figures 4.19 through 4.21 show the distribution of particles based on form index for CA1, CA2, and CA3 sizes of aggregates, respectively. For CA1 and CA2 aggregates, a significant difference was found in the form of the different types of aggregates ($p<0.05$) (Figures 4.19 through 4.21, Table 4.4). A multi-comparison test identifies that rhyolite and limestone aggregates had high form indices compared to granite aggregates**,** indicating that granite aggregates are less elongated compared to the other two. No significant difference was observed between the forms of limestone and rhyolite

aggregates. For CA3 aggregates, no significant difference was observed in the form of the different types of aggregates, indicating that smaller sizes of aggregate may have the same form irrespective of aggregate type (Figures 4.19 through 4.21, Table 4.4).

4.4.2.4 Sphericity

Figures 4.22 through 4.24 are the distribution of particles based on the sphericity index. In general, for larger size aggregates (i.e., CA1 and CA2), granite and rhyolite aggregates were found to have a higher sphericity index (i.e., more cubical particles) compared to limestone aggregates (Figures 4.22 through 4.24, Table 4.4). Similar to the form, the sphericity index of the smaller size aggregate (CA3) was observed to be the same for the three types of aggregates (Table 4.4), indicating that smaller size aggregates may have similar sphericity irrespective of the aggregate type.

4.4.2.5 Distribution of Flat and Elongated Particles

Figures 4.25 through 4.27 show the distribution of F&E particles for CA1, CA2, and CA3 aggregates, respectively. It can be seen from these figures that all types of aggregate had less than 10% of particles with maximum to minimum dimensions with a ratio of 5:1, indicating that the aggregates pass the Superpave requirement (i.e., F&E particles<10%). In general, limestone aggregates had a higher percentage of elongated particles compared to granite and rhyolite aggregates. Similarly, the larger size aggregates (CA1 and CA2) had 3:1 particles less than 20%. On the other hand, CA3 aggregates had more 20% particles with a 3:1 dimension, thus failing the limiting criterion (i.e., F&E<20%) (Vavrik et al., 1999). The plot provides a wealth of information for characterizing the aggregates for quality control purposes, which cannot be obtained using the Superpave method.

4.4.3 Ranking of Aggregates

The ranking of aggregates was done based on the value of the composite shape index (CI) factor (Pan et al., 2006). A similar approach is used by Pan et al. (2006) in quantifying the effect of coarse aggregates morphology on permanent deformation behavior of asphalt mix. Equation (4.1) was used to calculate CI for three different types of aggregates. This equation uses mean shape parameter (a_i) of particular sizes of aggregates (i.e., CA1, CA2, and CA3) (Table 4.2) and percentage retained particles (x_i) on respective sieves (Table 4.1). CI for shape parameters were named as: composite angularity index (CAI), composite form index (CFI), composite texture index (CTI), and composite sphericity index (CSI).

$$CI = \frac{\sum_{i=1}^{n}[(a_i)(x_i)]}{\sum_{i=1}^{n} x_i} \tag{4.1}$$

where,

CI = composite shape index parameter (i.e., CAI, CFI, CTI, and CSI),

a_i = mean shape parameter for a selected sieve size, and

x_i = percentage retained aggregates on selected sieve sizes.

The following example shows the calculation of CAI, CFI, CTI, and CSI factors for granite aggregates. Table 4.5 summarizes 'a_i' and 'x_i' values for this aggregate. The CAI, CFI, CTI, and CSI values for this aggregates are found to be 10.56, 7.31, 144, and 0.70, respectively, as shown in Equations (4.2) through (4.5) and in Table 4.5. Similar CI values were calculated for rhyolite and limestone aggregates (Table 4.6).

$$CAI = \frac{[(8\times 9)+(21\times 9.7)+(49\times 10)]}{(8+21+49)} = 9.79 \quad (4.2)$$

$$CTI = \frac{[(8\times 392)+(21\times 355)+(49\times 259)]}{(8+21+49)} = 298.7 \quad (4.3)$$

$$CFI = \frac{[(8\times 6.47)+(21\times 6.93)+(49\times 7.61)]}{(8+21+49)} = 7.3 \quad (4.4)$$

$$CSI = \frac{[(8\times 0.76)+(21\times 0.72)+(49\times 0.68)]}{(8+21+49)} = 0.70 \quad (4.5)$$

4.4.3.1 Angularity Criterion

The rhyolite aggregates had the highest CAI, followed by limestone and granite aggregates (i.e., $CAI_{rhyolite}$>$CAI_{limestone}$>$CAI_{granite}$) (Table 4.5). The angular aggregates are expected to produce better aggregate interlock, and consequently a more stable aggregate structure. Thus, the rhyolite aggregate was ranked first followed by limestone and granite aggregates (Table 4.5).

4.4.3.2 Texture Criterion

CTI for the granite aggregates was found to be the highest, followed by rhyolite and limestone aggregates (i.e., $CTI_{granite}$>$CTI_{rhyolite}$>$CTI_{limestone}$) (Table 4.6). The rough surface particles are helpful in developing better resistance to shear. Based on this criterion, the granite aggregate was ranked first, followed by rhyolite and limestone (Table 4.6).

4.4.3.3 Form Criterion

CFI for the granite aggregates was found to be the lowest, followed by rhyolite and limestone aggregates, indicating that the granite aggregates had less elongated particles compared to the others (i.e., $CFI_{limestone}>CFI_{rhyolite}>CFI_{granite}$) (Table 4.6). Therefore, granite was ranked first, followed for rhyolite and limestone aggregates (Table 4.6).

4.4.3.4 Sphericity Criterion

CSI of the granite aggregates was observed to be the highest, followed by rhyolite and limestone aggregates, indicating that the granite aggregates had more cubical particles compared to the other two (i.e., $CSI_{granite}>CSI_{rhyolite}>CSI_{limestone}$) (Table 4.6). The cubical particles are considered to create a better aggregate interlock. Thus, based on the sphericity criteria, the granite aggregates was ranked first, followed by rhyolite and limestone aggregates (Table 4.6).

4.4.3.5 Overall Rank

As discussed above, the rank of the aggregates depends upon the relative value of CI (i.e., CAI, CTI, CFI, and CSI). In the present study, the overall rank of the aggregates was decided based on the number of the highest ranks given to them on the basis of CI. It can be seen that the granite aggregates received the highest rank based on texture, form, and sphericity criteria; therefore, it was ranked first, followed by rhyolite and limestone aggregates (i.e., granite>rhyolite>limestone) (Table 4.6). It is recommended that the ranking of the aggregates be verified by conducting the performance tests (i.e., rutting and fatigue distresses) on asphalt mixes composed of these aggregates.

4.5 Summary of Results

The present study was undertaken to compare shape parameters (i.e., angularity, texture, form, and sphericity) of different types and sizes of coarse aggregates. The following conclusions can be drawn from the results and discussion presented in this chapter.

(1) No significant difference was observed in the angularity of difference sizes of aggregates.

(2) Larger size particles were found to be rougher and more cubical compared to the smaller size aggregates (i.e., high texture, low form, and high sphericity), indicating that the particles become smooth and elongated as their size decreases.

(3) A comparison of the different types of aggregates shows that the granite aggregate was rougher (high texture) and more cubical (low form and high sphericity) compared to rhyolite and limestone aggregates.

(4) The rhyolite and limestone aggregates were observed to be more angular compared to granite aggregates, contrary to what was expected. It is believed that the aggregate production process might have altered the angularity of granite aggregates. No difference was observed in the angularity of limestone and rhyolite.

(5) The rank of the aggregates was decided based on the composite shape index factor. The overall rank sequence for the aggregates was found to be as follows: granite>rhyolite>limestone, indicating that the performance of granite aggregates would be better compared to the other two aggregates.

It is recommended that performance tests be conducted on asphalt mixes prepared with different types of aggregates. The information obtained from the AIMS can be utilized to develop an aggregate library where shape properties of different source and types of aggregates can be stored for quality assurance and quality control purposes. It is expected that this study will be helpful in understanding differences in the shape parameters of aggregates.

Table 4.1 Aggregate Source, Gradation, and Test Results

	Aggregate 1	Aggregate 2	Aggregate 3
Aggregates Type	Granite	Rhyolite	Limestone
Aggregates Source	Martin Marietta@Snyder Pit No. 3802 (OK)	Hanson@Davis Pit No.5008 (OK)	Martin Marietta@Davis Pit No. 5005 (OK)
Gradation of Aggregates (% Passing)			
Sieve Size (mm)	Granite	Rhyolite	Limestone
25	100	100	100
19	100	100	100
12.5	92	91	89
9.5	71	49	54
4.75	22	1	3
2.36	5	1	1
1.18	3	1	1
0.6	2	1	1
0.3	2	1	1
0.15	2	1	1
0.075	1.2	0.5	0.4
Superpave Test	Granite	Rhyolite	Limestone
F&E particles (%)	0	0	0
Fractured Faces	100/100	100/100	100/100
LA Abrasion (%)	20	15	24
Micro-Deval (%)	2.7	7.9	9.7
Durability Index	93	80	81

Table 4.2 AIMS Test Results for All Types of Aggregates

Radius Angularity							
Aggregates	Size	Granite		Rhyolite		Limestone	
Type	(mm)	Mean	Stdev.	Mean	Stdev.	Mean	Stdev.
CA1	P19.5 - R12.5	9.0	3.0	10.2	3.6	10.5	3.7
CA2	P12.5 - R9.5	9.7	3.3	11.4	3.5	11.5	3.8
CA3	P9.5 - R4.75	10.0	3.4	11.2	3.5	10.8	3.2
Texture							
Aggregates	Size	Granite		Rhyolite		Limestone	
Type	(mm)	Mean	Stdev.	Mean	Stdev.	Mean	Stdev.
CA1	P19.5 - R12.5	392	90	195	69	220	71
CA2	P12.5 - R9.5	355	86	198	63	206	82
CA3	P9.5 - R4.75	259	73	152	52	142	60
Form							
Aggregates	Size	Granite		Rhyolite		Limestone	
Type	(mm)	Mean	Stdev.	Mean	Stdev.	Mean	Stdev.
CA1	P19.5 - R12.5	6.47	1.38	7.19	1.38	7.65	2.15
CA2	P12.5 - R9.5	6.93	1.55	7.50	1.41	7.82	2.51
CA3	P9.5 - R4.75	7.61	2.08	8.11	1.85	7.91	2.08
Sphericity							
Aggregates	Size	Granite		Rhyolite		Limestone	
Type	(mm)	Mean	Stdev.	Mean	Stdev.	Mean	Stdev.
CA1	P19.5 - R12.5	0.76	0.09	0.76	0.09	0.70	0.11
CA2	P12.5 - R9.5	0.72	0.10	0.68	0.10	0.68	0.10
CA3	P9.5 - R4.75	0.68	0.11	0.68	0.10	0.65	0.10

P19-R12.5 : Aggregates Passing on a 19 mm sieve and Retained on a 12.5 mm sieve
P12.5-R9.5 : Aggregates Passing on a 12.5 mm sieve and Retained on a 9.5 mm sieve
P9.5-R4.75 : Aggregates Passing on a 9.5 mm sieve and Retained on a 4.75 mm sieve

Table 4.3 Statistical Summary of Comparison of Different Sizes of Aggregates

ANOVA- One way Statistics Summary						
Shape	Granite		Rhyolite		Limestone	
Parameter	p	Sig.	p	Sig.	p	Sig.
Angularity	0.060	No	0.032	Yes	0.118	No
Texture	0.000	Yes	0.000	Yes	0.000	Yes
Form	0.000	Yes	0.000	Yes	0.712	No
Sphericity	0.000	Yes	0.000	Yes	0.001	Yes

Yes : Sig. difference exists, multi-comparison test required
No : Sig. difference does not exist, multi-comparison test not required

ANOVA-Multi-Comparison Statistics Summary							
Shape	Size	Granite		Rhyolite		Limestone	
Parameter	Comparison	Sig.	Remark	Sig.	Remark	Sig.	Remark
Angularity	CA1 vs. CA2	NA		Yes	CA1<CA2	NA	
	CA1 vs. CA3			No			
	CA2 vs. CA3			No			
Texture	CA1 vs. CA2	Yes	CA1>CA2	No	-	No	-
	CA1 vs. CA3	Yes	CA1> CA3	Yes	CA1>CA3	Yes	CA1>CA3
	CA2 vs. CA3	Yes	CA2>CA3	Yes	CA2>CA3	Yes	CA2>CA3
Form	CA1 vs. CA2	No	-	No	-	NA	
	CA1 vs. CA3	Yes	CA1<CA3	Yes	CA1<CA3		
	CA2 vs. CA3	Yes	CA2<CA3	Yes	CA2<CA3		
Sphericity	CA1 vs. CA2	Yes	CA1>CA2	Yes	CA1>CA2	No	-
	CA1 vs. CA3	Yes	CA1>CA3	Yes	CA1>CA3	Yes	CA1>CA3
	CA2 vs. CA3	Yes	CA2>CA3	No		No	

NA: Not Applicable

Table 4.4 Statistical Summary of Comparison of Different Types of Aggregates

ANOVA- Statistics Summary						
Shape	CA1		CA2		CA3	
Parameter	p	Sig.	p	Sig.	p	Sig.
Angularity	0.002	Yes	0.000	Yes	0.028	Yes
Texture	0.000	Yes	0.000	Yes	0.000	Yes
Form	0.000	Yes	0.002	Yes	0.174	No
Sphericity	0.000	Yes	0.004	Yes	0.076	No

Yes : Sig. difference exists, multi-comparison test required
No : Sig. difference does not exist, multi-comparison test not required

Multi-Comparison Statistics Summary							
Shape	Aggregate	CA1		CA2		CA3	
Parameter	Comparison	Sig.	Remark	Sig.	Remark	Sig.	Remark
Angularity	G vs R	Yes	G<R	Yes	G<R	Yes	G<R
	G vs L	Yes	G<L	Yes	G<L	No	-
	R vs L	No	-	No	-	No	-
Texture	G vs R	Yes	G>R	Yes	G>R	Yes	G>R
	G vs L	Yes	G>L	Yes	G>L	Yes	G>L
	R vs L	Yes	L>R	No	-	No	-
Form	G vs R	Yes	G<R	No	-	NA	
	G vs L	Yes	G<L	Yes	G<L		
	R vs L	No	-	No	-		
Sphericity	G vs R	No	-	Yes	G>R	NA	
	G vs L	Yes	G>L	Yes	G>L		
	R vs L	Yes	R>L	No	-		

G: Granite; R: Rhyolite; L: Limestone; NA: Not Applicable

Table 4.5 Calculation of Composite Shape Parameter

Granite					
Aggregate Size	Particle (x_i) %	Mean Value of Shape Parameters (a_i)			
		Angularity	Texture	Form	Sphericity
CA1	8	9.0	392	6.47	0.76
CA2	21	9.7	355	6.93	0.72
CA3	49	10.0	259	7.61	0.68
Composite Index		CAI	CTI	CFI	CSI
		9.79	298.7	7.3	0.70

Table 4.6 Composite Shape Parameters and Ranking of Aggregates

Aggregate	CAI	CTI	CFI	CSI
Granite	9.79	298.7	7.3	0.70
Rhyolite	11.16	175.1	7.7	0.69
Limestone	11.03	173.8	7.8	0.67

Ranking of Aggregates					
Aggregate	Angularity	Texture	Form	Sphericity	Overall
Granite	3	1	1	1	1
Rhyolite	1	2	2	2	2
Limestone	2	3	3	3	3

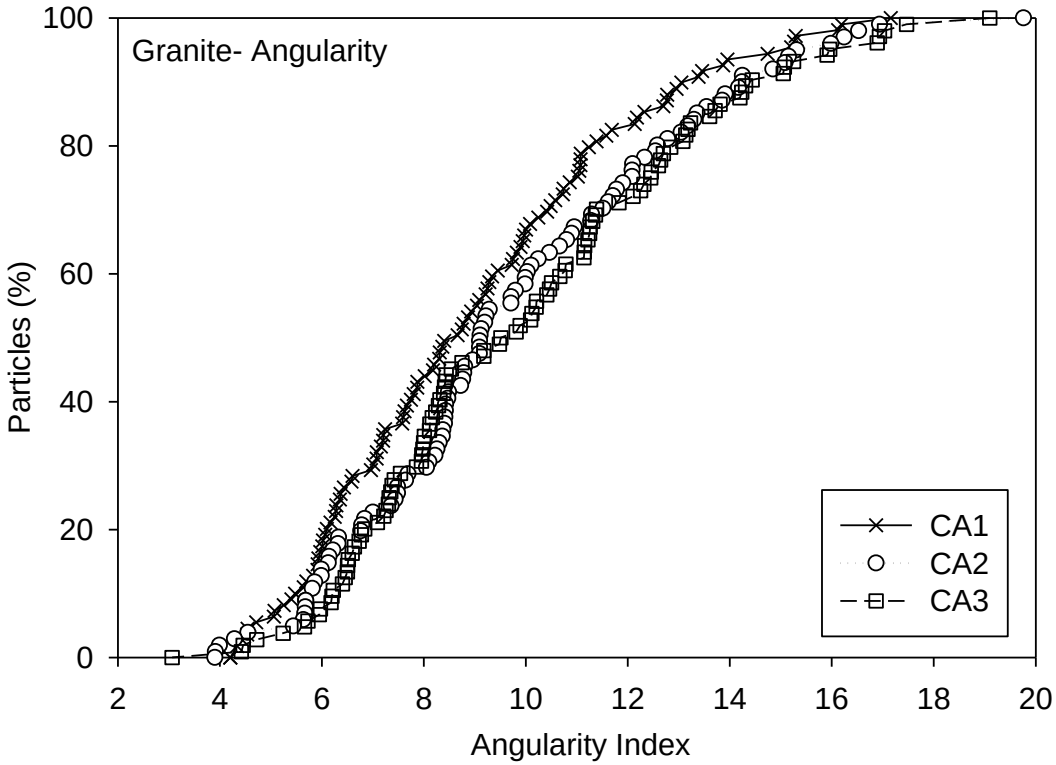

Figure 4.1 Comparison of Angularity for Different Sizes of Granite Aggregates

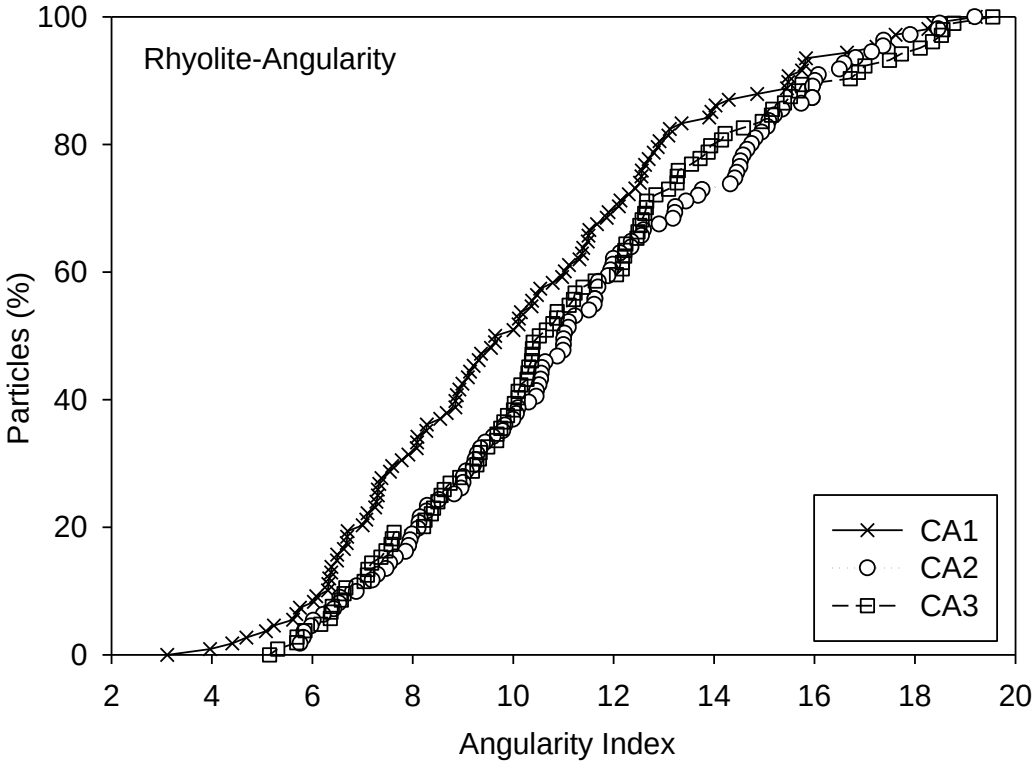

Figure 4.2 Comparison of Angularity for Different Sizes of Rhyolite Aggregates

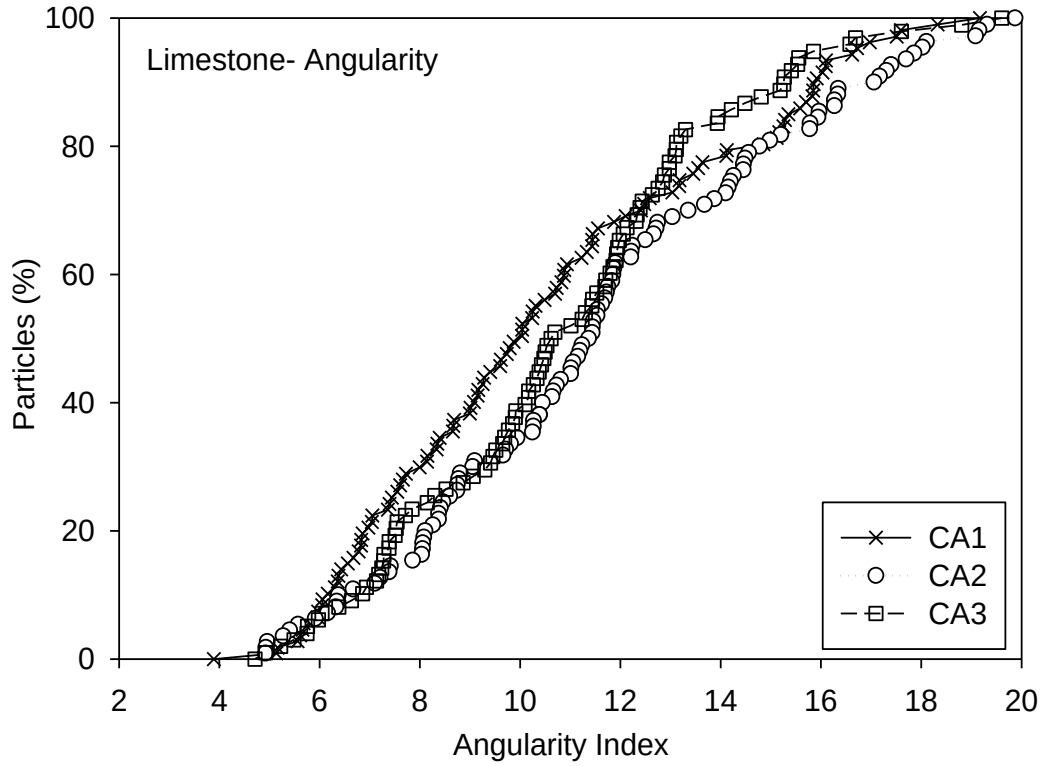

Figure 4.3 Comparison of Angularity for Different Sizes of Limestone Aggregates

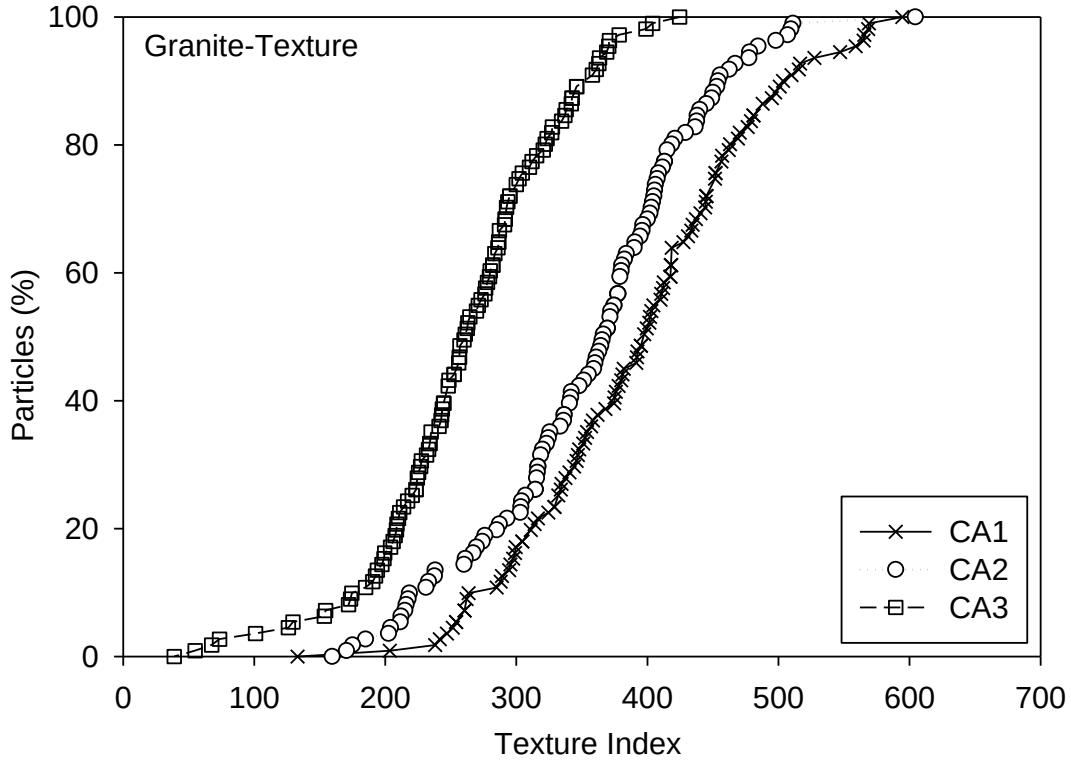

Figure 4.4 Comparison of Texture for Different Sizes of Granite Aggregates

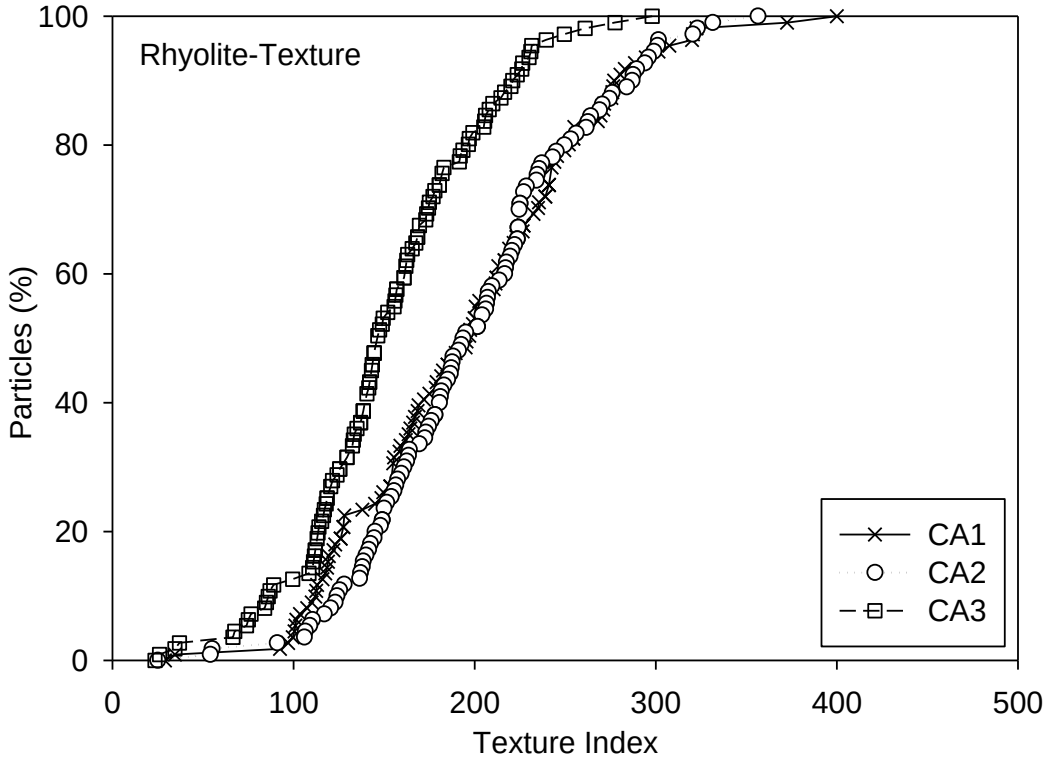

Figure 4.5 Comparison of Texture for Different Sizes of Rhyolite Aggregates

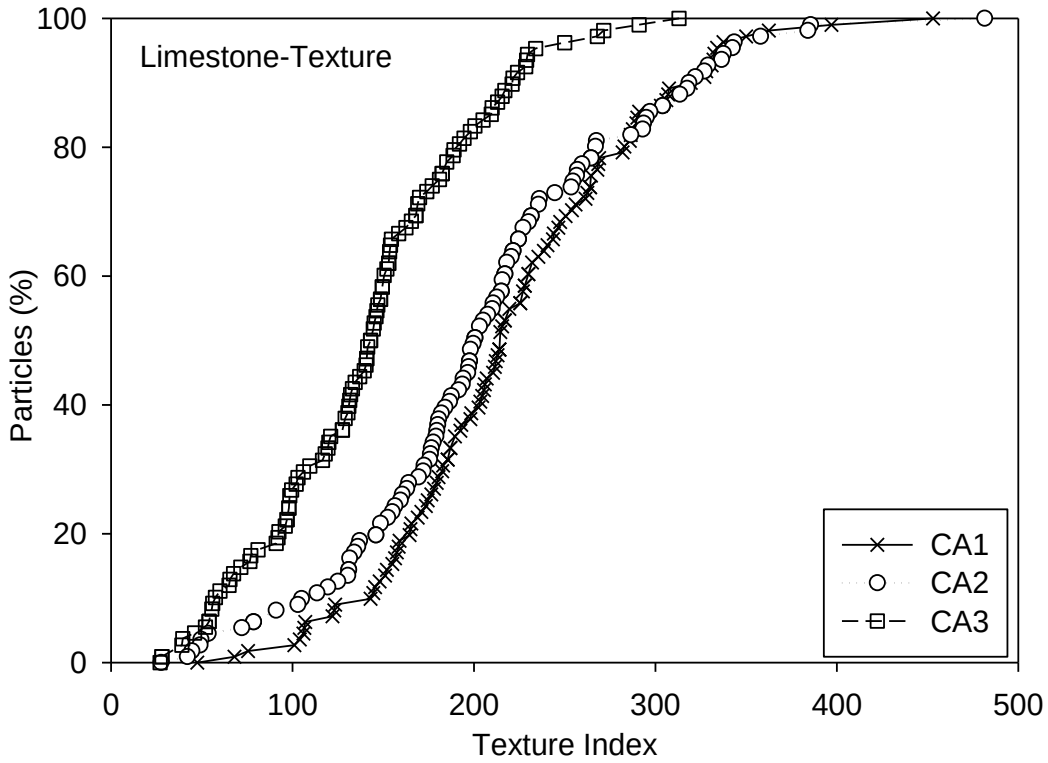

Figure 4.6 Comparison of Texture for Different Sizes of Limestone Aggregates

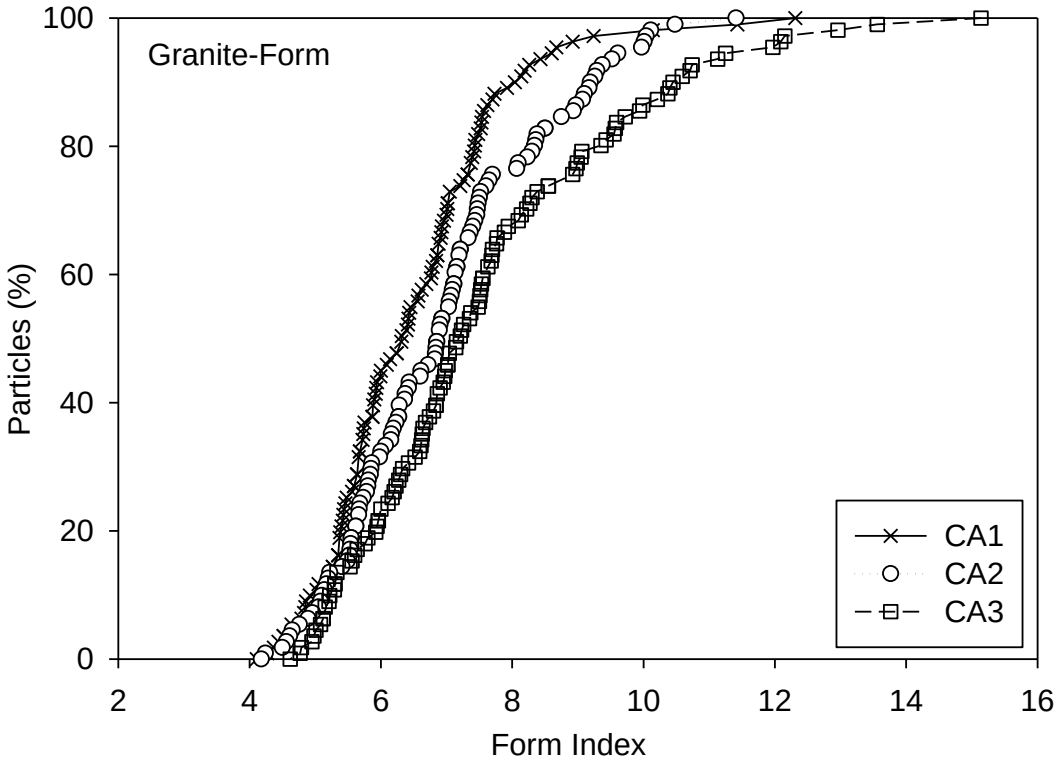

Figure 4.7 Comparison of Form for Different Sizes of Granite Aggregates

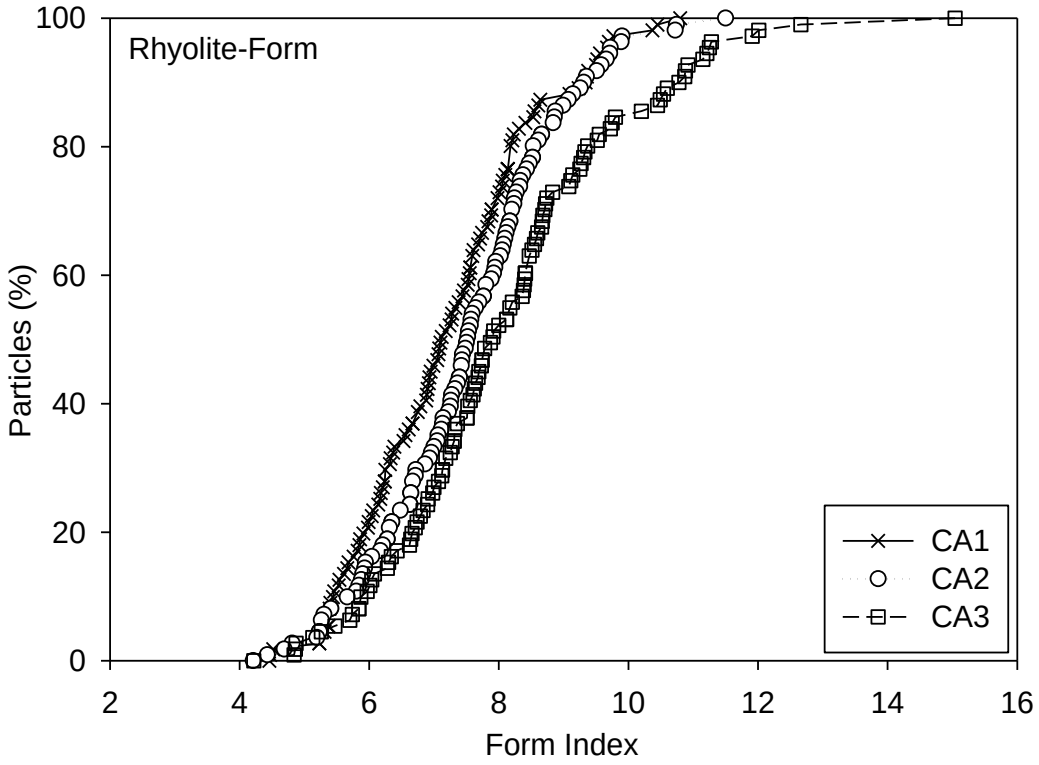

Figure 4.8 Comparison of Form for Different Sizes of Rhyolite Aggregates

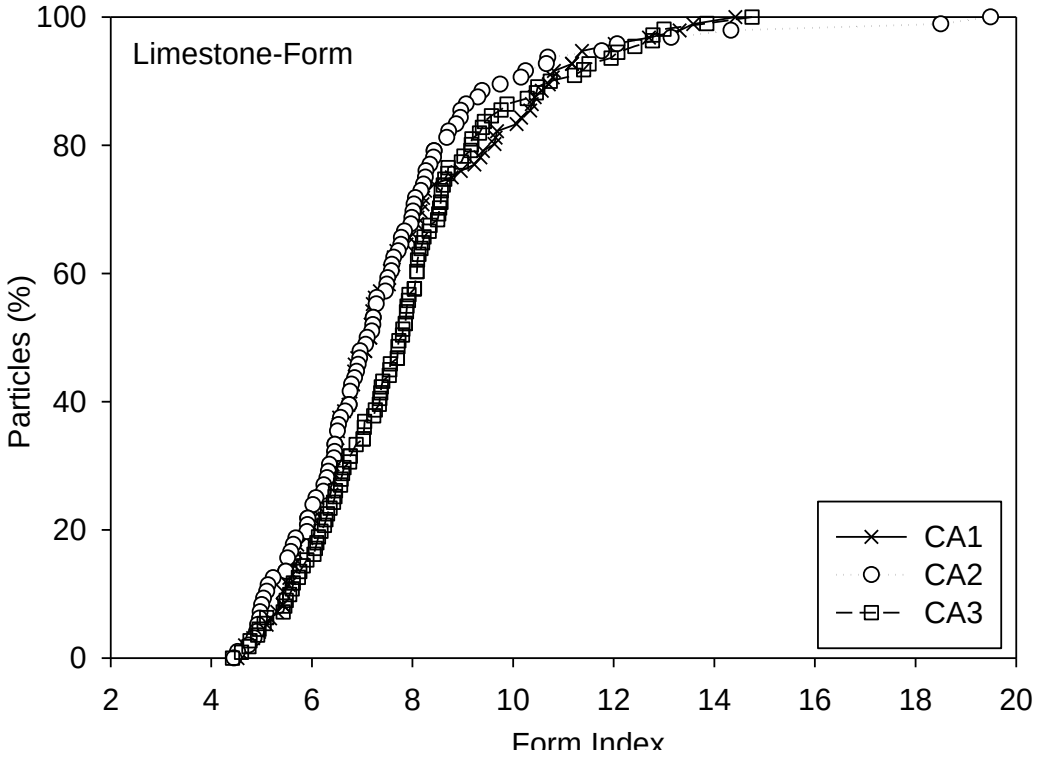

Figure 4.9 Comparison of Form for Different Sizes of Limestone Aggregates

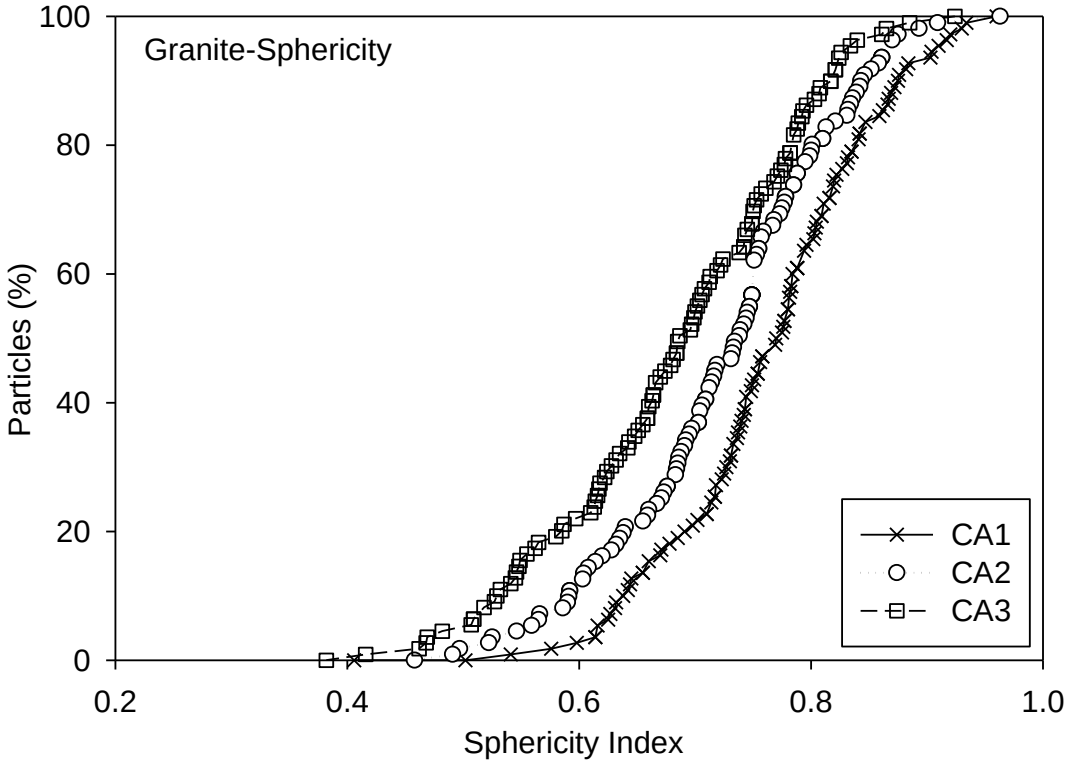

Figure 4.10 Comparison of Sphericity for Different Sizes of Granite Aggregates

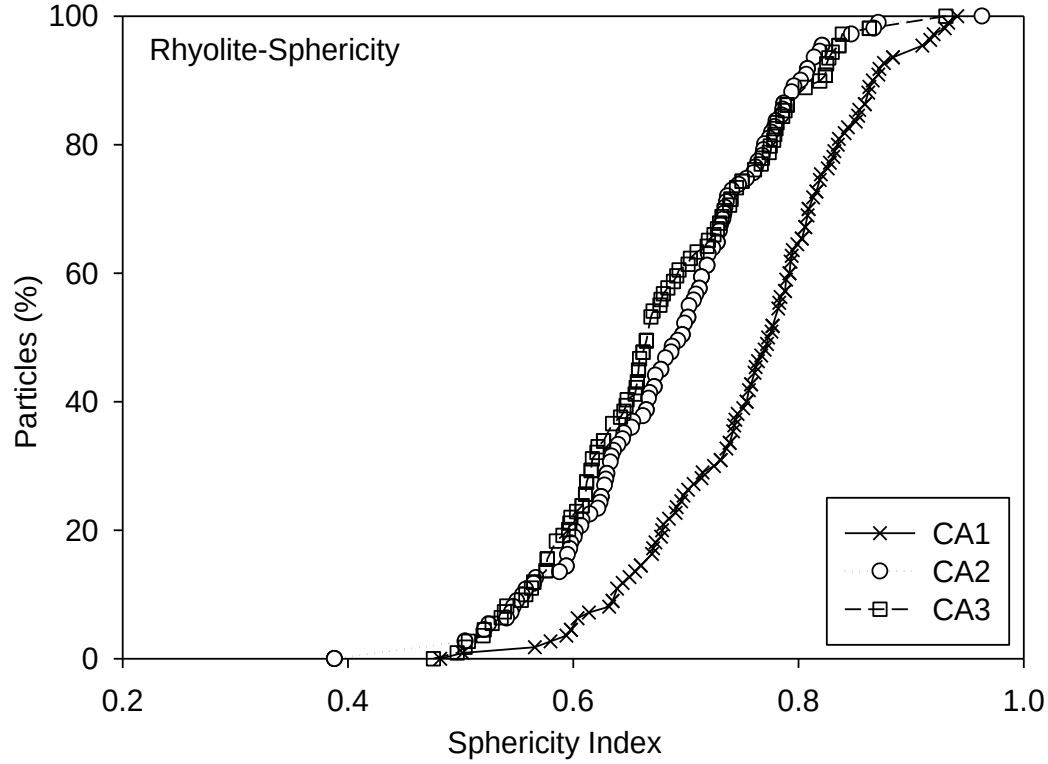

Figure 4.11 Comparison of Sphericity for Different Sizes of Rhyolite Aggregates

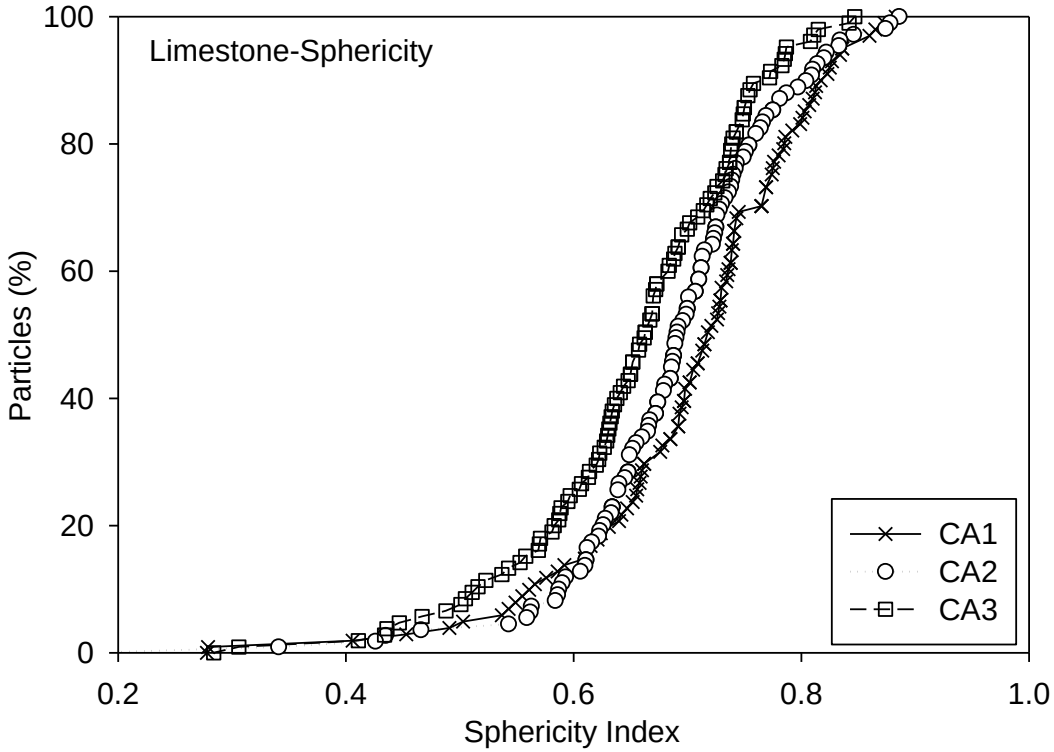

Figure 4.12 Comparison of Sphericity for Different Sizes of Limestone Aggregates

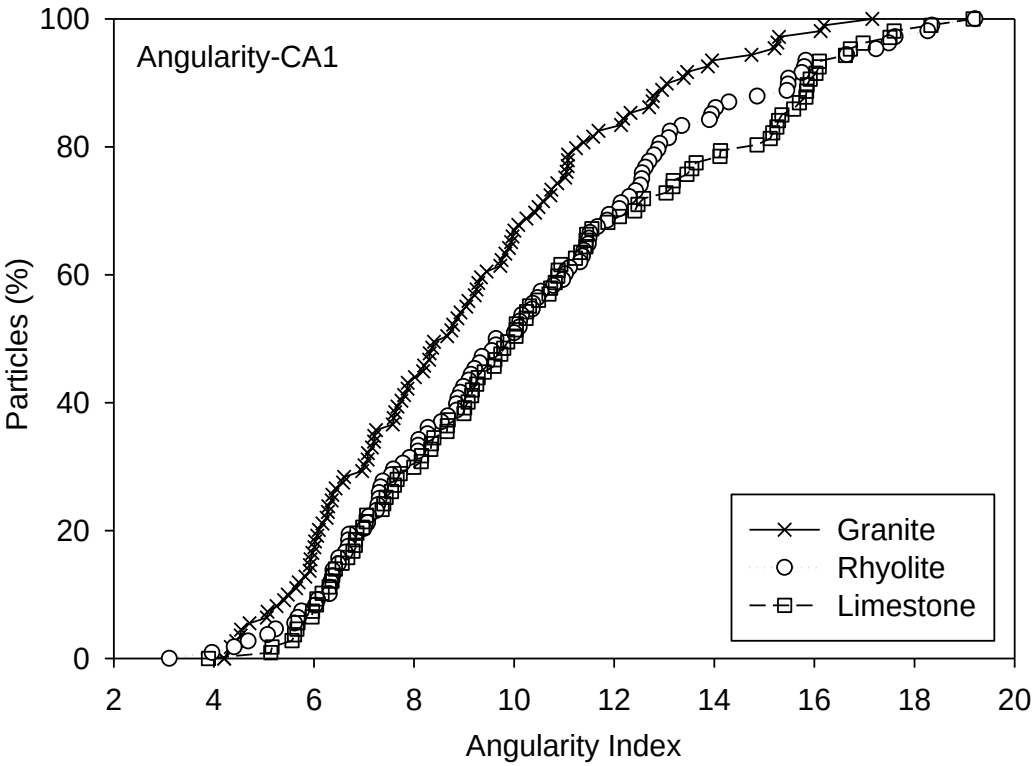

Figure 4.13 Comparison of Angularity for Different Types of CA1 Aggregates

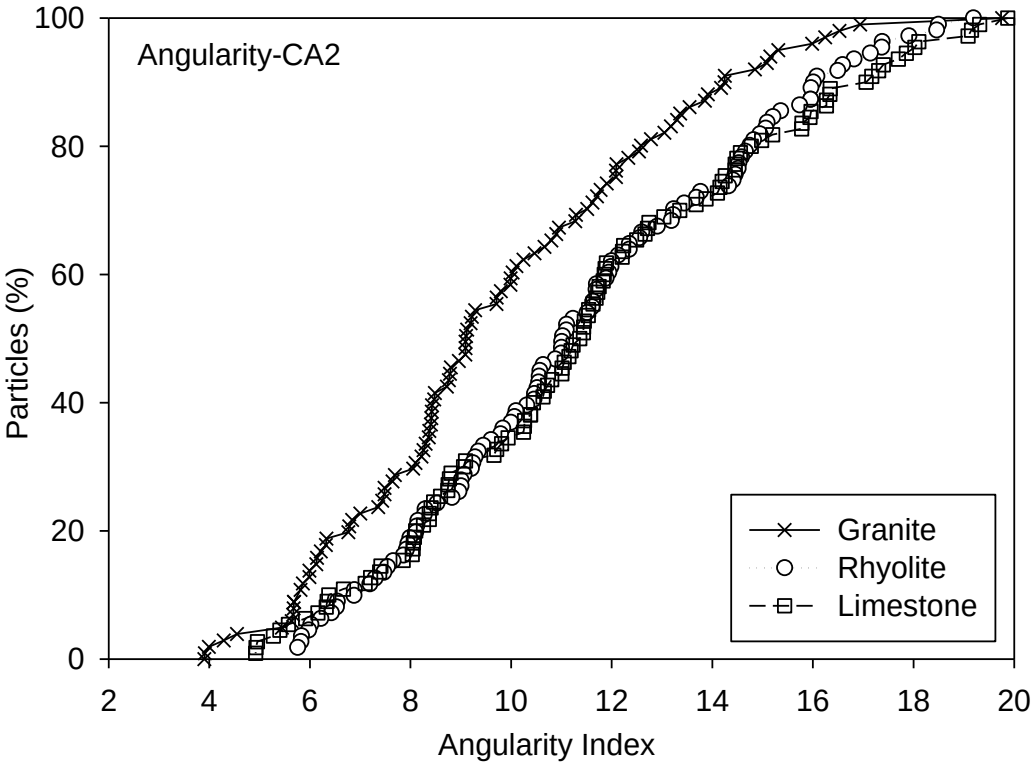

Figure 4.14 Comparison of Angularity for Different Types of CA2 Aggregates

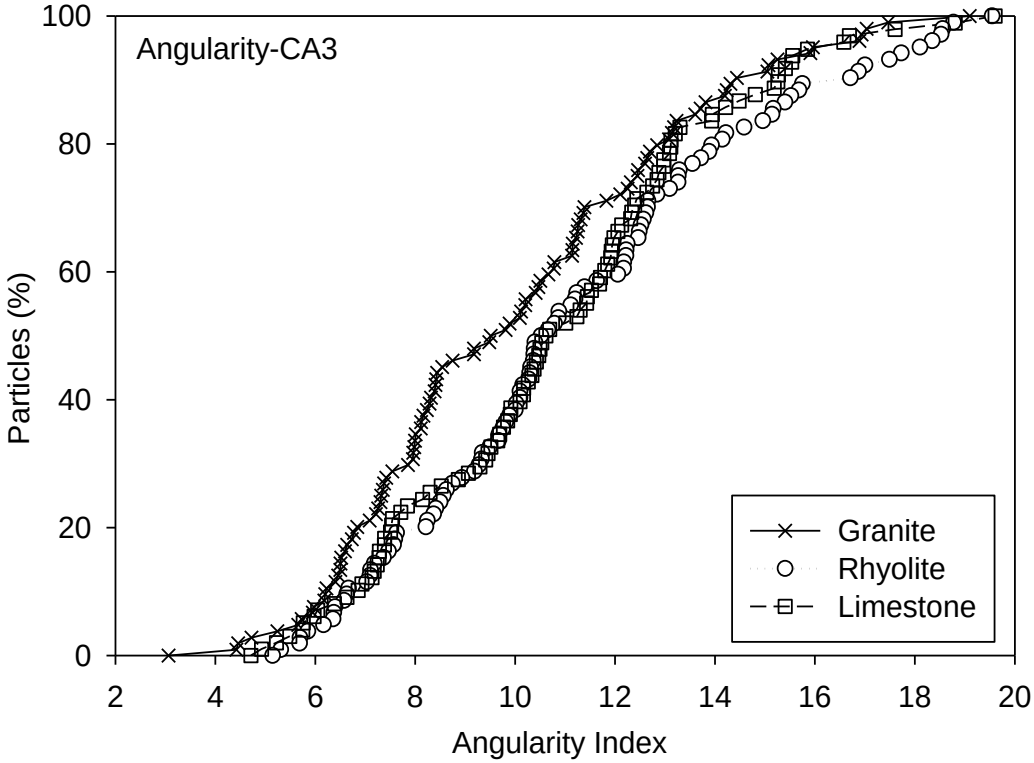

Figure 4.15 Comparison of Angularity for Different Types of CA3 Aggregates

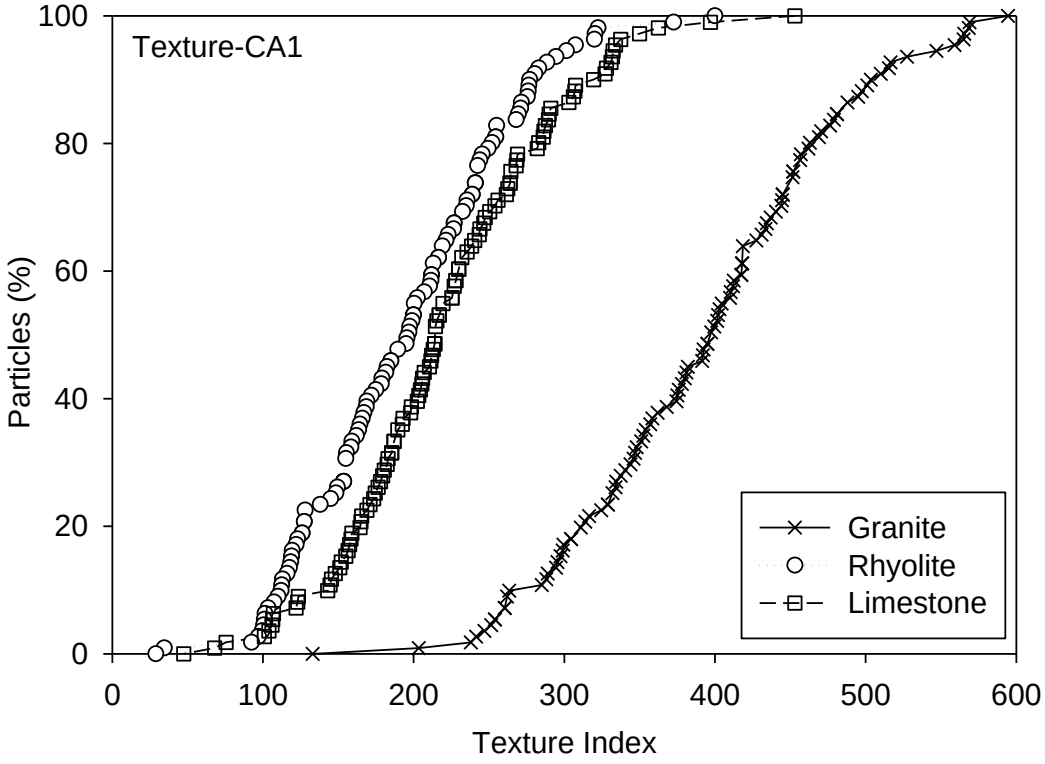

Figure 4.16 Comparison of Texture for Different Types of CA1 Aggregates

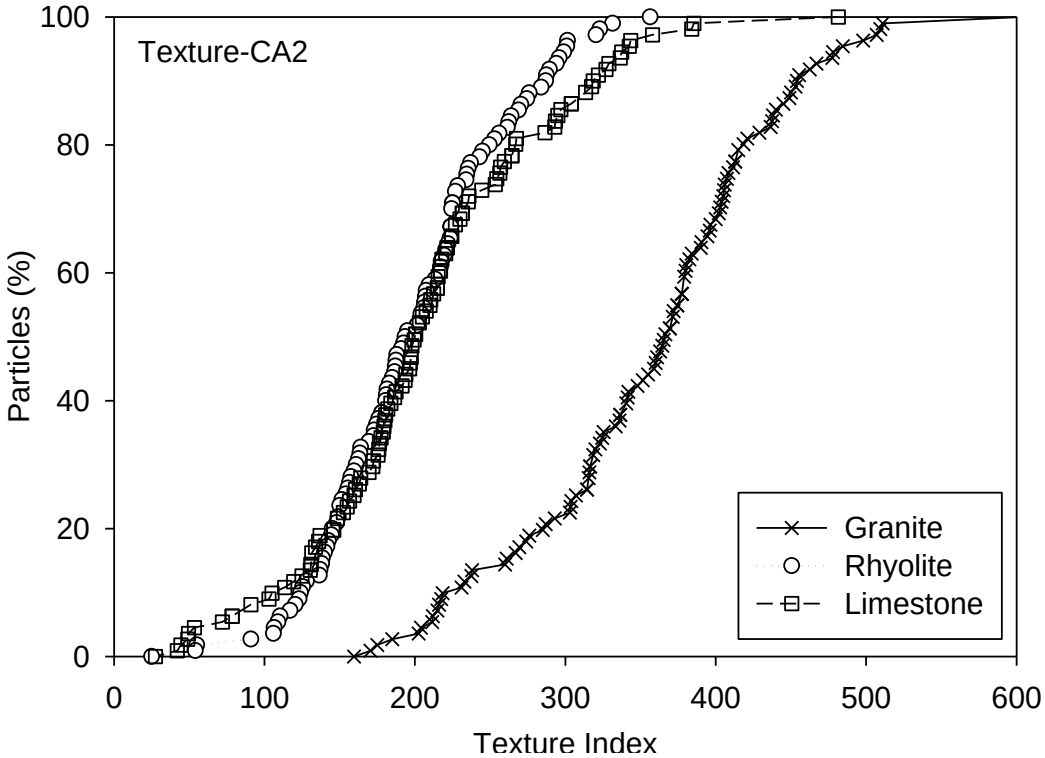

Figure 4.17 Comparison of Texture for Different Types of CA2 Aggregates

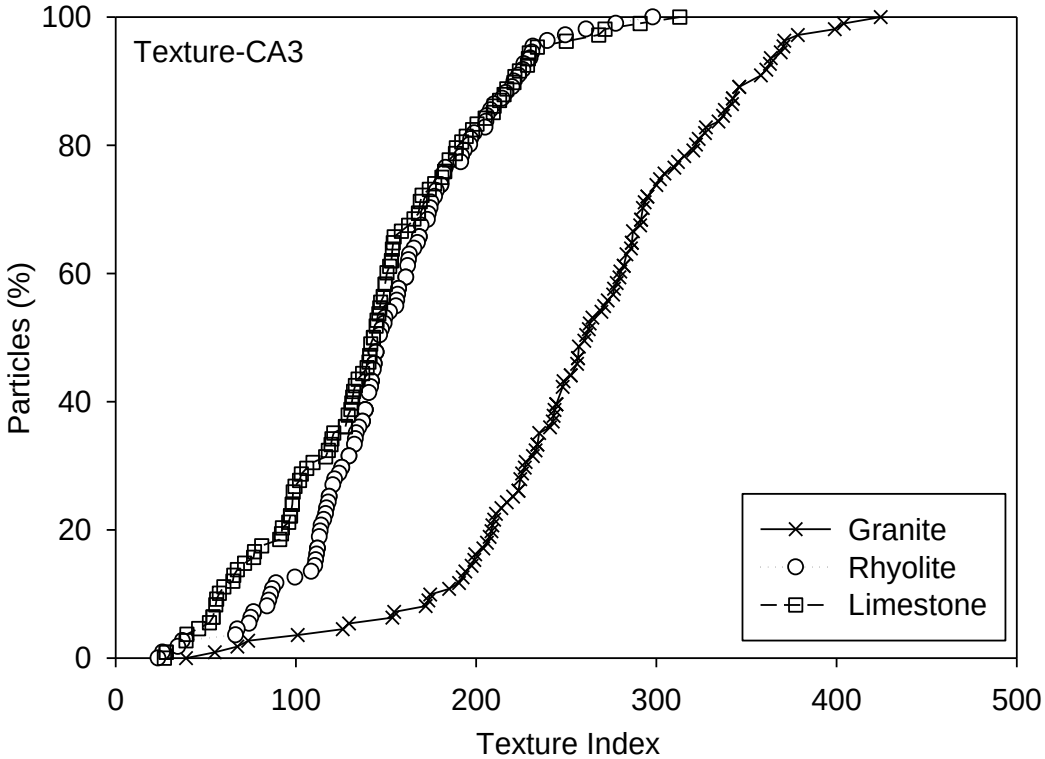

Figure 4.18 Comparison of Texture for Different Types of CA3 Aggregates

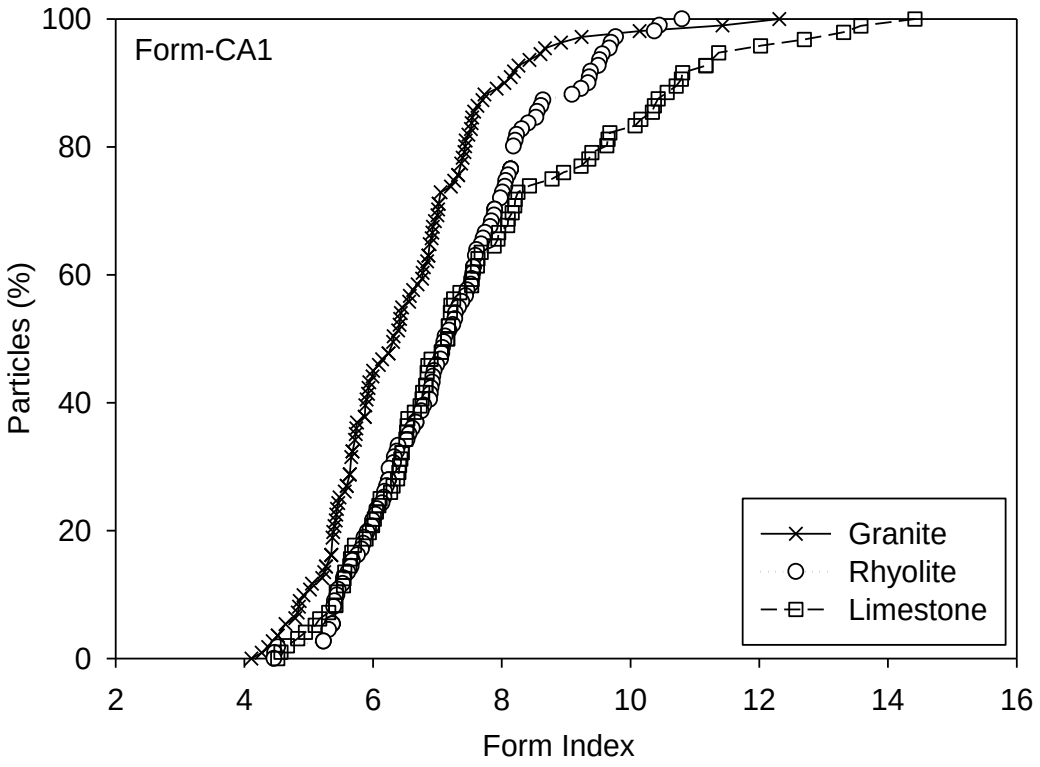

Figure 4.19 Comparison of Form for Different Types of CA1 Aggregates

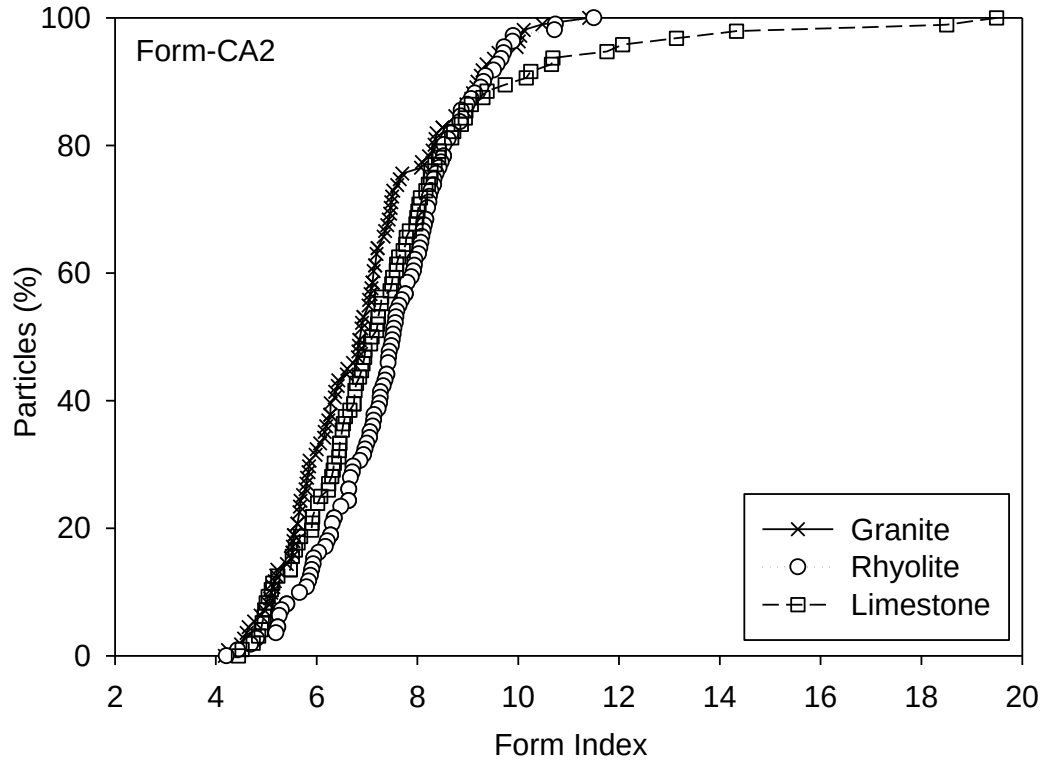

Figure 4.20 Comparison of Form for Different Types of CA2 Aggregates

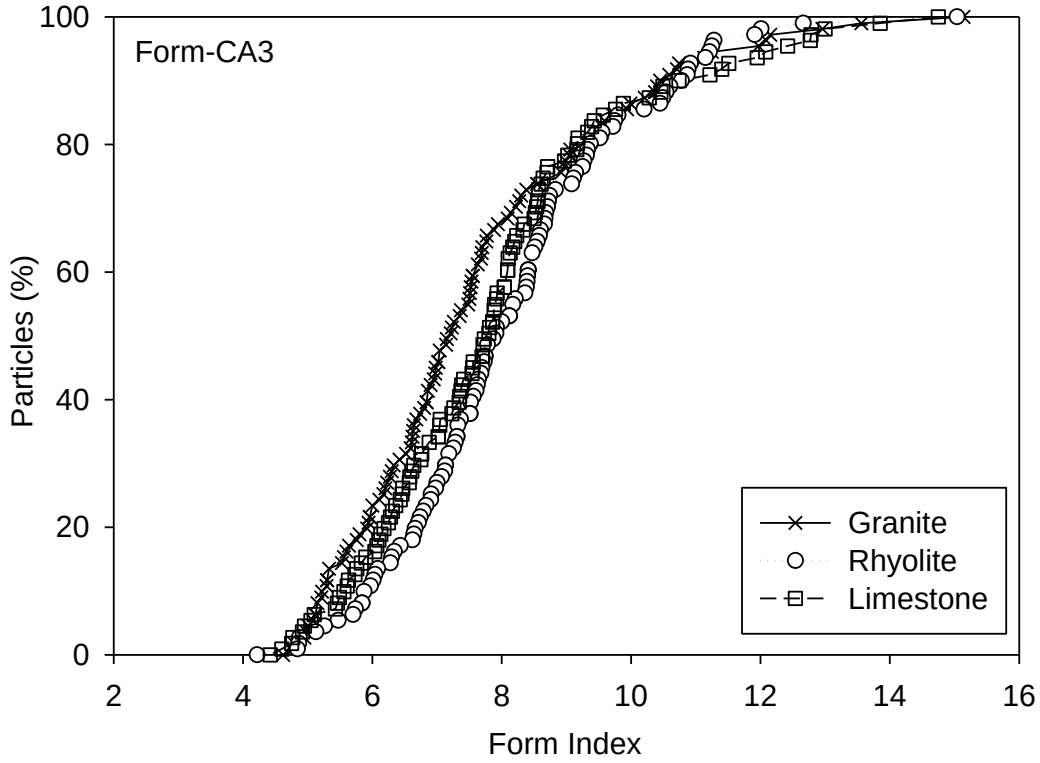

Figure 4.21 Comparison of Form for Different Types of CA3 Aggregates

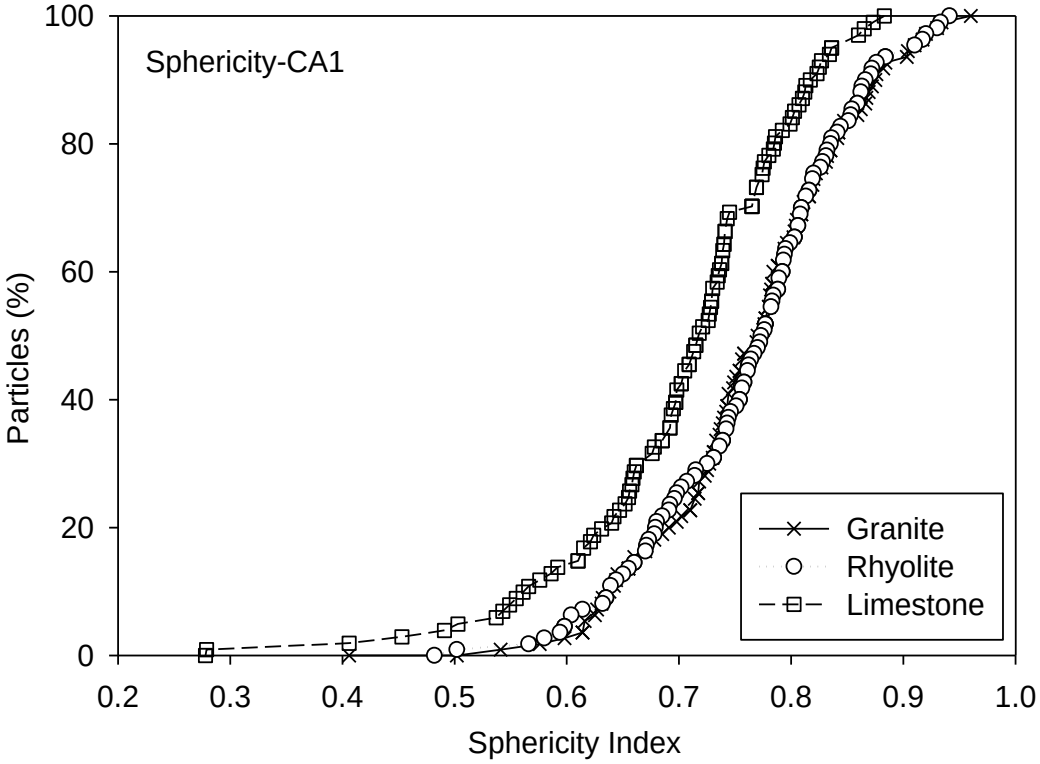

Figure 4.22 Comparison of Sphericity for Different Types of CA1 Aggregates

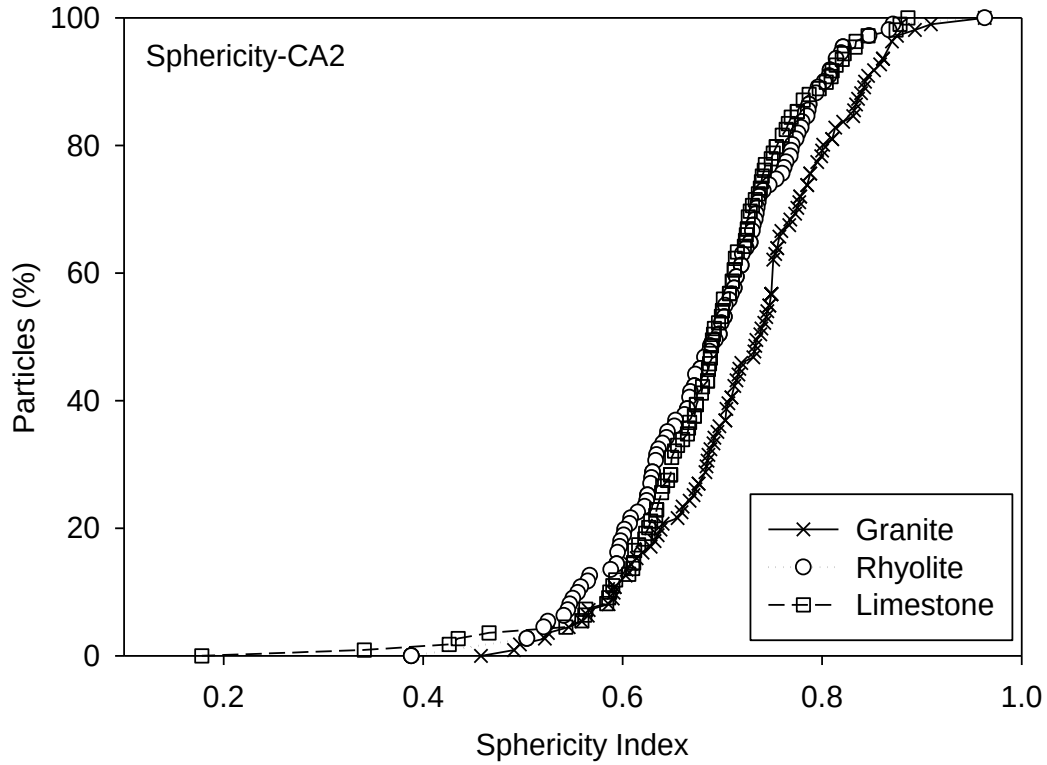

Figure 4.23 Comparison of Sphericity for Different Types of CA2 Aggregates

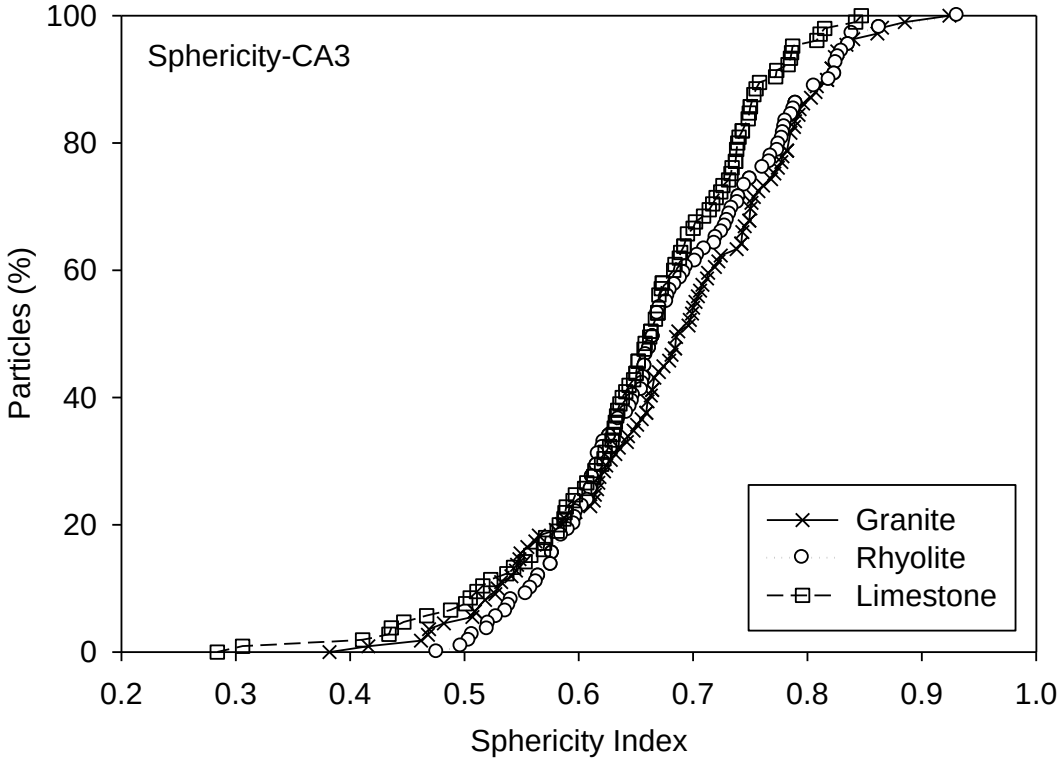

Figure 4.24 Comparison of Sphericity for Different Types of CA3 Aggregates

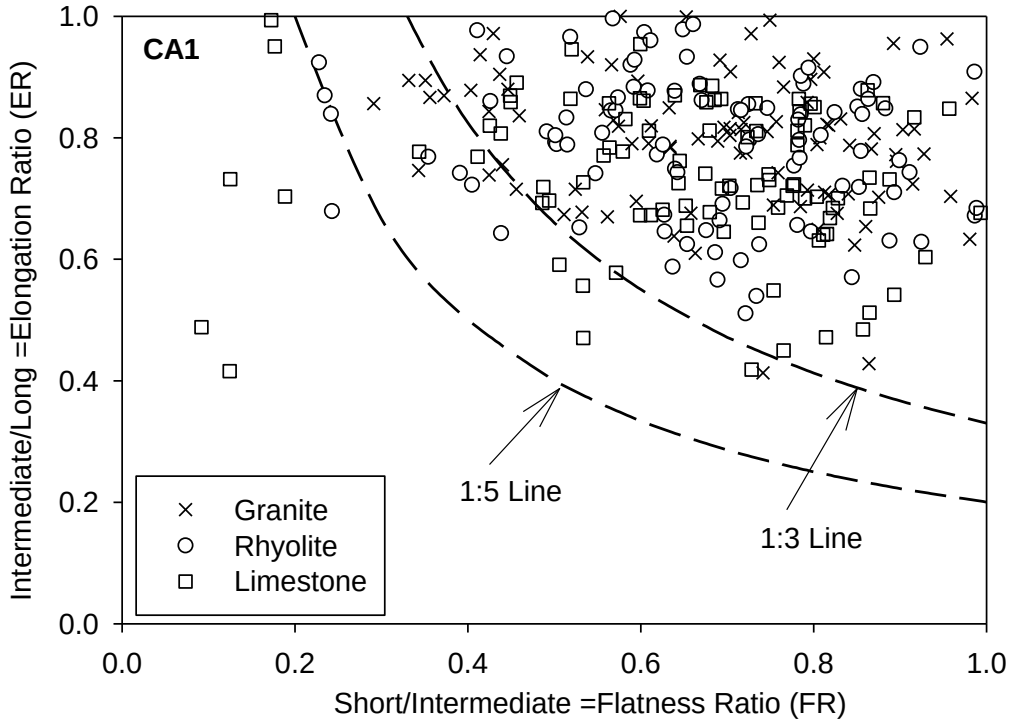

Figure 4.25 Distribution of Flat and Elongated Particles for Different Types of CA1 Aggregates

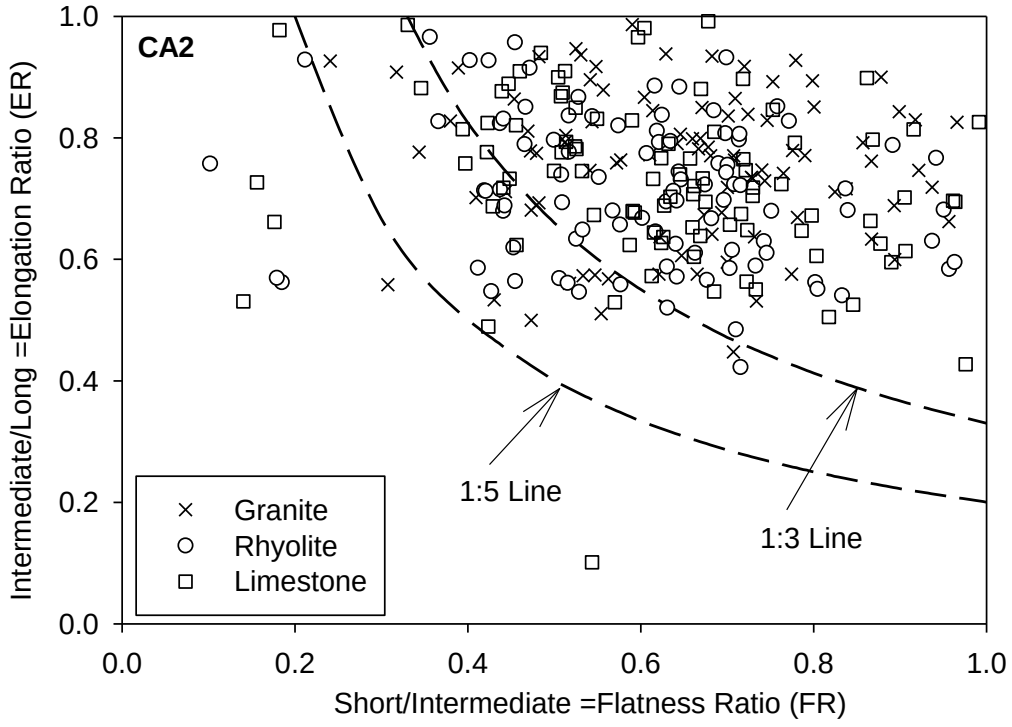

Figure 4.26 Distribution of Flat and Elongated Particles for Different Types of CA2 Aggregates

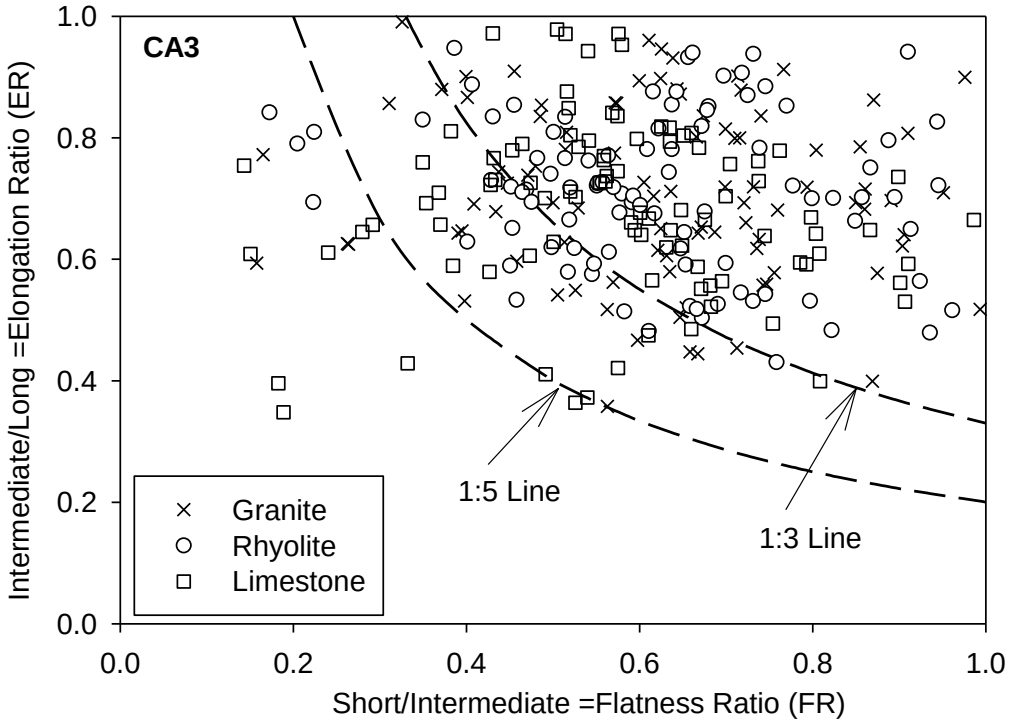

Figure 4.27 Distribution of Flat and Elongated Particles for Different Types of CA3 Aggregates

CHAPTER 5 : EVALUATION OF DYNAMIC MODULI FOR DIFFERENT MEPDG LEVELS

5.1 Introduction

The mechanistic empirical pavement design guide (MEPDG) uses a hierarchical approach for the selection of dynamic modulus (|E*|) depending on the desired reliability and available information (AASHTO, 2004). It offers three different levels of input: Level 1, Level 2, and Level 3. Of the three specified levels, Level 1 is considered the most accurate, while Level 2 and Level 3 are assumed to be an intermediate and the lowest level of accuracy, respectively. |E*| values for Level 1 are measured in the laboratory at selected combinations of temperature and loading frequency. |E*| values for Level 2 and Level 3 on the other hand, are predicted using the Witczak 1999 model (Birgisson et al., 2005; Tran and Hall, 2005; AASHTO, 2004; Andrei et al., 1999). Although the measurement of |E*| in the laboratory (i.e., Level 1) is highly desirable, it is not always feasible to conduct this test because of its tedious and time consuming nature (Gopalakrishnan and Kim, 2011; Tran and Hall, 2005). Consequently, prediction of |E*| (i.e., Level 2 and Level 3) using the Witczak 1999 model is an alternative choice for designers (Loulizi et al., 2006; Birgisson et al., 2005; Tran and Hall, 2005; AASHTO, 2004).

Several studies have been conducted in past to check the predictive power of this model for modified and unmodified mixes. For example, Bennert (2009) reported that the percent difference between the measured and the predicted |E*| increases with modified asphalt binders. Consequently, caution should be taken while predicting |E*| for modified asphalt binders. One reason for such discrepancy might be due to the fact that the Witczak 1999 model was developed using a very few polymer-modified asphalt binders.

Insufficient binder information could result in this model performing poorly for modified mixes (Bennert, 2009; Dongre et al., 2005). Zeghal et al. (2005) compared the predictions of this model for Level 3 designs for mixes prepared with PG 58-22, PG 64-34, and PG 52-34 asphalt binders. It was reported that this model over-predicted |E*| with an average error of approximately 100% and 300% at intermediate and high temperatures, respectively. Similarly, for Level 2 and Level 3, Harran et al. (2009) reported that the predicted |E*| ranged from 65% to 250% of the values measured in the laboratory at intermediate and high temperatures. However, their study was limited to unmodified asphalt mixes.

Tran and Hall (2005) compared the measured (i.e., Level 1) and the predicted (i.e., Level 3) |E*| of several asphalt mixes prepared with modified binders: PG 70-22 and PG 76-22. It was found that this model resulted in significant error for Level 3. Consequently, calibration factors were suggested to reduce the error in this model. However, they did not study the performance of this model for Level 2. In another study, Azari et al. (2007) compared the predictions for Level 3 designs for mixes prepared with unmodified, air blown, and polymer-modified asphalt binders. It was reported that |E*| for all kinds of mixes were over-predicted. However, the research was limited to one air void level (i.e. 7%), and the accuracy of the model at Level 2 was not evaluated. Similarly, Mohammad et al. (2008) studied the performance of this model for the modified and unmodified mixes for Level 3 and reported that the model over-predicted |E*|. However, their conclusions were based on the combined dataset of modified and unmodified mixes for samples compacted at 7% air void. In a recent study, Zhu et al. (2011) studied the performance of this model for different polymer-modified asphalt

mixes. It was reported this model may be applicable for polymer-modified asphalt mixes. However, the research was limited to one air voids level (i.e., 4%). Moreover, results were based on the combined dataset of all four mixes that might result in the change in the prediction power of the model. Furthermore, it was not clear from their reported results if the accuracy of the model was checked at Level 2 or Level 3. In a similar study, Singh et al. (2011d, 2011i) evaluated the strengths and weaknesses of this model for Level 3 and reported that this model over-predicted |E*|. However, the findings were based on the combined dataset of modified and unmodified mixes.

The results from the literature presented above conclusively demonstrates that the accuracy of input Level 2 and Level 3 |E*| is largely dependent on the type of mix, binder, air voids, and test temperature. The predictive model performs differently for modified and unmodified asphalt mixes. Such a significant difference between the measured and the predicted |E*| values may produce inaccurate designs and discourage users from implementing the proposed guide Zeghal et al. (2005). Therefore, it is important for state agencies and pavement designers to study different hierarchical levels of the MEPDG for predicting |E*| for the modified and un-modified asphalt mixes and develop correction factors to improve the accuracy of the predictive models for the asphalt mixes specific to their state.

In the present study, |E*| of modified and unmodified mixes that are commonly used in the construction of pavements in Oklahoma was evaluated for the three levels of input (i.e., Level 1, Level 2, and Level 3) of the MEPDG. The comparison was made by estimating the relative errors and by comparing the master curves constructed for these levels. Correction factors to reduce the prediction errors were developed for both the

mixes. It is anticipated that the present study would provide the designer more insight into the effect of modified mixes on the stiffness and result aid in the accurate estimation of |E*|.

5.2 Modified and Unmodified Mixes

Two Superpave asphalt mixes (i.e., Mix-3 and Mix-4) are used for this purpose (see Chapter 2, Tables 2.1). The nominal maximum aggregate size of both the mixes was 12.5 mm. Mix-3 was prepared with 4.5% of styrene-butadiene-styrene (SBS)-modified PG 70-28 binder, and it was named as modified mix (MM), while Mix-4 was prepared using 5.1% unmodified PG 64-22 binder, and it was designated as an unmodified mix (UM). The composition of aggregates in the mixes and the gradations are given in Chapter 2 (see Tables 2.1 and 2.2). Specimens were compacted using a Superpave Gyratory Compactor (SGC) at 6, 8, 10, and 12% target air voids (±0.5%) as discussed in Chapter 2. Volumetric analyses were conducted to obtain effective binder content (V_{beff}), voids in mineral aggregates (VMA), voids filled with asphalt (VFA), and air voids (V_a) for both the mixes (Chapter 2, Tables 2.5 and 2.6).

5.3 Measurement of Dynamic Modulus for Input Level 1

|E*| values for input Level 1 were measured in the laboratory in accordance with AASHTO TP62 specifications (AASHTO, 2006). The detailed procedure of measurement of dynamic modulus and construction of master curve are discussed in Chapter 2. A total of 576 |E*| values (2 mixes x 3 specimens x 4 air voids x 4 temperatures x 6 frequencies) were measured in the laboratory.

5.4 Prediction of Dynamic Modulus for Input Level 2 and Level 3

|E*| values for input Level 2 and Level 3 are predicted using the Witczak 1999 model (Equation (5.1)). The predictions are based on a mix of volumetric properties, aggregate gradation, binder viscosity, and loading frequencies.

$$Log E^{*} = -1.249937 + 0.029232\,\rho_{200} - 0.001767\,(\rho_{200})^{2} - 0.002841\,\rho_{4} - 0.058097\,V_{a} - 0.8022\,\frac{V_{beff}}{(V_{beff} + V_{a})} + \frac{3.87197 - 0.0021\,\rho_{4} + 0.003958\,\rho_{38} - 0.000017\,(\rho_{38})^{2} + 0.00547\,\rho_{34}}{1 + e^{(-0.603313 - 0.31335 \log(f) - 0.393532 \log(\eta))}} \quad (5.1)$$

where,

|E*| = dynamic modulus in 10^5 psi,

η = viscosity of binder in 10^6 poise,

f = loading frequency in Hz,

V_a = air voids in the mix (percentage by volume),

V_{beff} = effective binder content (percentage by volume),

ρ_{200} = percentage passing # 200 (0.075 mm) sieve,

ρ_4 = cumulative percentage retained on # 4 (4.75 mm) sieve,

ρ_{38} = cumulative percentage retained on 3/8 in (9.5 mm) sieve, and

ρ_{34} = cumulative percentage retained on 3/4 in (19 mm) sieve.

The viscosity of an asphalt binder used as an input in the model can be determined from the viscosity-temperature equation (ASTM, 2009). This equation needs two inputs: intercept (A) and slope (VTS) pertaining to the temperature susceptibility line of an asphalt binder. Level 2 designs use the laboratory measured A and VTS values, while Level 3 uses default values as provided in the MEPDG (AASHTO, 2004).

The A and VTS values for PG 70-28 and PG 64-22 were measured in the laboratory as: 9.78,-3.233; and 10.590, -3.537, respectively (Chapter 2, Table 2.11). The default A and VTS values were taken from the MEPDG guide as: 9.7515, -3.217; and 10.98, -3.68; for PG 70-28 and PG 64-22, respectively (AASHTO, 2004). The model input parameters, namely V_{beff}, VMA, VFA, V_a, and the gradation of the mixes are listed in Chapter 2 (see Tables 2.5 and 2.6). |E*| values were predicted for Level 2 and Level 3 for both of the mixes at different air voids, temperature, and frequencies as mentioned above. A total of 576 |E*| values were estimated for each level.

5.5 Master Curves for Level 1, Level 2, and Level 3

The master curves were developed for all three input levels (i.e., Level 1, Level 2, and Level 3). Level 1 and Level 2 require laboratory measured A-VTS values, while Level 3 uses the default binder properties provided in the MEPDG. The master curves were generated at a reference temperature of 21^{o}C. The detail discussion on the construction of the master curve is provided in Chapter 2.

5.6 Results and Discussion

The modulus values obtained for both MM and UM mixes for Level 1, Level 2, and Level 3 of the MEPDG design are compared in this section to determine the relative accuracy of each method in determining the stiffness of the mix specimen. In addition, the master curves were compared for all the three levels of the MEPDG.

5.6.1 Relative Error (RE) for Modified (MM) and Unmodified (UM) Mixes

The relative error (RE) (%) in prediction of |E*| for Level 2 and Level 3 was calculated using Equation (5.2). The negative and positive errors indicate under-prediction and over-prediction of |E*|, respectively. Figure 5.1 shows the distribution of RE (%) for both the mixes estimated for all temperature and air voids levels.

$$RE = \frac{(|E^*|_p - |E^*|_m)}{|E^*|_m} \times 100 \quad (5.2)$$

where,

RE = relative error (%),

$|E^*|_p$ = predicted dynamic modulus in MPa for Level 2 or Level 3, and

$|E^*|_m$ = laboratory measured dynamic modulus in MPa (Level 1).

RE (%) for the MM mix ranged from -45% to 300% and from -60% to 285% for Level 2 and Level 3, respectively. In general, the distribution of the points above the zero line indicate that the model over-predicted |E*| for a majority of the cases (Figure 5.1 (a)). Similarly for the UM mix, RE (%) ranged approximately from -45% to 50%, and from -50% to 60% for Level 2 and Level 3, respectively. It can be seen from the plot that maximum number of points are below the zero line, indicating that the model under-predicted |E*| for these levels (Figure 5.1(b)). It is important to note that the model performs differently for modified and unmodified asphalt mixes used in the present study. For example, it over-predicts |E*| for MM mix and under-predicts |E*| for UM mix. A comparison of both the mixes shows that this model performs slightly better for UM mix compared to MM mix. This could be due to the fact that the database used to develop this model primarily contains the unmodified mixes (Bennert, 2009; Dongre et al., 2005). Consequently, its performance is better for unmodified mixes.

5.6.2 Average Relative Error (ARE) for Modified (MM) and Unmodified (UM) Mixes

To better assess the performance of this model, it is necessary to estimate the percentage average relative error (ARE) for each air void and temperature levels. For this purpose, |E*| data for a particular mix (i.e., MM or UM mix) was separated into four

levels of air voids (i.e., 6%, 8%, 10%, and 12%). For each air void, the data was further partitioned into four temperature groups (i.e., 4, 21, 40, and 55^{o}C). For example, at 6% air voids, the measured and the predicted |E*| were divided into 4, 21, 40, and 55^{o}C group. The ARE was estimated for each temperature using Equation (5.3).

$$ARE = \frac{\sum_{i=1}^{N} \frac{(|E^*|_p - |E^*|_m)}{|E^*|_m} \times 100}{N} \quad (5.3)$$

where,

ARE = average relative error (%),

$|E^*|_p$ = predicted dynamic modulus in MPa for Level 2 or Level 3,

$|E^*|_m$ = laboratory measured dynamic modulus in MPa (Level 1), and

N = number of observations.

5.6.2.1 Modified Mix (MM)

Figure 5.2 shows the plot of ARE for MM mix, estimated at Level 2 and Level 3 for all four air voids and test temperatures. It can be seen from this figure that the accuracy of both levels varies with air voids and temperature. Both levels resulted in the lowest ARE at 6% air voids, indicating that predictions are good at this air voids. This plot also shows that the model resulted in significant error at higher air voids (i.e., air voids > 6%) for both the levels.

At each air void the model prediction is influenced by the test temperature. The results show that the model over-predicted |E*| at all test temperatures for both levels of the MEPDG. For example, this model shows the highest error at 21^{o}C followed by 4, 40, and 55^{o}C, indicating that model deviates significantly at low and intermediate temperatures. Surprisingly, Level 3 results exhibit comparatively smaller error compared

to Level 2. Thus, although the MEPDG considers Level 2 more accurate compared to Level 3 (AASHTO, 2004), that is not seen for the modified mix used in the present study.

5.6.2.2 Unmodified Mix (UM)

Figure 5.3 shows ARE (%) plot for the UM mix. At low air voids (i.e., 6%), the model under-predicted |E*| for all the test temperatures. The model exhibited less error for high air voids. The highest error ranged from -10% to -40% for high temperatures, indicating that the model under-predicted |E*| at this temperature. Such errors at high temperatures limit the ability of this model to capture the rutting behavior of a pavement. Level 2 predictions show a slightly lower magnitude of error compared to Level 3, indicating that the predictions are similar to those mentioned in the MEPDG.

5.6.3 Comparison of Modified (MM) and Unmodified (UM) Mixes

Figures 5.4 through 5.7 show a comparison of MM and UM mixes at Level 2 and Level 3 for all four levels of air voids and test temperatures. These plots are helpful in understanding the accuracy of the predicted |E*| as a function of the mix type. Figure 5.4 depicts the ARE (%) for Level 2 and Level 3 designs at 6% air voids. For both of these levels, at low and intermediate temperatures (i.e., 4 and 21^{o}C) the model under-predicted |E*| for the UM mix, while it over-predicted |E*| for the MM mix. The resulting magnitude of error for the UM mix was found to be smaller compared to the error for the MM mix, indicating that the model performs better for the UM mix. On the other hand, at high temperature (i.e., 55^{o}C), the model works better for the MM mix compared to the UM mix. It can be concluded that at 6% air voids and a high temperature, the model performs better for the MM mix.

Similarly, Figure 5.5 shows the distribution of ARE (%) for Level 2 and Level 3 for 8% air voids. It is important to see that the performance of the model is different for

both mixes. The model over-predicted |E*| significantly for the MM mix with ARE (%) ranging from 20% to 130%, while it resulted in a smaller magnitude of error (i.e., <30%) for the UM mix, indicating that the model works better for the UM mix compared to the MM mix. Similar trends were observed for 10% and 12% air voids (Figure 5.6 and Figure 5.7). The model over-predicted |E*| for the MM mix, while it predicted reasonably well for the UM mix. This could be due to the fact that the database used to develop this model primarily contains the unmodified mixes (Bennert, 2009; Dongre et al., 2005); consequently, its performance is better for unmodified mixes.

5.6.4 Comparison of the Master Curves for Modified (MM) and Unmodified (UM) Mixes

The master curve can be used as a means to compare of |E*| over a wide range of temperature and frequency. For this comparison, the master curves were generated for all three levels (i.e., Level 1, Level 2, and Level 3) at 21^{o}C reference temperature. Figures 5.8 through 5.11 show the master curves for MM and UM mixes generated for different levels of air voids. It is seen from the figures that for the MM mix, the master curves at Level 2 and Level 3 designs did not match with the master curve developed for Level 1. Also, the master curve for Level 2 lies above Level 3, indicating that Level 2 results in greater error compared to Level 3. For the UM mix, the Level 2 and Level 3 predictions match with Level 1, indicating that the model performs better for this mix. At a low frequency (high temperature), the model under-predicts |E*| for both the mixes. It is expected that at high temperatures the aggregate shape parameters dominate; consequently, the modulus at this temperature indicates an elastic modulus of aggregates (Huang et al., 2008). The fact that the model does not include any shape parameters might be a reason for this model to under-predict |E*| at high temperature.

Such errors in the estimation of |E*| can result in some performance issues. For example, a higher predicted value would result in a thinner pavement section, and consequently premature rutting failure of a pavement. Similarly, lower predicted |E*| would result in thicker pavement section that would increase the possibility of low temperature cracking of the pavement while simultaneously increasing the cost of its construction. Therefore, prior to the use of the predictive model for the Level 2 and Level 3 design of the MEPDG, it is important to understand the nature of the prediction error and its magnitude.

5.7 Development of Correction Factors

An accurate estimation of |E*| is important to enhance the performance of pavements. Selection of |E*| can significantly affect the thickness of pavement and its response characteristics. As discussed in the previous sections, the prediction of |E*| for Level 2 and Level 3 varies with type of mix, air voids, and temperatures. Consequently, correction factors are required to account for the variability in the model. The correction factors were calculated for each test temperature using Equations (5.4) through (5.7). First, the slope 'm' was determined by fitting a regression line passing through the origin for combinations of temperatures and air voids (Equation (5.4). This slope represents the calibration factor that is used to multiply the predicted |E*| to get a range of modulus close to the laboratory measured |E*|. Second, the relationship between 'm' and air voids (Equation (5.6) was developed to estimate coefficients 'a' and 'b'. Equation (5.7) along with factors 'a' and 'b' listed in Table 5.1 can be used to estimate |E*| at selected air voids and temperature.

$$|E^*|_{Measured(Level1)} = m\,|E^*|_{Predicted(Level2\ or\ Level3)} \quad (5.4)$$

The correction factor 'm' can be a function of temperature and air voids (Equation (5.5.).

$$m = f(T, V_a) \tag{5.5}$$

For a constant temperature, T = constant, Equation (5.5) can be written in form of Equation (5.6). The power relation was selected as it fitted the best with the dataset.

$$m = f(V_a) = a(V_a)^b \tag{5.6}$$

Substituting the value of 'm' (i.e., Equation (5.6)) in Equation (5.4), the final form of relationship can be written as shown in Equation (5.7).

$$|E^*|_{Measured\,(Level1)} = a(V_a)^b \, |E^*|_{Predicted\,(Level2\ or\ Level3)} \tag{5.7}$$

where,

m = the slope of regression line,

T = temperature (^oC),

V_a = air voids (%),

|E*| = dynamic modulus (MPa), and

a and b = fitting coefficients for any particular temperature (Table 5.1).

Figure 5.12 and Figure 5.13 show the relationship between correction factor and air voids at different temperatures for MM and UM mixes, respectively. It is anticipated that use of calibration factors would be helpful in estimating |E*| accurately without conducting actual modulus tests in the laboratory. Calibration factors are useful for estimating a reasonable range of |E*| used for input Level 2 and Level 3 of the MEPDG.

5.8 Summary of Results

The present study was undertaken to compare |E*| for the three input levels (i.e., Level 1, Level 2, and Level 3) of the MEPDG for modified and unmodified mixes. The analyses of results show that the performance of the Witczak model varies with the type of mix, air voids, and temperature. The accuracy of the model was evaluated by calculating average relative error (%), and by plotting master curves. The following conclusions can be drawn from the results and discussions presented in the preceding sections.

(1) At low air voids, for example 6%, the model works better for the modified mix than the unmodified mix.

(2) For higher air voids (i.e., 8%, 10%, and 12%), the model over-predicted and under-predicted |E*| for modified and unmodified mixes, respectively, indicating that performance of the model changes with type of mix.

(3) For the modified mix, Level 2 resulted in a higher magnitude of error compared to Level 3, which is contrary to the expectation that the Levels 1, 2, and 3 are in decreasing order of accuracy.

(4) For the unmodified mix, Level 2 resulted in less error compared to Level 3, indicating that assuming default viscosity values from the MEPDG works well for unmodified mix used in the present study.

(5) The Witczak model is very sensitive to input parameters pertaining to the viscosity-temperature relationship.

(6) Correction factors developed in this study for both the mixes at different temperatures and air voids can be used as correction factors in the estimating |E*|, resulting in |E*| values comparable to Level 1.

It is recommended that similar studies be conducted for mixes from different sources with different types of binders and aggregates. Furthermore, several mixes should be tested to develop common correction factors applicable for wide range of mixes.

Table 5.1 Correction Factor Parameters for Level 2 and Level 3

Mix Type : MM						
T	Level 2			Level 3		
(^oC)	a	b	R^2	a	b	R^2
4	2.71	-0.83	0.96	3.33	-0.84	0.95
21	5.94	-1.28	0.80	7.93	-1.29	0.79
40	8.46	-1.32	0.93	11.22	-1.32	0.94
55	3.53	-0.82	0.75	4.55	-0.82	0.76

Mix Type : UM						
T	Level 2			Level 3		
(^oC)	a	b	R^2	a	b	R^2
4	2.02	-0.35	0.63	1.94	-0.35	0.63
21	2.53	-0.41	0.80	2.51	-0.41	0.80
40	3.48	-0.51	0.87	3.64	-0.51	0.87
55	2.80	-0.41	0.92	3.01	-0.41	0.92

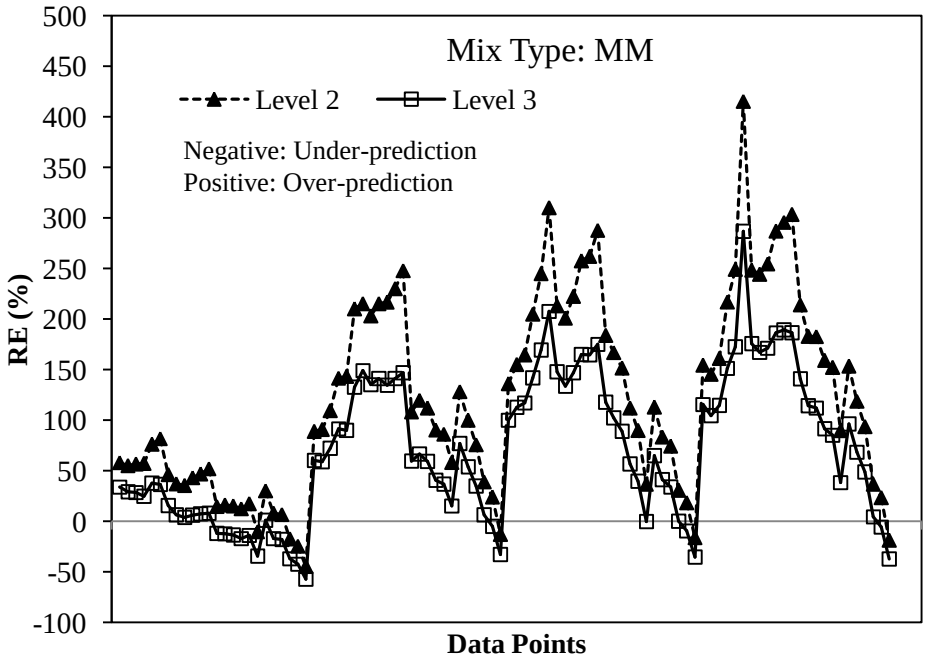

(a)

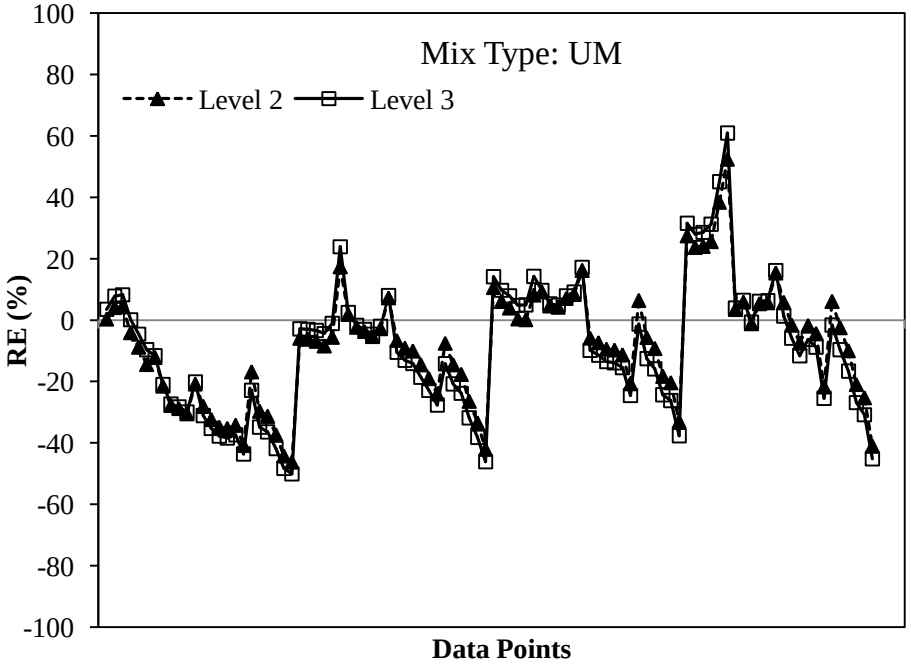

(b)

Figure 5.1 Variation of Relative Error for Level 2 and Level 3 (a) MM Mix, and (b) UM Mix

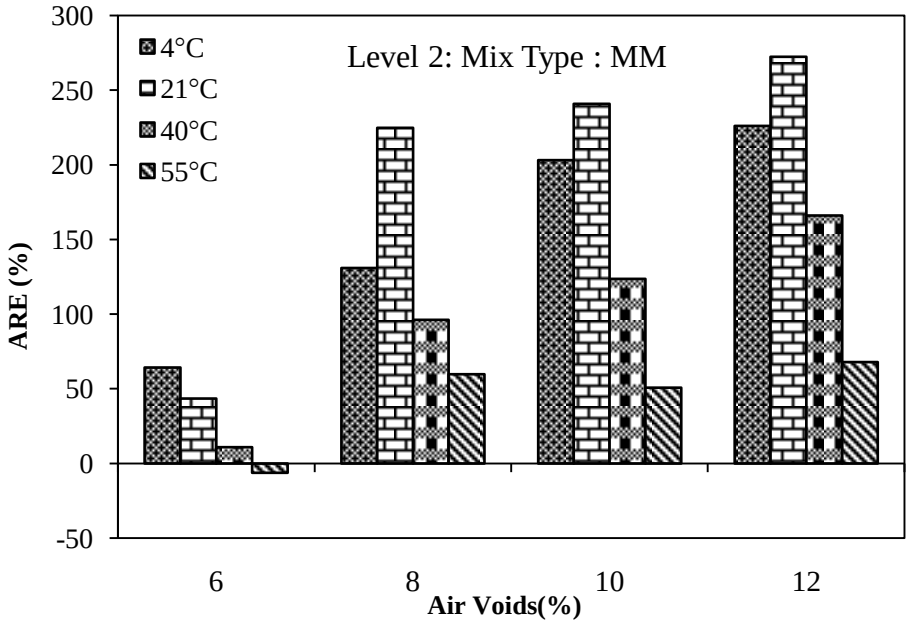

(a)

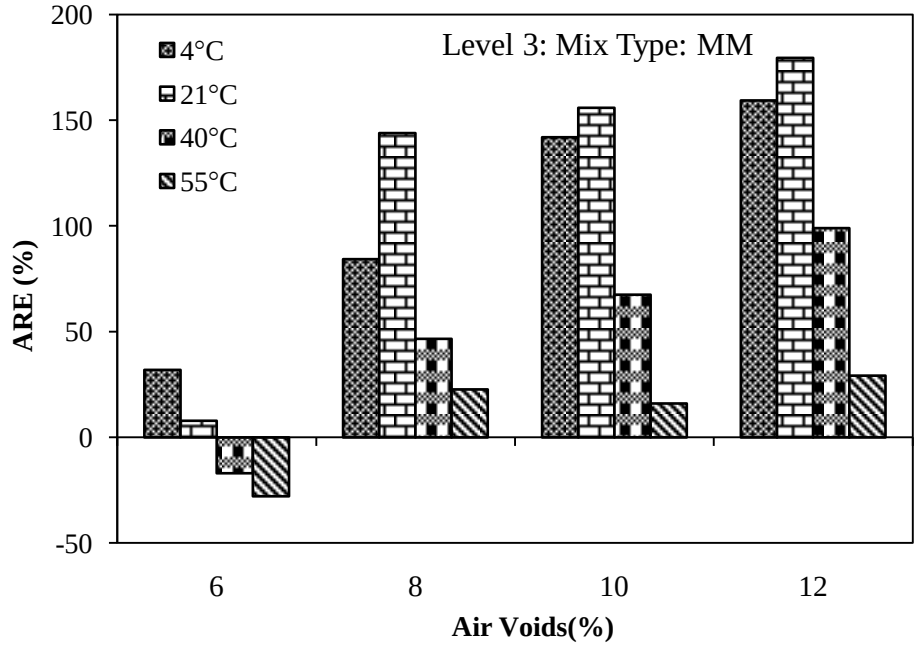

(b)

Figure 5.2 Average Relative Error for MM Mix (a) Level 2, and (b) Level 3

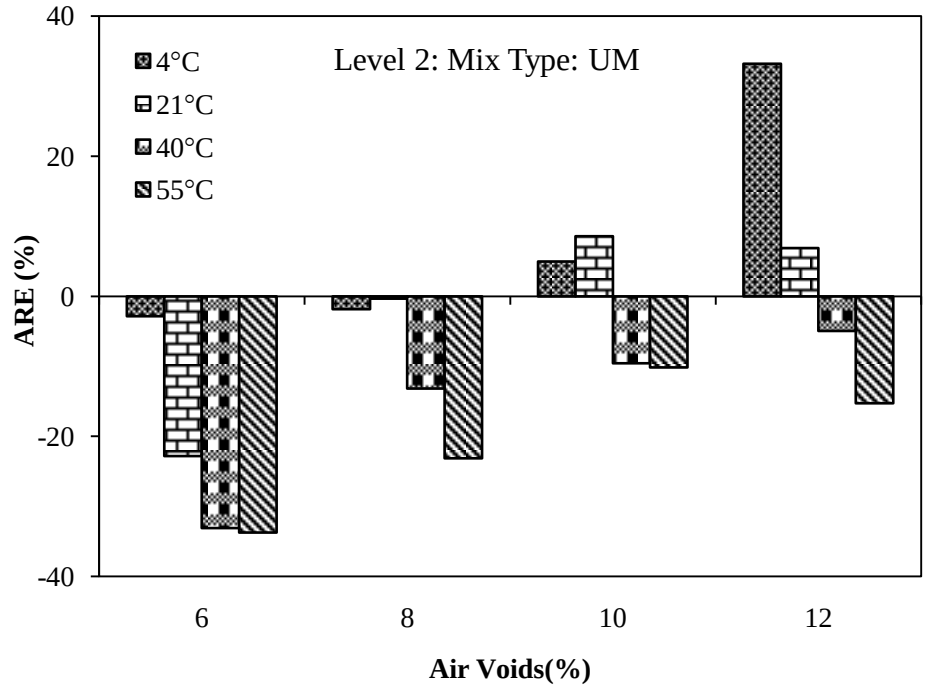

(a)

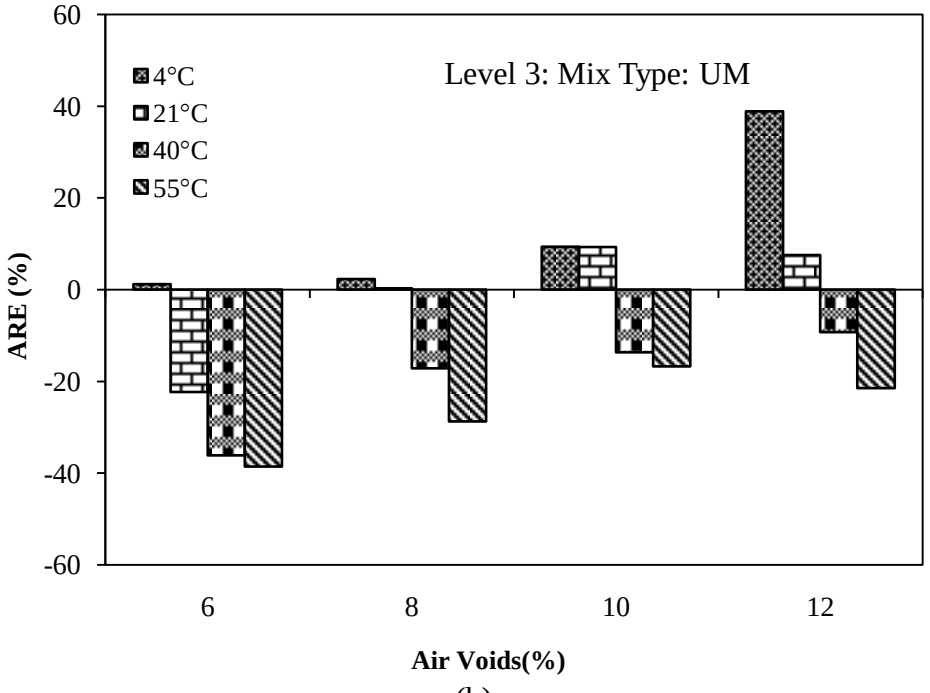

(b)

Figure 5.3 Average Relative Error for UM Mix (a) Level 2, and (b) Level 3

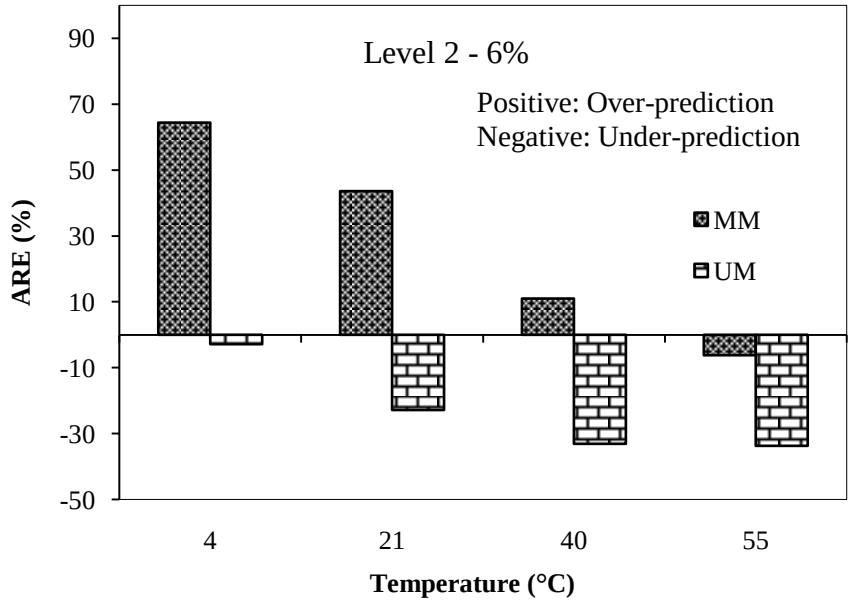

(a)

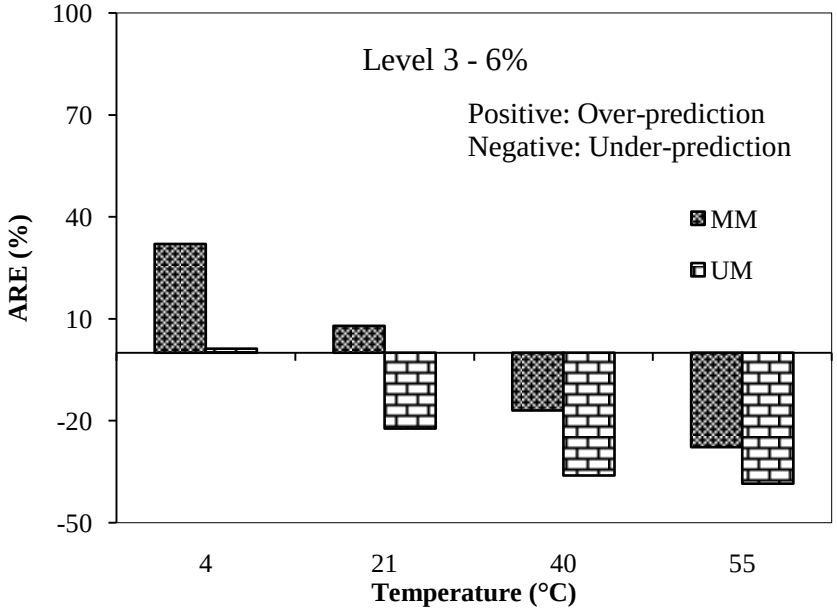

(b)

Figure 5.4 Comparison of MM and UM Mix at 6% Air Voids (a) Level 2, and (b) Level 3

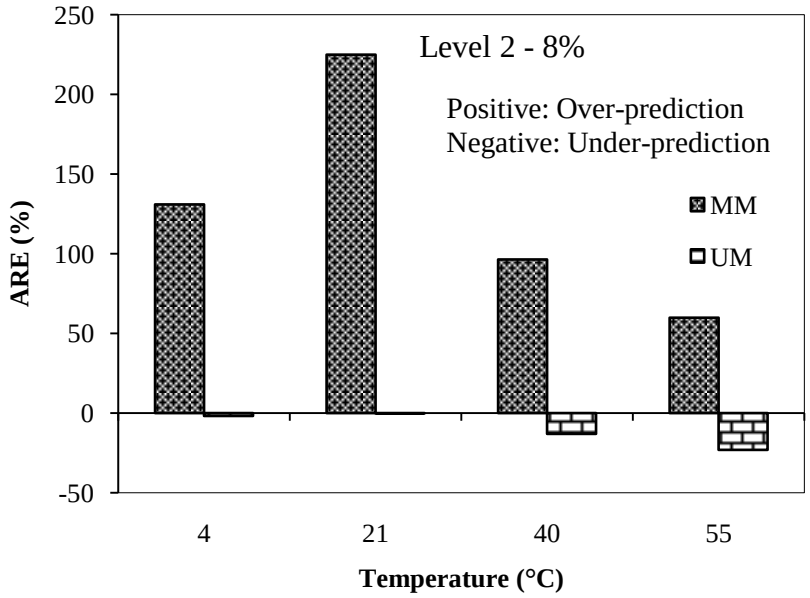

(a)

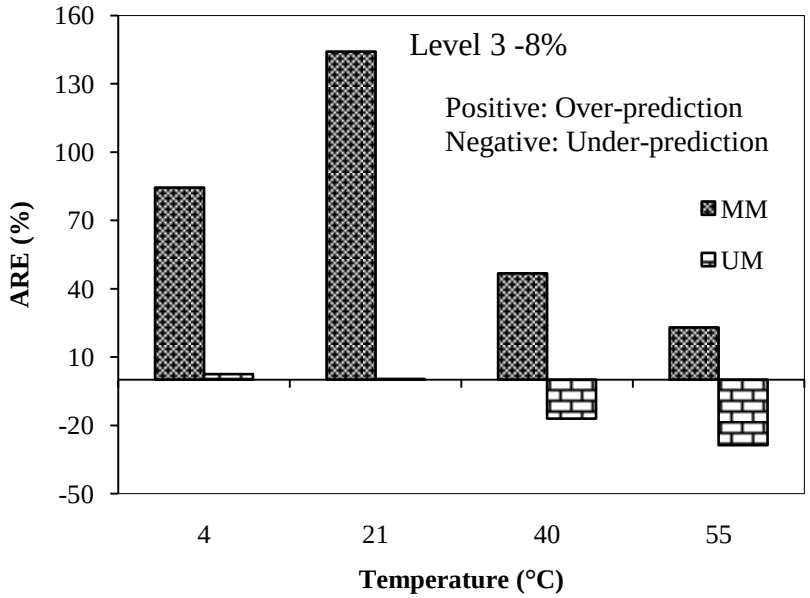

(b)

Figure 5.5 Comparison of MM and UM Mix at 8% Air Voids (a) Level 2, and (b) Level 3

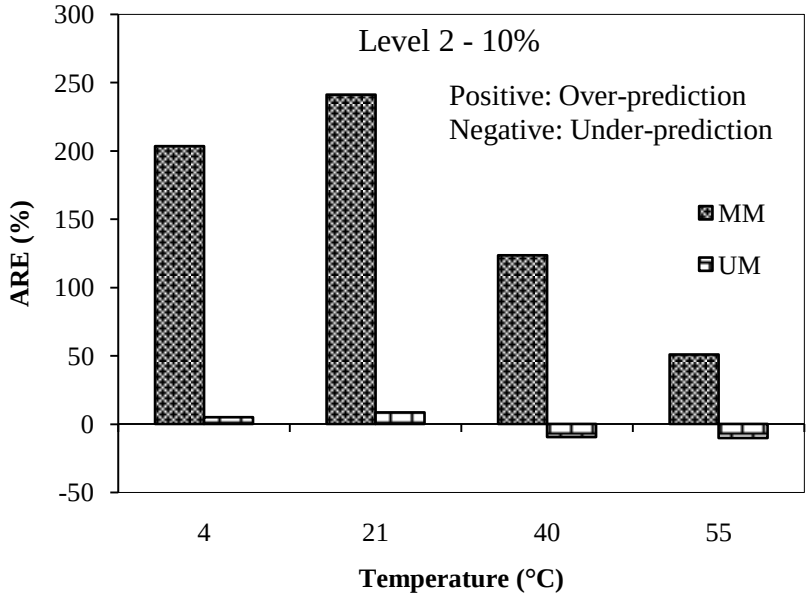

(a)

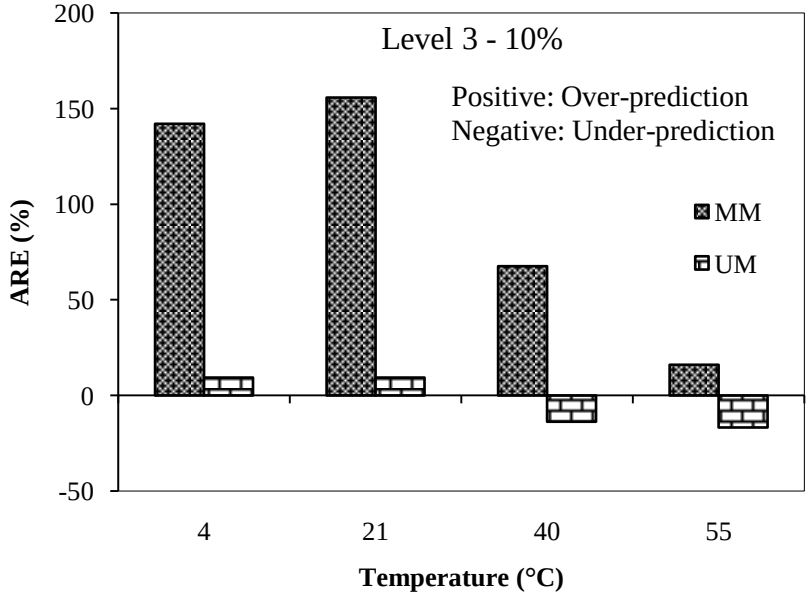

(b)

Figure 5.6 Comparison of MM and UM Mix at 10% Air Voids (a) Level 2, and (b) Level 3

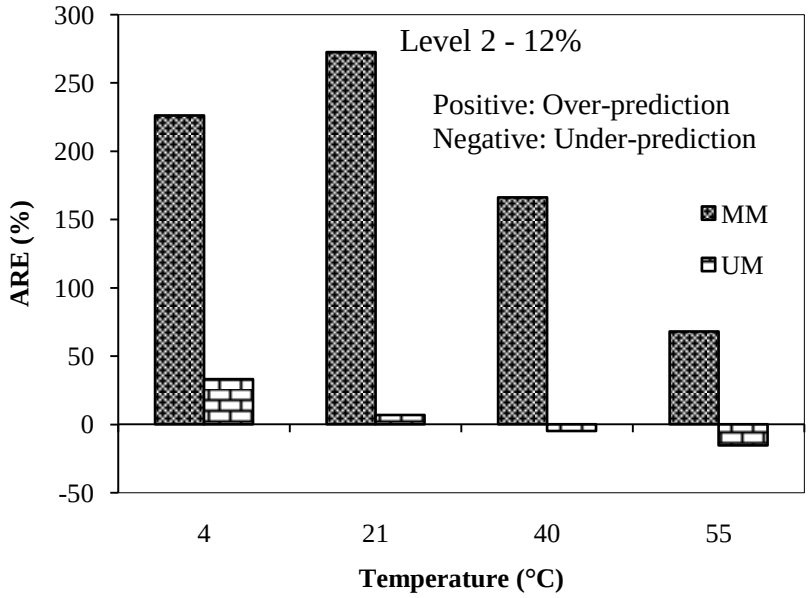

(a)

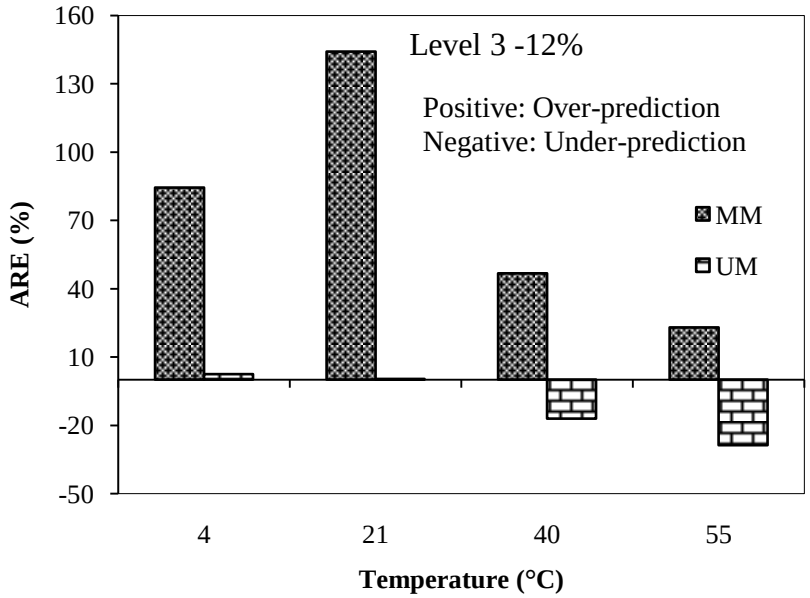

(b)

Figure 5.7 Comparison of MM and UM Mix at 12% Air Voids (a) Level 2, and (b) Level 3

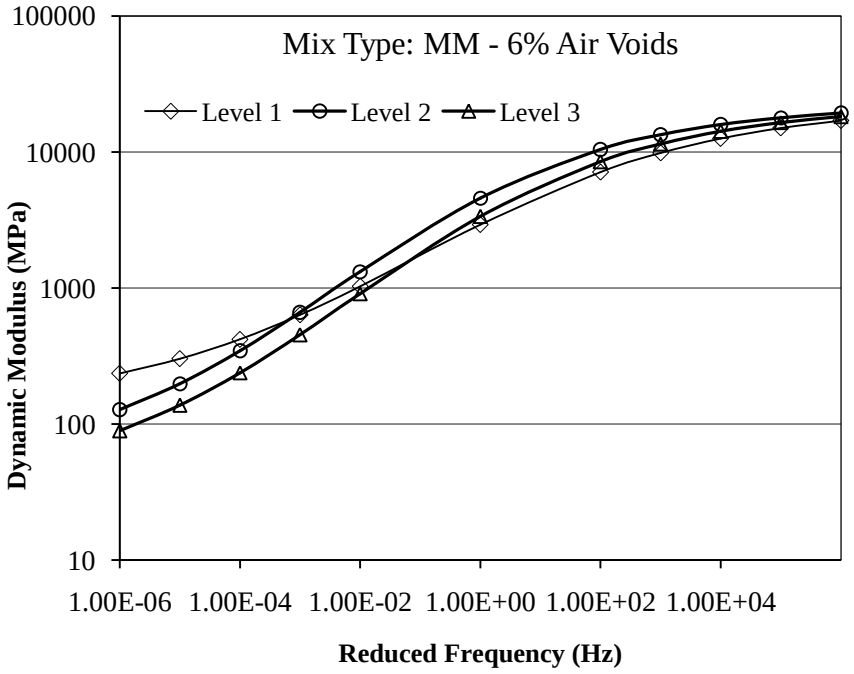

(a)

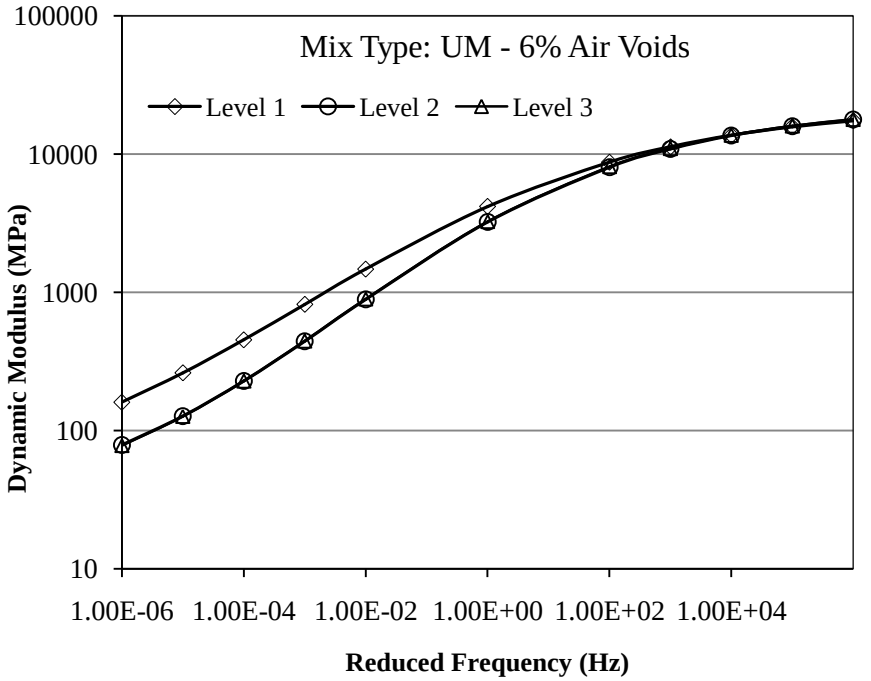

(b)

Figure 5.8 Master Curve Comparisons for Level 1, Level 2, and Level 3 at 6% Air Voids (a) MM Mix, and (b) UM Mix

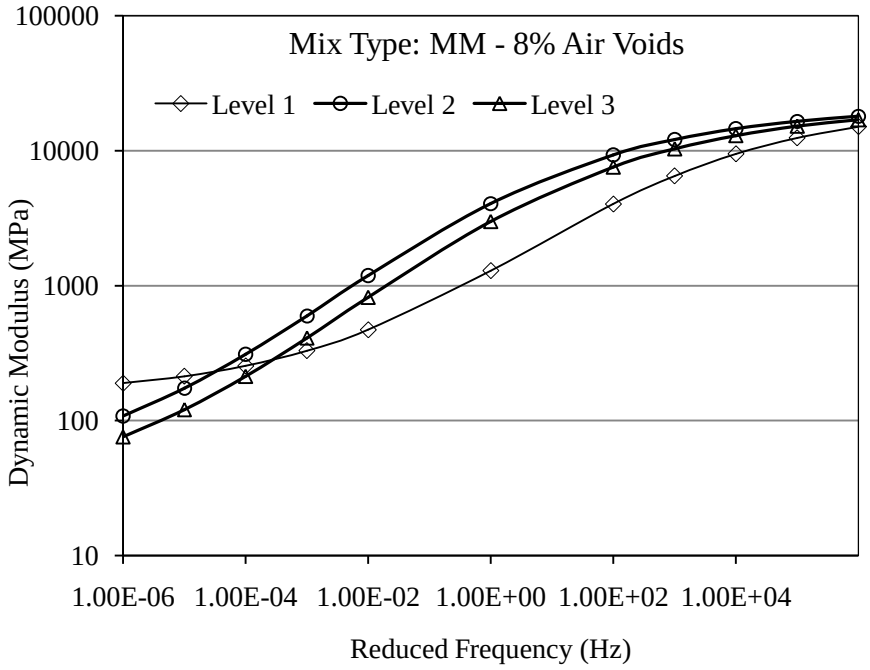

(a)

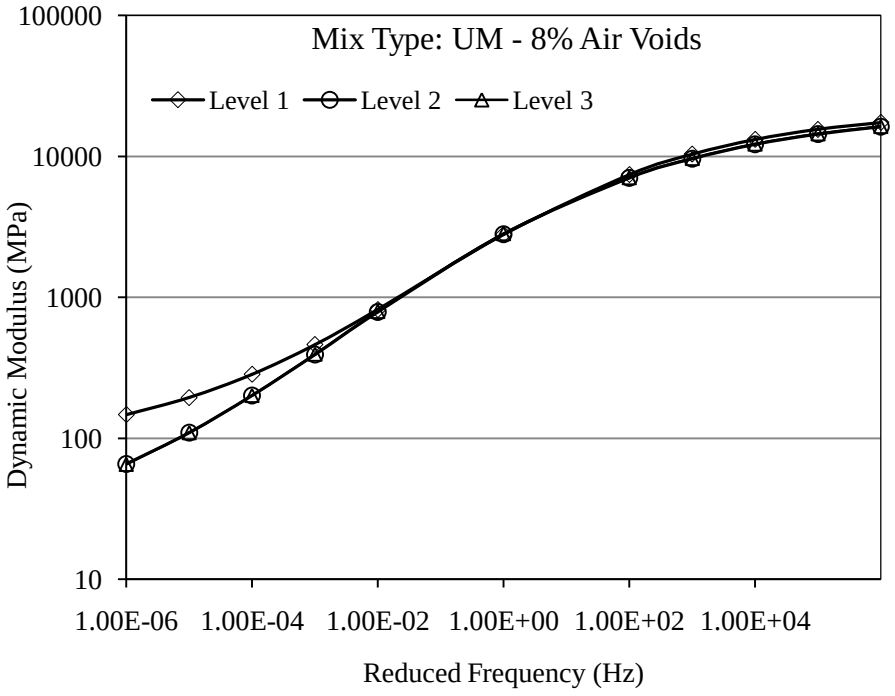

(b)

Figure 5.9 Master Curve Comparisons for Level 1, Level 2, and Level 3 at 8% Air Voids (a) MM Mix, and (b) UM Mix

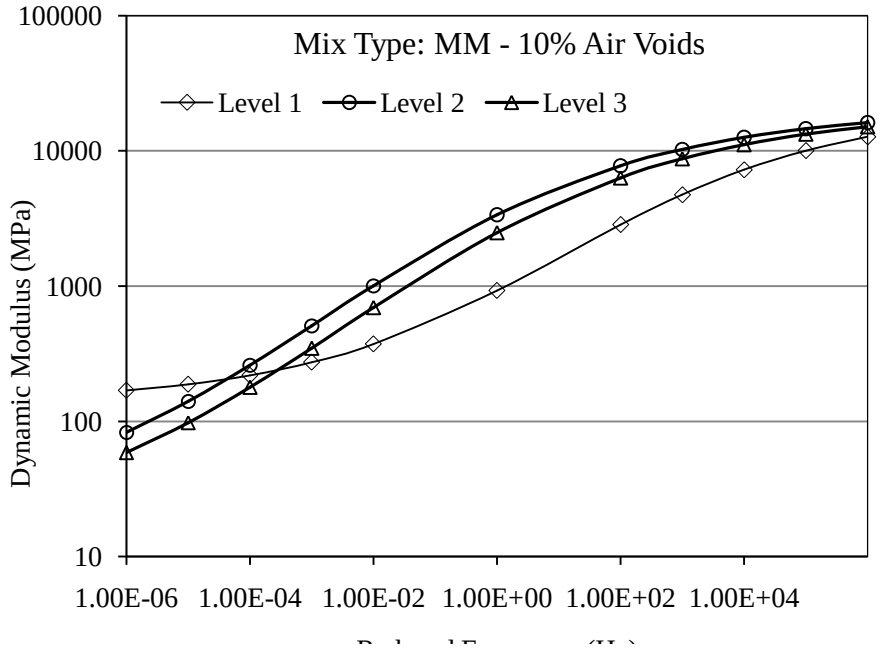

(a)

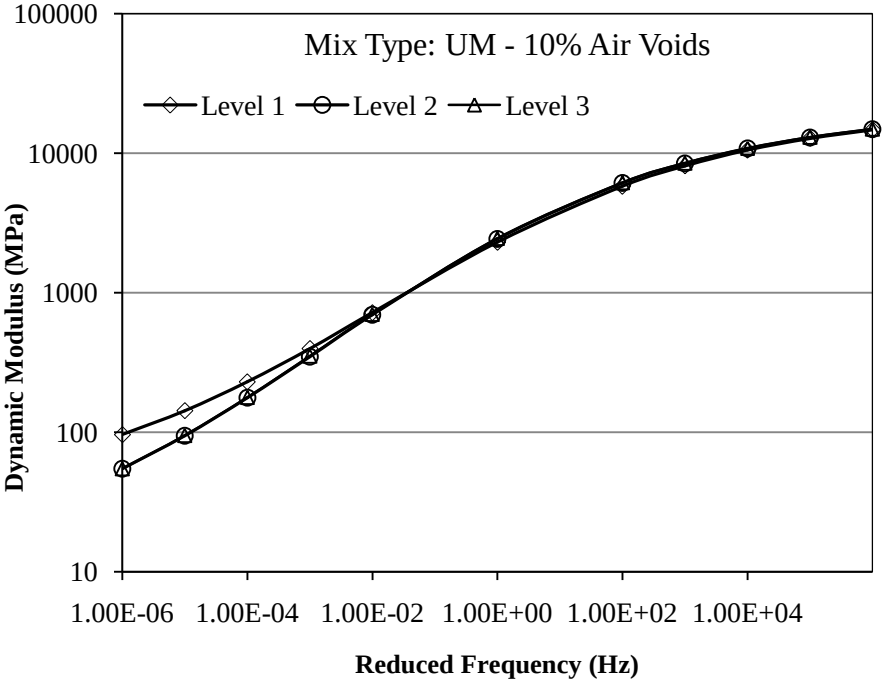

(b)

Figure 5.10 Master Curve Comparisons for Level 1, Level 2, and Level 3 at 10% Air Voids (a) MM Mix, and (b) UM Mix

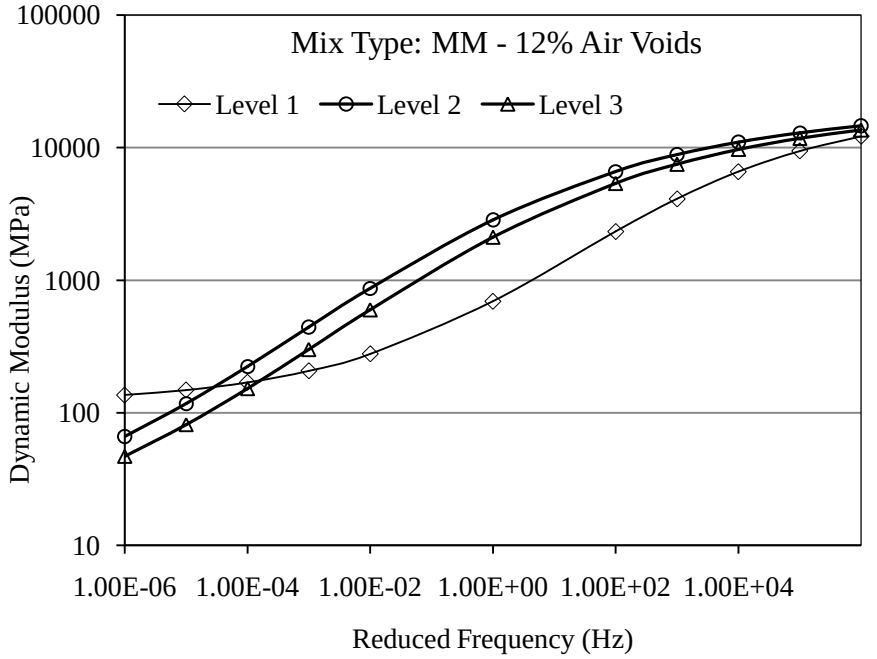

(a)

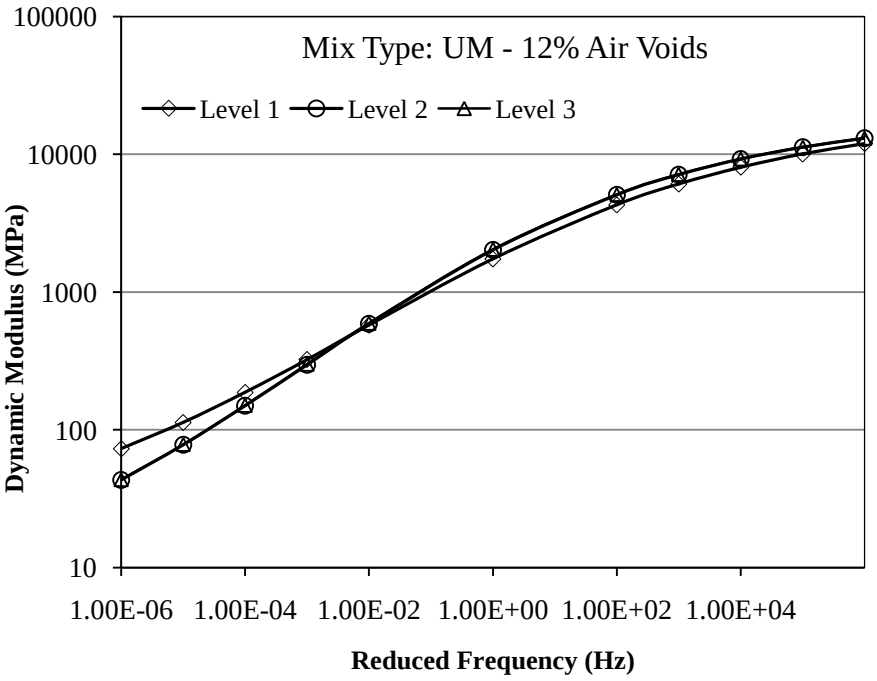

(b)

Figure 5.11 Master Curve Comparisons for Level 1, Level 2, and Level 3 at 12% Air Voids (a) MM Mix, and (b) UM Mix

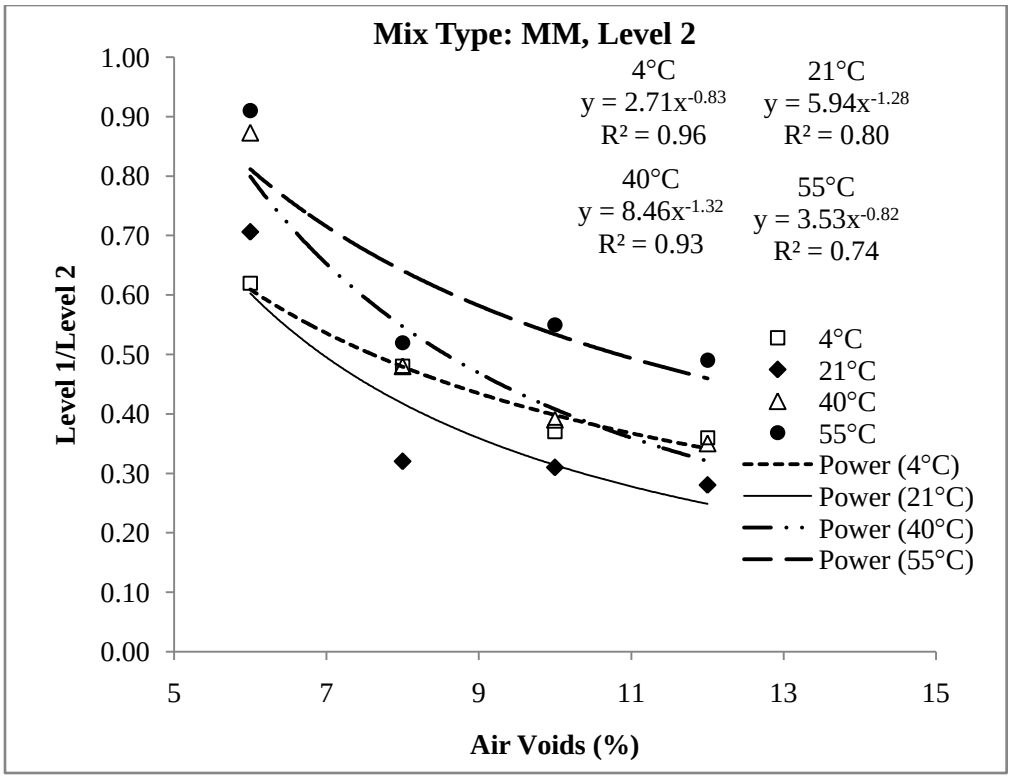

(a)

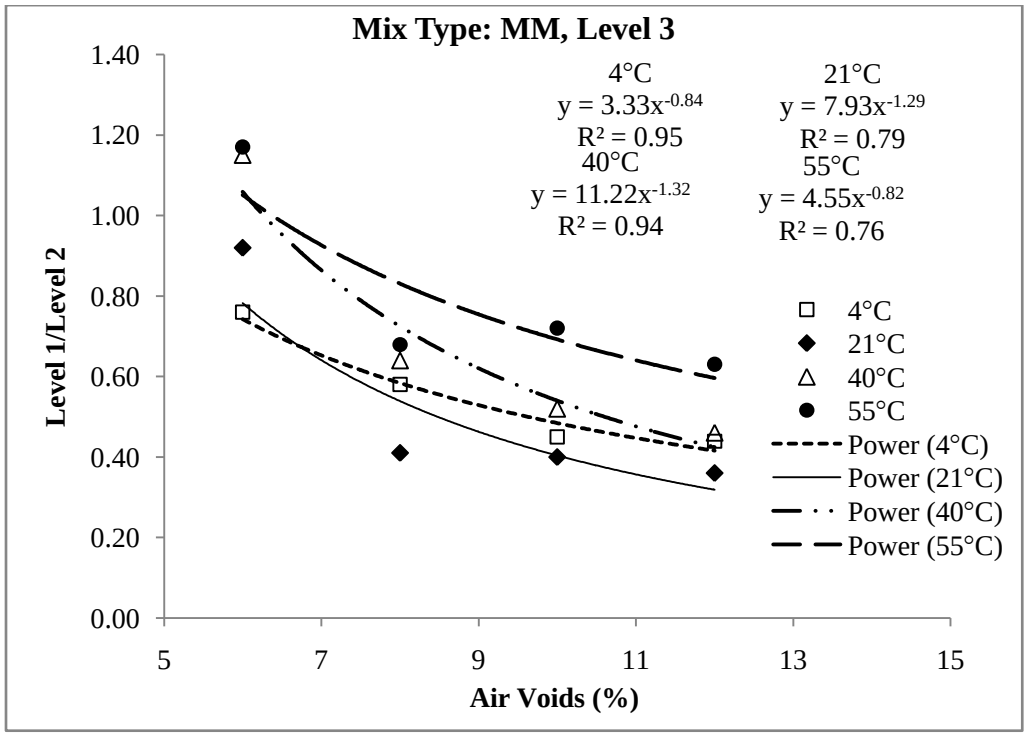

(b)

Figure 5.12 Correction Factor for MM Mix (a) Level 2, and (b) Level 3

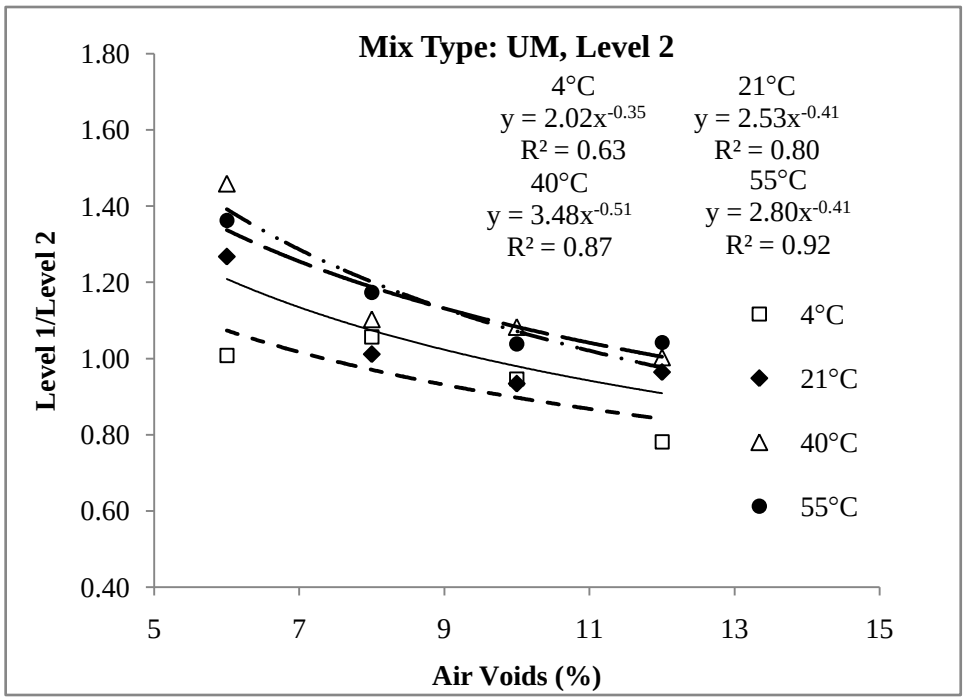

(a)

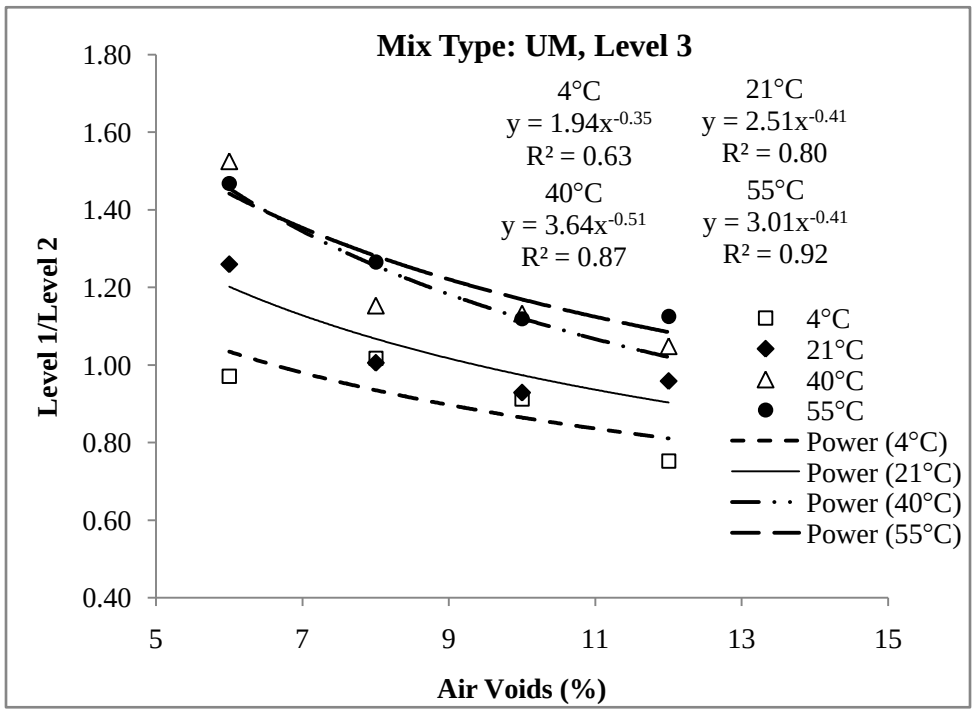

(b)

Figure 5.13 Correction Factor for UM Mix (a) Level 2, and (b) Level 3

CHAPTER 6 : EVALUATION OF PREDICTIVE MODELS FOR ESTIMATING DYNAMIC MODULUS

6.1 Introduction

The measurement of dynamic modulus in the laboratory is not always feasible, as it is a tedious experiment, and may take several days to develop a single master curve (Azari et al., 2007; Obulareddy, 2006; Birgisson et al., 2005). Moreover, it requires costly equipment and trained personnel for specimen preparation, testing, and data analysis (Azari et al., 2007*)*. To overcome these difficulties, several predictive models were developed for estimation of dynamic modulus of asphalt mixes. These models utilize the volumetric properties of a mix, aggregate gradation, loading frequency, and viscosity of an asphalt binder to predict dynamic modulus (Al-Khateeb et al., 2006; Tran and Hall, 2005; Christensen et al., 2003; Andrei et al., 1999).

In recent years, the Witczak 1999 (Andrei et al., 1999), Witczak 2006 (Bari and Witczak, 2006), Hirsch (Christensen et al., 2003), and Al-Khateeb (Al-Khateeb et al., 2006) models have been increasingly used to estimate the dynamic modulus of asphalt mixes. While predictive models are convenient, their performance varies with the type of mixes and volumetric properties (Azari et al., 2007; Bari and Witczak, 2006; Obulareddy, 2006; Birgisson et al., 2005; Dongre et al., 2005; Kim et al., 2005; Schwartz, 2005; Tran and Hall, 2005; Pellinen and Witczak, 2002). Obulareddy (2006), Tran and Hall (2006), Birgisson et al. (2005), Kim et al. (2005), and evaluated the performance of the Witczak 1999 model for mixes that are commonly used in Louisiana, Arkansas, Florida, and North Carolina respectively. Their research revealed that the Witczak 1999 model over-predicted dynamic modulus. The performance of this model was also found to be inconsistent across different types of asphalt mixes (Azari et al., 2007; Bari and Witczak,

2006; Dongre et al., 2005; Schwartz, 2005; Pellinen and Witczak, 2002). The revised Witczak 2006 model was introduced to improve the prediction accuracy of the Witczak 1999 model. The revised Witczak 2006 model has been the subject of many recent studies (Abdo et al., 2009; Ceylan et al., 2009a, 2009b; Far et al., 2009; Azari et al., 2007). It was observed that this model also over-predicts dynamic modulus and exhibits increased error at extremely high and low temperature conditions. Ceylan et al. (2008), Bari and Witczak (2006), Obulareddy (2006), and Kim et al. (2005) conducted studies to check the performance of the Hirsch model. It was reported that this model under-predicted dynamic modulus compared to the measured values. The Al-Khateeb model, on the other hand, showed substantial bias at low temperatures and a reduced sensitivity at high temperatures (Far et al., 2009).

A high dynamic modulus (high stiffness) improves the load carrying ability of asphalt layers and reduces the stress-strain on the underlying layers. However, excessive stiffness can reduce the durability of the pavement and increase the possibility of thermal cracking in the surface layers. On the other hand, a low dynamic modulus (low stiffness) decreases the load bearing capacity and can possibly result in the rutting failure of the pavement. Therefore, the use of these predictive models in the mechanistic-empirical design of asphalt pavements will be error prone if the performance of these models is not accounted for in the design process. Therefore, it is important to evaluate the performance of each model for a wide range of asphalt mixes at different air voids and test conditions.

The main objectives of the present study were (1) to evaluate the performance of four predictive models: Witczak 1999, Witczak 2006, Hirsch, and Al-Khateeb for

estimation of dynamic modulus of selected asphalt mixes that are commonly used in Oklahoma, and (2) to develop calibration factors for each of these models for Level 2 and Level 3 designs of the mechanistic empirical pavement design guide (MEPDG).

To achieve the objectives, a total of five different loose asphalt mixes as discussed in Chapter 2 are used for evaluating the models. The gradation and volumetric properties of the mixes used in the tests are given in Tables 2.1 and 2.2 (see Chapter 2). The dynamic modulus of each mix was measured as discussed in Chapter 2. A total of 1440 dynamic modulus values (5 mixes x 4 air voids x 3 samples x 4 temperatures x 6 frequencies) were measured in the laboratory.

6.2 Dynamic Modulus Predictive Models

6.2.1 Witczak 1999 Model

Andre et al. (1999) developed the Witczak 1999 model using 2750 test data points from 205 asphalt mixes. This model is currently used in the Level 2 and Level 3 designs of the MEDPG. This model uses mixture volumetric properties, gradation, binder viscosity, and loading frequencies as input variables to predict the dynamic modulus of asphalt mixtures. The temperature dependency of the predicted modulus value is taken into account in the viscosity term of the binder, which is measured at the same temperature that the mixture stiffness is predicted. The viscosity of the asphalt binder at the temperature of interest is determined from the ASTM viscosity temperature relationship (ASTM, 2009). The Witczak 1999 model had excellent goodness-of-fit statistics for its original database of 2750 data points, with S_e/S_y = 0.25 and R^2 = 0.94 results in logarithmic scale, and S_e/S_y = 0.34 and R^2 = 0.89 in arithmetic scale. The model is given by Equation (6.1).

$$LogE^{*} = -1.249937 + 0.029232\,\rho_{200} - 0.001767\,(\rho_{200})^{2} - 0.002841\,\rho_{4} - 0.058097\,V_{a} - 0.8022\,\frac{V_{beff}}{(V_{beff} + V_{a})} + \frac{3.87197 - 0.0021\,\rho_{4} + 0.003958\,\rho_{38} - 0.000017\,(\rho_{38})^{2} + 0.00547\,\rho_{34}}{1 + e^{(-0.603313 - 0.31335\log(f) - 0.393532\log(\eta))}} \quad (6.1)$$

where,

E* = asphalt mix dynamic modulus (10^5 psi),

η = viscosity of binder (10^6 poise),

f = loading frequency (Hz),

V_a = air voids in the mix (% by volume),

V_{beff} = effective binder content (% by volume),

ρ_{200} = passing # 200 (0.075 mm) sieve (%),

ρ_4 = cumulative retained on # 4 (4.75 mm) sieve (%),

ρ_{38} = cumulative retained on 3/8 inch (9.5 mm) sieve (%), and

ρ_{34} = cumulative retained on 3/4 inch (19 mm) sieve (%).

6.2.2 Witczak 2006 Model

Bari and Witczak (2006) revised the Witczak 1999 model, using 7400 data points from 346 asphalt mixes. The Witczak 2006 model uses dynamic shear modulus ($|G_b^*|$) and phase angle (δ_b) of binder as input parameters. It is reported that the Witczak 2006 model represents a better prediction, unbiased, and statistically sound performance compared to the Witczak 1999 model. The goodness-of-fit statistics for the Witczak 2006 model was found to be excellent with correlation coefficient ($R^2 = 0.90$), and a very small S_e/S_y (0.32) in logarithmic scale; however, it was reduced to very good when the goodness-of-fit statistics were calculated at normal scale with correlation coefficient ($R^2 = 0.80$), and a S_e/S_y (0.45). The revised model can be expressed as (Equation (6.2)):

$$Log_{10}E^{*} = -0.349 + 0.754\,(|G_b^{*}|^{-0.0052}) \times \left(\begin{array}{l} 6.65 - 0.032\,\rho_{200} + 0.0028\,(\rho_{200})^2 + 0.011\,\rho_4 - 0.0001\,\rho_4{}^2 \\ + 0.006\,\rho_{38} - 0.00014\,(\rho_{38})^2 - 0.08\,V_a - 1.06\dfrac{V_{beff}}{(V_{beff} + V_a)} \end{array} \right)$$
$$+ \frac{2.56 + 0.03\,V_a + 0.71\dfrac{V_{beff}}{(V_{beff} + V_a)} + 0.012\,\rho_{38} - 0.0001\,(\rho_{38})^2 - 0.01\,\rho_{34}}{1 + e^{(-0.7814 - 0.5785\,\log(|G_b^{*}|) + 0.8834\log(\delta_b))}} \qquad (6.2)$$

where,

E* = dynamic modulus (psi),

ρ_{200} , ρ_4 , ρ_{38} , ρ_{34} , V_a, V_{beff} as defined previously in Equation (6.1),

$|G_b^{*}|$ = dynamic shear modulus of asphalt binder (psi), and

δ_b = phase angle of asphalt binder (degree).

6.2.3 Hirsch Model

Christensen et al. (2003) modified the Hirsch model for estimating dynamic modulus of asphalt mixes. The model is based on the rule of mixtures which results in a simple predictive expression that includes: volumetric parameters (VMA and VFA), the stiffness of binder $|G_b^{*}|$, and aggregate contact volume (P_c). The developer reported R^2 = 0.98 (logarithmic scale) for Hirsch model. Their model is given in Equations (6.3) and (6.4).

$$\left|E^{*}\right|_m = P_c\left[4{,}200{,}000\left(1 - \frac{VMA}{100}\right) + 3\left|G^{*}\right|_b\left(\frac{(VMA)(VFA)}{10{,}000}\right)\right] + \frac{1 - P_c}{\left[\dfrac{(1 - \frac{VMA}{100})}{4{,}200{,}000} + \dfrac{VMA}{3\left|G^{*}\right|_b(VFA)}\right]} \qquad (6.3)$$

$$P_C = \frac{\left(20 + \dfrac{3\left|G^{*}\right|_b(VFA)}{VMA}\right)^{0.58}}{650 + \left(\dfrac{3\left|G^{*}\right|_b(VFA)}{VMA}\right)^{0.58}} \qquad (6.4)$$

where,

$|E^*|_m$ = absolute value of asphalt mixture dynamic modulus (psi),

$|G^*|_b$ = absolute value of asphalt binder complex shear modulus (psi),

VMA = voids in mineral aggregates in compacted mixture (%), and

VFA = voids filled with asphalt in compacted mixture (%).

6.2.4 Al-Khateeb Model

Al-Khateeb et al. (2006) developed a new model for predicting the dynamic modulus of asphalt mixture at a wider range of temperatures and loading frequencies. The new model was developed based on the law of mixtures, where composite materials were modeled in a simple three-phase system. In this three-phase system, the aggregate, the asphalt binder, and the air voids phases were placed in parallel arrangement with each other. To develop this model, several asphalt mixtures, including laboratory and field produced mixture and field cores with different performance grades covering highly modified and unmodified asphalt binders, were tested. The Al-Khateeb model requires no more than two inputs: asphalt binder complex shear modulus value $|G^*|_b$, and VMA of the compacted asphalt mixture. The glassy shear modulus ($|G^*|_g$) of the asphalt binder is also used in the model, which is equivalent to 1 GPa. The model is shown in Equation (6.5).

$$\left|E^*\right|_m = 3\left(\frac{100 - VMA}{100}\right)\left[\frac{\left(90 + 1.45\frac{\left|G^*\right|_b}{VMA}\right)^{0.66}}{1100 + \left(0.13\frac{\left|G^*\right|_b}{VMA}\right)^{0.66}}\right]\left|G^*\right|_g \qquad (6.5)$$

where,

$|E^*|_m$ = absolute value of dynamic modulus (Pa),

VMA = voids in mineral aggregate in compacted mixture (%),

$|G^*|_b$ = complex shear modulus of asphalt binder (Pa), and

$|G^*|_g$ = complex shear modulus of asphalt binder in glassy state (Pa).

6.3 Estimation of Dynamic Modulus

The Witczak 1999, Witczak 2006, Hirsch, and Al-Khateeb models (Equations (6.1) through (6.5)) were used for estimating the dynamic modulus of all the five mixes. The viscosity of each asphalt binder used for the Witczak 1999 model was calculated using the viscosity–temperature relationship (ASTM, 2009), as discussed in Chapter 2.

The regression parameters in the above equation - the intercept (A) and the slope (VTS) - pertaining to the temperature-viscosity relationship for three asphalt binders (i.e., PG 64-22, PG 70-28, and PG 76-28) were taken from the MEPDG guide (AASHTO, 2004). The $|G^*|_b$ and δ required for the Witczak 2006, Hirsch, and Al-Khateeb models were calculated using the model developed by Bari and Witczak (2007*)*.A total of 1440 dynamic modulus values were estimated using each predictive model.

6.4 Evaluation of the Performance of the Predictive Models

The performance of each predictive model was evaluated using three different criteria: goodness-of-fit statistics, comparison of the measured and the predicted values with the line of equality (LOE), and the use of local bias statistics (slope, intercept, and average error).

The goodness-of-fit statistics includes the ratio of the standard error of estimate (S_e) to the standard deviation (S_y), and the coefficient of determination (R^2). S_e, S_y, and R^2 for each of the models were calculated according to Equations (6.6) through (6.8). In the analysis of the data, S_e represents the likely error in the prediction. The ratio S_e/S_y

can, therefore, be used to assess the accuracy of the predictive model. While S_e/S_y is a measure of the accuracy of the estimates, R^2 represents the accuracy of the model. Together, these two measures can be used to standardize the results in a "subjective goodness" classification (Witczak et al., 2002a). The criteria used in the classification are shown in Table 6.1.

$$S_e = \sqrt{\frac{\sum (y - \hat{y})^2}{(n-k)}} \tag{6.6}$$

$$S_y = \sqrt{\frac{\sum (y - \bar{y})^2}{(n-1)}} \tag{6.7}$$

$$R^2 = 1 - \frac{(n-k)}{(n-1)}\left(\frac{s_e}{s_y}\right)^2 \tag{6.8}$$

where,

S_e = standard error of estimate,

S_y = standard deviation,

R^2 = correlation coefficient,

y = measured dynamic modulus,

$\hat{y}$ = predicted dynamic modulus,

$\overline{y}$ = mean value of measured dynamic modulus,

n = sample size, and

k = number of independent variables in the model.

The measured and the predicted dynamic modulus values were also compared by plotting them on the LOE plot. If the matching points are clustered along the LOE line, then this would indicate that the predictive model has a good correlation to the measured

data. It is to be noted that the goodness-of-fit statistics and matching the predicted and the measured dynamic modulus values on the LOE line do not conclusively address the model accuracy (Ceylan et al., 2009b). Under certain conditions, systemic or local bias in the models can cause significant reduction in the accuracy of the predicted modulus. Therefore, the local bias statistics (slope, intercept) and the average error for each of the predictive models were used to determine the existence of bias. The intercept and slope were calculated by fitting an unconstrained linear trend line that does not pass through the origin (Ceylan et al., 2009b). A non-zero slope and average error indicate a consistent over-prediction or under-prediction by the model (Ceylan et al., 2009b; Obulareddy, 2006; Tran and Hall, 2005).

6.5 Results and Discussion

6.5.1 Overall Performance Evaluation

6.5.1.1 Goodness-of-Fit Criterion

To assess the overall performance of these models (i.e., Witczak 1999, Witczak 2006, Hirsch, and Al-Khateeb), the goodness-of-fit statistics (S_e/S_y, R^2) were calculated for a combined dataset of the five mixes used in the present study. A total of 1440 laboratory measured dynamic modulus values were used to check the strengths and weaknesses of each model. The S_e/S_y and R^2 values were calculated at logarithmic and arithmetic scales using Equations (6.7) through (6.9).

Table 6.2 summarizes the goodness-of-fit statistics calculated at logarithmic and arithmetic scales. It can be seen that the performance of the Witczak 1999 and Hirsch models was rated as 'good' in both the logarithmic and the arithmetic scales (Figure 6.1(a), Table 6.2). These results are consistent with those reported by Bari and Witczak, (2006) and Tran and Hall (2005). In comparison, the performance of both the Witczak

2006 and the Al Khateeb models were seen to be inferior to the performance of the Witczak 1999 and Hirsch models.

6.5.1.2 LOE Criterion

The predicted and the measured dynamic modulus values were plotted on the LOE plot. Figure 6.2 shows that the predictions obtained using the Witczak 1999 model are tightly clustered around the LOE. This indicates that the dynamic modulus values predicted by the Witczak 1999 model are in 'good' match with the measured dynamic modulus. The modulus values predicted by the Witczak 2006 model match well with the measured values at lower stiffness values; however, there is a significant mismatch exists between the measured and the predicted values at higher stiffness (Figure 6.3). Similarly, the modulus values predicted by the Hirsch model are dispersed around the LOE line, indicating that this model exhibits significant error (Figure 6.4). The Al-Khateeb model exhibits large deviations at low stiffness, indicating that this model is not sensitive at low values of modulus (Figure 6.5)

6.5.1.3 Local Bias Statistics Criterion

The relationship between the predicted and the measured values was investigated to determine the intercept, slope, and average error for each of the four models (Figure 6.1 (b)). The Witczak 1999 model shows a low intercept (0.40 GPa) and a slope close to 1 (i.e., 1.2). The average error for this model was calculated as 0.87 GPa, indicating that it over-estimates the dynamic modulus. Similar observations were also reported by other researchers (Abdo et al., 2009; Obulareddy, 2006; Tran and Hall, 2005). The Witczak 2006 model demonstrated the highest average error (3.1 GPa) and maximum slope (1.97 GPa) in comparison with the corresponding values for the other models. Thus, this model over-estimates dynamic modulus of the mix significantly. The Hirsch model exhibits the

lowest intercept (0.14 GPa) and the lowest average error (-0.16 GPa), indicating that a low bias exists for this model. The Al-Khateeb model shows the highest intercept (0.47 GPa), indicating that a significant bias exists in this model.

Based on the discussion above, it can be concluded that the performance of the Witczak 1999 model and the Hirsch model is ‘good’, while the Witczak 2006 and the Al-Khateeb model produce relatively ‘poor’ estimates of dynamic modulus.

6.5.2 Performance Evaluation at Individual Level of Air Voids

6.5.2.1 Goodness-of-Fit Criterion

Strengths and weaknesses of each predictive model were checked at four levels of air voids (i.e., 6%, 8%, 10%, and 12%). The Witczak 1999 model shows an 'excellent' goodness-of-fit statistics at 6% air voids (Figure 6.6, Table 6.3). In addition, the performance of this model was rated 'good' at three other levels of air voids (i.e., 8%, 10%, and 12%) (Table 6.3). It is important to note that with increasing air voids (i.e., 6% to 12%), S_e/S_y ratio increases and R^2 value decreases, indicating that the model results in significant errors at higher air voids.

The performance of the Witczak 2006 model deteriorates rapidly with increasing air voids. The performance of the model is 'good' at 6% air voids, while the accuracy deteriorates at higher levels of air voids (Figure 6.6, Table 6.3). The Hirsch model was rated 'fair' at 6% air voids, and it was rated 'good' at higher air voids (Figure 6.6, Table 6.3). The performance of the Al-Khateeb model was found to be 'poor' at all four levels of air voids (Figure 6.6, Table 6.3).

6.5.2.2 LOE Criterion

Figures 6.7 through 6.10 show the LOE plots of the measured and the predicted dynamic modulus. The performance of the Witczak 1999 model can be rated between

'excellent' and 'good' depending on the air voids of a compacted sample. In addition, it is seen from the Figure 6.7 that this model over-predicts dynamic modulus at higher air voids. The Witczak 2006 model over-predicts dynamic modulus at high modulus values for all air voids levels (Figure 6.8). The performance of the Hirsch model can be rated 'good' at high air voids (Figure 6.9). The Al-Khateeb model's predictions fit poorly with the LOE line, indicating that this model under- predicts dynamic modulus at all levels of air voids (Figure 6.10).

6.5.2.3 Local Bias Statistics Criterion

The slope, intercept, and average error for all the models calculated at four different levels of air voids are presented in Figure 6.11. The intercept for the Witczak 1999 model was observed to be less than 0.5 GPa (Figure 6.11 (a)). The slope increases with increasing air voids, indicating that this model over-predicts dynamic modulus at higher air voids (Figure 6.11 (b)). Similarly, the Witczak 2006 model yields the highest slope, indicating over-estimation of modulus. The slope calculated for the Hirsch and the Al-Khateeb models was observed close to 1 (Figure 6.11 (b)). The average error was found to be maximum for the Witczak 2006 model, while it was less than 1 GPa for other models (Figure 6.11 (c)).

It can be concluded that the performance of the Witczak 1999 model can be rated as 'excellent' at lower levels of air voids. However, the accuracy of the predicted dynamic modulus values reduces as the air voids increase. The performance of the Hirsch model is rated 'good' at higher levels of air voids. The Witczak 2006 and the Al-Khateeb models perform poorly at all levels of air voids.

6.5.3 Performance Evaluation with Temperature

The performance of each predictive model was evaluated at four temperatures: 4, 21, 40, and 55^{o}C. Figures 6.12 through 6.15 present the plot of average error calculated for different levels of air voids and temperatures. The negative and positive errors indicate under-prediction and over-prediction, respectively.

At 4^{o}C, the Hirsch and the Al-Khateeb models show the lowest average error for all levels of compaction (Figure 6.12). The Witczak 2006 model, on the other hand, had the largest error for all levels of compaction. The Witczak 1999 model performed well at lower air voids; however, it over-predicts dynamic modulus at higher air voids (Figure 6.12). These findings are consistent with the results reported in the literature (Ceylan et al., 2009a, 2009b; Far et al., 2009; Ceylan et al., 2008; Birgisson et al., 2005; Dongre et al., 2005).

The accuracy of the Hirsch and the Al-Khateeb models is poor at 21^{o}C. The Hirsch model under-predicts dynamic modulus for all levels of air voids, while the Al-Khateeb model over-predicts the modulus at higher air voids. The Witczak 1999 model shows excellent accuracy at 6% air voids, however, it shows poor accuracy at higher air voids. Both the Witczak 1999 and the Witczak 2006 models over-estimate dynamic modulus at higher air voids (Figure 6.13).

The Witczak 1999 and the Witczak 2006 models show small average errors (< 0.30 GPa) at high temperatures (40^{o}C, 55^{o}C) for all levels of air voids. At higher test temperatures (40^{o}C, 55^{o}C), both the Hirsch and the Al-Khateeb models under-predict dynamic modulus for all levels of air voids (Figure 6.14 and Figure 6.15).

It can be concluded that the Witczak 1999 model performs reasonably well at intermediate and high temperatures; however, it over-estimates modulus at lower

temperatures. The Witczak 2006 model over-predicts dynamic modulus at low and intermediate temperatures, while its performance is excellent at high temperatures. The Hirsch and the Al-Khateeb models under-predict dynamic modulus at higher temperatures.

6.6 Development of Calibration Factors

From the discussion in the previous sections, the dynamic modulus estimated by the Witczak 1999, Witczak 2006, Hirsch, and Al-Khateeb models depends on the temperature, as well as the level of compaction of a specimen. This error has to be corrected before the model can be used in Level 2 and Level 3 designs of the MEPDG. In this study, a linear regression model is used to determine the calibration factor (i.e., the slope required for such a correction). It can be seen from Figure 6.16 that the slope (correction factor) of the linear regression line decreases with increasing air voids for each of the prediction models considered in this study. Therefore, the accuracy of the estimated modulus can be improved by considering the calibration factor at the corresponding air voids rather than using the average calibration factor determined across all the air voids. Failure to account for the variation in the estimated modulus due to air voids can result in significant errors. Figure 6.17 shows the percent error in the predicted modulus when an average calibration factor is used instead of a calibration factor determined at the appropriate air voids. This error in the estimation of dynamic modulus might impact the performance of flexible pavements (i.e., rutting, fatigue cracking, and thermal cracking). The relationship between the air voids and the calibration factor for all four predictive models is shown in Figure 6.18.

It is anticipated that use of calibration factors would be helpful in estimating dynamic modulus without conducting actual modulus tests. Moreover, calibration factors are important for the Level 2 and Level 3 designs of the MEPDG.

6.7 Summary of Results

In the present study, the performance of four predictive models (i.e., Witczak 1999, Witczak 2006, Hirsch, and Al-Khateeb) was evaluated for selected mixes that are commonly used in Oklahoma. The following conclusions can be drawn from the results and discussion presented in this chapter.

(1) The performance of each predictive model varies with the air voids and temperature of the test specimen.

(2) The Hirsch and the Al-Khateeb models were seen to perform with good accuracy at low temperatures. The Witczak 1999 and the Witczak 2006 models performed with good accuracy at high temperatures.

(3) None of the models performed well at low temperatures and high air voids.

(4) Calibration factors were developed at individual air void levels to account for the inaccuracies in the model.

(5) The relationship between air voids and the calibration factor is important to assist state agencies and pavement designers for Level 2 and Level 3 designs of the MEPDG for asphalt mixes commonly used in Oklahoma. It is anticipated that the use of calibration factors would be helpful in estimating dynamic modulus without conducting actual modulus tests in the laboratory.

Table 6.1 Criteria for Subjective classification of the goodness-of-fit

Criteria	R^2	S_e/S_y
Excellent	> 0.90	< 0.35
Good	0.70 - 0.89	0.36 - 0.55
Fair	0.40 - 0.69	0.56 - 0.75
Poor	0.20 - 0.39	0.76 - 0.90
Very Poor	< 0.19	> 0.90

Table 6.2 Overall Performance Evaluation on Combined Dataset: Goodness-of-fit Statistics

Model	Logarithmic Scale			Arithmetic Scale		
	S_e/S_y	R^2	Rating	S_e/S_y	R^2	Rating
Witczak 1999	0.39	0.85	Good	0.53	0.72	Good
Witczak 2006	0.62	0.61	Fair	1.57	< 0.19	Very Poor
Hirsch	0.52	0.73	Good	0.41	0.83	Good
Al-Khateeb	0.82	0.33	Poor	0.51	0.74	Good

Table 6.3 Goodness-of-Fit Statistics at Individual Level of Air Voids

Witczak 1999						
Air Voids	Logarithmic Scale			Arithmetic Scale		
(%)	S_e/S_y	R^2	Rating	S_e/S_y	R^2	Rating
6	0.33	0.91	Excellent	0.31	0.91	Excellent
8	0.37	0.86	Good	0.52	0.73	Good
10	0.4	0.82	Good	0.74	0.46	Fair
12	0.5	0.75	Good	0.89	0.20	Poor
Witczak 2006						
Air Voids	Logarithmic Scale			Arithmetic Scale		
(%)	S_e/S_y	R^2	Rating	S_e/S_y	R^2	Rating
6	0.47	0.78	Fair/Good	1.16	<0.19	Very Poor
8	0.58	0.66	Fair	1.51	<0.19	Very Poor
10	0.7	0.54	Fair	2.02	<0.19	Very Poor
12	0.8	0.38	Poor	2.45	<0.19	Very Poor
Hirsch						
Air Voids	Logarithmic Scale			Arithmetic Scale		
(%)	S_e/S_y	R^2	Rating	S_e/S_y	R^2	Rating
6	0.66	0.56	Fair	0.39	0.85	Good
8	0.51	0.74	Good	0.37	0.86	Good
10	0.5	0.77	Good	0.45	0.80	Good
12	0.5	0.79	Good	0.63	0.60	Fair
Al-Khateeb						
Air Voids	Logarithmic Scale			Arithmetic Scale		
(%)	S_e/S_y	R^2	Rating	S_e/S_y	R^2	Rating
6	0.98	0.05	Very Poor	0.45	0.80	Good
8	0.81	0.34	Poor	0.43	0.82	Good
10	0.8	0.36	Poor	0.56	0.68	Fair
12	0.8	0.36	Poor	0.90	0.19	Very Poor

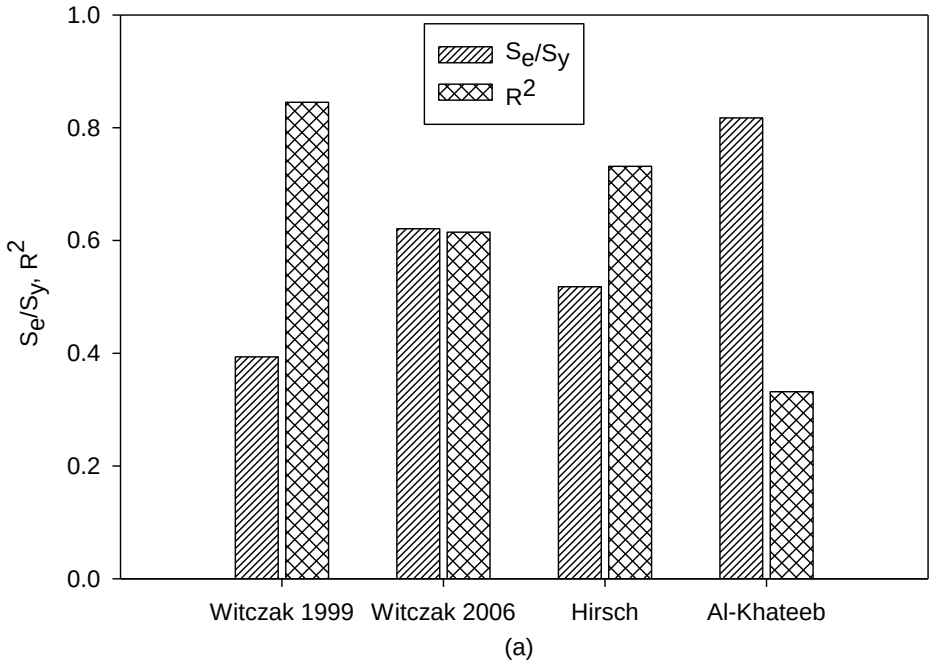

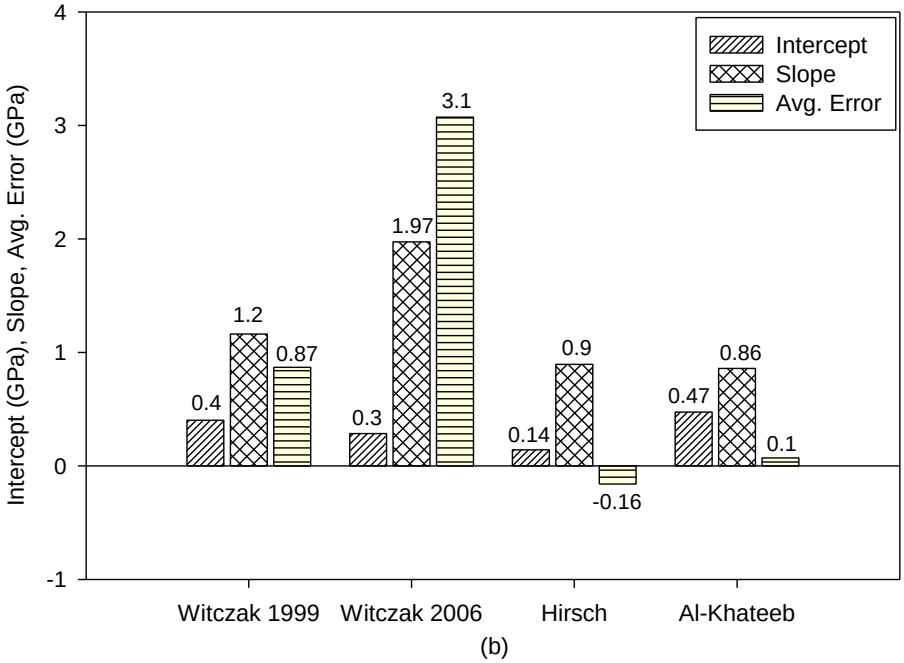

Figure 6.1 Overall Performance Evaluation (a) S_e/S_y, R^2 (b) Intercept, Slope, and Average Error

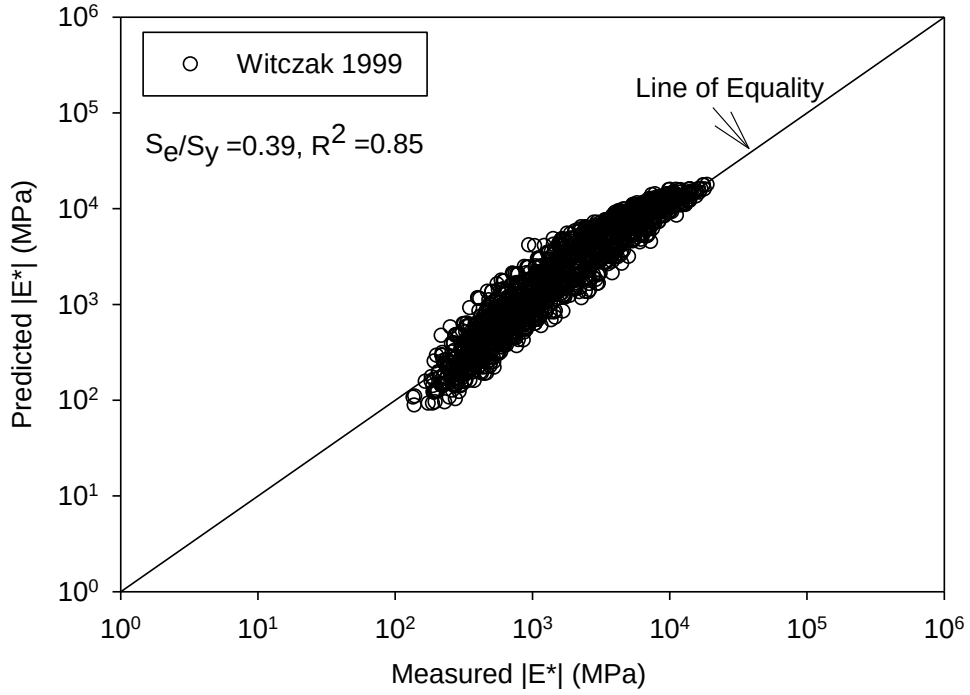

Figure 6.2 LOE Plot of Witczak 1999 Model for Overall Performance

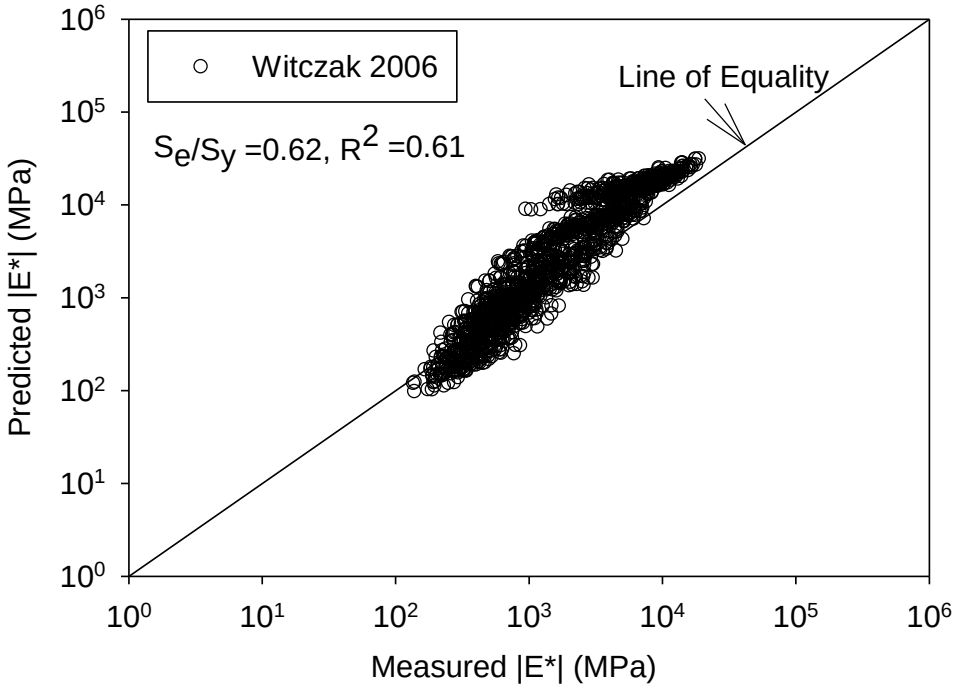

Figure 6.3 LOE Plot of Witczak 2006 Model for Overall Performance

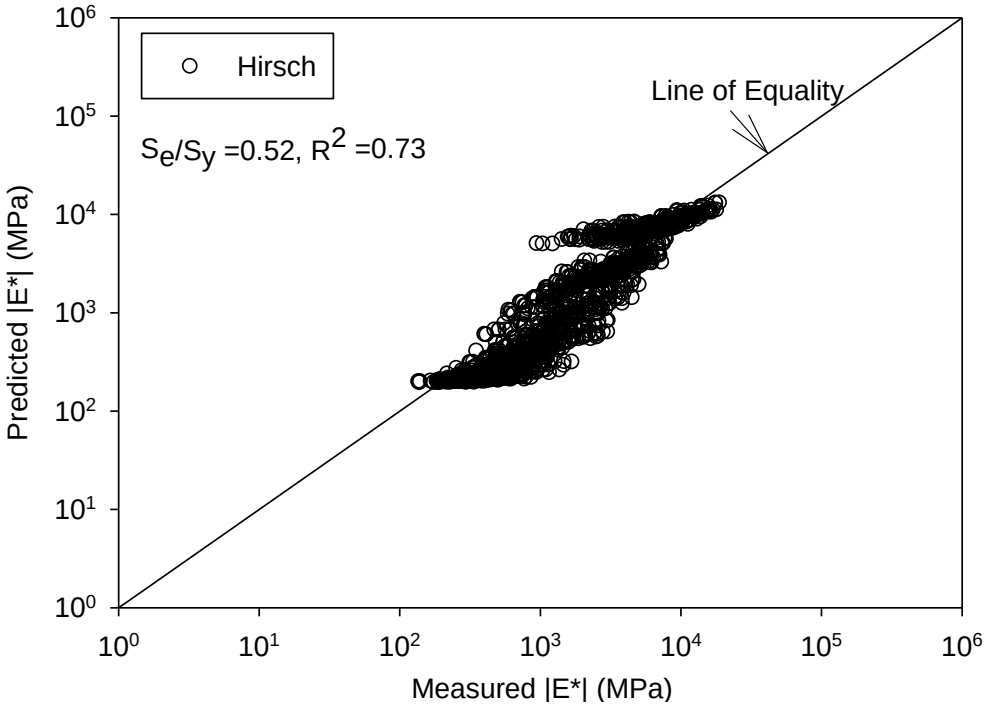

Figure 6.4 LOE Plot of Hirsch Model for Overall Performance

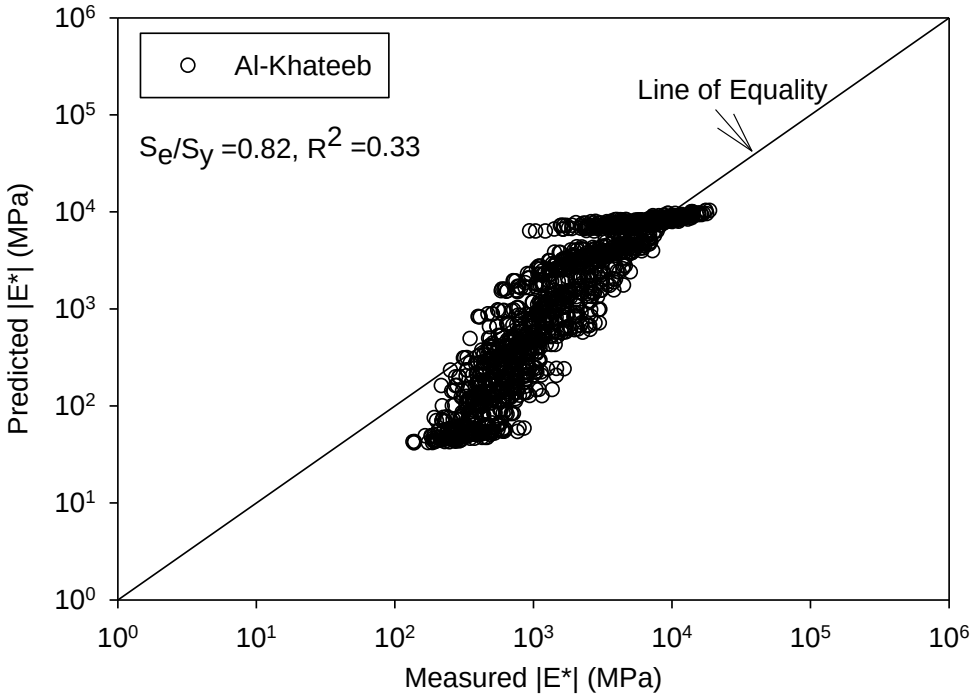

Figure 6.5 LOE Plot of Al-Khateeb Model for Overall Performance

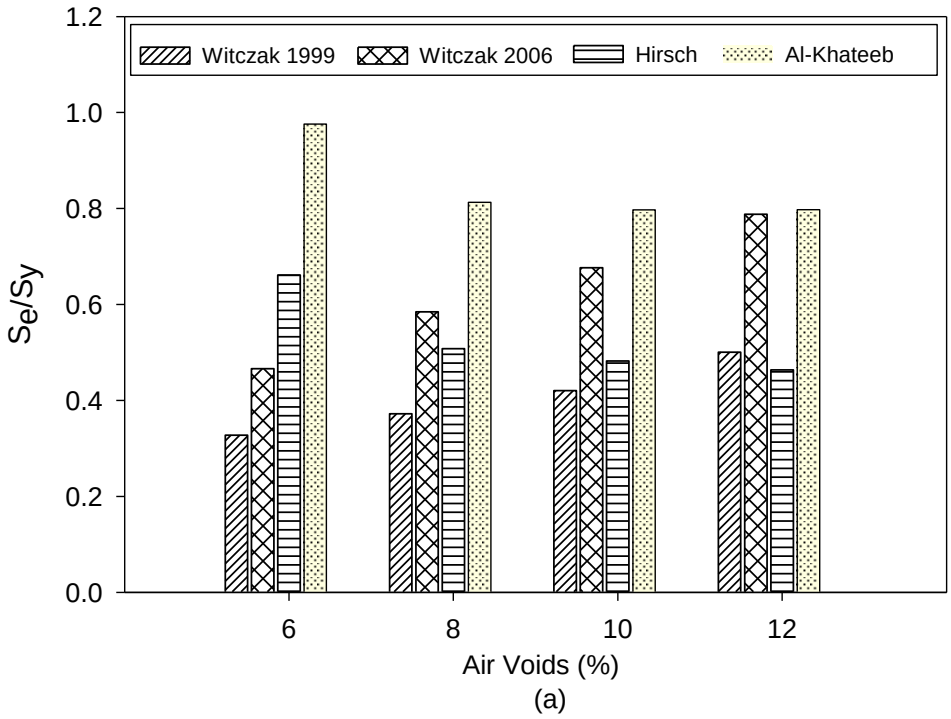

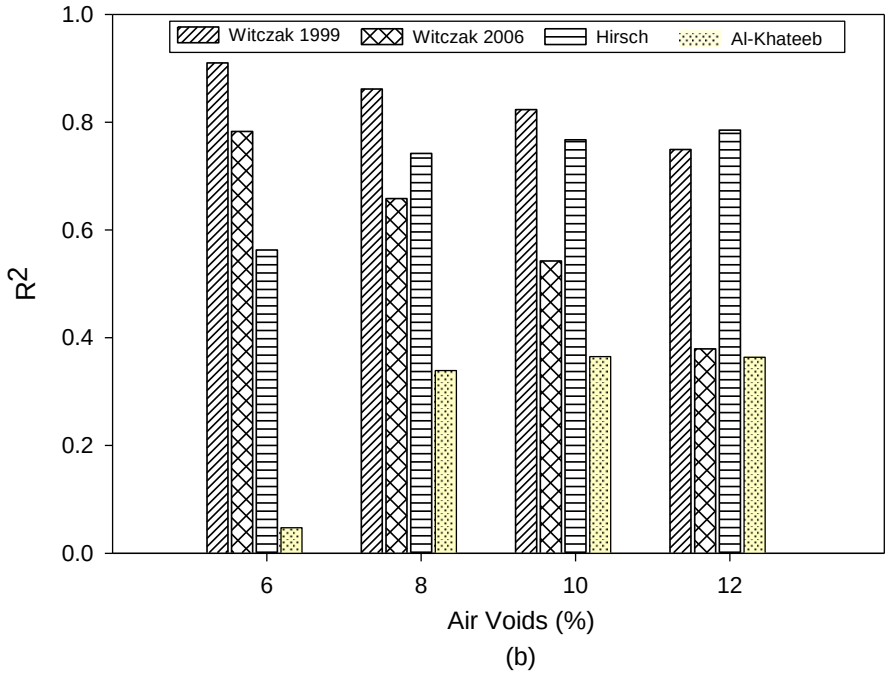

Figure 6.6 Goodness-of-Fit Statistics at Each Level of Air Voids (a) S_e/S_y (b) R^2

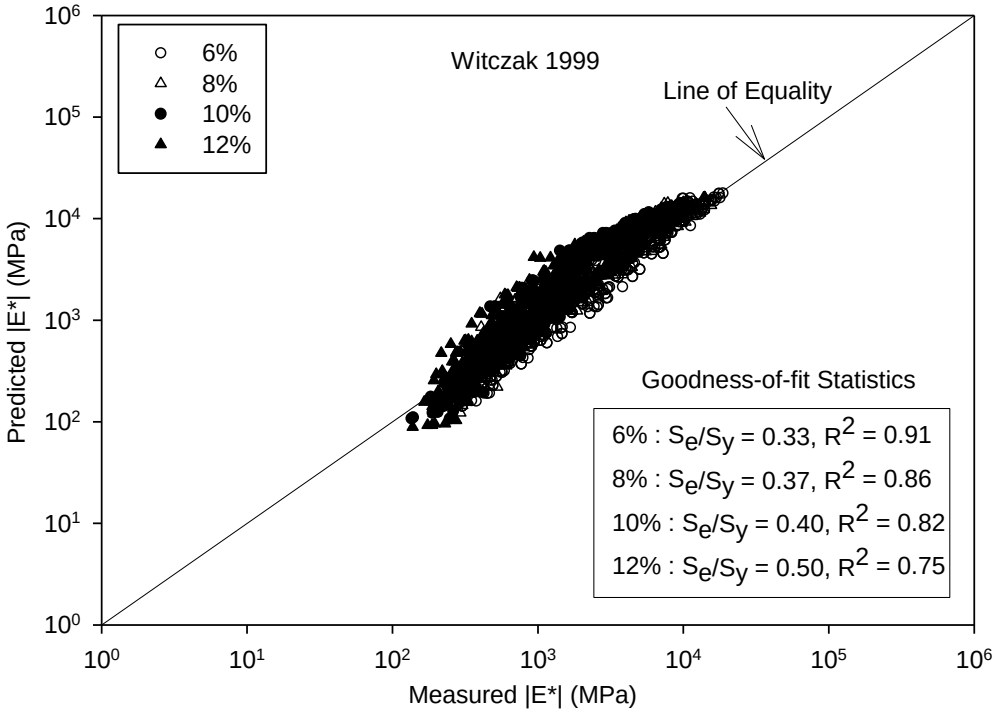

Figure 6.7 LOE Plot at Each Level of Air Voids for Witczak 1999 Model

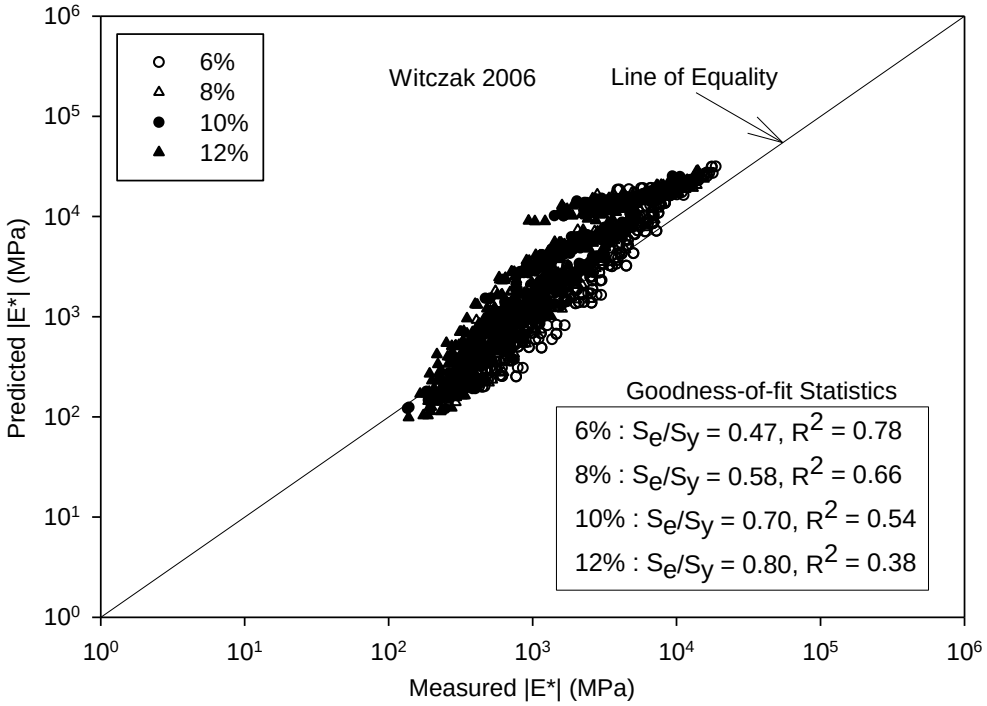

Figure 6.8 LOE Plot at Each Level of Air Voids for Witczak 2006 Model

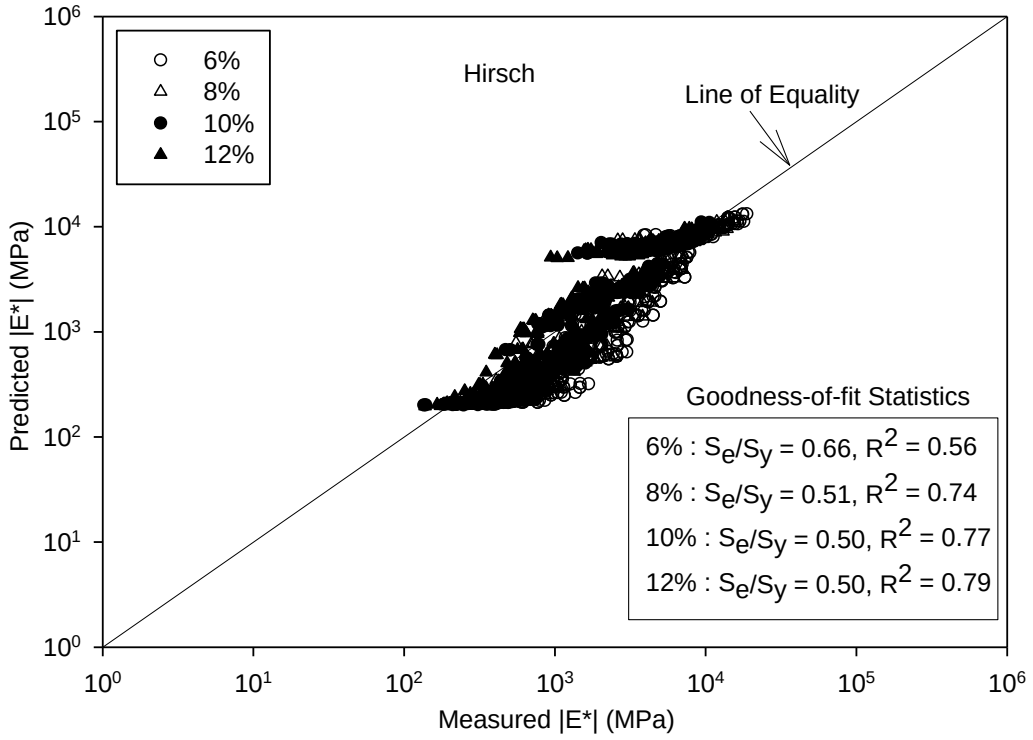

Figure 6.9 LOE Plot at Each Level of Air Voids for Hirsch Model

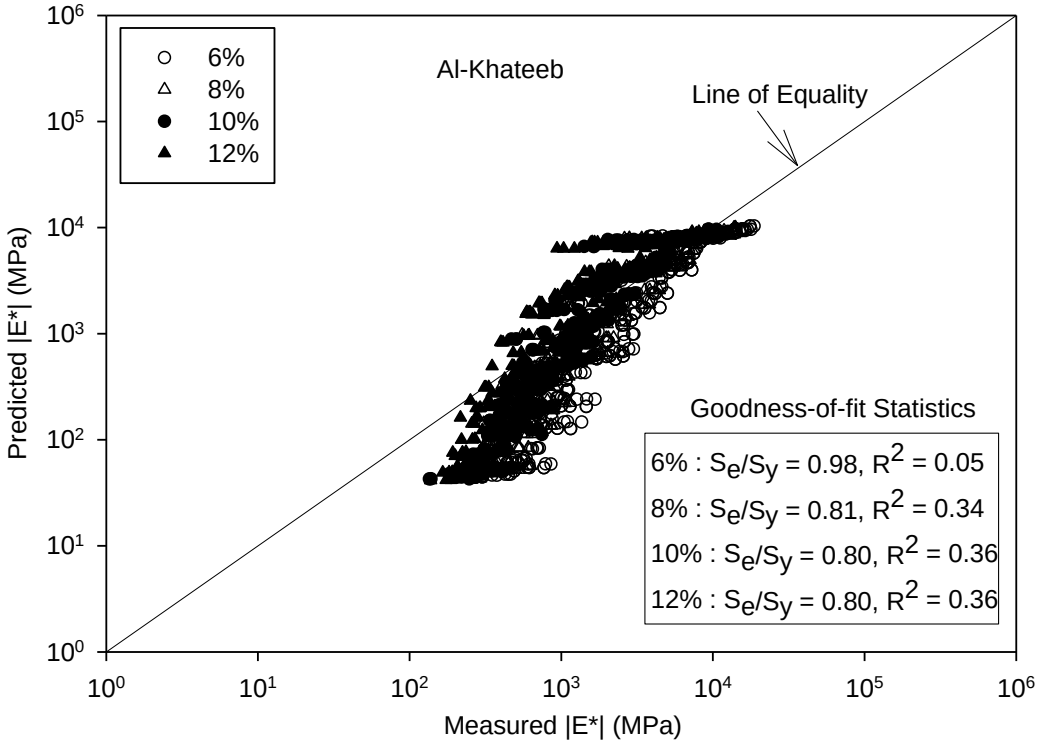

Figure 6.10 LOE Plot at Each Level of Air Voids for Al-Khateeb Model

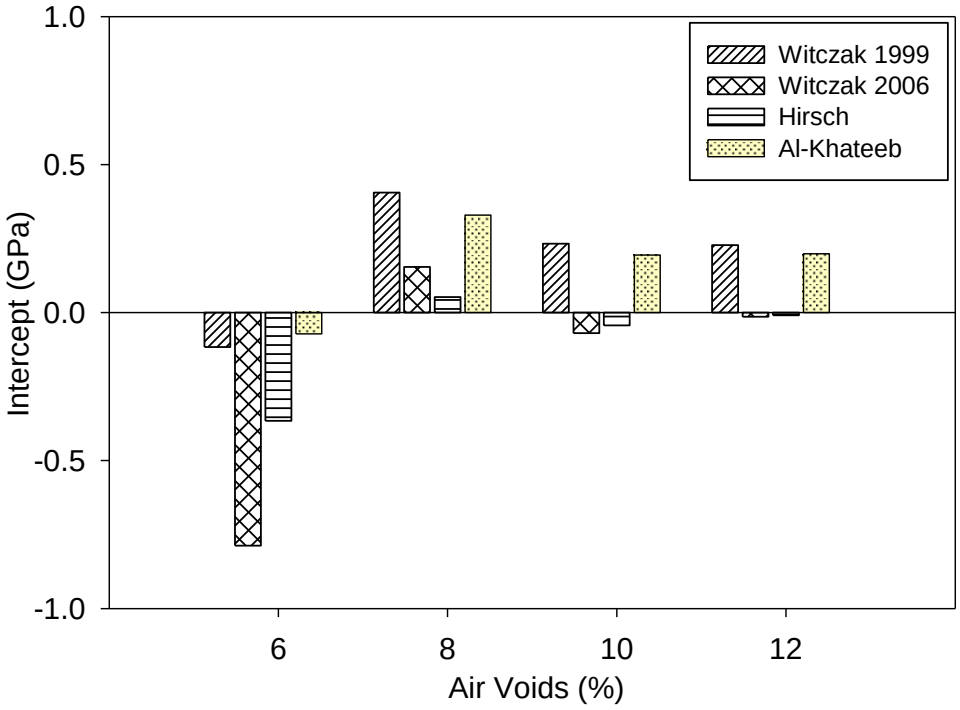
1.0
0.5
0.0
-0.5
-1.0
Intercept (GPa)
Witczak 1999
Witczak 2006
Hirsch
Al-Khateeb
6
8
10
12
Air Voids (%)

(a)

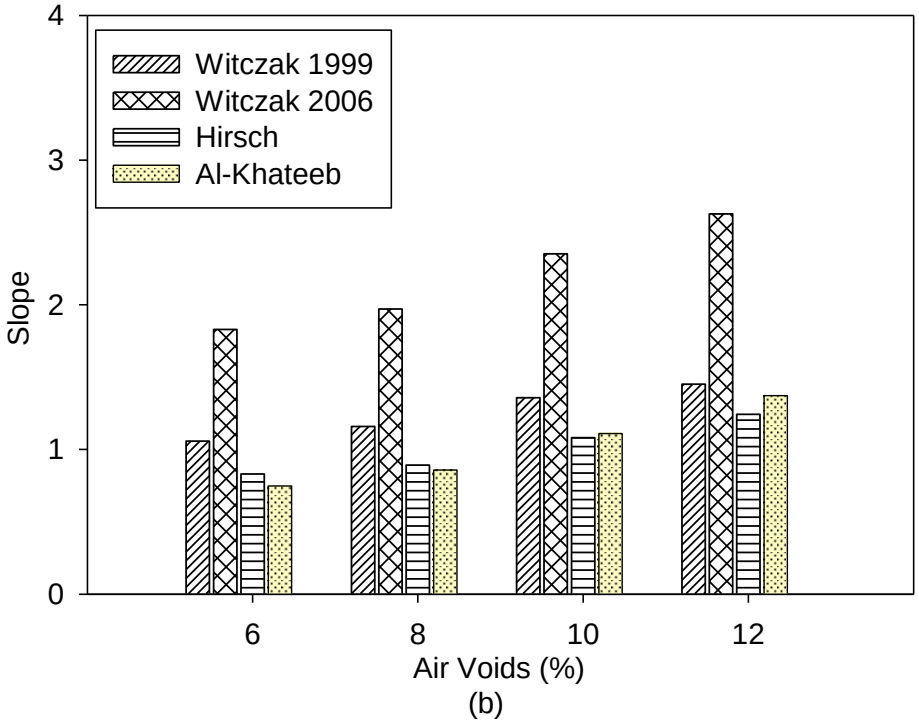
4
3
2
1
0
Slope
Witczak 1999
Witczak 2006
Hirsch
Al-Khateeb
6
8
10
12
Air Voids (%)

(b)

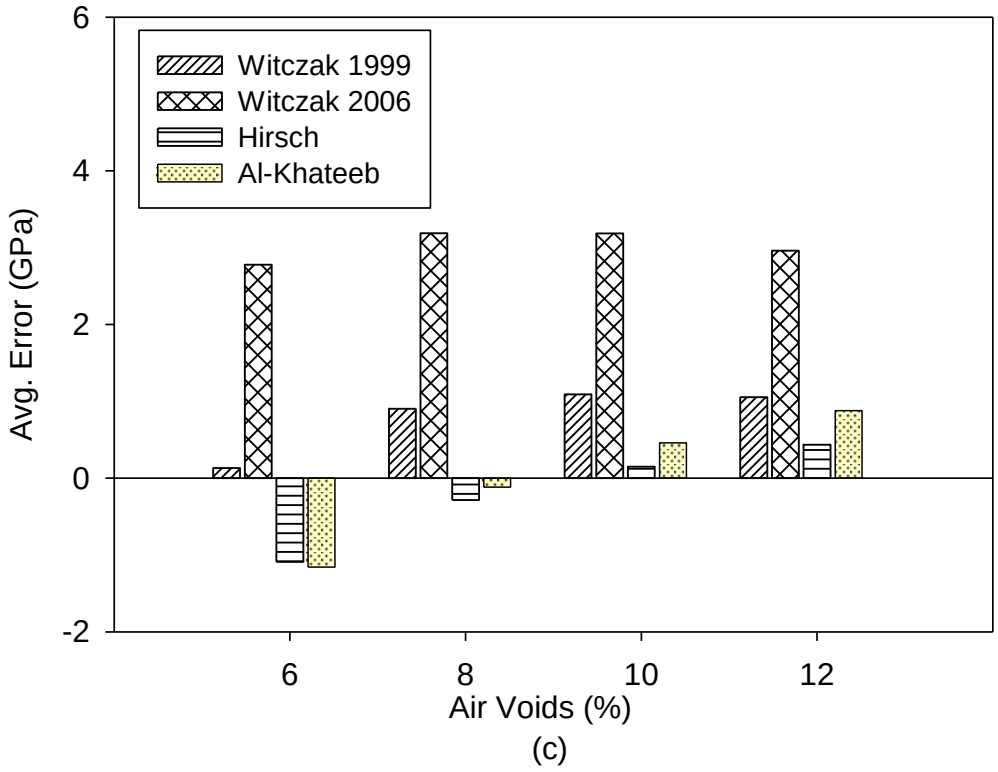

Figure 6.11 Local Bias Statistics at Each Level of Air Voids (a) Intercept, (b) Slope, and (c) Average Error

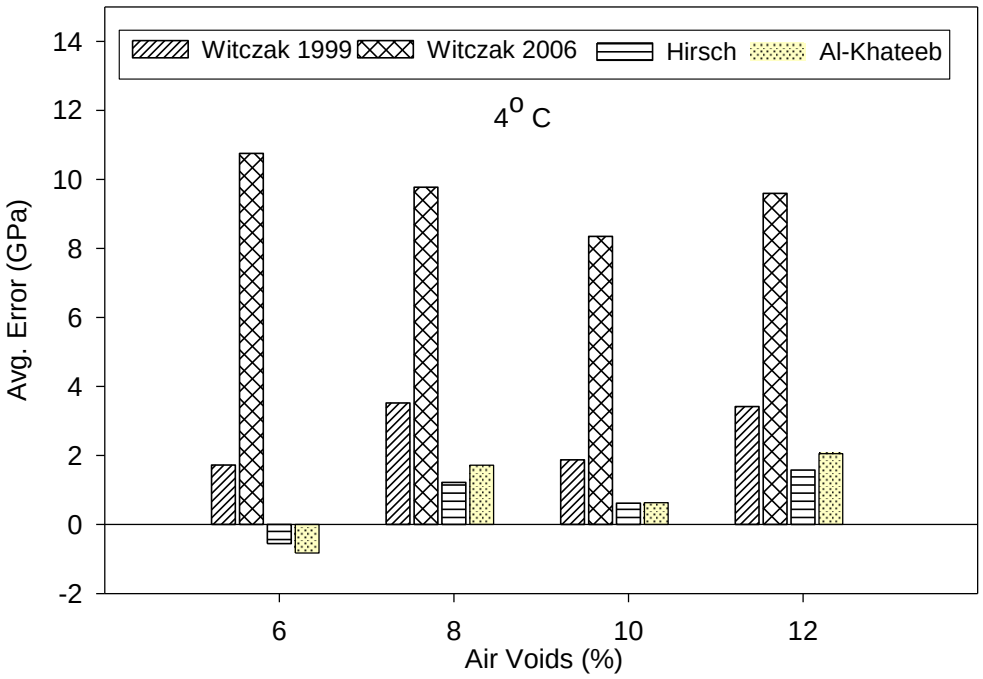

Figure 6.12 Average Errors at 4°C for Each Level of Air Voids

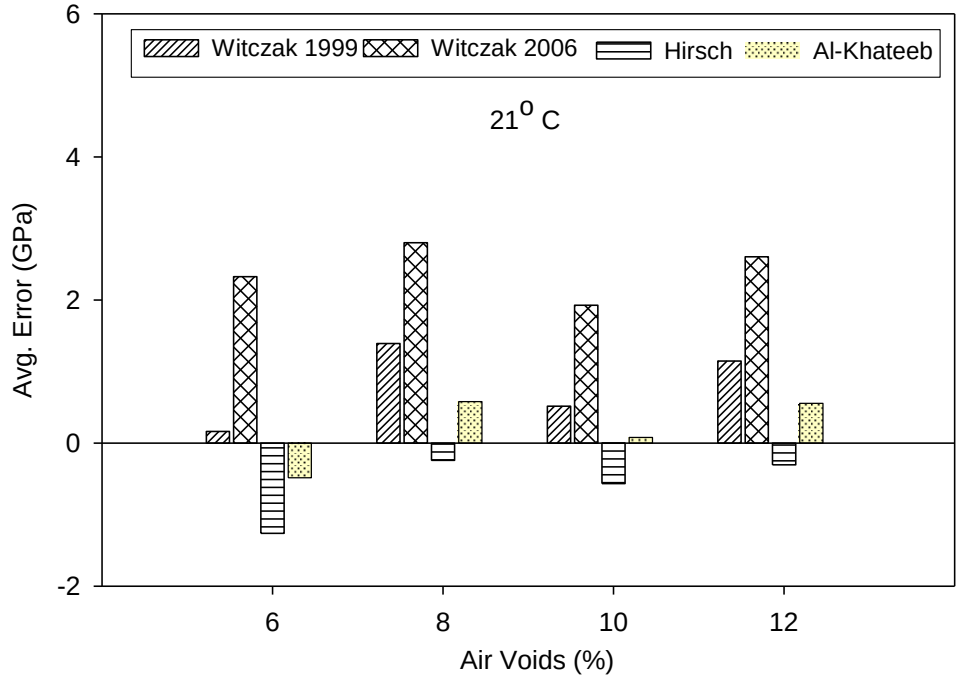

Figure 6.13 Average Errors at 21°C for Each Level of Air Voids

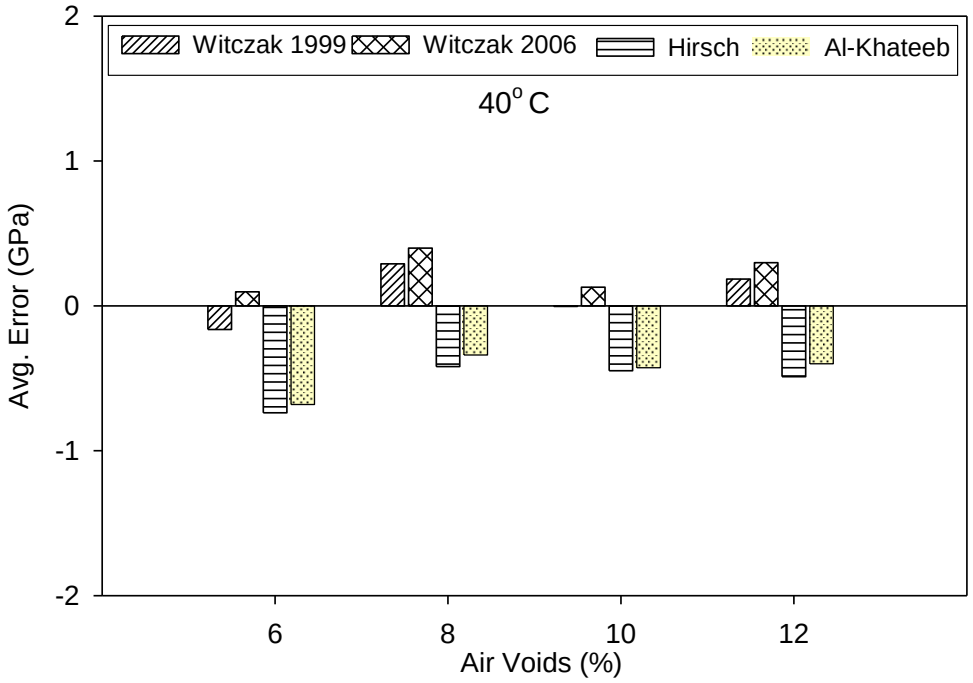

Figure 6.14 Average Errors at 40°C for Each Level of Air Voids

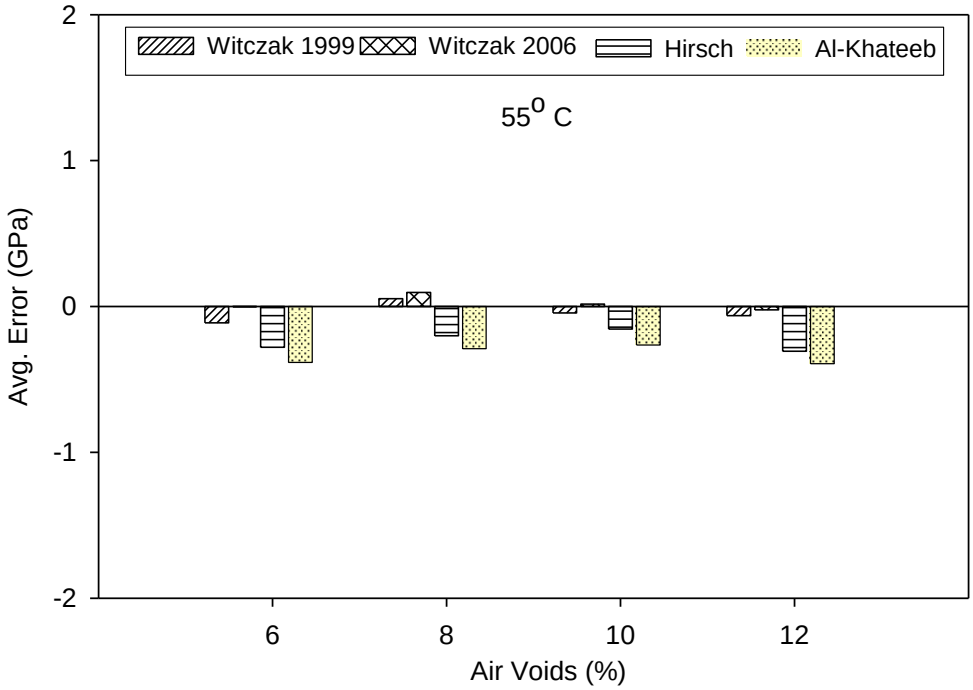

Figure 6.15 Average Errors at 55°C for Each Level of Air Voids

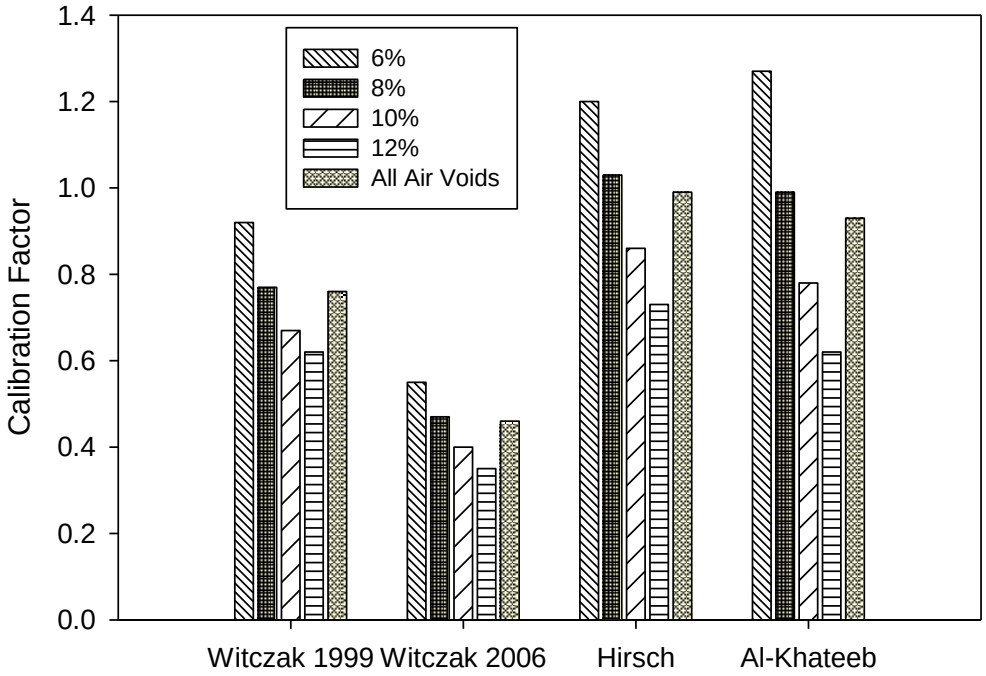

Figure 6.16 Calibration Factor at Each Level of air Voids

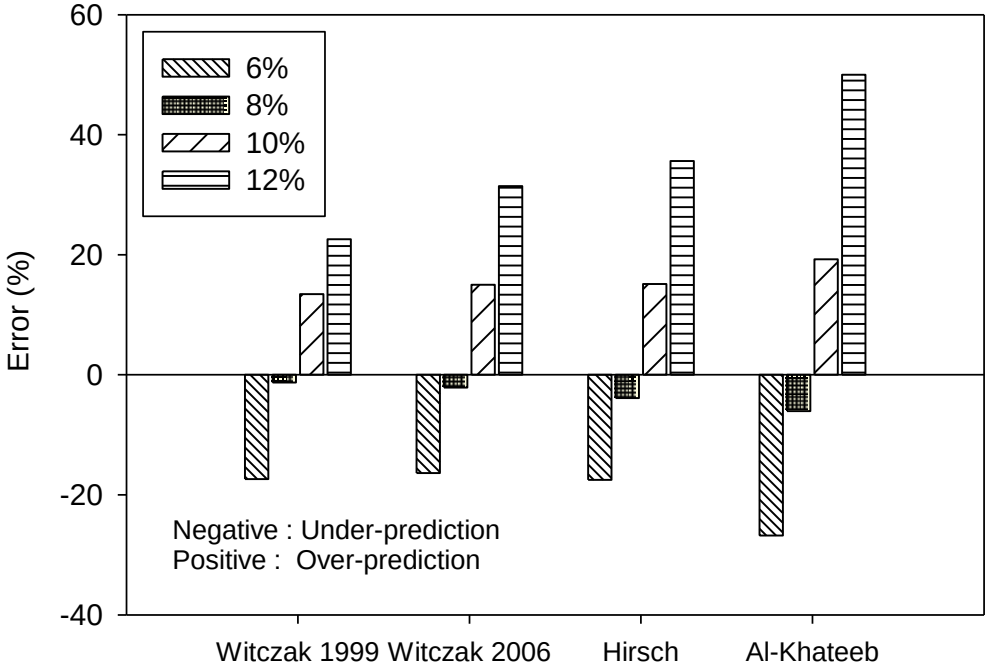

Figure 6.17 Estimated Error Associated with Calibration Factor

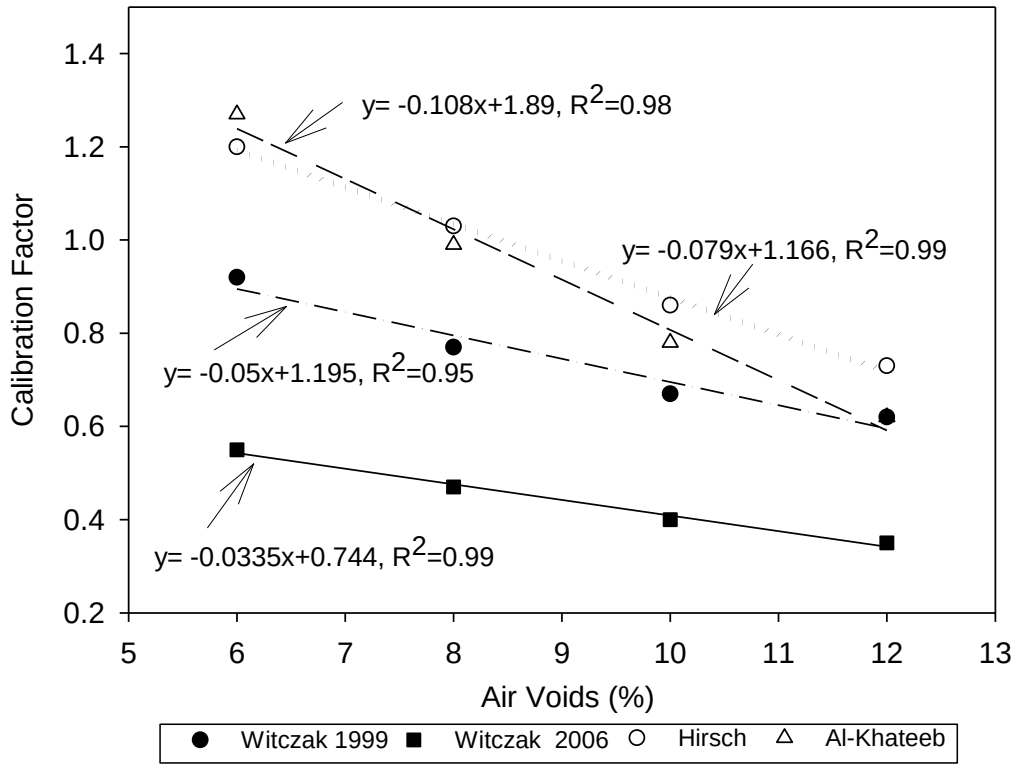

Figure 6.18 Relationship between the Calibration Factors and Air Voids

CHAPTER 7 : STATISTICAL AND NEURAL NETWORK MODELING OF DYNAMIC MODULUS

7.1 Introduction

Currently several predictive models (i.e., Witczak, Hirsch, and Al-Khateeb models) (see Chapter 6) are available in the literature to estimate the dynamic modulus of asphalt mixes. The input parameters of these models include: aggregate gradation (i.e., percentage passed and retained on selected sieve sizes), viscosity of asphalt binder, shear modulus of asphalt binder, and volumetric properties of the mix (i.e., air voids, frequency, voids in mineral aggregates, effective binder). Although these models consider the gradation of the aggregate, none of the model takes into account the aggregate shape properties as input parameters in the estimation of dynamic modulus. Since the volumetric properties of the mix depend on the shape parameters (i.e., angularity, texture, form, and sphericity) of the aggregates, it is expected that these shape parameters would directly influence the dynamic modulus values as well.

Furthermore, at high temperatures, asphalt mixes behave like a granular non-linear elastic material; therefore, aggregate gradation and shape parameters play an important role (Bari and Witczak, 2006). Generally, rough-textured surfaces result in stronger mixes by providing more friction between aggregate faces (Kandhal and Mallick, 2001; Ahlrich, 1996; Roberts et al., 1996; Sousa et al., 1991; Brown and Bassett, 1990; Button et al., 1990). Similarly, angular aggregates provide a better interlock, and consequently an increase in rut resistance (Kandhal and Mallick, 2001; Sousa et al., 1991; Brown and Bassett, 1990; Button et al., 1990). Several researchers have reported that shape characteristics of aggregates have a direct influence on the performance and the serviceability of pavements (Liu and You, 2011; Wang et al., 2008; Lynn et al., 2007;

Masad et al., 2007a, 2007b; Alvarado et al., 2006; Pan et al., 2006; Fletcher et al., 2002; `Kuo, 2002; Masad et al., 2001b; Coree and Hislop, 2000). Bari and Witczak (2006) mentioned that two mixes with different aggregate shape parameters but the same aggregate gradation and volumetric properties could possibly result in different dynamic modulus values. Researchers have emphasized that these aggregate shape parameters need to be considered to enhance the prediction capability of a model (Ceylan et al., 2009a, 2009b; Harran and Shalaby, 2009; Bari and Witczak, 2006; Dongre et al., 2005). However, there is no model available at the present that considers these shape parameters as an input variable in estimation of dynamic modulus.

Usually, the finite element method (FEM) (Dai and You, 2007; Papagiannakis et al., 2002; Masad et al., 2001a) and discrete element method (DEM) (Liu and You, 2011; You et al., 2008; You and Buttlar, 2006; Abbas et al., 2005) are used to simulate the heterogeneity of asphalt mixture including aggregates and asphalt binder. Dai (2010) simulated the structure of asphalt mixture using a FEM approach. The results indicated that micromechanical FEM-based models provided reasonable predictions of dynamic modulus and phase angle over a range of frequencies. Similarly, Aragao et al. (2010) developed a FEM micromechanics model to estimate the dynamic modulus of asphalt mixes. They compared the performance of FEM model with the Witczak model. It was reported that FEM model can directly account for geometric complexity and inelastic mixture component properties.

Recently Liu and You (2011) have reported a DEM-based model to study the impact of aggregate sphericity, orientation, and angularity on creep stiffness of asphalt mixes. It was found that as the sphericity increases, the creep stiffness of the asphalt

mixture increases or decreases, depending on the angles of aggregate orientation. Aggregate particles with two or three fractured faces can improve asphalt mixture creep stiffness better than those with one fractured face. In another study, Bennert et al. (2011) observed that asphalt pavement analyzer (APA) rut and flow numbers are sensitive to the angularity of aggregates. Similarly, Kuo (2002) reported a strong correlation between permanent deformation of asphalt mixtures and aggregate geometric irregularities.

Recognizing the importance of aggregate morphological properties, the present study was undertaken to develop an aggregate shape-based model for estimating dynamic modulus of asphalt mixes. To achieve this objective, dynamic modulus tests on several mixes were conducted as per AASHTO TP62 (AASHTO, 2006). The aggregate shape properties of different coarse and fine aggregates were measured using the aggregate image measurement system (AIMS). Two different types of models: statistical and neural network-based are developed for estimating the dynamic modulus of asphalt mixes. It is anticipated that the present study would be helpful in characterizing the mixes in more accurate manner.

7.2 Materials and Testing

A total of five mixes are used to develop the models (see Chapter 2). Each mix was subdivided into four different groups. The division of a mix into groups was done based on the target air voids at which the samples were prepared. A total of four different levels of air voids: 6%, 8%, 10%, and 12% were selected. Therefore, a total of 20 different groups of mixes (M11 through M54) were prepared out of five mixes (5 mixes x 4 groups each for one level of air voids) (Table 7.1). Three samples were compacted for each mix. Therefore, a total of 60 samples were compacted out of 20 mixes (3 samples x 20 mixes). Table 7.1 shows the volumetric properties of the compacted samples for all

the mixes. Dynamic modulus testing was conducted on each compacted sample in accordance with AASHTO TP62 (AASHTO, 2006). A total of 1440 (20 mixes x 3 samples x 4 temperatures x 6 frequencies) dynamic modulus values were measured in the laboratory.

After the dynamic modulus test, the aggregates from each of the compacted samples of all the mixes were retrieved by burning them in the NCAT ignition oven. The aggregates were processed and the gradation was analyzed. The aggregates of each mix were divided into three different sizes of coarse aggregates (CA): passing a 19 mm sieve and retained on a 12.5 mm sieve (P19-R12.5), passing a 12.5 mm sieve and retained on a 9.5 mm sieve (P12.5-R9.5), and passing a 9.5 mm sieve and retained on a 4.75 mm sieve (P9.5-R4.75). Similarly, the aggregates were divided into two different sizes of fine aggregates (FA): passing a 4.75 mm sieve and retained on a 2.36 mm sieve (P4.75-R2.36), and passing a 2.36 mm sieve and retained on a 1.18 mm sieve (P2.36-R1.18). Therefore, each mix was divided into three sizes of coarse aggregates (i.e., P19-R12.5, P12.5-R9.5, and P9.5-R4.75) and two sizes of fine aggregates (i.e., P4.75-R2.36 and P2.36-R1.18). Table 7.2 shows the percentage of particles retained for each size of aggregate.

A slight difference in the gradation of the mix compacted at different levels of air voids was observed. This variation could be due to the fact that the mixes compacted at different air voids exert different pressure inside the SGC, resulting in a change in the gradation of aggregates. Although, the gradation plot is helpful in understanding the change in aggregate size, it cannot provide the information on change in aggregate shape parameters. Since aggregate in a mix undergo different laboratory processes, namely

compaction, coring and sawing in the laboratory, it is quite possible that the aggregates extracted from the compacted specimen have different shape parameters. Therefore, gradation and shape parameters of each mix have to be analyzed separately.

7.3 Measurement of Shape Parameters

Pine's AIMS was used to measure angularity, texture, form, and sphericity of different sizes of coarse and fine aggregates. The AIMS was operated as per the guidelines and specifications provided in Masad (2005). The additional details on the AIMS can be found in Chapter 3. Table 7.3 summarizes the AIMS test matrix for all the aggregates. A total of 120 coarse aggregate samples comprising of 6720 aggregates particles (2 samples x 56 particles x 3 sizes x 20 mixes) were tested in the AIMS. Similarly, a total of 40 fine aggregates samples (1 sample x 2 sizes x 20 mixes) were tested for fine aggregates. In general, coarse aggregates were found to be more angular compared to fine aggregates.

7.4 Composite Index (CI) Factor

As mentioned before, the shape parameters of three different sizes of coarse aggregates (i.e., P19-R12.5, P12.5-R9.5, and P9.5-R4.75) and two different sizes of fine aggregates (i.e., P4.75-R2.36, and P2.36-R1.18) were measured using the AIMS. Therefore, to come up with a single shape index factor for coarse and fine aggregates, a composite index (CI) factor was estimated for each shape parameter using Equation (7.1).

$$CI = \frac{\sum_{i=1}^{n}[(a_i)(x_i)]}{\sum_{i=1}^{n} x_i} \tag{7.1}$$

where,

CI = composite shape index parameter,

a_i = mean shape parameter for a selected sieve size, and

x_i = percentage retained aggregates on selected sieve sizes.

This equation uses mean shape parameter (a_i) for each size of aggregates and percentage retained particles (x_i) on selected sieves. CI for coarse aggregates was named as: composite angularity index for coarse aggregates (COAI), composite form index for coarse aggregates (COFI), and composite texture index for coarse aggregates (COTI). CI for fine aggregates was named as: composite angularity index for fine angularity (FAI).

7.5 Statistical Modeling

7.5.1 Development of Statistical Model

For the purpose of developing a model, a comprehensive database was developed. The measured dynamic modulus values, loading frequency, viscosity of asphalt binders, aggregate shape parameters, and volumetric properties of the compacted samples are used in developing the database. Sixteen different mixes (M11 through M44) were used in developing the model. The following independent variables were selected: viscosity (η) (10^6 poise), frequency (f) (Hz), COAI, COFI, COTI, FAI, air voids (V_a) (%), and effective asphalt binder (% volume) (V_{beff}). Dynamic Modulus (|E*|) (MPa) was selected as dependent variable.

The intercept (A) and slope (VTS) values pertaining to the temperature-viscosity relationship of each asphalt binder were estimated (see Chapter 2). The viscosity of the asphalt binders at the test temperatures (i.e., 4, 21, 40, and 55^{o}C) was calculated using the ASTM equation (ASTM, 2009) (see Chapter 2).

The 'x_i' values for the mixes are provided in Table 7.2, while 'a_i' values were measured in the AIMS. CI factors for all the mixes (M11 to M54) are calculated using

Equation (7.1). Table 7.4 summarizes the COAI, COFI, COTI, and FAI for all the mixes. No specific correlation was observed among different shape indices.

Table 7.5 summarizes the descriptive statistics of the database. The database covered a large range of viscosities (0.01×10^6 to 3070×10^6 Poise), frequencies (1 Hz to 25 Hz), air voids (5.4% to 12.4%), V_{beff} (8.1% to 11.3%), and shape parameters. The modeling was done using commercially available software called Statistical Package for the Social Sciences (SPSS®16). For each mix (M11 through M44), data were arranged in the SPSS data manager. A non-linear regression method was used to develop a relationship between dynamic modulus and its associated parameters. Several combinations of the model were tried, and finally Equation (7.2) was considered to be the best fit model.

$$Log|E^*| = 2.0331 + 0.08644\ (COAI) + 0.2914\ (COFI) - 0.0022\ (COTI) - 0.03258\ (FAI) - 0.0624\ V_a + 0.0418\ (V_{beff}) + \left(\frac{-5.0921 + 0.1195\ (COAI) - 0.0548\ (COFI) + 0.00326\ (COTI) + 0.1196\ (FAI)}{1 + \exp\ (-0.1861 + 0.4039\ \log\ (f) + 0.4474\ \log\ (\eta))}\right) \quad (7.2)$$

where,

$|E^*|$, η, f, V_a , V_{beff} , COAI, COFI, COTI, FAI, are as defined above.

The performance of the developed model (Equation (7.2)) was assessed by calculating coefficient of correlation (R^2) and S_e/S_y at logarithmic and arithmetic scales. Moreover, mean absolute relative error (MARE) was estimated to measure the accuracy of the model. The R^2 is a measure of correlation between the predicted and the measured values. The R^2 value close to 1 indicates that the predictions of a model are in good agreement with the measured data. Similarly, the lower S_e/S_y and MARE represent that the model would result in lesser amount of error in the prediction. Therefore, a higher

value of R^2 and a lower value of S_e/S_y and MARE are desired for a better performance of a model.

Figure 7.1 shows the plot of the measured and the predicted dynamic modulus for sixteen different mixes. R^2 and S_e/S_y for the developed model was found to be 0.95, 0.22; and 0.92, 0.29 on logarithmic and arithmetic scales, respectively. The MARE was found to be 21.9%, which is close to the estimated limit of accuracy using two LVDTs (AASHTO, 2006). The variability in the measured dynamic modulus can be reduced by increasing the number of LVDTs and specimens. The results indicate that the model has a strong correlation with its parameters. The developed model has a similar form as the Witczak model. However, it is worthwhile to note that the developed model (Equation (7.2)) uses the aggregate shape parameters, while the Witczak model considers gradation of the aggregates.

7.5.2 Validation of the Developed Model

The performance of the developed model was checked for M51, M52, M53, and M54. These mixes were not used in the development process. It was found that shape parameters of samples compacted at M51 and M52 were out of range of the database used for the development of the model; therefore they were not considered for the validation purpose. Thus, only mixes M53 and M54 were selected for the purposes of validation. The volumetric properties, percentage aggregate retained, and CI of these mixes are summarized in Table 7.1, Table 7.2, and Table 7.4, respectively. Equation (7.2) was used to estimate dynamic modulus for these mixes. It was decided to compare the performance of the developed model with the Witczak model (Andrei et al., 1999).

Figure 7.2 and Figure 7.3 show the predicted and the measured dynamic modulus for M53 (i.e., 10% air voids) and M54 (i.e., 12% air voids) mixes, respectively. At 10%

air voids (M53) (Figure 7.2), R^2 and S_e/S_y for the developed model were found to be 0.87, 0.39; and 0.97, 0.19 on logarithmic and arithmetic scales, respectively. MARE was found to be as 22.5%. These statistics indicate that the model predictions were excellent. On the other hand, the Witczak model correlated poorly with $R^2 = 0.47$, $S_e/S_y = 0.76$; and $R^2 = 0.0$, $S_e/S_y = 1.79$ on logarithmic and arithmetic scale, respectively. MARE for this model was estimated at 92.8%, which was approximately 4 times higher than the developed model. Similar results were observed for 12% air voids (M54) (Figure 7.3). In both the cases, it was observed that the developed model has excellent performance compared to the Witczak model. However, both models under-predicted the modulus at higher temperatures. It is expected that the relationship between shape parameters and dynamic modulus is not a straight forward task. Therefore, a neural network (NN)-based model considering aggregates shape parameters was also developed. This NN-based model will be discussed in a later part of this chapter.

7.5.3 Effect of Shape Parameters on Dynamic Modulus

The developed model (Equation (7.2)) was used to establish the relationship between the dynamic modulus and the shape parameters (i.e., angularity, form, and texture). A selected shape parameter was varied within its ranges, while keeping the other variables constant. For this purpose, a mix with 6% of air voids and 4.1% of PG 64-22 type of asphalt binder was selected. The variation of the dynamic modulus with shape parameters were plotted for high temperatures (i.e., 40^{o}C and 55^{o}C) and for a low loading frequency (i.e., 0.1 Hz). It is expected that at high temperatures, binder starts flowing and it does not hold aggregate particles together; consequently, aggregate interlock and friction among particles play an important role to maintain the stability of the structure. On the other hand, at low temperatures, binder becomes stiff and does not allow

aggregates particles to mobilize. Though, temperature might have a significant effect on dynamic modulus of asphalt mix, the effect aggregate shape parameters cannot be neglected particularly at higher temperatures.

Figure 7.4 shows the variation of dynamic modulus with COAI (i.e., angularity). It can be seen that the dynamic modulus increases with an increase in COAI, indicating that angularity has a significant effect on dynamic modulus. Angularity creates greater interlock between particles, therefore resulting in better stability of a mix**.** Similarly, Figure 7.5 shows that dynamic modulus increases with an increase in form index (i.e., COFI). An increase in form index indicates lesser amounts of rounded particles. The effect of texture (COTI) on dynamic modulus can be seen in Figure 7.6. It shows that an increase in texture resulted in an increase in dynamic modulus. Texture is important for developing a strong friction surface among the aggregates, resulting in a stable structure of aggregates compared to the smooth aggregates. Similarly, the effect of fine aggregate angularity (FAI) is plotted in Figure 7.7. Similar to COAI, an increase in FAI resulted in an increase in dynamic modulus. The results indicate that higher values of angularity, texture, and form develop a strong aggregate structure and consequently, higher dynamic modulus. Furthermore, the use of high angular and textured particles is beneficial to resist rutting deformation under load at high temperatures. The change in aggregate shape parameters can affect the behavior of the mix significantly. It is believed that in the future shape-based models will be used to estimate the modulus of an asphalt mix at different input levels of the mechanistic empirical pavement design guide (MEPDG).

Overall above graphs show a trend of dynamic modulus with different shape parameters. To better quantify the effect of these parameter on dynamic modulus, it is

recommended the database be increased and comprehensive laboratory testing be conducted. It is expected that this study would be helpful in characterizing the asphalt mixes in more accurate manner.

7.5.4 Summary of Results

A study was undertaken to utilize aggregate shape parameters (i.e., angularity, texture, and form) in the estimation of dynamic modulus. Twenty different mixes were tested for dynamic modulus. The coarse and fine aggregates were recovered from each mix, and their shape parameters were measured using an automated aggregate image measurement system (AIMS). A nonlinear regression model was developed to estimate the dynamic modulus of the mix in terms of its aggregate gradation, aggregate shape parameters (i.e., angularity, form, and texture), viscosity of asphalt binder, and volumetric properties. The following conclusions can be drawn from the results and discussion presented above.

(1) The correlation coefficient (R^2) for the developed model was found to be 0.95 and 0.92 on logarithmic and arithmetic scales, respectively, with a mean average relative error (MARE) of 21.9%.

(2) The performance of this model was compared with the widely accepted Witczak model that does not use the shape parameters of the aggregates. The MARE for the Witczak model was estimated to be approximately 92.8%, which was approximately 4 times higher than the developed model.

(3) Results show that the dynamic modulus of the mix increases with an increase in angularity and texture of aggregates and that the inclusion of shape parameters can enhance the prediction capability of a model.

(4) The developed model is observed to perform better than empirical models that do not take aggregate shape parameters into account.

It is recommended that additional mixes be tested for the development and the validation of the shape-based model. Furthermore, artificial neural network-based modeling should be developed to enhance the relationship between shape parameters and dynamic modulus. In addition, a similar approach should be used to develop the models for estimating the resilient modulus of aggregates. It is expected that the shape-based model would be helpful in characterizing the performance of asphalt mix and aggregate base layers in an accurate manner. It is believed that in the future shape-based models will be used to estimate the modulus of an asphalt mix at different input levels of the MEPDG. An accurate estimation of modulus properties of asphalt mixes and aggregates is expected to help designers to design long lasting pavements.

7.6 Neural Network (NN) Modeling

7.6.1 Application of NN in Pavement Field

Neural Networks (NNs) represent a class of models designed to perform the mapping of an input vector into an output vector (Zaman et al., 2010; Ceylan et al., 2009a, 2009b; Ceylan et al., 2008; Lacroix et al., 2008; Tarefder et al., 2005a, 2005b; Tarefder et al., 2003; Hagan et al., 1996). The architecture and operation of these networks is an over simplification of those of the biological nervous system. Therefore, NNs are massively parallel systems that adapt according to stimuli induced by an external environment. In other words, NNs are designed to learn incrementally from examples presented to them (Zaman et al., 2010; Ceylan et al., 2009a, 2009b, 2008; Lacroix et al., 2008; Tarefder et al., 2005a, 2005b). Recently several researchers have successfully used NN tools for modeling complex problems in pavement and geotechnical fields (Demircan

et al., 2011; Kutay et al., 2010; Xiao et al., 2010; Zaman et al., 2010; Ceylan et al., 2009a, 2009b; Far et al., 2009; Xiao et al., 2009; Ceylan et al., 2008; Lacroix et al., 2008; Tarefder et al., 2005a, 2005b).

Zaman et al. (2010) demonstrated that NN is a useful resource to model the complex relationship between the resilient modulus and routine properties of subgrade soils. Similarly, Xiao et al. (2009) used the NN approach to estimate the stiffness behavior of rubberized asphalt mix containing reclaimed asphalt pavement. In another study, Xiao et al. (2010) developed a NN model for predicting the viscosity of crumb rubber modified binders using four input variables: asphalt binder source, rubber size, mixing duration, and rubber content. Recently, Demircan et al. (2011) compared NN and nonlinear models for estimating gelling time and maximum curing temperature rise in polymer grouts, and found that NN predictions are better compared to nonlinear model. NN has also been widely used in estimating the dynamic modulus of asphalt mixes. For example, Lacroix et al. (2008) developed NN models for back calculating the dynamic modulus from the resilient modulus of asphalt mix. Similarly, Far et al. (2009) and Ceylan et al. (2009a, 2009b, 2008) reported that NN is a promising tool to estimate dynamic modulus.

The one of the objective of the present study was to develop a NN-based model that includes the aggregate shape parameters in estimation of dynamic modulus.

7.6.2 Database

The independent parameters considered for NN model were slightly different than those considered in the statistical modeling. For example, in NN modeling, combined shape index for both coarse and fine aggregates are used, instead of their individual composite shape index (i.e., COAI, COFI, COTI, and FAI). The combined coarse and

fine aggregates shape parameters are named as follows: composite angularity index (CAI), composite form index (CFI), composite texture index (CTI), and composite sphericity index (CSI).

The following eight variables were selected as independent varaibles: binder viscosity (η), frequency (f), air voids (V_a), effective asphalt binder (V_{beff}) (% volume), CAI, CFI, CTI, and CSI. The viscosities of asphalt binders were estimated at four different temperature (i.e., 4, 21, 40, and 55^{o}C), using the ASTM equation (ASTM, 2009). The A and VTS values for PG 64-22, PG 70-28, and PG 76-28 asphalt binders were taken as 10.98, -3.68; 9.715, -3.217; and 9.2, -3.024, respectively (AASHTO, 2004).

CI values for twenty different mixes were calculated as shown in Table 7.6. Figure 7.8 and Figure 7.9 show the relationship of CAI with CFI and with CSI, respectively. It can be seen that these parameters are very poorly correlated. In general, CFI and CSI increase with an increase in the angularity of particles. However, this trend should not be generalized, as the three properties of a particle are independent of each other (Masad, 2005). Similarly, Figure 7.10 shows the relationship between CSI and CFI. It is noted that CSI and CFI indicate 3D and 2D forms of a particles, respectively. The texture of the particles (CTI) is also poorly correlated with CAI, as expected (Figure 7.11). The texture indicates a micro-level property of a particle, while angularity, form, and sphericity represent the overall shape and sharpness of a particle.

Descriptive statistics (maximum, minimum, mean, and standard deviation) of all the variables are summarized in Table 7.7. The V_a and V_{beff} for the database ranged from 5.4% to 12.4%; and 8.08 to 11.30, respectively. The maximum and minimum dynamic modulus values were found to be as 135 MPa and 18729 MPa, respectively. Similarly,

the viscosity ranged from 0.01×10^6 Poise to 1805.42×10^6 Poise. The highest and the lowest viscosities were observed at 4 and 55°C, respectively. The frequency ranged from 0.1 Hz to 25 Hz. The composite shape parameters CAI, CFI, CTI, and CSI ranged from 10.2 to 11.1; 7.23 to 7.28; 123.6 to 235.1; 0.68 to 0.76, respectively.

7.6.3 Normalization of the Data

Normalization of the input and output variables is an important step to achieve the best network performance of NN models (Singh et al., 2011j, 2011k; Far et al., 2009; Tarefer et al., 2005a, 2005b). In the present study, each variable was normalized so that the mean and variance became zero and unity, respectively.

7.6.4 Division of Dataset

The first step in the formulation of an NN model is to separate the available dataset into two sets, one for training and another for testing of the developed model. This separation should be done randomly, but it should also be done in a manner such that the training dataset has the range of variables seen in the testing dataset or expected to be seen in further applications of the model. NNs are similar to regression models in this respect, and they should not be expected to perform well when they are used to extrapolate beyond the data used for training. In the present study, a total dataset of 1440 data points was randomly divided into the training and the testing datasets. Approximately 80% (i.e., 1152) and 20% (i.e., 288) of the data points were used for training and testing purposes, respectively.

7.6.5 Neural Network Model Formulation

The architecture of a simple NN model is a collection of nodes distributed over an input layer, hidden layer(s), and an output layer (Figure 7.12). In the present study, a four layer (one input, two hidden, and one output layers) network was used (Figure 7.12). The

input layer contains the independent variables (i.e., η, f, V_a, V_{beff}, CAI, CFI, CTI, and CSI) and the output layer contains the dependent variables (i.e., dynamic modulus). The output for this configuration of network was calculated using Equation (7.3). A hyperbolic tangent (called 'tansig') function was selected as an activation function for the hidden layer (Equation (7.4)), while a pure linear function (called 'purelin') was used for the output layer (Equation (7.5)). These functions are considered to be best suited to estimate the modulus of asphalt mixes (Lacroix et al., 2008).

$$O = f_o\left[b_o + \sum_{k=1}^{q} W_k{}^{o} f_h\left\{b_k{}^{2h} + \sum_{j=1}^{n} W_{jk}{}^{2h} f_h(b_j{}^{1h} + \sum_{i=1}^{m} W_{ij}{}^{1h} P_i)\right\}\right] \tag{7.3}$$

$$f_h(T) = \frac{2}{1+e^{-2T}} - 1 \tag{7.4}$$

$$f_o(T) = T \tag{7.5}$$

where,

i	=	subscript for input layer,
j	=	subscript for first hidden layer,
k	=	subscript for second hidden layer,
m	=	number of input parameters (i.e., 8),
n	=	number of nodes in first hidden layer (i.e., 20),
q	=	number of nodes in second hidden layer (i.e., 20),
f_h	=	transfer function for hidden layers (i.e., 'tansigmoid'),
f_o	=	transfer function for output layer (i.e., 'purelin'),
$W^{1h}{}_{ij}$	=	weight factors for first hidden layer (Size: n x m),
$W^{2h}{}_{jk}$	=	weight factors for second hidden layer (Size: q x n),
$W^{o}{}_{k}$	=	weight factors for output layer (Size: 1 x q),
$b^{1h}{}_{j}$	=	bias factors for first hidden layer (Size: n x 1),
$b^{2h}{}_{k}$	=	bias factors for second hidden layer (Size: q x 1),

b_o = bias factor for output layer (Size: 1 x1),

P_i = input variables (Size: m x 1), and

O = output value (Size: 1 x 1).

The next step was to select a training algorithm. A feed-forward back-propagation algorithm was used to train the neural network. Back-propagation is a supervised learning algorithm in which the network is trained and adjusted by reducing the error between the network output and the target output. The neural network training starts with the initiation of all the weights and biases with random numbers. The input vector is presented to the network. The difference between the target output and the network output represents the error. The error is then propagated backward through the network, and the weights and biases are adjusted to minimize the error in the next round of prediction. The interaction continues until the error goal is reached. In the present study, the Levenberg-Marquardt optimization algorithm was used for the training of the network. The NN codes were developed using commercial software, called MATLAB®.

7.6.6 Design of Network Architecture

The accuracy of the NN model depends upon the network architecture. The network architecture indicates the number of hidden layers and number of neurons in each hidden layer. There is no specific rule to select number of hidden layers and neurons. Usually a trial and error process is used to select these numbers. In the present study, several networks with 5-5, 10-10, 15-15, 20-20, and 25-25 numbers of neurons in first and second hidden layers were tried. It was found that a network with 20-20 neurons in each of the hidden layer was found to be performed best. This network (i.e., 1-20-20-1) was used to model the dynamic modulus in the present study.

7.6.7 Methodology for Estimate Network Output

Generally, the output of NN depends on the initialization of the weights in the minimization algorithms (Singh et al., 2011j, 2011k; Tarefder et al., 2005a, 2005b; Hagan, 1996). Ideally, the network should give close to the same answer regardless of the initial value of the weight, but in reality that may not be the case. This can be due to the fact that the error function may have multiple minima. It is possible that the optimization method is local in nature. Therefore, it is important to do several trials using different initial weights to get the global minima. In the present study, a statistical approach was used to get the final output from the network. The approach used here involved the random generation of starting values of weights to obtain a collection of different estimated weights. This collection is used in a simulation to determine distributions of outputs for a given input. The model was developed by randomly varying the weight by 100 times. Therefore, a total of 100 neural networks were trained, and then a histogram was generated for all the 100 outputs and the mean of this histogram was taken as the final output. Figure 7.13 shows the histogram of 100 NN outputs. It can be seen from this figure that the output (i.e., Log|E*|) ranged from 2 to 5, indicating the variability into the output because of the selection of initial weight. In addition, the mean of the histogram and the measured dynamic modulus values are approximately equal, indicating that this approach avoids the local minima of the optimization problem. The similar approach has been used by many other researchers (Singh et al., 2011j, 2011k; Tarefder et al., 2005a, 2005b).

7.6.8 Results of Neural Network Model

The model strength was evaluated using the two statistical parameters: R^2 and MARE. The plot of the measured and the predicted dynamic modulus for the training

dataset (i.e., 1152 dynamic modulus values) is shown in Figure 7.14. This figure shows that the NN model predictions are very close to the line of equality (LOE). The R^2 logarithmic and arithmetic scales were observed as 0.94 and 0.99, respectively, indicating that the trained model predictions are in excellent fit with the measured values. Similarly, the MARE was estimated as 10.2%, which is considered to be very minimal as compared to the variation existed between the measured dynamic modulus of two samples.

The trained model was checked for the testing dataset (i.e., 288 dynamic modulus values). These 288 dynamic modulus values were not used in the in training the NN. Figure 7.15 is the plot of the measured and the predicted dynamic modulus for the testing dataset. The R^2 was observed to be 0.90 and 0.98 on logarithmic and arithmetic scales, respectively. The MARE was found to be approximately 17.5%. Overall, the training and testing results indicate that using aggregate shape parameters can be a good approach in enhancing the accuracy of the predictive models.

The purpose of the study was to show the use of aggregate shape parameters in estimating of dynamic modulus. However, the current approach must be further validated by using an independent dataset before it could be implemented in practice.

7.6.9 Sensitivity Analysis of Input Variables

The sensitivity analysis of the input variables was examined by developing the relationship between an individual input parameter and dynamic modulus. For each input parameter, a separate NN model was trained and tested. For example, the relationship between the viscosity and dynamic modulus was established by developing an NN model. Similar models were developed for all other input variables. The network configuration of four layers (one input- two hidden- one output layers) was used for this purpose.

Table 7.8 summarized the statistics of the developed models for training and testing dataset on arithmetic scales. The viscosity of the asphalt binders was found to have the strongest correlation with the dynamic modulus with R^2 >0.70 and MARE less than 60%. Similarly, the combination of viscosity (η) and loading frequency (f) were found to have the highest correlation index with R^2 = 0.84 and 0.78 for training and testing dataset, respectively. In addition, the MARE was found to be less than 40%. However, the relationship of the frequency and dynamic modulus was found to have a poor correlation ((R^2 = 0, MARE = 118%).

The effect of asphalt volumetric properties (V_a, V_{beff}), loading frequency (f), and other aggregate shape parameters (i.e., CAI, CFI, CTI, CSI) can be observed from the statistics summary presented in Table 7.8. It can be seen that these parameters are poorly correlated with the dynamic modulus (R^2 = 0, MARE >120%). This poor correlation can be attributed due to the exclusion of the time and temperature effected represented by asphalt binder rheological properties.

7.6.10 Summary of Results

This study presents the development of a NN model for predicting the dynamic modulus of asphalt mixes considering the aggregate shape parameters. Dynamic modulus values of twenty different mixes were measured in the laboratory. The aggregates from each mix were retrieved and separated into different sizes of coarse and fine aggregates. An automated aggregate imaging system was used to measure the shape parameters (i.e., angularity, texture, form, and sphericity) of each size of aggregates. The combined shape factors (i.e., CAI, CTI, CFI, and CSI) considering aggregate gradations and shape parameters were estimated for each mix. A four layer (one input-two hidden-one output layers) network was used for developing the model. The input layers consisted eight

different parameters (i.e., η, f, V_a, V_{beff}, CAI, CFI, CTI, and CSI) and the output layer had one parameter (i.e., dynamic modulus). The following conclusions can be drawn from the results and discussion presented above.

(1) There was no significant correlation observed among the different shape parameters (i.e., CAI, CTI, CFI, and CSI).

(2) The training and testing results of the developed model show that the inclusion of aggregate shape parameters can be used as independent parameters of the model. It is believed these parameters would certainly enhance the prediction capability of the model.

(3) The sensitivity analysis of the input parameters show the viscosity of the asphalt binder has a strong correlation with dynamic modulus.

(4) The volumetric properties (V_a, V_{beff}) and shape parameters were found to be very poorly correlated.

The approach used in the present study needs to be validated using an independent dataset. Furthermore, it is recommended that database be increased to consider a wide range of aggregates and mix. It is expected that present study would be helpful in developing a better understanding of predicting the dynamic modulus using the aggregate shape parameters.

Table 7.1 Volumetric Properties of the Mixes

Mix Groups	V_a (%)			V_{beff} (%)		
	Sample 1	Sample 2	Sample 3	Sample 1	Sample 2	Sample 3
M11	5.4	5.6	5.6	8.78	8.76	8.77
M12	7.3	7.2	7.2	8.61	8.61	8.62
M13	9.3	9.6	9.1	8.42	8.39	8.44
M14	11.5	12.4	12.4	8.21	8.14	8.14
M21	6.5	6.4	6.4	8.94	8.95	8.95
M22	8.3	8.1	7.9	8.77	8.79	8.81
M23	9.6	10.2	9.8	8.64	8.58	8.62
M24	12.2	11.7	12	8.40	8.45	8.41
M31	6.2	6.3	6.2	9.52	9.51	9.52
M32	7.9	7.9	8.3	9.35	9.35	9.31
M33	10.2	10.3	10.2	9.11	9.10	9.11
M34	11.9	12.2	12.1	8.94	8.92	8.92
M41	6.1	5.9	6.3	11.28	11.3	11.26
M42	8.2	7.8	8.2	11.02	11.07	11.03
M43	9.9	9.6	9.9	10.82	10.86	10.82
M44	12.1	11.6	11.7	10.56	10.62	10.61
M51	6.2	6.3	6.1	8.65	8.63	8.65
M52	8.2	8.2	8.1	8.46	8.46	8.47
M53	9.7	9.7	9.2	8.32	8.32	8.37
M54	12.3	12	11.9	8.08	8.11	8.12

Table 7.2 Percentage Aggregates Retained for Different Types of Mixes

Mix Groups	Particles Retained (%)				
	Coarse Aggregates			Fine Aggregates	
	P19-R12.5	P12.5-R9.5	P9.5-R4.75	P4.75-R2.36	P2.36-R1.18
M11	7.2	4.6	13.8	23.1	15.2
M12	7.2	4.2	12.8	23.8	15.7
M13	7.0	5.1	14.0	23.4	15.5
M14	8.5	5.2	14.2	23.2	15.2
M21	4.6	3.2	12.0	25.8	15.8
M22	5.2	3.9	12.7	25.4	15.4
M23	7.5	4.1	12.4	25.6	14.6
M24	6.5	4.7	11.1	26.5	15.0
M31	2.6	6.8	20.9	20.6	13.0
M32	2.0	6.9	20.1	20.9	13.3
M33	2.0	4.9	19.2	21.6	14.1
M34	2.2	6.4	18.6	21.3	14.0
M41	4.5	5.2	14.7	23.3	14.5
M42	4.0	5.3	15.2	23.3	14.2
M43	4.3	4.5	15.5	23.2	14.6
M44	4.2	4.5	14.7	23.7	14.7
M51	2.4	6.9	20.9	18.9	14.2
M52	2.6	7.1	22.0	18.8	13.8
M53	3.2	7.6	22.0	19.2	13.4
M54	2.4	7.6	21.3	19.1	14.2

P19-R12.5 : Aggregates Passing on a19 mm and Retained on a 12.5 mm
P12.5-R9.5 : Aggregates Passing on a 12.5 mm and Retained on a 9.5 mm
P9.5-R4.75 : Aggregates Passing on a 9.5 mm and Retained on a 4.75 mm
P4.75-R2.36 : Aggregates Passing on a 4.75 mm and Retained on a 2.36 mm
P2.36-R1.18 : Aggregates Passing on a 2.36 mm and Retained on a 1.18 mm

Table 7.3 AIMS Test Matrix

	Coarse Aggregates		Fine Aggregates	
	Sizes	No. Samples	Sizes	No. Samples
M11	P19-R12.5, P12.5-R9.5, and P9.5-4.75	6	P4.75-R2.36,and P2.36-R1.18	2
M12		6		2
M13		6		2
M14		6		2
M21		6		2
M22		6		2
M23		6		2
M24		6		2
M31		6		2
M32		6		2
M33		6		2
M34		6		2
M41		6		2
M42		6		2
M43		6		2
M44		6		2
M51		6		2
M52		6		2
M53		6		2
M54		6		2
	Total	120		40

Table 7.4 Composite Index Factors of Different Mixes for Statistical Modeling

Mix	COAI	COFI	COTI	FAI
M11	10.83	7.66	144.0	10.39
M12	10.60	7.81	154.7	10.52
M13	10.88	7.82	153.4	10.70
M14	10.79	7.88	146.9	10.77
M21	10.55	7.55	138.8	10.52
M22	10.78	7.67	142.3	11.08
M23	10.81	7.71	142.4	10.74
M24	10.81	7.48	141.5	10.52
M31	11.05	7.61	235.1	10.42
M32	10.15	7.15	202.6	10.71
M33	10.57	7.10	211.9	10.50
M34	10.25	7.25	223.4	10.95
M41	10.41	7.48	147.4	11.00
M42	10.61	7.53	123.6	10.27
M43	10.74	7.57	149.4	10.66
M44	10.35	8.35	146.9	10.11
M51	10.72	7.39	141.8	0.76
M52	11.10	7.64	143.4	0.75
M53	10.31	7.20	140.8	0.71
M54	10.84	7.50	142.2	0.69

Table 7.5 Descriptive Statistics for Statistical Modeling

Parameters	Minimum	Maximum	Mean	Std. Dev.
V_a (%)	5.4	12.4	8.9	2.2
V_{beff} (%)	8.1	11.3	9.3	1.0
COAI	10.1	11.1	10.6	0.2
COFI	7.1	8.4	7.6	0.29
COTI	123.6	235.1	162.8	33.3
FAI	10.1	11.1	10.6	0.25
f (Hz)	0.1	25.0	6.9	8.8
Viscosity (10^6 Poise)	0.01	3070	535.2	985.1
E* (MPa)	135	18729	2951	3417

Table 7.6 Composite Index Factors of Different Mixes for NN Modeling

Mix Type	CAI	CFI	CTI	CSI
M11	10.56	7.31	144.04	0.7
M12	10.55	7.37	154.7	0.69
M13	10.77	7.42	153.36	0.68
M14	10.78	7.55	146.93	0.69
M21	10.53	7.33	138.76	0.69
M22	10.98	7.46	142.29	0.7
M23	10.77	7.43	142.36	0.69
M24	10.62	7.31	141.54	0.7
M31	10.72	7.57	235.13	0.69
M32	10.45	7.34	202.64	0.69
M33	10.53	7.23	211.91	0.72
M34	10.65	7.49	223.36	0.69
M41	10.77	7.53	147.44	0.69
M42	10.41	7.34	123.6	0.69
M43	10.69	7.38	149.41	0.71
M44	10.2	7.68	146.93	0.71
M51	10.81	7.46	141.77	0.76
M52	11.08	7.78	143.4	0.75
M53	10.4	7.3	140.8	0.71
M54	10.6	7.51	142.16	0.69

Table 7.7 Descriptive Statistics for Neural Network Modeling

Parameters	Minimum	Maximum	Mean	Std. Dev.
V_a (%)	5.4	12.4	8.9	2.2
V_{beff} (%)	8.08	11.30	9.1	1.0
CAI	10.2	11.1	10.6	0.20
CFI	7.23	7.78	7.4	0.13
CTI	123.6	235.1	158.6	30.9
CSI	0.68	0.76	0.7	0.02
f (Hz)	0.1	25	6.9	8.8
Viscosity (10^6 Poise)	0.01	1805.42	318.8	590.6
E* (MPa)	135	18729	2864	3262

Table 7.8 Sensitivity Analysis of Input Parameters on Arithmetic Scale

Arithmetic Scale					
Input	ANN	R^2		MARE (%)	
Parameter	Model	Training	Testing	Training	Testing
n	1-20-20-1	0.70	0.69	48.2	56.8
f	1-20-20-1	0.00	0.00	119.0	117.9
n,f	2-20-20-1	0.84	0.78	31.3	37.1
V_a	1-20-20-1	0.00	0.00	123.7	124.4
V_{beff}	1-20-20-1	0.00	0.00	124.2	123.8
V_a,V_{beff}	2-20-20-1	0.00	0.00	123.2	123.6
CAI	1-20-20-1	0.00	0.00	124.7	120.7
CFI	1-20-20-1	0.00	0.00	126.1	125.4
CTI	1-20-20-1	0.00	0.00	123.7	128.5
CSI	1-20-20-1	0.00	0.00	130.1	128.6

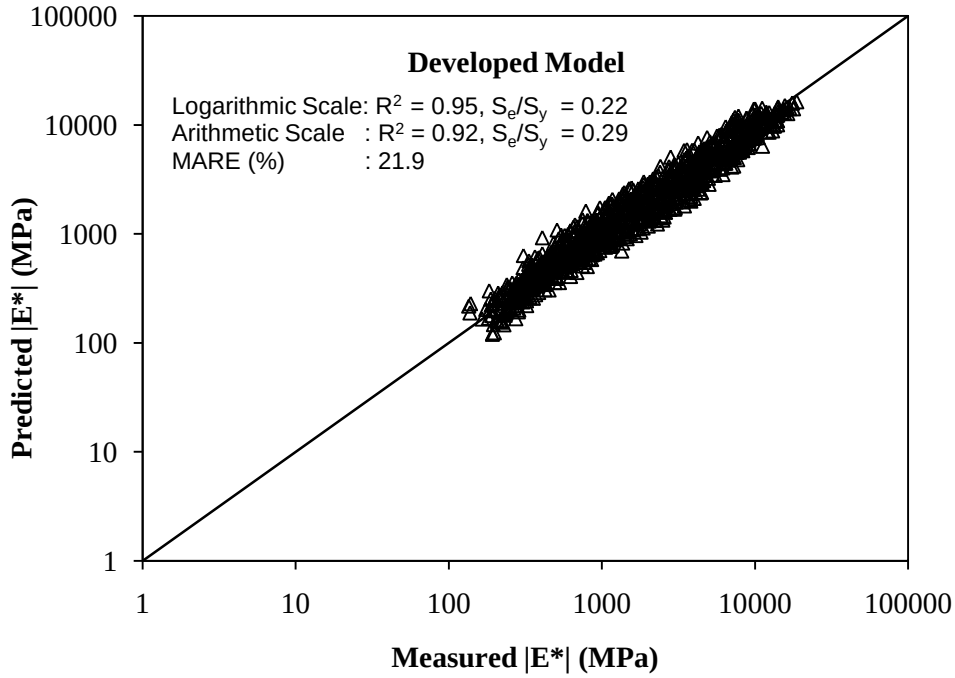

Figure 7.1 Measured and Predicted Dynamic Modulus Values for Development Dataset

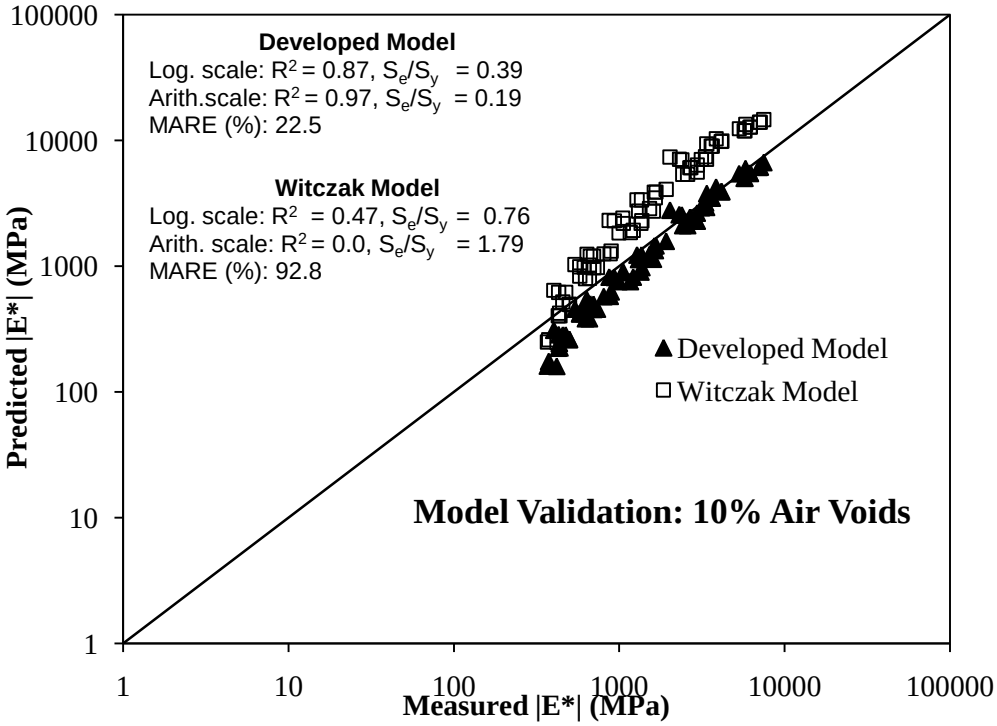

Figure 7.2 Validation of the Developed Model: Measured and Predicted Dynamic Modulus Values for Mix-M53 (10% Air Voids)

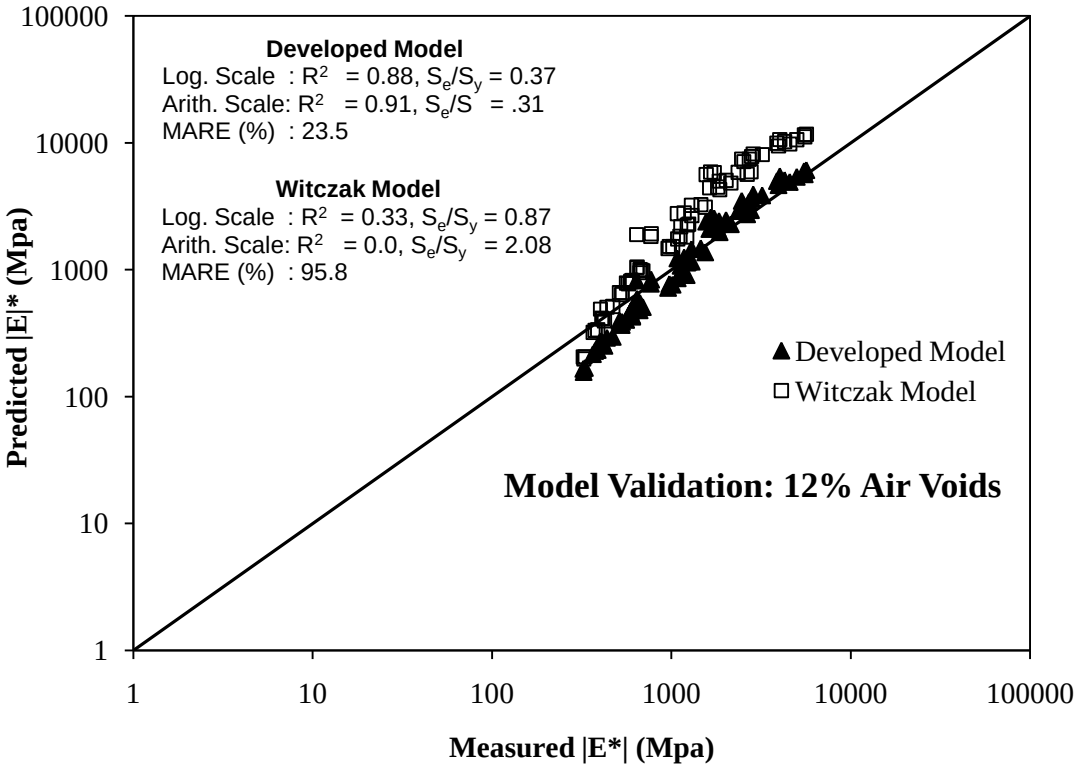

Figure 7.3 Validation of the Developed Model: Measured and Predicted Dynamic Modulus Values for Mix-M54 (12% Air Voids)

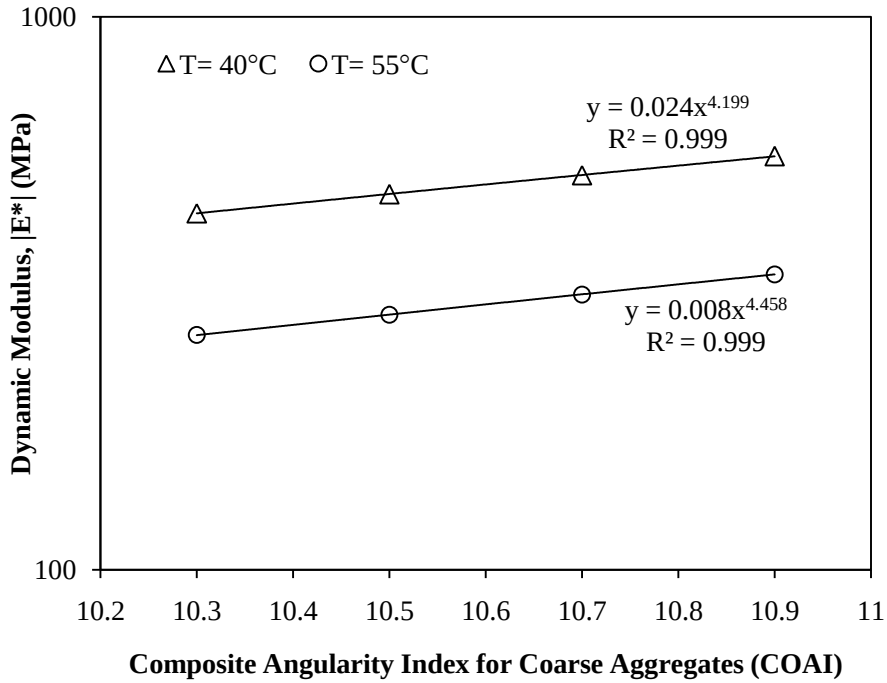

Figure 7.4 Variation of Dynamic Modulus Value with Composite Angularity Index of Coarse Aggregates (COAI)

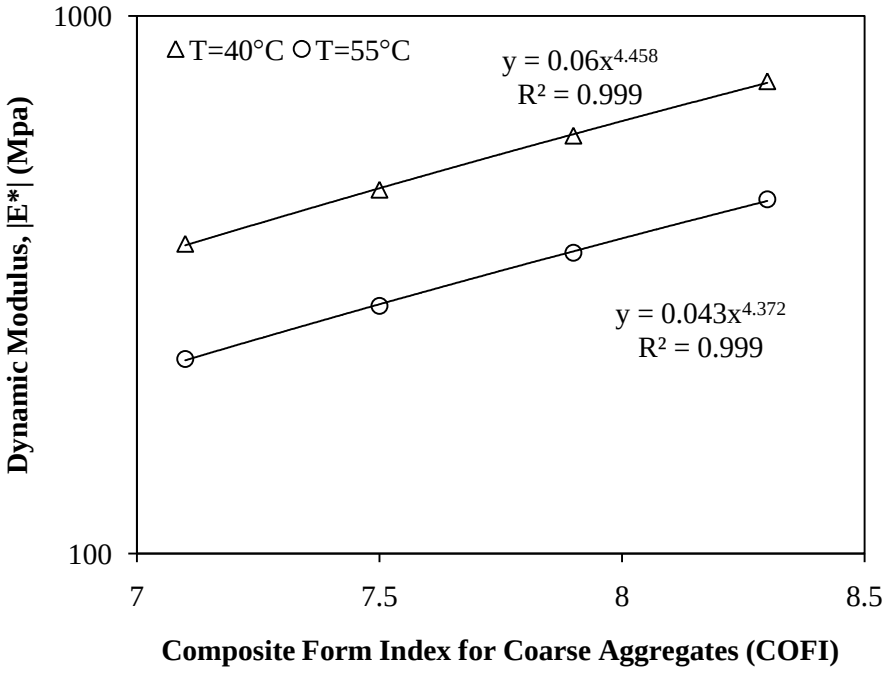

Figure 7.5 Variation of Dynamic Modulus Value with Composite Form Index of Coarse Aggregates (COFI)

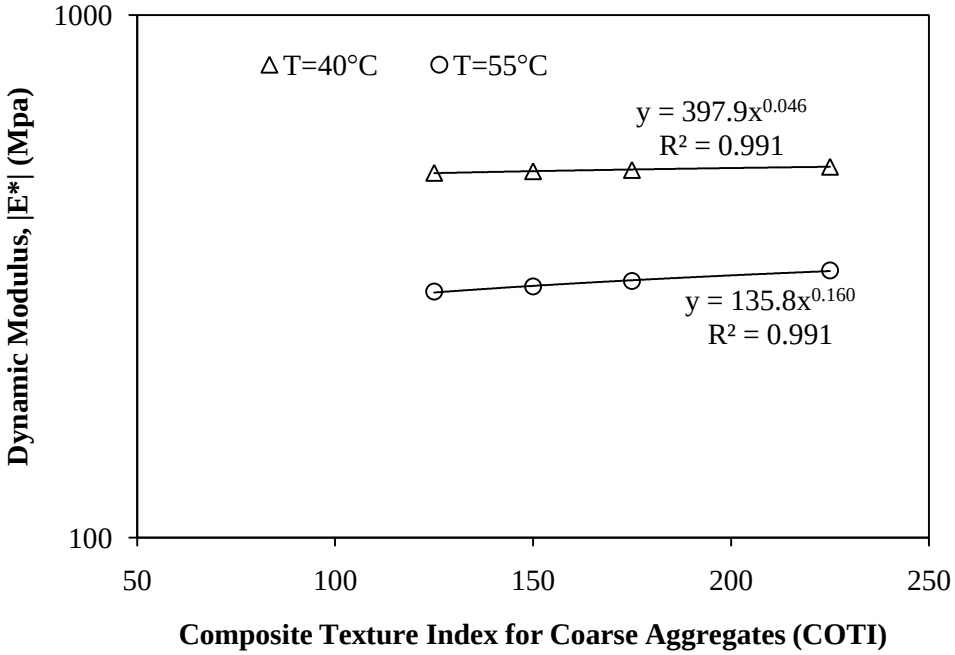

Figure 7.6 Variation of Dynamic Modulus Value with Composite Texture Index of Coarse Aggregates (COTI)

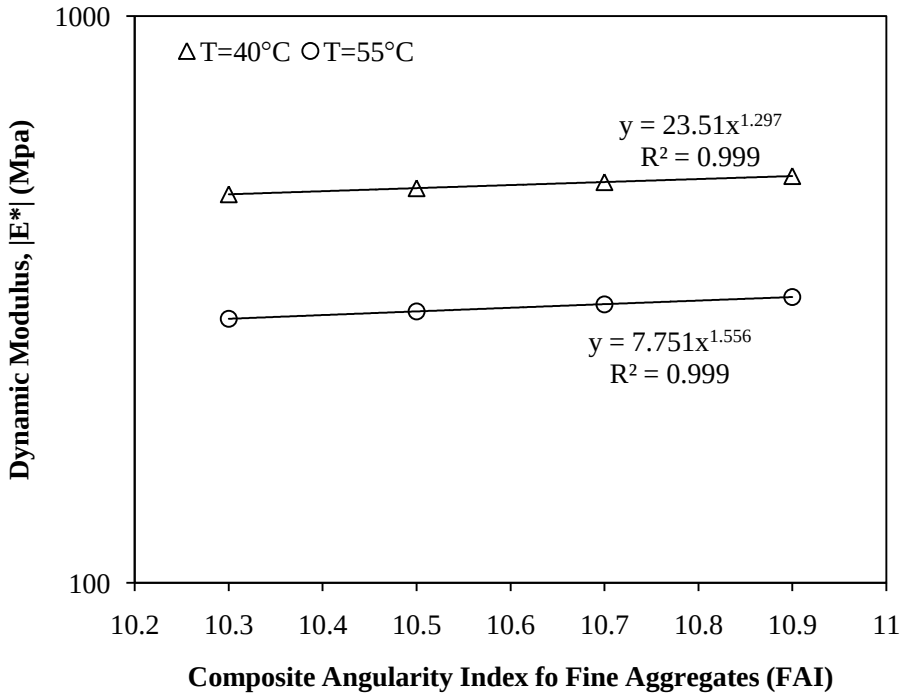

Figure 7.7 Variation of Dynamic Modulus Value with Composite Angularity Index of Fine Aggregates (FAI)

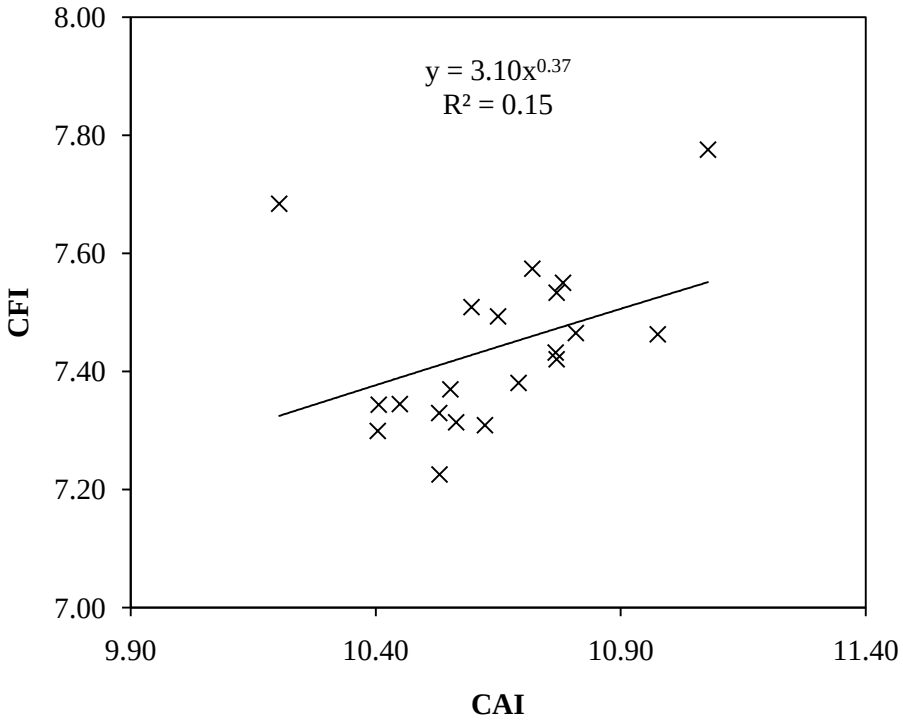

Figure 7.8 Relationship of Composite Angularity Index (COAI) and Composite Form Index (COFI)

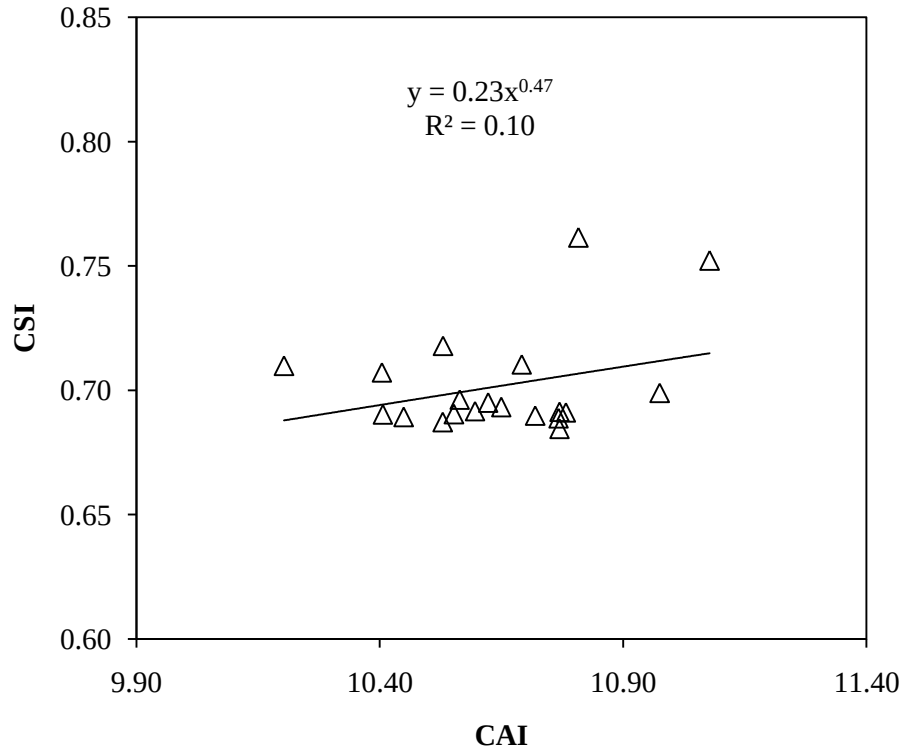

Figure 7.9 Relationship of Composite Angularity Index (COAI) and Composite Sphericity Index (COSI)

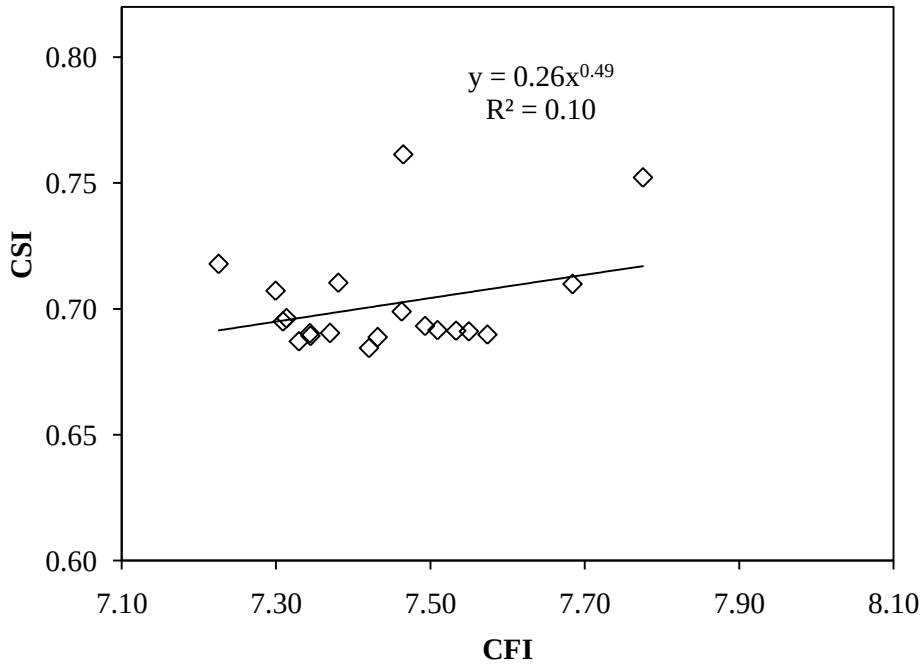

Figure 7.10 Relationship of Composite Form Index (COFI) and Composite Sphericity Index (COSI)

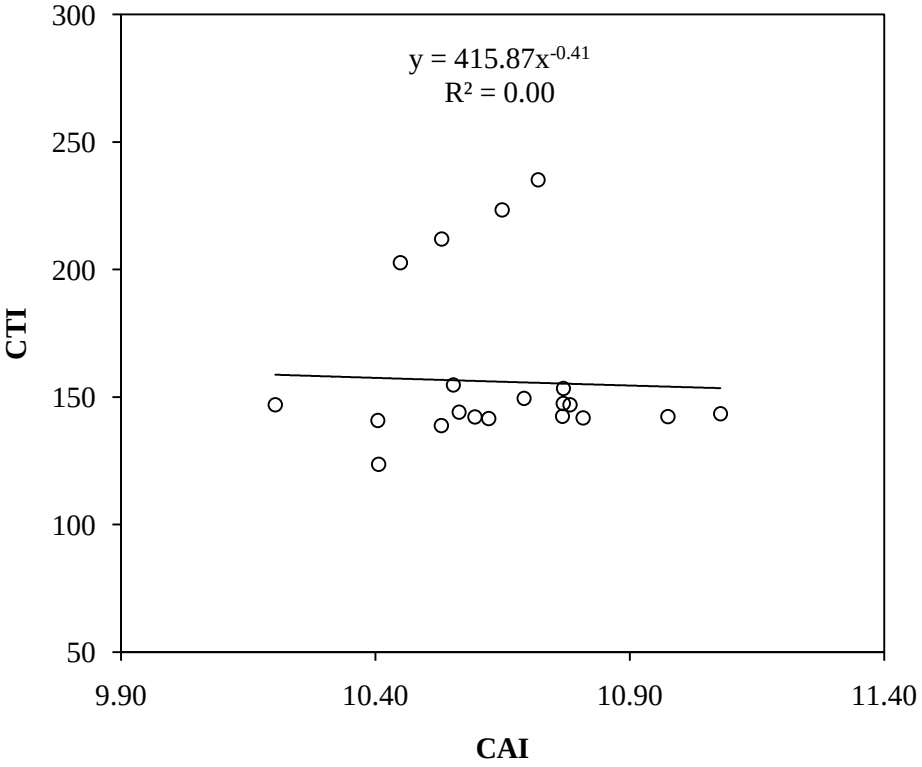

Figure 7.11 Relationship of Composite Angularity Index (COAI) and Composite Texture Index (COTI)

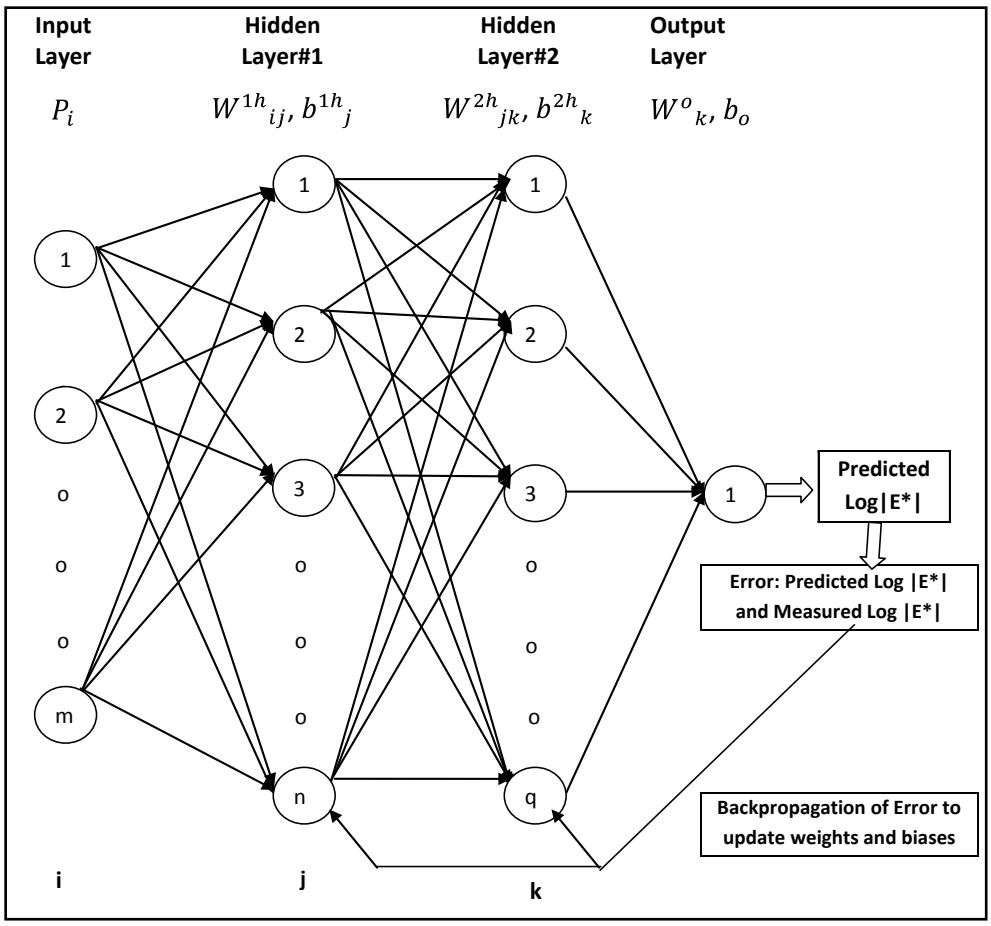

Figure 7.12 Flow Diagram of Neural Network

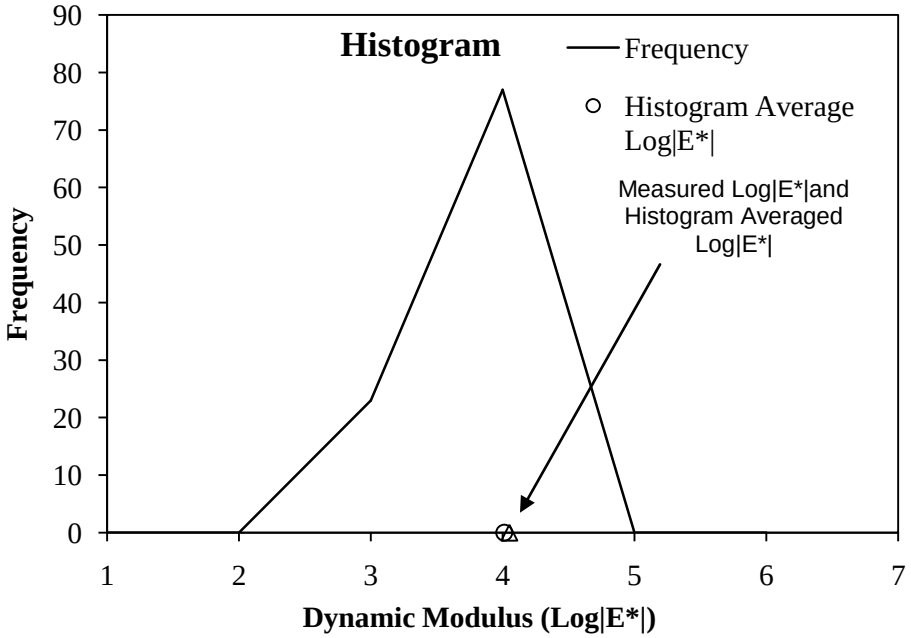

Figure 7.13 Histogram for 100 NN Outputs

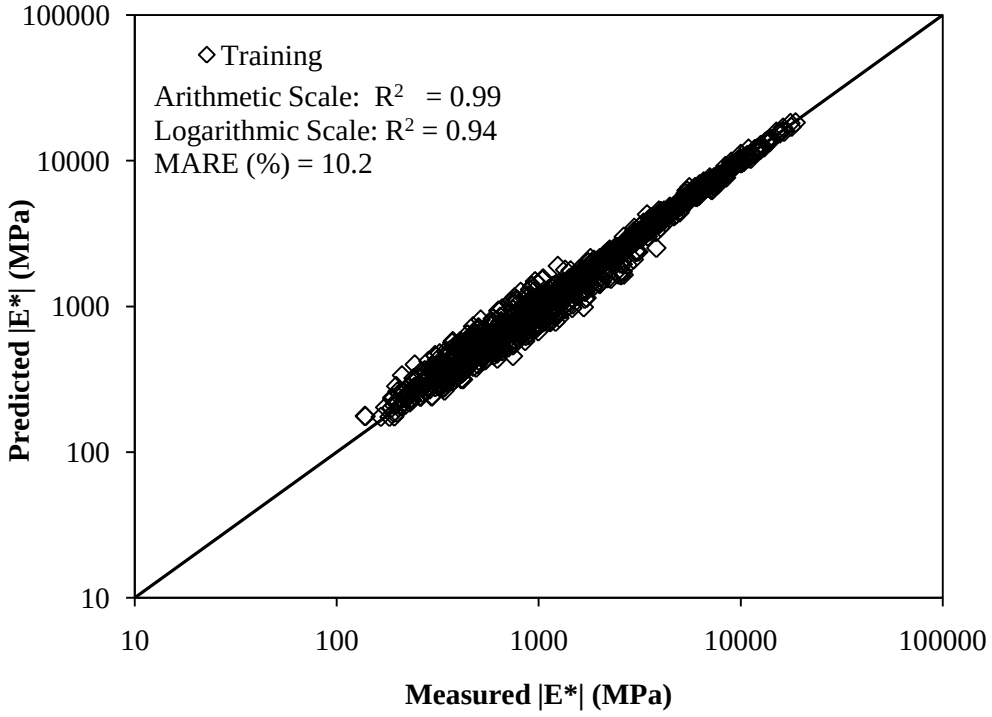

Figure 7.14 Measured and Predicted Dynamic Modulus for Training Dataset

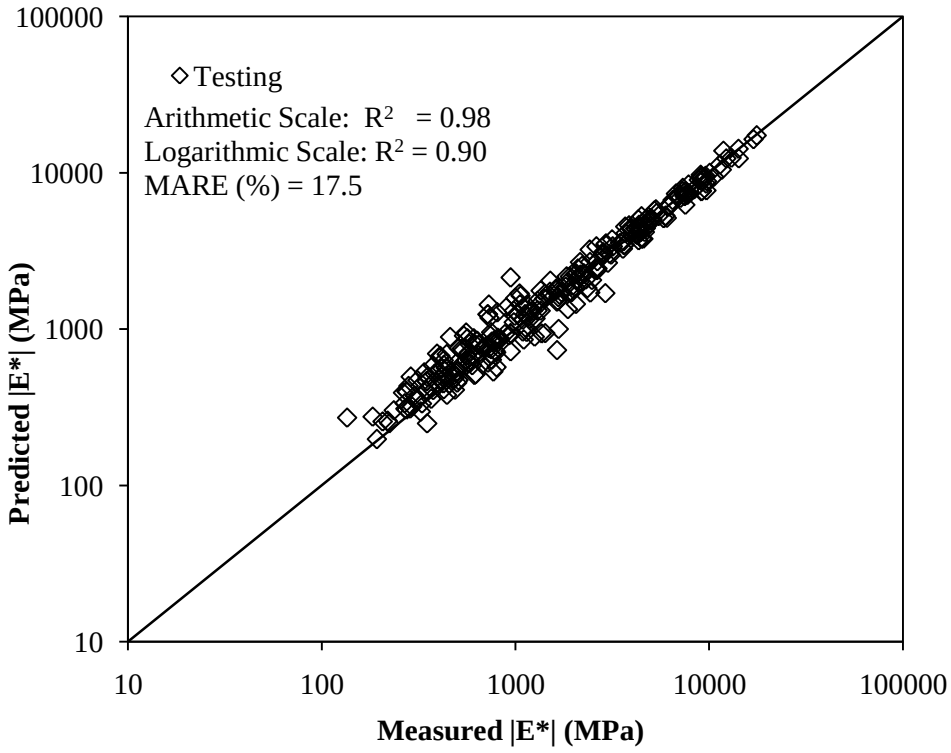

Figure 7.15 Measured and Predicted Dynamic Modulus for Testing Dataset

CHAPTER 8 : EFFECT OF AGING ON DYNAMIC MODULUS

8.1 Introduction

Reclaimed asphalt pavement (RAP) is a recycled pavement material containing coated aggregates with asphalt binder (FHWA, 2010; Al-Qadi et al., 2007; McDaniel and Anderson, 2001). According to the U.S. Environmental Protection Agency and the Federal Highway Administration, about 90 million tons of asphalt pavements is reclaimed each year, and over 80 percent (73 million tons) of it is being reused in the production of asphalt mixes (FHWA, 2010). The use of RAP in the asphalt mix has been favored over the use of virgin materials due to the increasing cost of raw materials and the reduced environmental impacts (FHWA, 2010; Al-Qadi et al., 2007; Kennedy et al., 1998; Page and Murphy, 1987). Furthermore, the addition of RAP is beneficial in resisting permanent deformation at high temperatures (Huang et al., 2004; Li et al., 2004; Kandhal et al., 1989; Brown, 1984; Meyers et al., 1983; Little et al., 1981; Little and Epps, 1980). On the other hand, excessive RAP content may reduce the resistance to cracking at low temperatures (Li et al., 2008).

Many studies have been conducted to evaluate the effect of RAP amounts on the performance of asphalt mix. McDaniel et al. (2007) reported that adding small amounts of RAP does not significantly alter mix properties. As RAP content increases, some effect on mix properties was noted. However, the change was not in proportion to the amount of RAP being added. Similarly, Kandhal et al. (1997) found that that up to 15% RAP could be used without changing the PG binder grade. In general, most studies on laboratory produced mixes concluded that the effect of RAP on mixes' properties is negligible at RAP contents within 15% to 20% (Li et al., 2008; McDaniel et al., 2007;

McDaniel et al., 2002; McDaniel et al., 2000). A low RAP content did not significantly affect stiffness and strength of a mix at low and high temperatures. However, an increase in RAP contents beyond 20% increased the mix stiffness and strength, resulting in an increase in the rutting resistance (Li et al., 2008; McDaniel et al., 2007; Xiao et al., 2007; Li et al., 2004; McDaniel et al., 2001).

Limited studies have been conducted, so far, to investigate the effect of long-term oven (LTO)-aging on plant produced asphalt mixes prepared containing RAP. Daniel et al. (1998) and Francken et al. (1997) studied the effect of aging on asphalt mixes. Specimens were compacted and subjected to three different levels of long-term aging. It was reported that the aging of mix increased |E*|. However, they did not study the effect of aging on mix containing RAP. Therefore, evaluation of the effect of short-term and long-term aging on performance of RAP contained mixes would be helpful in understanding the response (stress-strain behavior) of a flexible pavement (Houston et al., 2005). Furthermore, it is known that for a given virgin asphalt mix (without any RAP), with a given aggregate gradation, aggregate type, and binder content, a mix with stiffer binder grade (i.e., PG 76-28) is expected to result in a higher |E*|, compared to a mix with a softer binder grade (i.e., PG 64-22). However, such behavior may not be reflected in a mix containing RAP, because it changes the rheological property and grade of the binder compared to the virgin mix. Hence, it becomes important to evaluate the performance of RAP contained asphalt mix at the design phase of a flexible pavement.

The present study was undertaken to examine the effect of LTO-aging on two different asphalt mixes contained different PG grade binders and RAP, using |E*| test. |E*| is recommended as one of the fundamental properties of a mix to evaluate long-term

performance of a flexible pavement (fatigue cracking and rutting) (MEPDG, 2004). It is anticipated that the present study would be helpful in understanding the behavior of RAP contained mixes.

8.2 Reclaimed Asphalt Pavement (RAP) Mixes

Two different types of plant produced RAP mixes, namely Mix-1 and Mix-2, were collected (see Chapter 2). The gradations and other volumetric properties of these mixes are tabulated in Chapter 2 (see Tables 2.1 and 2.2). Both mixes had similar aggregate type (primarily limestone), and the same nominal maximum aggregate size (NMAS) of 19 mm. Mix-1 had 25 percent RAP, and 4.1 percent an unmodified PG 64-22 binder, while Mix-2 had 15 percent RAP and 4.1 percent PG 76-28 styrene-butadiene-styrene (SBS) modified binder. RAP used for the production of these two mixes was taken from the same stockpile maintained at the plant site. These mixes are commonly used for paving in Oklahoma.

The samples were compacted using the Superpave Gyratory Compactor (SGC) at four different levels of air voids (i.e., 6%, 8%, 10%, and 12%). The details of the sample preparation method and volumetric properties of the compacted samples are tabulated in Chapter 2 (see Tables 2.3 and 2.4). The samples compacted without subjecting LTO-aging of the mix is referred to as 'unaged' sample. Therefore, the measured dynamic modulus on 'unaged' samples is called 'unaged |E*|.' Similarly, samples subjected LTO-aging is referred to as 'aged' sample; thus the measured dynamic modulus for these samples are called 'aged |E*|.' LTO-aging procedure of the compacted sample is described later in this chapter.

Dynamic modulus testing was done on both unaged and LTO-aged specimens in accordance with AASHTO TP62 (AASHTO, 2006). The detailed testing procedure is

described in Chapter 2. The master curves for both the mixes were constructed as per the method discussed in Chapter 2.

8.3 Long-Term Oven (LTO) Aging

Since dynamic modulus testing is considered to be a non-destructive testing, the same samples can be used for further testing. Therefore, after dynamic modulus testing on unaged samples, the samples were kept for LTO-aging. The samples compacted at four different air voids (i.e., 6, 8, 10, and 12%) were LTO-aged in accordance with the AASHTO R30 method (AASHTO, 2002), which recommends aging of compacted specimens in a forced draft oven for 5 days at 85^{o}C temperature. This standard is expected to simulate the long-term aging of a mix in the field over a period of 5 to 7 years, irrespective of the environmental conditions and mix properties. To avoid or minimize the slump during aging, the specimens were wrapped in a wire mesh (Figure 8.1). Three steel clamps were used to hold the mesh in place. This method facilitated the highest amount of air circulation without allowing for any slump. Specimens were taken out of oven after 5 days and allowed to cool down at room temperature. Dynamic modulus testing was run on LTO-aged specimens at combinations of temperatures and different frequencies.

8.4 Results and Discussion

8.4.1 Effect of Air Voids on Dynamic Modulus

To show the effect of air voids on |E*|, one particular frequency (10 Hz) and one temperature (21^{o}C) were selected. Changes in |E*| with air voids are shown in Figure 8.2. For both mixes (Mix-1 and Mix-2), |E*| decreases with increasing air voids. For example, an increase in air voids from 6% to 12% causes an approximately 44% and 53% reduction in |E*| for Mix-1 and Mix-2, respectively. A similar reduction was observed at

other combinations of temperature and frequency. The results manifest that the degree of compaction has a significant effect on |E*|. An increase in air voids indicates the formation of a loose asphalt mix structure (low compaction), which causes a reduction in |E*|.

8.4.2 Effect of Frequency on Dynamic Modulus

Figure 8.3 shows the variation of |E*| with the test frequency at 6% air voids and 21^{o}C test temperature. Under a constant test temperature (21^{o}C), |E*| increases with an increasing test frequency. For example, for Mix-1, at 0.1 Hz @ 21^{o}C, |E*| was measured as 2679 MPa; it increased to 7360 MPa at 25 Hz frequency @ 21^{o}C. Similarly, for Mix-2, |E*| was measured as 1315 MPa at 0.1 Hz @21^{o}C, and it increased to 5381 MPa at 25 Hz frequency @21^{o}C. Similar results were observed for other air voids, and temperatures. The results indicate that the loading frequency significantly affects the magnitude of |E*|; hence, it is important to select an appropriate frequency while predicting performance of a flexible pavement.

8.4.3 Effect of Temperature on Dynamic Modulus

The variation of |E*| with temperature at 6% air voids, and 10 Hz loading frequency, is shown in Figure 8.4. Under a constant loading frequency (10 Hz), |E*| decreases with an increase in test temperature. For example, |E*| for Mix-1 (unaged condition) was measured to be 17003 MPa at 4^{o}C, and it reduced to 1013 MPa at 55^{o}C. A similar reduction was observed for Mix-2. Results show that changes in temperature have a significant impact on |E*|. At a high temperature |E*| value reaches a constant value for both mixes, indicating that the binder becomes softer at high temperature, and the influence of aggregates becomes more dominant (Huang et al., 2008). Similar reductions were observed for all other sets of frequencies and air voids. The above trends of |E*|

with temperature and frequency are consistent with the research results reported by other researchers (Bayat et al., 2010; Huang et al., 2008; You et al., 2008). It is interesting to note that at all air voids, temperatures, and frequencies, Mix-1 (PG 64-22 @25% RAP) resulted in higher |E*| compared to Mix-2 (PG 76-28 @15% RAP). Thus, it is expected that the inclusion of a higher percentage of RAP results in a stiffer structure compared to a lower percentage of RAP. Similar results were observed for LTO-aged |E*|.

8.4.4 Effect Aging on Dynamic Modulus

The effects of LTO-aging on |E*| for Mix-1 and Mix-2 are evaluated by plotting unaged and aged |E*| on the line of equality (LOE) plot. The LOE plot was divided into different regions by drawing lines at different slopes. For example, the LOE line is drawn at 45^{o} slope where ratio of aged and unaged |E*| is equal to 1; similar lines were drawn into the LOE plot at 0.5, 1.5, and 2 ratios. These lines are called the 0.5 line, 1.5 line, and 2 line, respectively. If a point falls on the 0.5 line, then it indicates that aged |E*| is 50% less than unaged |E*|. Similarly, if a point falls on the 1.5 and 2 lines, it indicates that the aged |E*| is 50% and 100% higher than the unaged |E*|. Figure 8.5 shows the different regions marked on the LOE plot.

Figure 8.5 shows a comparison of unaged and aged |E*| for Mix-1. It was found that LTO-aging caused a significant impact on |E*| at all air voids levels. Aged |E*| falls between the 2.0 line and the LOE line, indicating that aging increases |E*| by a factor greater than 1 (Figure 8.5). The process of oxidation in binders (aging) form polar compounds that tend to increase the amount of asphaltenes. These asphaltenes contribute to a solid structure of asphalt binder that leads to increased binder stiffness and viscosity (Li et al., 2009; Al-Azri et al., 2006; Farrar et al., 2006; Liu et al., 1998a; Liu et al., 1998b; Mirza and Witczak, 1995). The average percentage change in |E*| due to LTO-

aging for 6, 8, 10, and 12% air voids was observed to be approximately 42%, 53%, 50%, and 60%, respectively. Thus, it is observed that specimens with a higher percentage of air voids aged more compared to specimens with lower air voids. It is believed that specimens with higher air voids have an open structure of aggregates that allows free circulation of the air inside the specimen which causes more hardening of the binder, whereas the structure with lower air voids narrows down the free circulation of the air inside the specimen, resulting in relatively less aging of the binder. Similar observations were made for Mix-2, where the change in |E*| was observed in the range of 60% to 64% (Figure 8.6). It is interesting to note that LTO-aging causes more impact on Mix-2 compared to Mix-1. For example, the increase in |E*| due to LTO-aging varied from 40% to 60%, and 60% to 64% for Mix-1 and Mix-2, respectively. This could be due to the fact that Mix-1 contained a higher percentage of RAP (25%) compared to Mix-2 (15%). It is expected that the higher percentage of RAP causes Mix-1 to age slowly. Kiggundu et al. (1985) showed that mixes prepared from the recycled binder generally age at a slower rate than virgin mixes. It is believed that RAP binder has already undergone oxidation which tends to retard the rate of hardening (Kiggundu et al., 1985; Meyers et al., 1983). Moreover, the mixing of a higher percentage of RAP with virgin binder causes significant changes in the chemical and rheological properties of the binder and forms a complex structure. It is important to note that aging is a very complex process that is influenced by many factors such as temperature, moisture, traffic, ultra-violet ray, air voids distribution, and thickness of pavement layers. The results in the present study are consistent with the previous study done by Daniel et al. (1998) and Francken et al. (1997) and Kiggundu et al. (1985).

8.4.5 Comparison of Mix-1 and Mix-2

8.4.5.1 Unaged Condition

The performance of Mix-1 and Mix-2 was compared for both unaged and LTO-aged conditions. A comparison of the two mixes was done by using two different approaches namely, plotting |E*| of Mix-1 and Mix-2 on the LOE plot and comparing the master curve constructed at 21^{o}C reference temperature.

Figure 8.7 shows the measured |E*| for Mix-1 and Mix-2 for different air voids and temperatures. The measured |E*| for Mix-1 falls above the LOE, indicating that Mix-1 results in higher |E*| compared to Mix-2. At high temperatures, Mix-1 and Mix-2 resulted in approximately equal |E*|, which indicates that at high temperatures, the effect of binder is not significant. However, since Mix-1 contained higher amounts of RAP (25%) as compared to Mix-2 (15%), it was expected that Mix-1 would still result in higher |E*| at high temperatures. To understand further, the ratio of |E*| for Mix-1 and Mix-2 (Mix-1/Mix-2) with air voids were plotted at four different temperatures (Figure 8.8). It was found that at all temperatures, Mix-1 resulted in a higher |E*| compared to Mix-2. The average |E*| ratio ranged from 1.2 to 1.7 depending upon air voids and temperatures. As noted earlier, a virgin mix (without any RAP) with a stiffer grade binder (i.e., PG 76-28) would result in a higher modulus compared to a mix with a lower grade binder (i.e., PG 64-22). However, analyses of results show that this behavior is not true if mixes contain RAP. The binder in a RAP has already undergone aging in the field, causing a change in its chemical composition. Mixing RAP binder with unmodified or modified binders forms a more complex structure that is not easily understood. Thus, the inclusion of RAP binder has significant impact on stiffness of asphalt mix. For example, in the present study, Mix-1 with unmodified PG 64-22 binder and 25% of RAP resulted

in higher |E*| compared to Mix-2 with SBS modified PG 76-28 binder and 15% RAP. The higher modulus at high temperatures is beneficial to the control of rutting; however, it is not considered good at lower temperatures, as it might result in low temperature cracking. Therefore, it is important to examine such behavior of RAP contained asphalt mixes for predicting performance of flexible pavements.

A comparison of Mix-1 and Mix-2 was further made by comparing master curves constructed at 21^{o}C reference temperature for all four air voids. Figures 8.9 through 8.12 show the master curves for both mixes. A comparison of Mix-1 and Mix-2 using the master curve is an important technique, as it allows comparing |E*| at a wide range of temperatures and frequencies. It is observed that, in general, Mix-1 (25% of RAP) produces higher |E*| compared to Mix-2 (15% of RAP) at all combinations of temperature and frequency, expect at high temperatures (low frequency). It is believed that at a high temperatures binder starts flowing, and it does not hold aggregate particles together, therefore, aggregate's morphology, namely angularity and texture, plays an important role.

8.4.5.2 Aged Condition

A comparison of LTO-aged |E*| of Mix-1 and Mix-2 was made by plotting them on the LOE graph and generating master curves at 21^{o}C. Figure 8.13 shows the LOE plots for both mixes. At all temperatures, Mix-1 shows a higher |E*| compared to Mix-2. The average modulus ratio ranged from 1.4 to 1.5 depending upon air voids and temperatures (Figure 8.14). It is important to note that the difference in |E*| for Mix-1 and Mix-2 decreased after LTO-aging. For example, in unaged condition the highest ratio of |E*| for Mix-1 and Mix-2 was observed 1.7, while in LTO-aged condition this ratio was calculated approximately 1.5.

A comparison of master curves of LTO-aged |E*| is presented in Figures 8.15 to 8.18. It is seen that Mix-1 results in a higher |E*| compared to Mix-2 for all combinations of temperature and frequency. In aged condition, master curves for both mixes seem closer at particular air voids, indicating less difference between the two mixes. The master curves depict that the modulus reaches an equilibrium stage at lower and higher temperatures.

8.4.6 Statistical Analysis

The performance of Mix-1 and Mix-2 was further compared by conducting a statistical analysis called 'student t-test' at a significance level of 0.05. The null hypothesis for this analysis was that the difference in mean |E*| for Mix-1 and Mix-2 is equal to zero ($H_0 = \mu_{Mix\text{-}1} = \mu_{Mix\text{-}2}$). Statistically, a significant factor p-value less than 0.05 indicates that the null hypothesis was rejected and the means of the data sets are not statistically equal. Comparisons were made for both unaged and LTO-aged conditions at four different air voids, four temperatures, and at a frequency of 10 Hz. Table 8.1 shows the results of the statistical analyses. At low air voids (6%), statistical analyses show that Mix-1 (PG 64-22 @25% RAP) results in a higher |E*| compared to Mix-2 (PG 76-28@15%RAP) at all temperatures. No statistically significant differences exist between Mix-1 and Mix-2 at higher air voids (8 to 12%) and higher temperature (55^oC), which indicates that at a higher temperature, binder does not influence |E*|, and aggregate structure plays a more dominant role. Overall, the statistical analyses reveal that a higher percentage of RAP causes a higher magnitude of |E*|, compared to a mix with lower percentage of RAP.

8.5 Summary of Results

The present study was undertaken to evaluate the effect of aging on RAP mixes. The following conclusions can be drawn from the results and discussions presented in the preceding sections.

(1) The degree of compaction (amount of air voids), temperature, and frequency have a significant impact on |E*|. A proper selection of these parameters is important in predicting the response of a flexible pavement.

(2) LTO-aging resulted in an approximately 42% to 60% increase in |E*|, depending upon the amount of RAP and air voids. Specimens having higher air voids aged more rapidly compared to specimens with lower air voids.

(3) Mixes with higher percentages of RAP aged slowly compared to mixes with a lower percentage of RAP.

(4) The higher the quantity of RAP, the stiffer the asphalt mix and the higher the |E*| values, irrespective of binder grade.

It is expected that the present study would be helpful in the selection of RAP in asphalt mix designs and in pavement construction. It is recommended that similar studies be conducted for mixes produced with other grade of unmodified and polymer modified binders and having different amounts of RAP.

Table 8.1 Statistical Analyses of Unaged and Aged Dynamic Modulus

Unaged @ 10 Hz Frequency

T (^{o}C)	Air Voids (%)							
	6		8		10		12	
	p value	Sig.	p value	Sig.	p value	Sig.	p value	Sig.
4	0	Y	0.027	Y	0	Y	0.014	Y
21	0.023	Y	0.022	Y	0	Y	0.027	Y
40	0	Y	<0	Y	0.078	N	0.109	N
55	0	Y	0.153	N	0.262	N	0.064	N

Aged @ 10 Hz Frequency

T (^{o}C)	Air Voids (%)							
	6		8		10		12	
	p value	Sig.	p value	Sig.	p value	Sig.	p value	Sig.
4	0.026	Y	0.023	Y	0.093	N	0.051	N
21	0.01	Y	0	Y	0	Y	0	Y
40	0	Y	0.013	Y	0.019	Y	0.061	N
55	0	Y	0.32	N	0.119	N	0.12	N

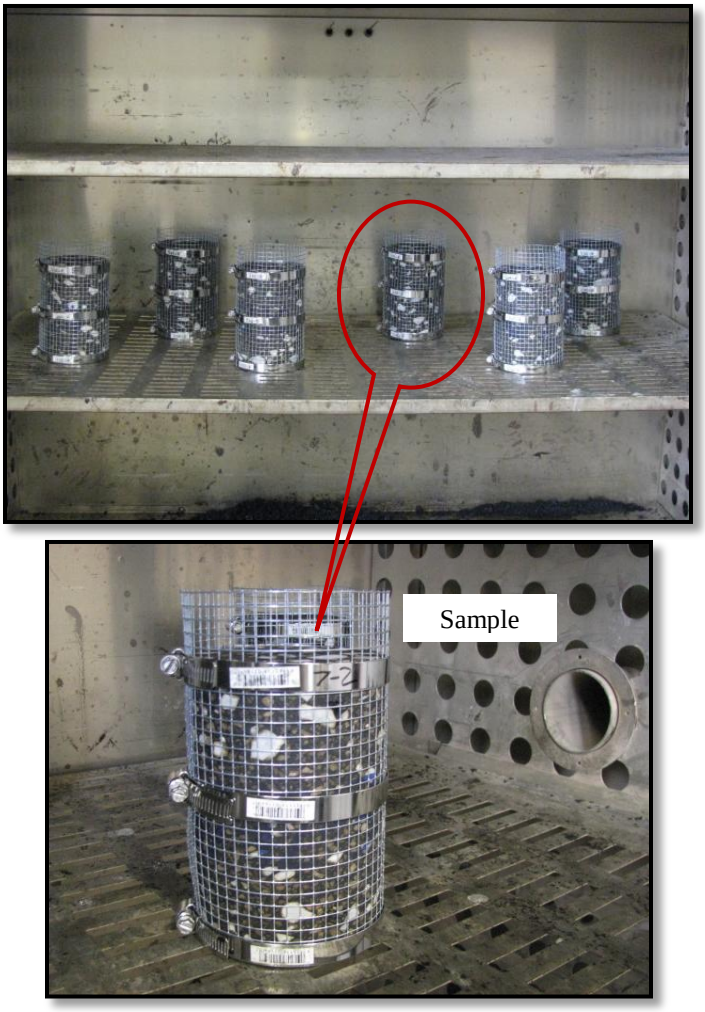

Figure 8.1 Long Term-Oven Aging of Compacted Samples

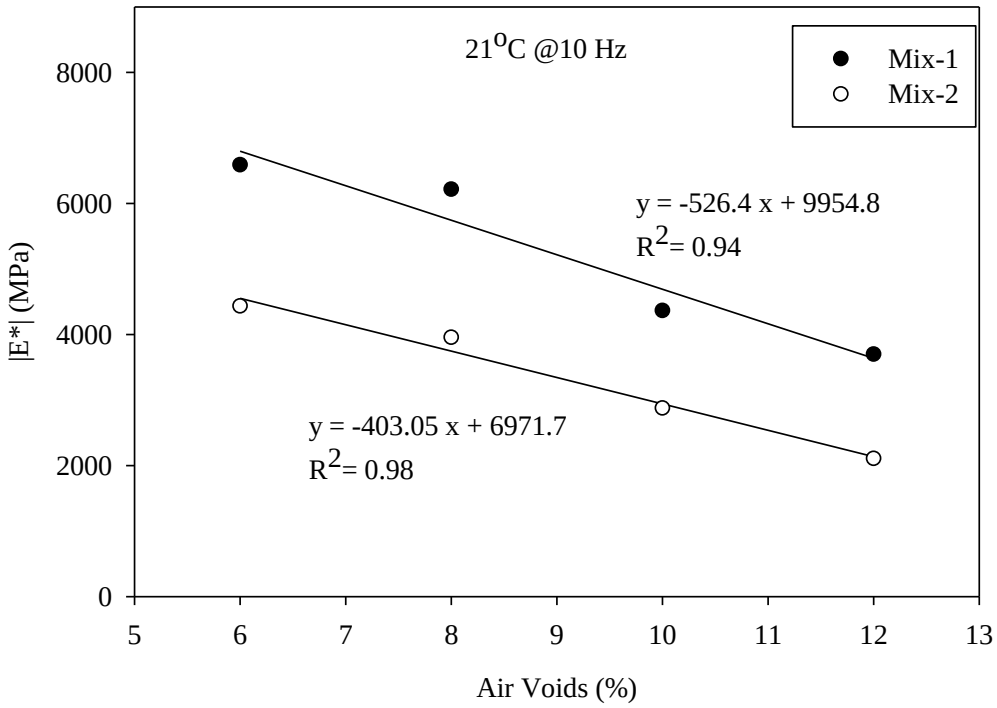

Figure 8.2 Variation of |E*| with Air Voids

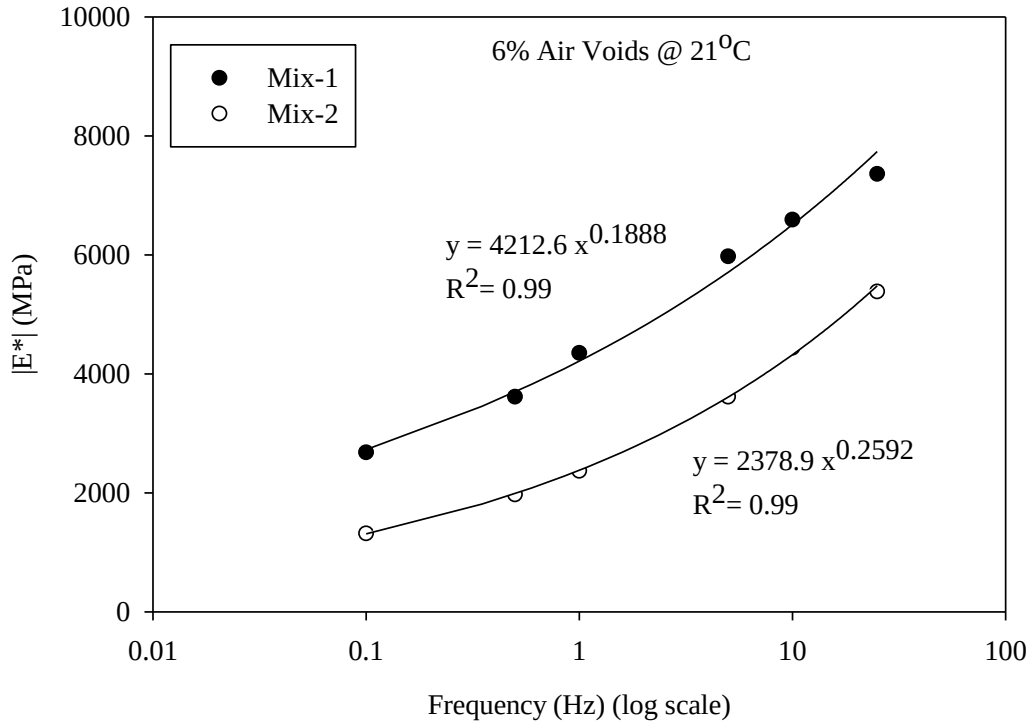

Figure 8.3 Variation of |E*| with Frequency

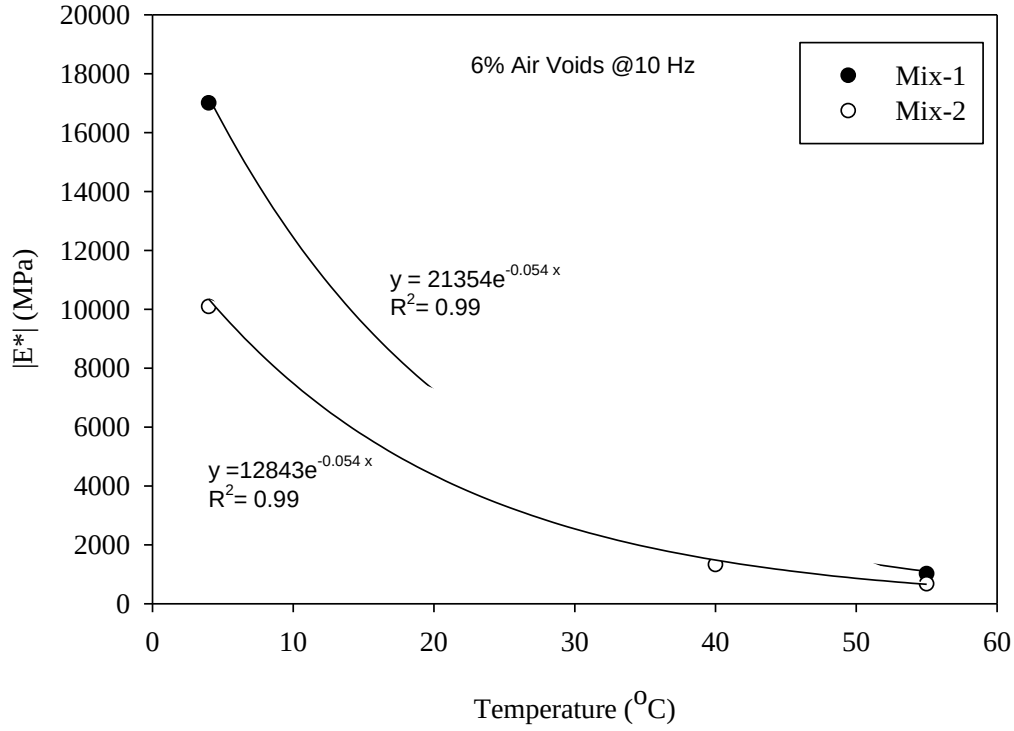

Figure 8.4 Variation of |E*| with Temperature

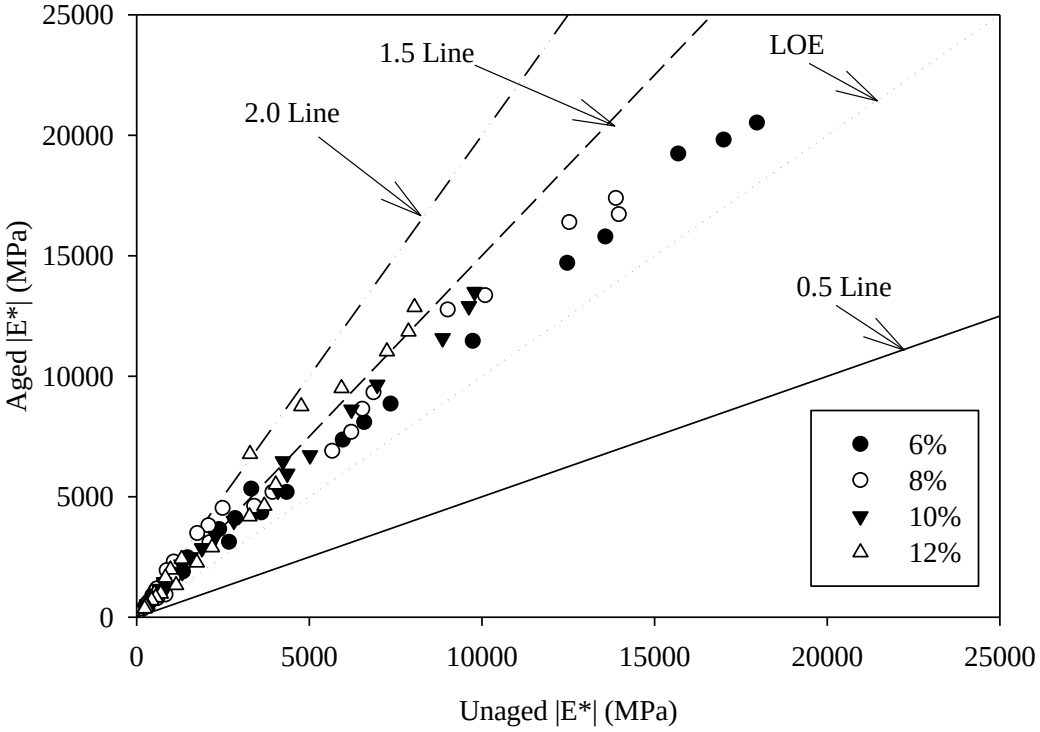

Figure 8.5 Effect of LTO-Aging on Mix-1

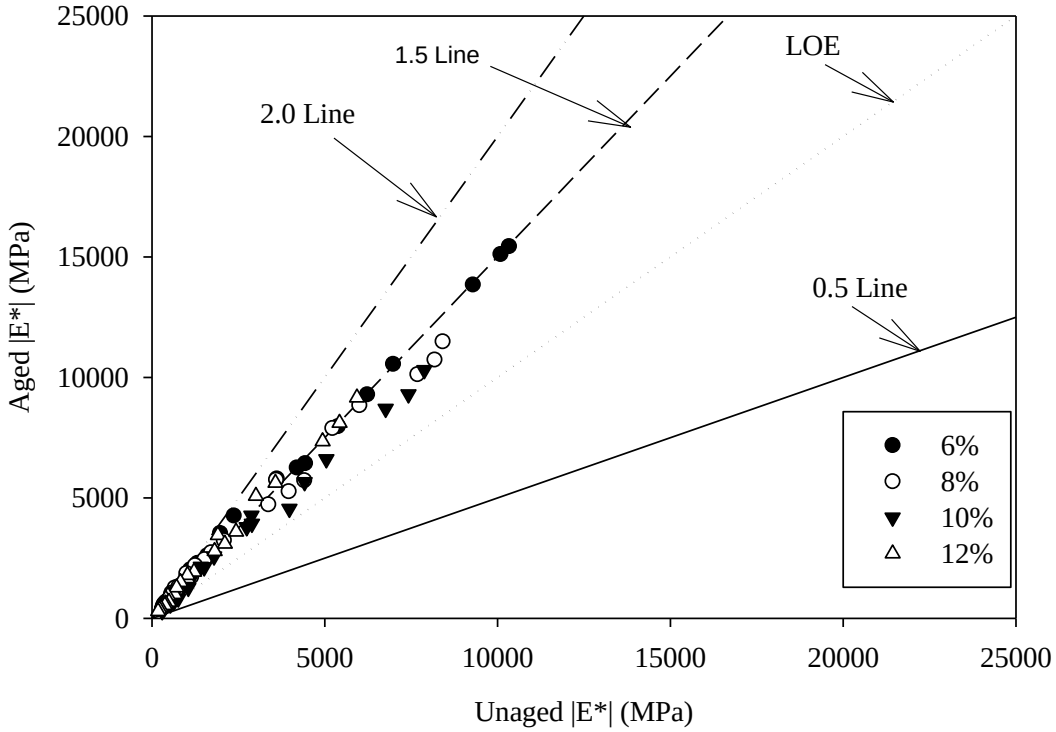

Figure 8.6 Effect of LTO-Aging on Mix-2

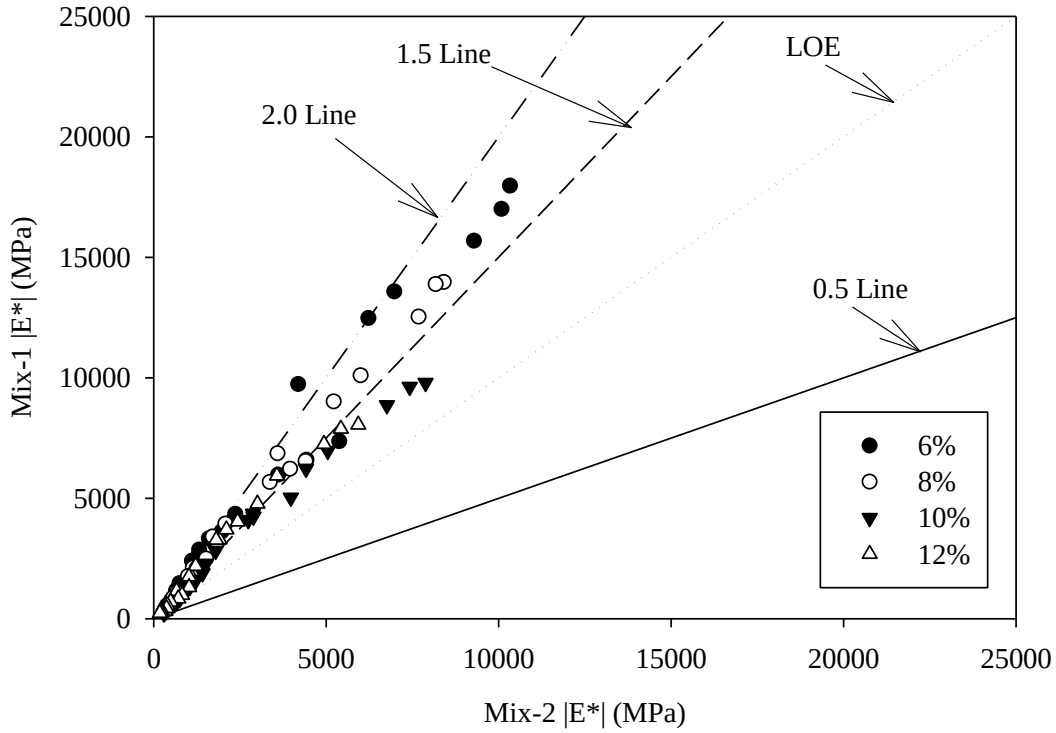

Figure 8.7 Comparison of |E*| for Mix-1 and Mix-2 for Unaged Condition

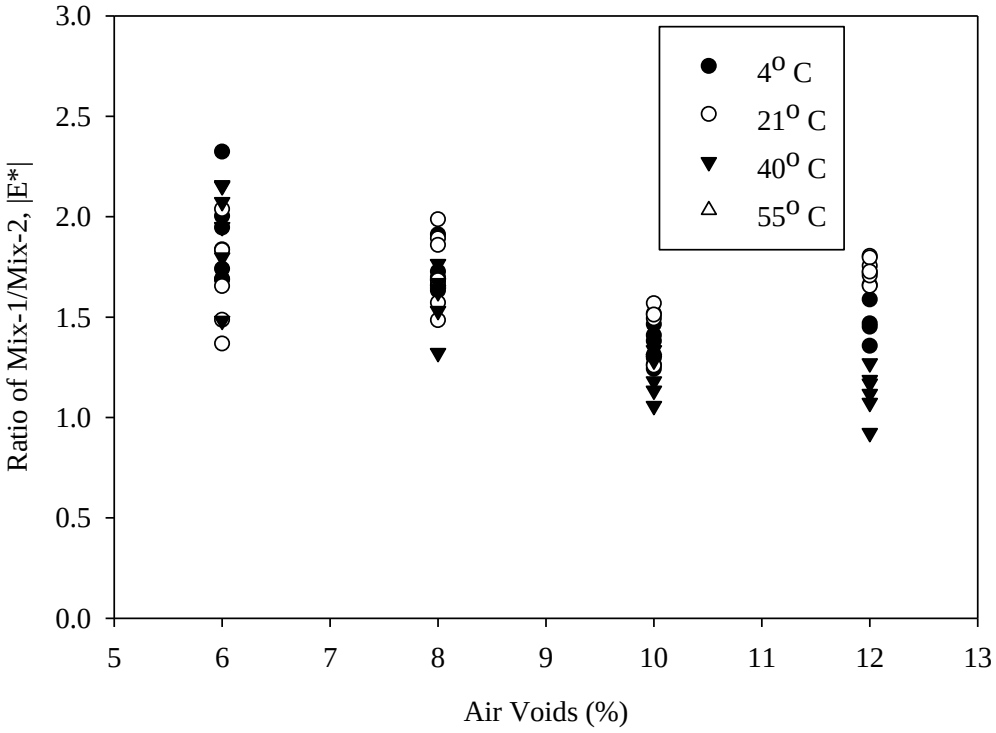

Figure 8.8 Spread of Ratio of |E*| for Mix-1 and Mix-2 for Unaged Condition

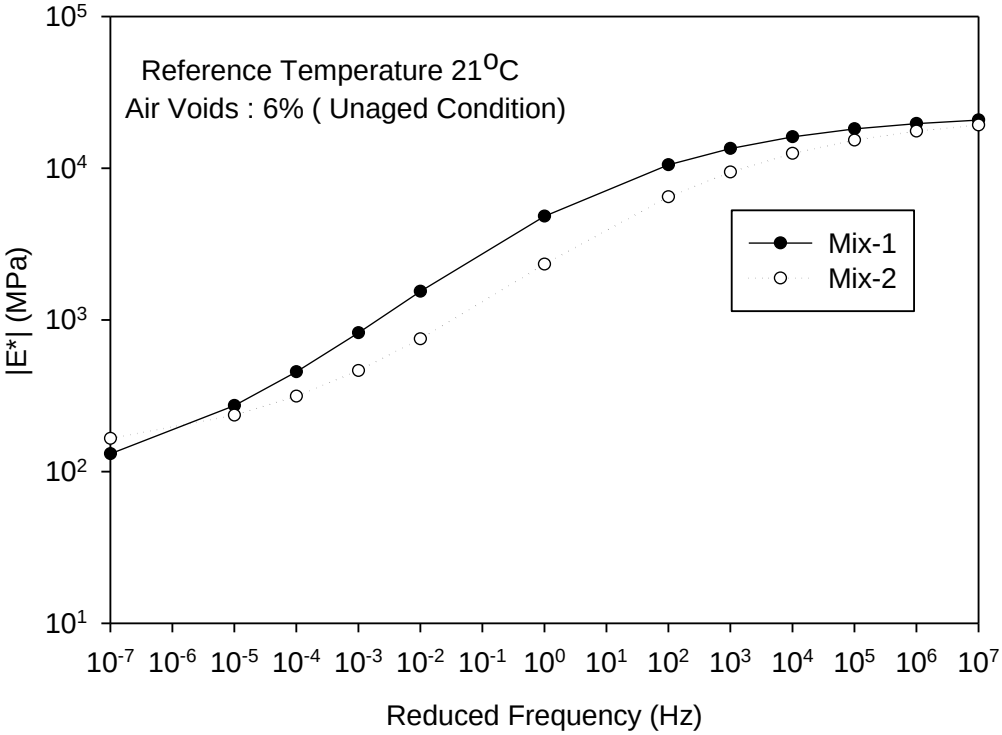

Figure 8.9 Master Curves for Unaged Condition at 6% Air Voids

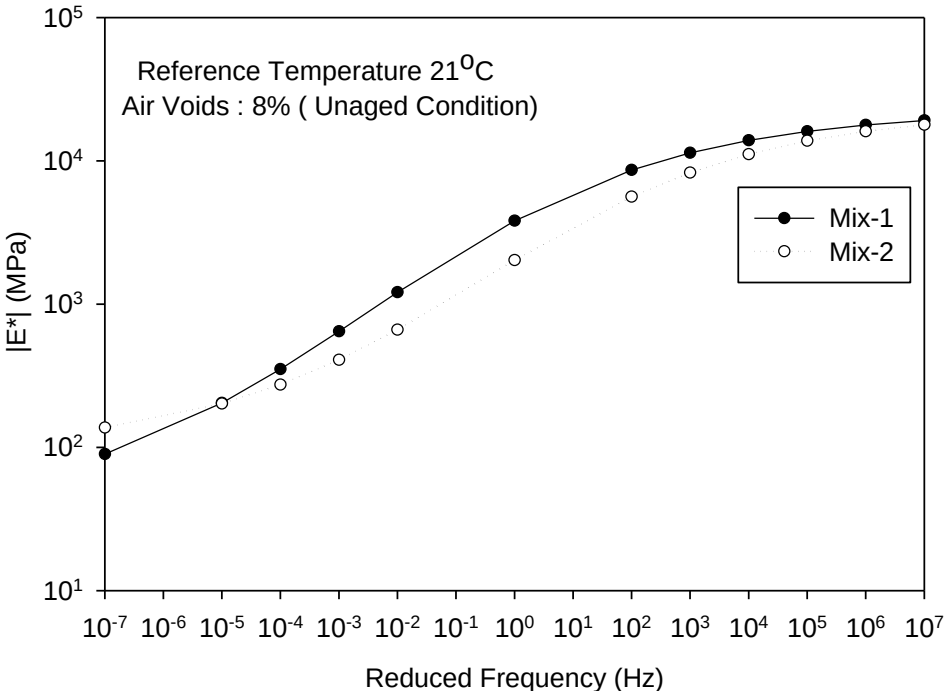

Figure 8.10 Master Curves for Unaged Condition at 8% Air Voids

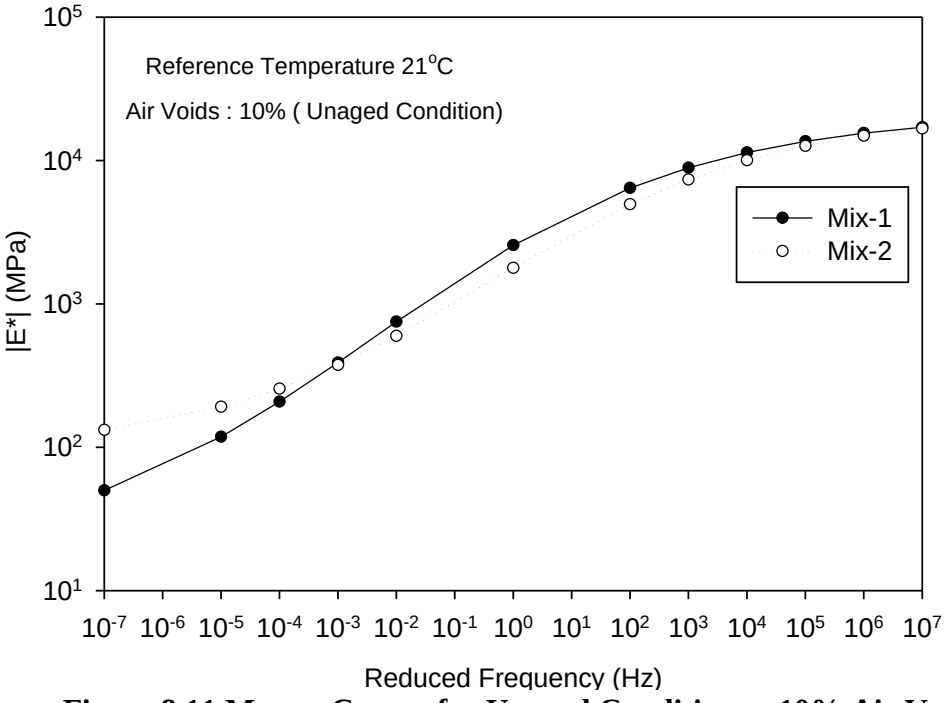

Figure 8.11 Master Curves for Unaged Condition at 10% Air Voids

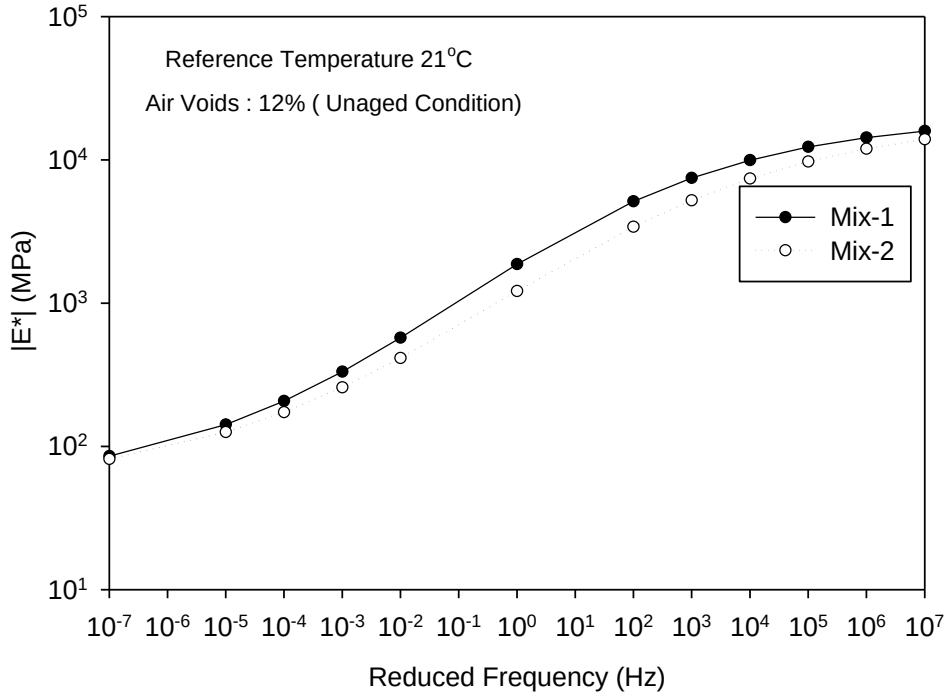

Figure 8.12 Master Curves for Unaged Condition at 12% Air Voids

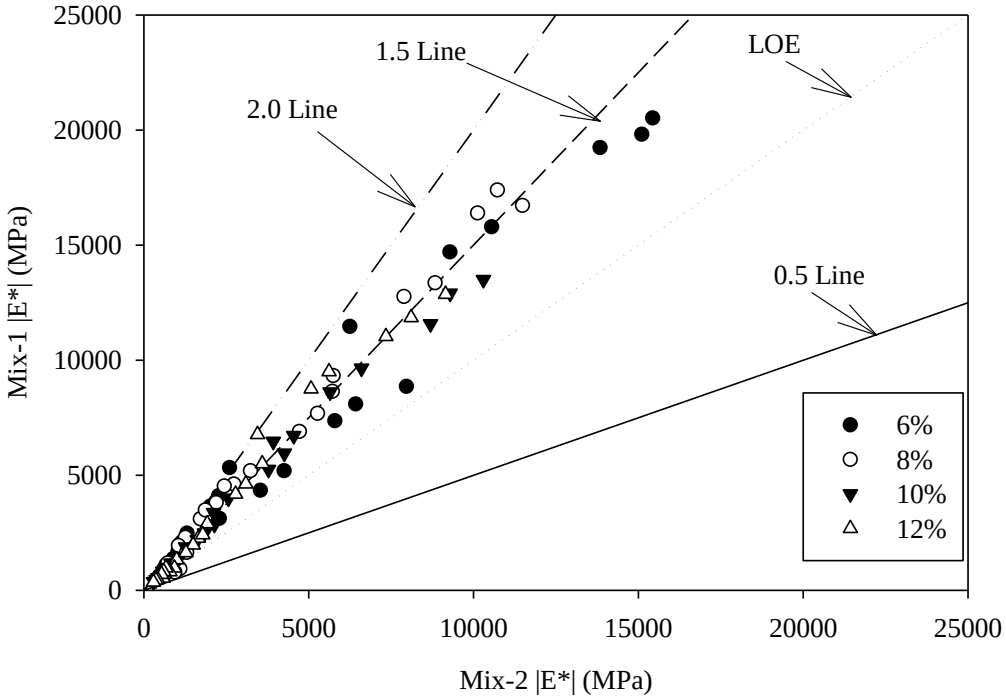

Figure 8.13 Comparison of |E*| for Mix-1 and Mix-2 for LTO-Aged Condition

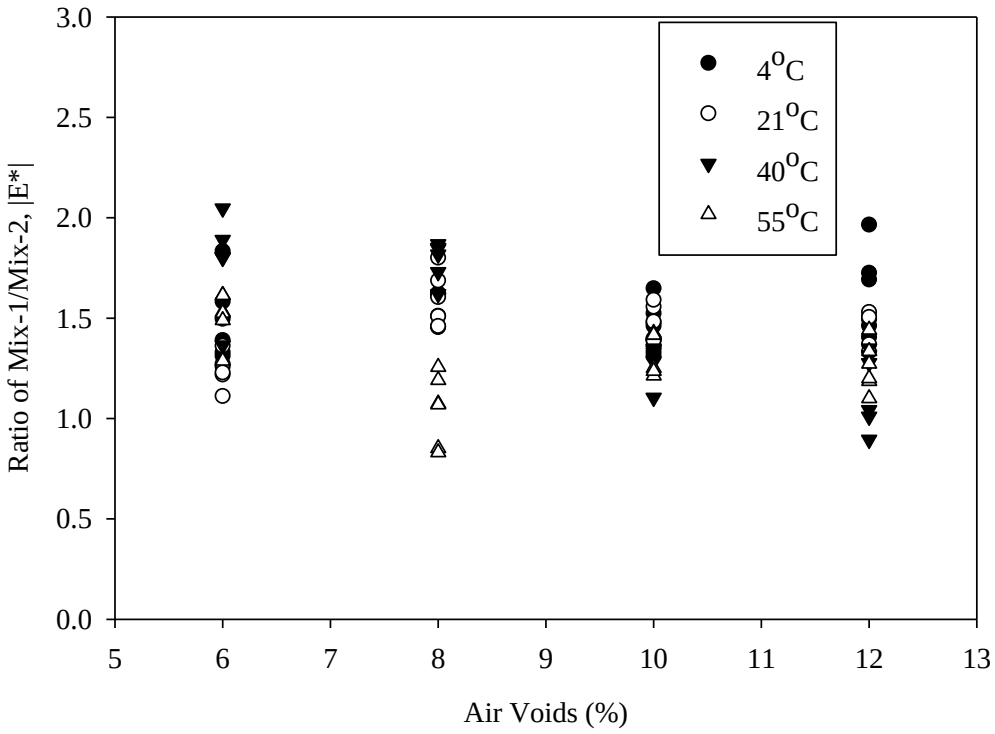

Figure 8.14 Spread of Ratio |E*| of Mix-1 and Mix-2 for LTO-Aged Condition

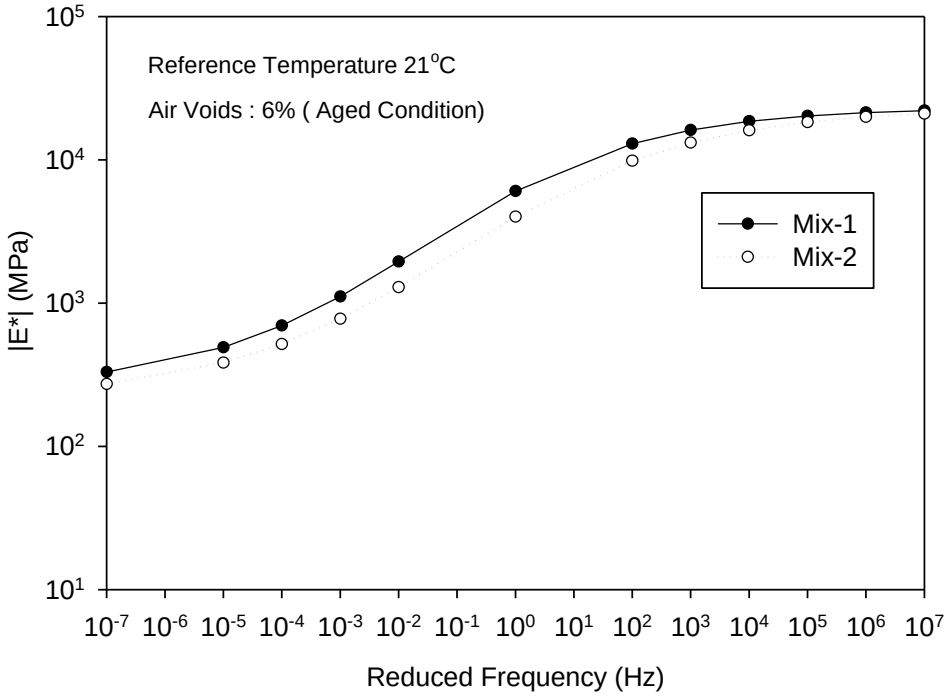

Figure 8.15 Master Curves for LTO-aged Condition at 6% Air Voids

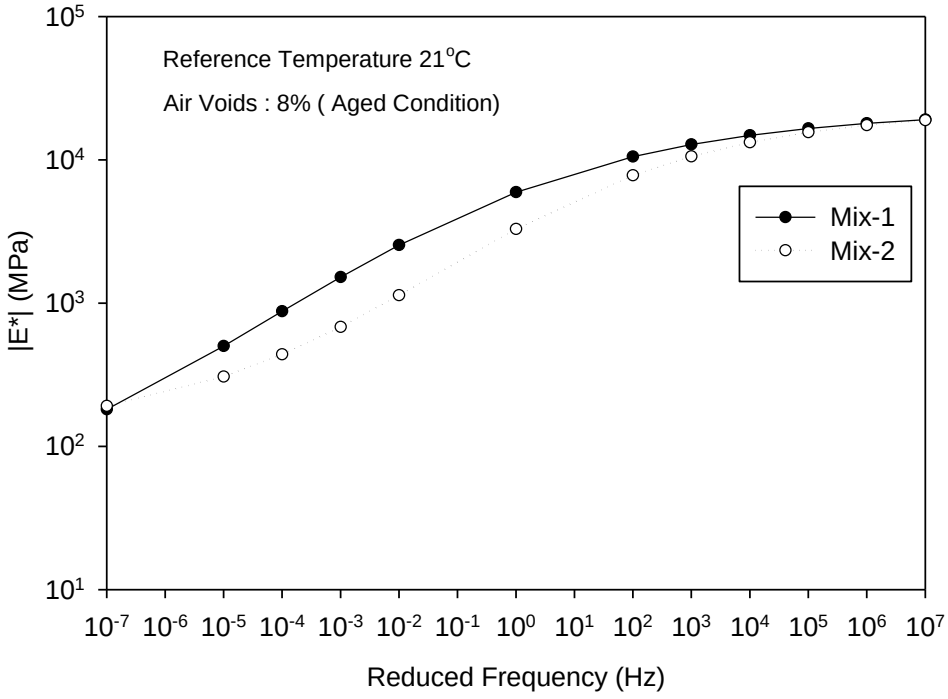

Figure 8.16 Master Curves for LTO-aged Condition at 8% Air Voids

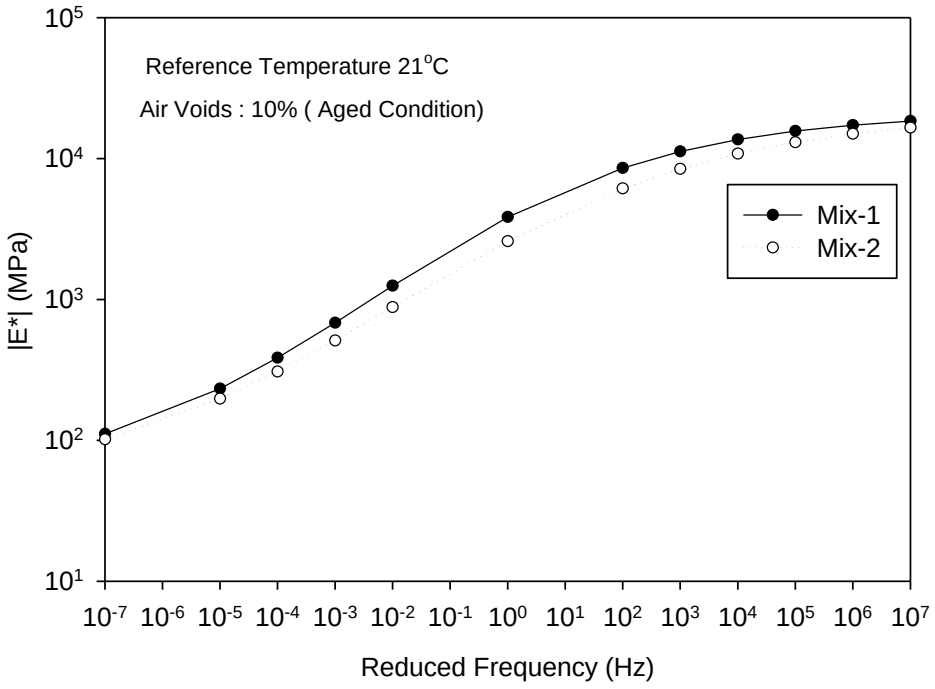

Figure 8.17 Master Curves for LTO-aged Condition at 10% Air Voids

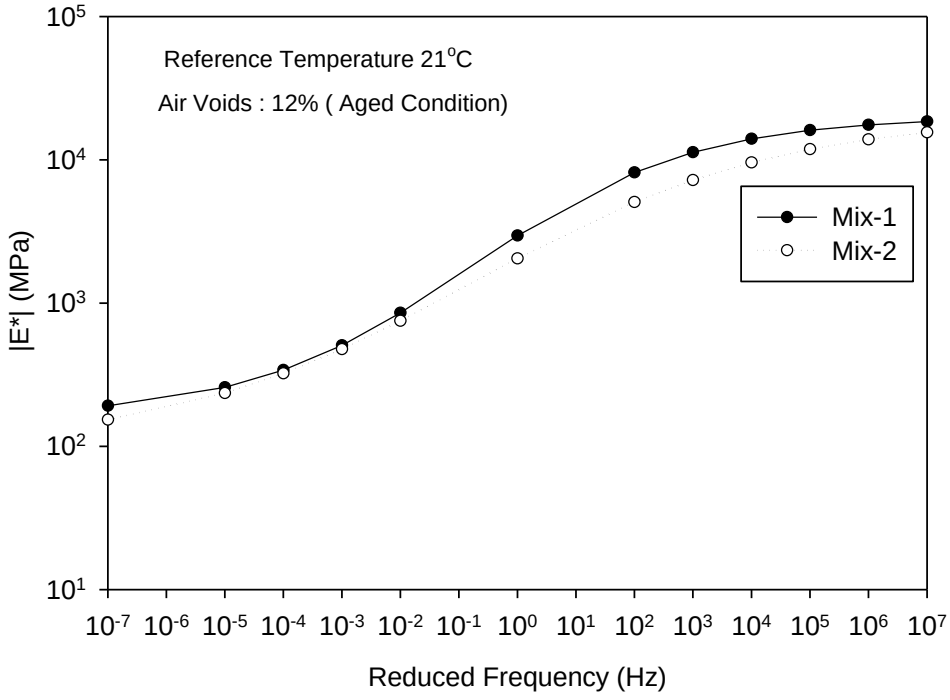

Figure 8.18 Master Curves for LTO-aged Condition at 12% Air Voids

CHAPTER 9 : SUMMARY, CONCLUSIONS, AND RECOMMENDATIONS

9.1 Summary

The mechanistic empirical pavement design guide (MEPDG) emphasizes using dynamic modulus of asphalt mixes at three different levels of design (i.e., Level 1, Level 2, and Level 3) for predicting the performance (i.e., rutting, fatigue, and low temperature cracking) of flexible pavements (MEPDG, 2004). Several studies have shown that dynamic modulus correlates better with the performance of pavements. The present study characterized selected asphalt mixes and aggregates that are commonly used in Oklahoma for the construction of flexible pavements. Five different asphalt mixes with varying aggregate sizes, types, sources, and different types of asphalt binders were collected from the production plant of Haskell Lemon Construction Company located in Norman. Samples were prepared using the Superpave gyratory compactor (SGC) at four different levels of air voids (i.e., 6%, 8%, 10%, and 12%). It is expected that selection of this wide range of air voids would cover the practical range of the compaction density achieved in the field (i.e., 88% to 94% of maximum theoretical density). Dynamic modulus values of compacted samples were measured in the laboratory at selected combinations of temperatures and frequencies. A total of 1440 dynamic modulus values were measured in the laboratory.

One of the objectives of this study was to develop the master curve and the shift factors for the asphalt mixes that are commonly used in Oklahoma. The master curves of each mix were constructed at a reference temperature of 21^{o}C (see Appendix A). The developed master curves and shift factors are useful for estimating dynamic modulus of a selected mix for a wide range of temperatures and frequencies.

One of the contributions of this study is to evaluate the effect of the production and sample preparation method on aggregate shape parameters (Singh et al., 2011a). Six different types of coarse and fine aggregates were tested, including original aggregates (OA) collected from the stockpile, plant mix (PM) aggregates extracted from the loose asphalt mix, and aggregates retrieved from the sample compacted at different density levels, called AV aggregates. Aggregate shape parameters were measured using an automated aggregate image measurement system (AIMS).

Another contribution of this study is the comparison of shape parameters of different types and sizes of coarse aggregates for quality control and quality assurance of the aggregates (Singh et al., 2011b). Currently, the Superpave mix design system is used to ensure the quality of aggregates by determining their consensus and source properties (Cominsky, 1994). However, several researchers have reported that the Superpave tests may not reflect the overall quality of the aggregates and consequently, contradictory results have been reported in the literature. In this study, three different types of aggregates (i.e., granite, rhyolite, and limestone) that are commonly used in Oklahoma were collected from the stockpiles. Each type of aggregate was divided into three different sizes of coarse aggregates (i.e., CA1, CA2, and CA3), with CA1 having the largest size, followed by CA2 and CA3.

Dynamic modulus values of modified and unmodified mixes were evaluated for three different levels of input (i.e., Level 1, Level 2, and Level 3) of the MEPDG (Singh et al., 2011c). Two Superpave asphalt mixes (i.e., Mix-3 and Mix-4), one containing a modified PG 70-28 binder and the other containing an unmodified PG 64-22 binder, are

used for this purpose. The dynamic modulus and master curves for these mixes are compared.

This study evaluates the performance of four predictive models (Witczak 1999, Witczak 2006, Hirsch, and Al-Khateeb) in estimating dynamic modulus of selected asphalt mixes (Singh et al., 2011d). Five different asphalt mixes were used for evaluating the models (see Chapter 2). Calibration factors were developed at individual air voids levels.

One of the most significant findings of this study is to develop the statistical and neural network (NN)-based models considering aggregates shape parameters (Singh et al., 2011e, 2011f). At present, no model is available that considers the shape parameters of aggregates in the estimation of dynamic modulus. A nonlinear regression model was developed to estimate the dynamic modulus of the mix. A four layer (one input-two hidden-one output layers) network was used for developing the NN model. The results from this study are expected to help in characterizing the performance of asphalt mix and aggregate base layers in an accurate manner.

This study also examined the effect of long term oven-aging on two different asphalt mixes contained reclaimed asphalt pavement (RAP) (Singh et al., 2011g).

9.2 Conclusions

Specific conclusions pertaining to specific topics were included in individual chapters. The pertinent overall conclusions are summarized as follows:

(1) It was observed that the texture of original coarse aggregates (i.e., OA aggregates) was higher compared to the plant mix coarse aggregates (i.e., PM aggregates), indicating that the plant production process lowers the texture of coarse aggregates.

(2) Aggregate compacted at different levels of air voids (i.e., AV aggregates) were found to have more texture compared to PM aggregates. It might be possible that the texture is altered during the process of sample preparation, coring, and sawing.

(3) The form of OA coarse aggregates was found to be higher than all other types of coarse aggregates. PM coarse aggregates were found to have the lowest value of form.

(4) For fine aggregates, the angularity and form were found to be very similar for all six types of aggregates, indicating that the plant production process and sample preparation method did not influence the shape properties of these particles significantly.

(5) The results showed that coarse aggregates were more angular and elongated compared to the fine aggregates, indicating that the particles become rounded and circular as its size decreases.

(6) Larger size particles were found to be rougher and more cubical compared to the smaller size aggregates (i.e., high texture, low form, and high sphericity), indicating that the particles become smooth and elongated as their size decreases.

(7) Granite aggregate was rougher (high texture) and more cubical (low form and high sphericity) compared to rhyolite and limestone aggregates.

(8) The ranking of the aggregates is done based on the composite shape index factor (CI). The overall rank sequence for the aggregates was found to be as follows: granite>rhyolite>limestone, indicating that the performance of granite aggregates would be better compared to the other two aggregates.

(9) For the modified mix, Level 2 resulted in a higher error compared to Level 3, which is contrary to the expectation that the Levels 1, 2, and 3 are in decreasing order of accuracy.

(10) For the unmodified mix, Level 2 resulted in lesser error compared to Level 3, indicating that assuming default viscosity values from the MEPDG would work well for the unmodified mix used in the present study.

(11) The Hirsch and the Al-Khateeb models were found to perform with good accuracy at low temperatures.

(12) The Witczak 1999 and the Witczak 2006 models performed well at high temperatures. None of these models performed well at low temperatures and high air voids.

(13) Calibration factors were developed at individual air voids levels. These calibration factors are important to assist state agencies and pavement designers for Level 2 and Level 3 designs of the MEPDG for mixes commonly used in Oklahoma.

(14) The correlation coefficient (R^2) for the developed statistical shape-based model was found to be 0.95 and 0.92 on logarithmic and arithmetic scales, respectively, indicating that aggregate shape parameters can enhance the predictive capability of the model.

(15) The performance of the statistical shape-based model was compared with the widely accepted Witczak model that does not use the shape parameters of the aggregates. The MARE for the Witczak model was estimated to be

approximately 92.8%, which was approximately 4 times higher than the developed model.

(16) The results show that the dynamic modulus of the mix increases with an increase in angularity and texture of aggregates and that the inclusion of shape parameters can enhance the prediction capability of a model.

(17) The training and testing results of the developed neural network (NN) model show that the inclusion of aggregate shape parameters can be used as independent parameters of the model.

(18) The sensitivity analysis of the input parameters shows that the viscosity of the asphalt binder has a strong correlation with dynamic modulus. The volumetric properties and shape parameters were found to be very poorly correlated.

(19) It was found that LTO-aging resulted in an approximately 42% to 60% increase in dynamic modulus, depending upon the amount of RAP, and air voids.

(20) Specimens having higher air voids aged more rapidly compared to specimens with lower air voids. Mixes with higher percentages of RAP aged slowly compared to mixes with a lower percentage of RAP.

(21) Results show that the degree of compaction (amount of air voids), temperature, and frequency have significant impact on dynamic modulus. A proper selection of these parameters is important while predicting the response of a flexible pavement.

9.3 Recommendations

Based on the observations from this study, the following recommendations are made for future studies:

(1) In the present study, the effect of the production and sample preparation methods was studied on limestone aggregates. It is recommended that similar studies be conducted on other types of aggregates (i.e., granite, sandstone, rhyolite, and gravel etc.) collected from different sources.

(2) The ranking of the aggregates based on the composite index (CI) factors need to be validated by conducting the performance test on the asphalt mixes made of different types of aggregates.

(3) The comparison of dynamic modulus on different levels of MEPDG need to be conducted for mixes from different sources with different types of binders and aggregates.

(4) This study developed a shape-based model for estimating dynamic modulus. It is recommended that additional mixes be tested for the development and the validation of the shape-based model. In addition, a similar approach should be used to develop the models for estimating the resilient modulus of aggregates.

(5) The performance of stone mastic asphalt (SMA) largely depends on stone-to-stone contact. Therefore, it is important to evaluate the effect of aggregate shape parameters on the performance of SMA mixes. In addition, emphasis should be given to establish the ranking of different shape parameters.

(6) It is important to investigate the contribution of mechanical properties (i.e., modulus of elasticity, Poisson's ratio) of aggregate on dynamic modulus of asphalt mixes.

(7) It is recommended that future studies be conducted to quantify the effect of aggregate shape parameters on dynamic modulus.

REFERENCES

1. AASHTO (1993). "AASHTO Guide for Design of Pavement Structures," *American Association of State Highway and Transportation Officials,* Washington, D.C.
2. AASHTO (2004). "Guide to the Mechanistic-Empirical Design of New and Rehabilitated Pavement Structures," 1-37A, NCHRP, Washington, D.C., *http://www.trb.org/mepdg/guide.htm (last accessed 3/10/2011).*
3. AASHTO R30 (2002). "Standard Practice for Mixture Conditioning of Hot Mix Asphalt," *American Association of State Highway and Transportation Officials,* Washington, D.C.
4. AASHTO T 240 (2003). "Standard Method of Test for Effect of Heat and Air on a Moving Film of Asphalt (Rolling Thin-Film Oven Test)," *American Association of State Highway and Transportation Officials,* Washington, D.C.
5. AASHTO T 316 (2002). "Standard Method of Test for Viscosity Determination of Asphalt Binder Using Rotational Viscometer," *American Association of State Highway and Transportation Officials,* Washington, D.C.
6. AASHTO T166 (2006). "Standard Method of Test for Bulk Specific Gravity of Compacted Bituminous Mixtures Using Saturated Surface Dry Specimens," *American Association of State Highway and Transportation Officials,* Washington, D.C.
7. AASHTO TP62-03 (2006). "Standard Method of Test for Determining Dynamic Modulus of Hot-Mix Asphalt Concrete Mixtures," *American Association of State Highway and Transportation Officials,* Provisional Standards.
8. AASHTO TP64-10 (2010a). "Calculating Aggregate Stockpile Shape Characteristics Values from Digital Image Analysis Shape Properties," *American Association of State Highway and Transportation Officials,* Washington, D.C.
9. AASHTO TP81-10 (2010b). "Determining Aggregate Shape Properties by Means of Digital Image Analysis," *American Association of State Highway and Transportation Officials,* Washington, D.C.
10. Abbas, A.M., Masad, E., Papagiannakis, T., and Shenoy, A. (2005). "Modelling asphalt mastic stiffness using discrete element analysis and micromechanics-based

models," *International Journal of Pavement Engineering,* Vol. 6, Issue: 2, pp.137-146.

11. Abdo, A.A., Bayomy, F., Nielsen, R., Weaver, T., and Jung, S.J. (2009). "Prediction of the Dynamic Modulus of Superpave Mixes," *Bearing Capacity of Roads, Railways and Airfields,* Taylor and Francis Group, London, pp. 305-314.
12. Abdul-Malak, M., Fowler, D., and Constantino, C. (1996). "Aggregate characteristics governing performance of seal coat highway overlays. Transportation Research Record, No. 1547, *Journal of the Transportation Research Board,* Washington, D.C., pp. 15–22.
13. Ahlrich, R.C. (1996). "Influence of Aggregate Properties on Performance of Heavy-Duty Hot-Mix Asphalt Pavements," Transportation Research Record, No. 1547, *Journal of the Transportation Research Board,* Washington, D.C., pp. 7-14.
14. Alam, J., Galal, K.A., and Diefenderfer, B.K. (2007). "Network-Level Falling Weight Deflectometer Testing: Statistical Determination of Minimum Testing Intervals and Number of Drop Levels on Virginia's Interstate System," Transportation Research Record, No. 1990, *Journal of the Transportation Research Board,* Washington, D.C., pp. 111-118.
15. Al-Azri, N. A., S. H. Jung, K. M. Lusford, A. Ferry, J. A. Bullin, R. R. Davison, and Glover, C. J. (2006). "Binder Oxidative Aging in Texas Pavements: Hardening Rates, Hardening Susceptibilities, and the Impact of Pavement Depth*," Transportation Research Board Presentation*, Washington, D.C.
16. Al-Khateeb, G., Shenoy, A., Gibson, N., and Harman, T. (2006). "A New Simplistic Model for Dynamic Modulus Predictions of Asphalt Paving Mixtures," *Journal of the Association of Asphalt Paving Technologists,* Vol. 75, pp. 1254–1293.
17. Al-Qadi, I.L., Elseifi, M.A., and Carpenter, S.H. (2007). "Reclaimed Asphalt Pavement- A Literature Review," Report No. FHWA-ICT-07-001. *Illinois Center for Transportation (ICT),* Urbana, IL.
18. Al-Rousan, T., Masad, E., Myers, L., and Speigelman, C. (2005). "New Methodology for Shape Classification of Aggregates," Transportation Research

Record, No. 1913, *Journal of the Transportation Research Board*, Washington, D.C., pp.11-23.

19. Alvarado, C., Mahmoud, E., Abdallah, I., Masad, E., Nazarian, S., Tandon, V., and Button, J. (2006). "Feasibility of Quantifying the Role of Coarse Aggregate Strength on Resistance to Load in HMA," Research Report FHWA/TX 06/0-5268-2, *Center for Transportation Infrastructure Systems,* The University of Texas at EI Paso, EI Paso, Texas.
20. Andrei, D., Witczak, M.W., Mirza, M.W. (1999). "Development of a Revised Predictive Model for the Dynamic (Complex) Modulus of Asphalt Mixtures," NCHRP 1-37A Interim Team Report, *University of Maryland.*
21. Anthony, A.M. (2007). "Effects of Manufactured Fine Aggregate on Physical and Mechanistic Properties of Saskatchewan Asphalt Concrete Mixes." M.S. Thesis, University of Saskatchewan.
22. Aragao, F.T., Kim, Y., Karki, P. (2010). "Semi-Empirical, Analytical, and Computational Predictions of Dynamic Modulus of Asphalt Concrete Mixtures," CD-ROM Publication, *Transportation Research Board,* Washington, D.C.
23. Aschenbrener, T. and MacKean, C. (1994). "Factors that Affect the Voids in the Mineral Aggregate of Hot-Mix Asphalt," Transportation Research Record, No. 1469, *Journal of the Transportation Research Board,* Washington, DC, pp. 1-8.
24. Asphalt Institute (1991). "Thickness Design-Asphalt Pavements for Highways & Streets," *Manual Series No.1.*
25. ASTM D2493-01 (2001). "Viscosity-Temperature Chart for Asphalt," *Annual Book of ASTM Standards,* Vol. 0.0403.
26. Ayres, M. Jr. and Witczak, M.W. (1998). "AYMA - A Mechanistic Probabilistic System to Evaluate Flexible Pavement Performance," Transportation Research Record, No. 1629, *Journal of the Transportation Research Board,* Washington D.C., pp. 137-148.
27. Azari, H., Al-Khateeb, G., Shenoy, A., and Gibson, N. (2007). "Comparison of Simple Performance Test |E*| of Accelerated Loading Facility Mixtures and Prediction |E*| use of NCHRP 1-37 A and Witczak's New Equations,"

Transportation Research Record, No. 1998, *Journal of the Transportation Research Board,* Washington, D.C., pp. 1-9.

28. Bari, J., and Witczak, M.W. (2006). "Development of a New Revised Version of the Witczak E* Predictive Model for Hot Mix Asphalt Mixtures," *Journal of the Association of Asphalt Paving Technologists,* Vol. 75, pp. 381-423.
29. Bari, J., and Witczak, M.W. (2007). "New Predictive Models for Viscosity and Complex Shear Modulus of Asphalt Binders for Use with Mechanistic-Empirical Pavement Design Guide," Transportation Research Record, No. 2001, *Journal of the Transportation Research Board,* Washington, D.C., pp. 9-19.
30. Barksdale, R. D., Pollard, C. O., Siegel, T., and Moeller, S. (1992). "Evaluation of the effects of aggregate on rutting and fatigue of asphalt," Research Report, *Georgia DOT Project 8812 and Georgia Tech Project E20-835,* Georgia Institute of Technology, Atlanta.
31. Bayat, A., Knight, M. (2010). "Investigation of Hot-Mix Asphalt Dynamic Modulus Using Field Measured Pavement Response," *CD-ROM Publication, Transportation Research Board,* Washington, D.C.
32. Bennert, T. (2009). "Dynamic Modulus of Hot Mix Asphalt," FHWA-NJ-2009-011, *New Jersey Department of Transportation, Trenton,* New Jersey, pp. 56-57.
33. Bennert, T., Cooley, L.A., Ericson, C., and Zavery, Z. (2011). "Evaluation of Coarse Aggregate Angularity Properties and Its Relationship to Permanent Deformation for New York State Gravel Aggregates," *CD-ROM Publication, Transportation Research Board,* Washington, D.C.
34. Bhasin, A., Button, J.W., Chowdhury, A., and Masad, E. (2006). "Selection of Optimum Gravel Aggregate Size to Resist Permanent Deformation in Hot-Mix Asphalt," Transportation Research Record, No. 1952, *Journal of the Transportation Research Board,* Washington, D.C., pp. 39-47.
35. Birgisson, B., Sholar, G., and Roque, R. (2005). "Evaluation of a Predicted Dynamic Modulus for Florida Mixture," Transportation Research Record, No. 1929, *Journal of the Transportation Research Board,* Washington, D.C., pp. 200-207.

36. Bonaquist, R., and Christensen, D.W. (2005). "Practical Procedure for Developing Dynamic Modulus Master Curves for Pavement Structural Design," Transportation Research Record, No. 1929, *Journal of the Transportation Research Board,* Washington, D.C., pp. 208-217.

37. Brown, E.R. (1984). "Evaluation of Properties of Recycled Asphalt Concrete Hot Mix," *U.S. Army Engineer Waterways Experiment Station,* Final Report # CL-84-2.

38. Brown, R.R., and Bassett, C.E. (1990). "Effects of Maximum Aggregate Size on Rutting Potential and Other Properties of Asphalt –Aggregate Mixtures," Transportation Research Record, No. 1259, *Journal of the Transportation Research Board, Washington,* D.C., pp. 107-119.

39. Button, J.W., Perdomo, D., and Lytton, R.L. (1990). "Influence of Aggregate on Rutting in Asphalt Concrete Pavements," Transportation Research Record, No. 1259, *Journal of the Transportation Research Board,* Washington, D.C., pp.141-152.

40. Ceylan, H., Gopalakrishnan, K., and Kim, S. (2008). "Advanced Approached to Hot Mix Asphalt Dynamic Modulus Prediction," *Canadian Journal of Civil Engineering,* Vol. 35, pp. 699-707.

41. Ceylan, H., Gopalakrishnan, K., and Kim, S. (2009a). "Looking to the future: the next-generation hot mix asphalt dynamic modulus prediction models," *International Journal of Pavement Engineering,* Vol.10, Issue: 5, pp.341-352.

42. Ceylan, H., Schwartz, C.W., Kim, S., and Gopalakrishnan, K. (2009b). "Accuracy of Predictive Models for Dynamic Modulus of Hot Mix Asphalt," *ASCE, Journal of Materials in Civil Engineering,* Vol. 21, No. 6, pp. 286-293.

43. Chadbourn, B. A., Skok, E. L., Newcomb, D. E., Crow, B. L., and Spindler, S. (1999). "Effect of Voids in Mineral Aggregate on Hot-Mix Asphalt Pavements," *Report MN/RC-2000-13. Minnesota Department of Transportation,* St. Paul.

44. Chehab, G. R. (2002). "Characterization of Asphalt Concrete in Tension Using a Visco-Elasto-Plastic Model," *Ph.D. Dissertation,* North Carolina State University, Raleigh.

45. Chehab, G., O'Quinn, R. E., and Kim, Y. R. (2000). "Specimen Geometry Study for Direct Tension Test Based on Mechanical Tests and Air Void Variation in Asphalt Concrete Specimens Compacted by Superpave Gyratory Compactor," Journal of Transportation Research Record, No. 1723, *Journal of the Transportation Research Board,* Washington, D.C., pp. 125–132.

46. Chen, J.S., and Huang, L.S. (2000). "Developing an Aging Model to Evaluate Engineering Properties of Asphalt Paving Binders," *Journal of Materials and Structures,* Vol. 33, pp. 559-565.

47. Christensen, D.W., Pellinen, T., and Bonaquist, R.F. (2003). "Hirsch Model for Estimating the Modulus of Asphalt Concrete," *Journal of the Association of Asphalt Paving Technologists,* Vol. 72, pp. 97–121.

48. Cline, T.R., Li, X., Marasteanu, M.O., and Skok, E.L. (2003). "Dynamic and Resilient Modulus of Mn/DOT Asphalt Mixes," *Final Report No. MN/RC-2003-09,* St. Paul, Minnesota, 4-14.

49. Collins, R., Watson, D., Johnson, A., and Wu, Y.P. (1997). "Effect of Aggregate Degradation on Specimens Compacted by Superpave Gyratory Compactor," Transportation Research Record, No. 1590, *Journal of the Transportation Research Board,* Washington, D.C., pp. 1-9.

50. Cominsky, R., Leahy, R.B., and Harrigan, E.T. (1994). "Level One Mix Design: Materials Selection, Compaction, and Conditioning," *SHRP A-408.* Washington, D.C.

51. Cominsky, R.J., Killingsworth, B.M., Anderson, R.M., Anderson, D.A., and Crockford, W.W. (1998). "Quality control and acceptance of superpave designed hot mix asphalt," Project D9-7, *NCHRP Report No. 409, Transportation Research Board,* Washington, D.C.

52. Commuri, S., Zaman, M., Singh, D.V., Mai, A., and Beainy, F. (2011). "Continuous Real Time Measurement of Pavement Quality during Construction" *Oklahoma Transportation Center, Report No. OTCREOS7.1-10-F, Oklahoma.*

53. Coree, B.J., Hislop, W.P. (2000). "A Laboratory Investigation into the Effects of Aggregate Related Factors of Critical VMA in Asphalt Paving Mixtures," Iowa Highway Research Board, Project TR-415, *Iowa Department of Transportation.*

54. D'Angelo, J. (1998). "Superpave mix design tests methods and requirement," *APWA International Public Works Congress,* Las Vegas, Nevada.

55. Dai, Q. (2010). "Prediction of Dynamic Modulus and Phase Angle of Stone-Based Composites Using a Micromechanical Finite-Element Approach," *ASCE, Journal of Materials in Civil Engineering,* Vol. 22, No.6, pp. 618-627.

56. Dai, Q., and You, Z. (2007). "Micromechanical finite element framework for predicting viscoelastic properties of asphalt mixtures," *Materials and Structures,* Vol. 41, pp. 1025-1037.

57. Daniel, J. S. (2001). "Development of a Simplified Fatigue Test and Analysis Procedure Using a Viscoelastic, Continuum Damage Model and Its Implementation to WesTrack Mixtures," *Ph.D. Dissertation,* North Carolina State University, Raleigh.

58. Daniel, J. S., Kim, Y. R., Lee, H. J. (1998). "Effects of Aging on Viscoelastic Properties of Asphalt-Aggregate Mixtures," Transportation Research Record, No. 1630, *Journal of the Transportation Research Board,* Washington, D.C., pp. 21-27.

59. Demircan, E., Harendra, S., Vipulanandan, C. (2011). "Artificial Neural Network and Nonlinear Models for Gelling Time and Maximum Curing Temperature Rise in Polymer Grouts," *ASCE, Journal of Materials in Civil Engineering,* Vol. 24, No.4, pp. 372-377.

60. DiBenedetto, H., Partl, M.N., De La Roche Saint Andre, C. (2001). "Stiffness Testing for Bituminous Mixtures, RILEM TC 182-PEB Performance Testing And Evaluation Of Bituminous Materials," *Materials and Structures,* Vol. 34, pp. 66-70.

61. Dongre, R., Myers, L., D'Angelo, J., and Gudimettla, J. (2005). "Field Evaluation of Witczak and Hirsch Models for Predicting Dynamic Modulus of Hot-Mix Asphalt," *Journal of the Association of Asphalt Paving Technologists,* Vol. 74.

62. Far, M.S.S., Underwood, B.S., Ranjithan, S.R., Kim, Y.R., and Jackson, N. (2009). "Application of Artificial Neural Networks for Estimating Dynamic Modulus of Asphalt Concrete," Transportation Research Record, No. 2127, *Journal of the Transportation Research Board,* Washington, D.C., pp. 173-186.

63. Farrar, M.J., Harnsberger, P.M., Thomas, K.P., and Wiser, W. (2006). "Evaluation of Oxidation in Asphalt Pavement Test Sections After Four Years of Service," *Proceedings of the International Conference on Perpetual Pavement,* Columbus, Ohio.

64. Federal Highways (FHWA). (2010a) "Aggregate Imaging Measurement System. Highways for LIFE Program," *Online access: http://www.fhwa.dot.gov/hfl/partnerships/aims2/aims2_00.cfm (Last accessed: June 30, 2011).*

65. Federal Highways Administration (FHWA). (2010b). Recycled Materials in Roadway Construction: The Many Ways of Going Green. *Online access: (http://www.fhwa.dot.gov/publications/focus/10apr/01.cfm (Last assessed: July 25, 2011).*

66. Fletcher, T., Chandan, C., Masad, E., and Sivakumar, K. (2003). "Aggregate Imaging System for Characterizing the Shape of Fine and Coarse Aggregates," Transportation Research Record, No. 1832, *Journal of the Transportation Research Board,* Washington, D.C., pp. 67-77.

67. Fletcher, T., Chandan, C., Masad, E., and Sivakumar, K (2002). "Measurement of Aggregate Texture and its Influence on Hot Mix Asphalt Permanent Deformation," *ASTM, Journal of Testing and Evaluation*, Vol. 30, No. 6, pp. 1-8.

68. Francken, L., Partl, M. (1996). "Complex Modulus Testing of Asphaltic Concrete: RILEM Inter-laboratory Test Program," Transportation Research Record, No. 1545, *Journal of the Transportation Research Board*, Washington, D.C., pp. 133-142.

69. Francken, L., Vanelstraete, A., and Verhasselt, A. (1997). "Long Term Ageing of Pure and Modified Bitumen: Influence on the Rheological Properties and Relation with the Mechanical Performance of Asphalt Mixtures," *8th International Conference on Asphalt Pavements,* Volume 2.

70. Gatchalian, D., Masad, E., Chowdhury, A., and Little, D. (2006). "Characterization of Aggregate Resistance to Degradation in Stone Matrix Asphalt Mixtures," Transportation Research Record, No. 1962, *Journal of the Transportation Research Board,* Washington, D.C., pp. 55-63.

71. Goh, S.W., You,Z., Williams, R.C., and Li, Xinjun. (2011). "Preliminary Dynamic Modulus Criteria of HMA for Field Rutting of Asphalt Pavements: Michigan's Experience," *ASCE, Journal of Transportation Engineering,* Vol. 137, No.1, pp.37-45.

72. Gopalakrishnan, K., Kim, S. (2011). "Support Vector Machine Approach to HMA Stiffness Prediction," *ASCE, Journal of Engineering Mechanics,* Vol. 137, No.2, pp. 138-146.

73. Gudimettla, J., Myers, L.A., and Paugh, C. (2006). "AIMS: The future in Rapid, Automated Aggregates Shape and Texture Measurement," *Proceeding of 51st Canadian Transportation Board Meeting,* Canada, pp. 179-207.

74. Hagan, M.T., Demuth, H.B., and Beale, M. (1996). "Neural Network Design," *International Thomson Publishing Inc.,* U.S.A.

75. Hand, A.J., Epps, J.A., and Sebaaly, P.E. (2000). "Precision of ASTM D5821 standard test method for determining the percentage of fractured particles in coarse aggregate," *ASTM, Journal of Testing and Evaluation,* Vol.28, No.2, pp.67-75.

76. Harran, G., and Shalaby, A. (2009). "Improving the prediction of the dynamic modulus of fine-graded asphalt concrete mixtures at high temperatures," *Canadian Journal of Civil Engineering,* Vol. 36, pp.180-190.

77. Hossain, M.S., Lane, D.S., and Schmidt, B.N. (2008). "Results of Micro-Deval Test for Coarse Aggregates from Virginia Sources," Journal of Transportation Research Record, No. 2059, *Journal of the Transportation Research Board,* Washington, D.C., pp. 1-10.

78. Houston, W.N., Mirza, M.W., Zapata, C.E., and Raghavendra, S. (2005). "Environmental Effects in Pavement Mix and Structural Design Systems," *National Cooperative Highway Research Program: Web Only Document 113: Part 1 of Final Report for NCHRP Project 9-23. http://www.basic.northwestern.edu/statguidefiles/oneway_anova_ass_viol.html (last accessed: April 12, 2011).*

79. Huang, B., Shu, X., and Bass, J. (2008). "Investigation of Simple Performance Characteristics of Plant-Produced Asphalt Mixtures in Tennessee," Transportation

Research Record: No. 2057, *Journal of the Transportation Research Board,* Washington, D.C., pp. 140-148.

80. Huang, B., Zhang, Z., and Kinger, W. (2004). "Fatigue Crack Characteristics of HMA Mixtures Containing RAP," *Proceedings, 5th International RILEM Conference on Cracking in Pavements,* Limoges, France.
81. Huber, G.A., Jones, J.C., Messersmith, P.E., and Jackson, N.M. (1998). "Contribution of Fine Aggregate Angularity and Particle Shape to Superpave Mixture Performance," Transportation Research Record, No.1609, *Journal of the Transportation Research Board,* Washington, D.C., pp.28-35.
82. Hughes, C.S., Simpson, A.L., Cominsky, R., Pendleton, O.J., Weed, R.M., and Wilson, T. (1998). "Measurement and Specification of Construction Quality," Volume I: Final Report No. FHWA-RD-98-077, *Brent Rauhut Engineering Inc.,* Austin, Texas, pp.83-85.
83. Jiang, Y., Selezneva, O., Mladenovic, G., Aref, S., and Darter, M. (2003). "Estimation of Pavement Layer Thickness Variability for Reliability-Based Design," Transportation Research Record, No. 1849, *Journal of the Transportation Research Board,* Washington, D.C., pp. 156-165.
84. Johnson, E., Li, X., Zofka, A., and Marasteanu, M.O., and Clyne, T.R. (2007). "Investigation of Superpave Fine Aggregate Angularity Criterion for Asphalt Concrete," Transportation Research Record, No. 1998, *Journal of the Transportation Research Board,* Washington, D.C., pp.75-81.
85. Kandhal, P. S., and Mallick, R. B. (1997). "Pavement Recycling Guidelines for State and Local Governments – Participant's Reference Book," Report No. FHWA-SA-98-042, *National Center for Asphalt Technology,* Auburn, Alabama.
86. Kandhal, P.S. and Frazier, P. (1998). "Aggregate Tests Related to Asphalt Concrete Performance in Pavements," *NCHRP Report No. 405,* Washington, D.C.
87. Kandhal, P.S., and Mallick. R.B. (2001). "Effect of Mix Gradation on Rutting Potential of Dense-Graded Asphalt Mixtures," Transportation Research Record, No. 1767, *Journal of the Transportation Research Board,* Washington, D.C., pp. 146-151.

88. Kandhal, P.S., Brown, E.R., and Cross, S. (1989). "Guidelines for Hot Mix Recycling in Georgia," *Georgia DOT Project No. 8807, Final Report.*

89. Kennedy, T. W., Tam, W. O., and Solaimanian, M. (1998). "Optimizing Use of Reclaimed Asphalt Pavement with the SuperPave System," *Journal of the Association of Asphalt Paving Technologists,* Vol. 67, pp. 311-333.

90. Kiggundu, B.M., Humphrey, B.N., and Zallen, D.M. (1985). Recycling Agent Selection and Tentative Specification. *Final Report # ESL-TR-84-47,* New Mexico Engineering Research Institute.

91. Kim, Y.R., King, M., and Momen, M. (2005). "Typical Dynamic Moduli Values of Hot Mix Asphalt in North Carolina and Their Prediction*" CD-ROM Publication, Transportation Research Board,* Washington, D.C.

92. Kuo, C.-Y. (2002). "Correlating Permanent Deformation Characteristics of Hot Mix Asphalt with Aggregate Geometric Irregularities," *ASTM, Journal of Testing and Evaluation,* Vol. 30, No. 2, pp. 136–144.

93. Kutay, M.E., Arambula, E., Gibson, N., and Youtcheff, J. (2010). "Three-dimensional Image Processing Methods to Identify and Characterize Aggregates in Compacted Asphalt Mixtures," *International Journal of Pavement Engineering,* Vol. 11, No.6, pp. 511-528.

94. Kutner, M. H., Nachtsheim, C. J., and Neter, J. (2004) "Applied Linear Regression Models" *McGraw-Hill Irwin,* Boston, MA.

95. Lacroix, A., Kim, Y.R., and Ranjithan, S.R. (2008). "Backcalcualtion of Dynamic Modulus from Resilient Modulus of Asphalt Concrete with an Artificial Neural Network," Transportation Research Record, No. 2057, *Journal of the Transportation Research Board,* Washington, D.C., pp.107-113.

96. Li, X., Clyne, T. R., and Marasteanu, M. O. (2004). "Recycled Asphalt Pavement (RAP) Effects on Binder and Mixture Quality. *Report No. MN/RC – 2005-02, Minnesota Department of Transportation, Research Services Section.*

97. Li, X., Marasteanu, M. O., Christopher W., and Clyne, T. R. (2008). "Effect of RAP (Proportion and Type) and Binder Grade on the Properties of Asphalt Mixtures," *CD-ROM Publication, Transportation Research Board,* Washington, D.C.

98. Li, X., William, R.C., Marateanu, M.O., Clyne, T.R., and Johnson, E. (2009). "Investigation of In-Place Asphalt Film Thickness and Performance of Hot-Mix Asphalt Mixtures," *ASCE, Journal of Materials in Civil Engineering,* Vol. 21, No. 6, 2009, pp. 262-270.

99. Lindman, H. R. (1974). "Analysis of variance in complex experimental designs," San Francisco: *W. H. Freeman & Co.*, p. 33.

100. Little, D.H., and Epps, J.A. (1980). "Evaluation of Certain Structural Characteristics of Recycled Pavement Materials," *Journal of the Association of Asphalt Paving Technologists,* Vol. 49, pp. 219-251.

101. Little, D.H., Holmgreen, R.J., and Epps, J.A. (1981). "Effect of Recycling Agents on the Structural Performance of Recycled Asphalt Concrete Materials," *Journal of the Association of Asphalt Paving Technologists,* Vol. 50, pp. 32-63.

102. Liu, M., Ferry, M.A., Davison, R.R., Glover, C.J., and Bullin, J.A. (1998a). "Oxygen Uptake as Correlated to Carbonyl Growth in Aged Asphalts and Asphalt Corbett Fractions," *Ind. & Eng. Chem. Res.,* 37(12), pp. 4669-4674.

103. Liu, M.M., Lin, M.S., Chaffin, J.M., Davison, R.R., Glover, C.J., and Bullin, J.A. (1998b). "Oxidation Kinetics of Asphalt Corbett Fractions and Compositional Dependence of Asphalt Oxidation," *Pet. Sci. & Tech.,* 16(7-8), p.827

104. Liu, Y., and You, Z. (2011). "Discrete-Element Modeling: Impacts of Aggregate Sphericity, Orientation, and Angularity on Creep Stiffness of Idealized Asphalt Mixtures," *ASCE, Journal of Engineering Mechanics,* Vol. 137, No.4, pp.294-303.

105. Loulizi, A., Flintsch, G., Al-Qadi, I., Mokarem, D. (2006). "Comparing Resilient Modulus and Dynamic Modulus of Hot Mix Asphalt as Material Properties for Flexible Pavement Design," Transportation Research Record, No. 1970, *Journal of the Transportation Research Board,* Washington, D.C., pp. 161-170

106. Loulizi, A., Flintsch, G.W., and McGhee, K. (2007). "Determination of in-Place Hot-Mix Asphalt Layer Modulus for Rehabilitation Projects by a Mechanistic-Empirical Procedure," Transportation Research Record, No. 2037, *Journal of the Transportation Research Board,* Washington, D.C., pp. 53-62.

107. Lynn, T., James, R.S., Wu, P.Y., and Jared, D.M. (2007). "Effect of Aggregate Degradation on Volumetric Properties of Georgia's Hot-Mix Asphalt,"

Transportation Research Record, No. 1998, *Journal of the Transportation Research Board,* Washington, D.C., pp. 123-131.

108. Maerz, N.H. (2004). "Technical and Computational Aspects of the Measurement of Aggregate Shape by Digital Image Analysis," *ASCE, Journal of Computing in Civil Engineering,* Vol. 18, No. 1, pp. 10-18.
109. Mahmoud, E., and Masad, E. (2007). "Experimental Methods for the Evaluation of Aggregate Resistance to Polishing, Abrasion, and Breakage," *ASCE, Journal of Materials in Civil Engineering,* Vol. 19, No. 11, pp.977-985.
110. Mallat, S. G. (1989). "A Theory for Multiresolution Signal Decomposition: The Wavelet Representation," I*EEE Transactions on Pattern Analysis and Machine Intelligence,* Vol. II, No. 7.
111. Masad, E., Al-Rousan, T., Bathina, M., McGahan, J., and Spiegelman, C. (2007a). "Analysis of Aggregate Shape Characteristics and Its Relationship to HMA Performance," *Road Materials and Pavement Design,* Vol. 8, No. 2, pp. 317-350.
112. Masad, E., Al-Rousan, T., Button, J., Little, D., and Tutumluer, E. (2007b). "Test methods for characterizing aggregate shape, texture and angularity," NCHRP Report No. 555, *National Cooperative Highway Research Program, National Research Council,* Washington, D.C.
113. Masad, E., Button, J., and Papagiannakis, T. (2000). "Fine Aggregate Angularity: Automated Image Analysis Approach," Transportation Research Record, No. 1721, *Journal of the Transportation Research Board,* Washington, D.C., pp. 66-72.
114. Masad, E., Little, D. N., Tashman, L., Saadeh, S., Al-Rousan, T., and Sukhwani, R. (2003). "Evaluation of Aggregate Characteristics Affecting HMA Concrete Performance," Research Report ICAR 203-1, *The Aggregate Foundation of Technology, Research, and Education,* Arlington, VA.
115. Masad, E., Niranjanan, S., Bahia, H., and Kore, S. (2001a). "Modeling and experimental measurements of localized strain distribution in asphalt mixes," *ASCE, Journal of Transportation Engineering,* Vol. 127, No. 6, pp. 477-485.
116. Masad, E., Olcott, D., White, T., and Tashman, L. (2001b). "Correlation of Fine Aggregate Imaging Shape Indices with Asphalt Mixture Performance,"

Transportation Research Record, No. 1757, *Journal of the Transportation Research Board,* Washington, D.C., pp. 148–156.

117. Masad, E.A. (2003). "The Development of a Computer Controlled Image Analysis System for Measuring Aggregate Shape Properties," National Cooperative Highway Research Program NCHRP-IDEA Project 77 Final Report, *Transportation Research Board,* Washington, D.C.
118. Masad, E.A. (2005). "Aggregate Image Measurement System (AIMS) Basics and Applications," Report No. FHWA/TX-05/5-1707-01-1. *Texas Transportation Institute,* The Texas A&M University System College Station, Texas.
119. McDaniel, R. S., Slah, A., Huber, G. A., and Gallivan, V. (2007). Investigation of Properties of Plant-Produced RAP Mixtures. CD-ROM Publication, *Transportation Research Board,* Washington, D.C.
120. McDaniel, R. S., Soleymani, H., and Shah, A. (2002). "Use of Reclaimed Asphalt (RAP) under Superpave Specifications," Final Report, a Regional Pooled Fund Project.
121. McDaniel, R. S., Soleymani, H., Anderson, R. M., Turner, P., and Peterson, R. (2000). "Incorporation of Reclaimed Asphalt Pavement in the Superpave System," *NCHRP 9-12,* Washington, D.C.
122. McDaniel,R., and Anderson, R.M.(2001). "Recommended Use of Reclaimed Asphalt Pavement in the Superpave Mix Design Method: Technician's Manual," *NCHRP Report No. 452,* Washington, D.C.
123. Medani, M., Huurman, M. (2003). "Constructing the Stiffness Master curves for Asphaltic Mixes," Report 7-01-127-3, ISSN 0169-9288, *Delft University of Technology,* Netherlands.
124. Meyers, F., Tessier, G.R., Haas, R., and Kennedy, T.W. (1983). "Study of Hot Mix Recycling of Asphalt Pavements," *Roads and Transportation Association of Canada,* Report # TP 2964 E, Ottawa, Ontario.
125. Mirza, M. W., and Witczak, M. W. (1995). "Development of a Global Aging System for Short and Long Term Aging of Asphalt Cements," *Journal of Association of Asphalt Paving Technologists,* Vol. 64, pp. 393-431.

126. Mishra, D., Tutumluer, E., and Butt, A.A. (2010). "Quantifying Effects of Particle Shape and Type and Amount of Fines on Unbound Aggregate Performance Through Controlled Gradation," Transportation Research Record, No. 2167, *Journal of the Transportation Research Board,* Washington, D.C., pp. 61-71.
127. Mohammad, L.N., Saadeh, S., Obulareddy, S., and Cooper, S. (2008). "Characterization of Louisiana Asphalt Mixtures Using Simple Performance Tests," *ASTM, Journal of Testing and Evaluation,* Vol. 36, No.1, pp.1-12
128. MTS System Corporation (2011). *URL: http://www.mts.com/ (Last accessed: July 12, 2011).*
129. NCHRP (2007). "Research Result Digest 324: Simulating the Effects of Hot Mix Asphalt Aging for Performance Testing and Pavement Structural Design," Washington, D.C.
130. NECEPT (2010). "Superpave System, Northeast Center of Excellence for Pavement Technology, Northeast Regional Superpave Center," *The Pennsylvania Transportation Institute,* Pennsylvania State University.
131. Obulareddy, S. (2006). "Fundamental Characterization of Louisiana HMA Mixtures for the 2002 Mechanistic-Empirical Design Guide," Master's Thesis, Louisiana State University.
132. Oklahoma Department of Transportation (ODOT) (2011). "Construction Engineering Standard, Specifications, Materials and Testing," *Online access: http://www.okladot.state.ok.us/cnstrctengr.htm (last accessed: June 30, 2011)*
133. Page, G. C., and Murphy, K. H. (1987). "Hot-Mix Recycling Saves Florida DOT $38 Million," *Asphalt,* Vol. 1, No.1, 1987.
134. Page, G. C., Musselman, J. A., and Romano, D. C. (1997). "Effects of Aggregate Degradation on Air Voids of Structural Asphalt Mixture in Florida," Transportation Research Record, No. 1583, *Journal of the Transportation Research Board,* Washington, D.C., pp. 19–27.
135. Pan, T., Tutumluer, E., and Carpenter, S.H. (2006). "Effect of Coarse Aggregate Morphology on Permanent Deformation Behavior of Hot Mix Asphalt," *ASCE, Journal of Transportation Engineering,* Vol. 132, No. 7, pp. 580-589.

136. Papagiannakis, A.T., Abbas, A., and Masad, E. (2002). "Micromechanical analysis of viscoelastic properties of asphalt concretes," Transportation Research Record, No. 1789, *Journal of the Transportation Research Board,* Washington, D.C., pp.113-120.

137. Pellinen, T.K., and Witczak, M.W. (2002). "Use of Stiffness of Hot-Mix Asphalt as a Simple Performance Test," Transportation Research Record, No. 1789, *Journal of the Transportation Research Board,* Washington, D.C., pp. 80-90.

138. Peterson, R.L, Mahboub, K.C., Anderson, R.M., Masad, E., and Tashman, L. (2003). "Superpave® Laboratory Compaction Versus Field Compaction," Transportation Research Record, No. 1832, *Journal of the Transportation Research Board,* Washington, D.C., pp.201-208.

139. Pintner, R. M., Vinson, T.S., and Johnson, E.G. (1987). "Nature of fines produced In aggregate processing," *ASCE, Journal of Cold Regions Engineering,* vol. 1, No. 1, pp. 10-21

140. PROPHET StatGuide (2011) "Do your data violate one-way ANOVA assumptions?," *Online access:*

141. Prowell, B.D. and Weingart, R. (1999). "Precisions of Flat and Elongated Particles Tests: ASTM D4791 and CDG-40 Videograder," Transportation Research Record, No. 1673, *Journal of the Transportation Research Board,* Washington, D.C., pp.73-80.

142. Prowell, B.D., Zhang, J., and Brown, E.R. (2005). "Aggregates Properties and the Performance of Superpave-Designated Hot Mix Asphalt," *NCHRP Report 539: Transportation Research Board,* Washington, D.C.

143. Ramsey, F., and Schafer, D. (2002). "The Statistical Sleuth- A Course in Methods of Data Analysis," *Pacific Grove,* CA: Daxbury.

144. Rao, C., Tutumluer, E., and Kim, I. T. (2002). "Quantification of Coarse Aggregate Angularity Based on Image Analysis," Transportation Research Record, No. 1787, *Journal of the Transportation Research Board,* Washington, D.C., pp. 117-124.

145. Roberts, F.L., Kandhal, P.S., Brown, E.R., Lee, D., and Kennedy, T.W. (1996). "Hot Mix Asphalt Materials, Mixture Design and Construction," 2nd Edition, *NAPA Education Foundation,* Lanham, Maryland.

146. Schwartz, C. (2005). "Evaluation of the Witczak Dynamic Modulus Prediction Model," *CD-ROM Publication, Transportation Research Board,* Washington, D.C.

147. Schwartz, C. W., Gibson, N., and Schapery, R. A. (2002). "Time–Temperature Superposition for Asphalt Concrete at Large Compressive Strains," Transportation Research Record No. 1789, *Journal of the Transportation Research Board,* Washington, D.C., pp. 101-112.

148. Shenoy, A., and Romero, P. (2002). "Standardized procedure for analysis of dynamic modulus (E*) data to predict asphalt pavement distresses," Transportation Research Record, No. 1789, *Journal of the Transportation Research Board,* Washington, D.C., pp. 173-182.

149. Singh, D.V., Zaman, M., and Commuri, S. (2011a). "Effects of Production and Sample Preparation Methods on Aggregate Shape Parameters," *International Journal of Pavement Engineering, (Accepted for Publication).*

150. Singh, D.V., Zaman, M., and Commuri, S. (2011b). "Comparison of Shape Parameters for Different Types and Sizes of Coarse Aggregates for Pavement Applications," ASTM, *Journal of Testing and Evaluation (Submitted October 2011: Under Review).*

151. Singh, D.V., Zaman, M., and Commuri, S. (2011c). "Evaluation of Dynamic Modulus (|E*|) for Modified and Unmodified Asphalt Mixes on Different Input Levels of the MEPDG," *International Journal of Pavement Research and Technology, (Accepted for Publication).*

152. Singh, D.V., Zaman, M., and Commuri, S. (2011d). "Evaluation of Predictive Models for Estimating Dynamic Modulus of HMA Mixes Used in Oklahoma," *Journal of Transportation Research Record, Washington, D.C. (Accepted for Publication).*

153. Singh, D.V., Zaman, M., and Commuri, S. (2011e). "Inclusion of Aggregate Angularity, Texture, and Form in Estimating Dynamic Modulus of Asphalt

Mixes," *International Journal of Road Materials and Pavement Design (Accepted for Publication).*

154. Singh, D.V., Zaman, M., and Commuri, S. (2011f) "Artificial Neural Network Modeling of Dynamic Modulus Using Aggregate Shape Properties," *ASCE, Journal of Materials in Civil Engineering (Submitted October 2011: Under Review*).
155. Singh, D.V., Zaman, M., and Commuri, S. (2011g). "Investigation on Effect of Long-Term Oven Aging on RAP Mixes Using Dynamic Modulus Test," *International Journal of Pavement Research and Technology* (*Accepted for Publication*).
156. Singh, D.V., Mai, A.T., Beainy, A.F., Commuri, S., and Zaman, M.M. (2011h). "In-situ Assessment of Stiffness during the Construction of HMA Pavements," *International Journal of Pavement Research and Technology,* Vol.4, Issue: 3, pp. 131-139.
157. Singh, D.V., Zaman, M., and Commuri, S. (2011i). "Evaluation of Measured and Estimated Dynamic Moduli for Selected Asphalt Mixes," *Journal of ASTM International (JAI) Vol.8. No.9, 19 pages.*
158. Singh, D.V., Zaman, M., and White, L. (2011j) "Neural Network Modeling of 85th Percentile Speed for Two-Lane Rural Highways," *Journal of Transportation Research Board (Submitted July 2011: Under Review).*
159. Singh, D.V., Zaman, M., and White, L. (2011k). "Modeling of 85th Percentile Speed for Rural Highways For Enhanced Traffic Safety" Oklahoma Department of Transportation, Final Report - FHWA-OK-11-07, Oklahoma.
160. Sousa J.B., Craus J., and Monismith, C.L. (1991). "Summary Report on Permanent Deformation in Asphalt Concrete," *Strategic Highways Research Program IR-91-104.*
161. Statsoft (2011). "Electronics Statistics Textbook" *http://www.statsoft.com/textbook/anova manova/?button=1 (last accessed: April 12, 2011).*
162. Tarefder, R.A. (2003) "Laboratory and Model Prediction of Rutting in Asphalt Concrete," Ph.D. Dissertation, University of Oklahoma, Norman, OK.

163. Tarefder, R.A., White, L., and Zaman, M. (2005a). "Development and Application of a Rut Prediction Model for Flexible Pavements," Transportation Research Record, No. 1936, *Journal of the Transportation Research Board,* Washington, D.C., pp. 201-209.

164. Tarefder, R.A., White, L., and Zaman, M. (2005b). "Neural Network Model for Asphalt Concrete Permeability." *ASCE, Journal of Materials in Civil Engineering,* Vol. 17, No.1, pp.19-27.

165. Tran, N.H., and Hall, K.D. (2005). "Evaluating the Predictive Equation in Determining Dynamic Moduli of Typical Asphalt Mixtures Used in Arkansas," *Journal of the Association of Asphalt Paving Technologists,* Vol. 74, pp. 1-17.

166. Tran, N.H., and Hall, K.D. (2006). "An Examination of strain levels used in the dynamic modulus testing," *Journal of Association of Asphalt Paving Technologist,* Vol. 75, pp. 321-343.

167. Uddin, M., Mahboub, K.C., and Goodrum, P.M. (2011). "Effects of Nonnormal Distribution on Highway Construction Acceptance Pay Factor Calculation," *ASCE, Journal of Construction Engineering and Management,* Vol. 137, No.2, pp. 108-118.

168. Vavrik, W., Fries, R., and Carpenter, S.H. (1999). "Effect of Flat and Elongated Coarse Aggregate on Characteristics of Gyratory Compacted Samples," Transportation Research Record, No. 1681, *Journal of the Transportation Research Board,* Washington, D.C., pp.28-36.

169. Wang, L., Lane, D.S., Lu, Y., and Druta, C. (2008). "Portable Image Analysis System for Characterizing Aggregate Morphology," *Report No. FHWA/VTRC 08-CR11,* Virginia Transportation Research Council.

170. Wang, L., Lane, D.S., Lu, Y., and Druta, C. (2009). "Portable Image Analysis System for Characterizing Aggregate Morphology," Transportation Research Record, No. 2104, *Journal of the Transportation Research Board,* Washington, D.C., pp. 3-11.

171. Witczak, M. (2005). "Simple Performance Tests: Summary of Recommended Methods and Database," *NCHRP Report No. 547, Transportation Research Board,* Washington, D.C.

172. Witczak, M. W., Kaloush, K., Pellinen, T., El-Basyouny, M., and Von- Quintus, H. (2002a). "Simple Performance Test for Superpave Mix Design," *NCHRP Report 465: Transportation Research Board,* Washington, D.C.

173. Witczak, M., Kaloush, K., and Von Quintus, H. (2002b). "Pursuit of the Simple Performance test for asphalt mixture rutting," *Journal of the Association of Asphalt Paving Technologies,* Vol. 71, pp. 671-691.

174. Woo W.J., Chowdhury, A., and Glover, C.J. (2008). "Field Aging of Unmodified Asphalt Binder in Three Texas Long-Term Performance Pavements," Transportation Research Record, No. 2051, *Journal of the Transportation Research Board,* Washington, D.C., pp. 15-22.

175. Wu, Y., Parker, F., and Kandhal, P. (1998). "Aggregate toughness/ abrasion resistance and durability/soundness tests related to asphalt concrete performance in pavements," Transportation Research Record, No. 1638, *Journal of the Transportation Research Board,* Washington, D.C., pp. 85–93.

176. Xiao, F., Amirkhanian, S., and Juang, C. H. M. (2007). "Rutting Resistance of Rubberized Asphalt Concrete Pavements Containing Reclaimed Asphalt Pavement Mixtures," *ASCE, Journal of Materials in Civil Engineering,* Vol. 19, No. 6, pp.475-483.

177. Xiao, F., and Amirkhanian, S.N. (2009). "Artificial Neural Network Approach to Estimating Stiffness Behavior of Rubberized Asphalt Concrete Containing Reclaimed Asphalt Pavement," *ASCE, Journal of Transportation Engineering,* Vol. 135, No.8, pp. 580-589.

178. Xiao, F., Putman, B.J., and Amirkhanian, S.N. (2010). "Viscosity Prediction of CRM Binders Using Artificial Neural Network Approach," *International Journal of Pavement Engineering,* iFirst article, pp. 1-11.

179. You, Z., Adhikari, S., and Dai, Q. (2008). "Three Dimensional Discrete Element Models for Asphalt Mixtures," *ASCE, Journal of Engineering Mechanics,* Vol. 134, No. 12, pp. 1053-1063.

180. You, Z., Adhikari, S., and Kutay, M.E. (2008). "Dynamic modulus simulation of the asphalt concrete using the X-ray computed tomography images," *Material and structures,* Vol., 59, No.3, pp.427-452.

181. You, Z., and Buttlar, W.G. (2006). "Micromechanical modeling approach to predict compressive dynamic moduli of asphalt mixtures using the distinct element method," Transportation Research Record, No. 1970, *Journal of the Transportation Research Board,* Washington, D.C., pp. 73-83.
182. Zaman, M., Solanki, P., Ebrahimi, A., and White, L. (2010). "Neural Network Modeling of Resilient Modulus Using Routine Subgrade Soil Properties," *ASCE, International Journal of Geomechanics,* Vol. 10, No.1, pp. 1-12.
183. Zeghal, M., Adam, Y.E., Ali, O., and Mohamed, E.H. (2005). "Review of the New Mechanistic-Empirical Pavement Design Guide-A Material Characterization Perspective," *Annual Conference of the Transportation Association of Canada,* Calgary, Alberta.
184. Zeghal, M., and Mohamed, E.H. (2008). "Assessment of analytical tools used to estimate the stiffness of asphalt concrete," *Canadian Journal of Civil Engineering,* Vol.35, pp. 268-275.
185. Zhu, H., Sun, L., Yang, J., Chen, Z., Gu, W. (2011). "Developing Master Curves and Predicting Dynamic Modulus of Polymer-Modified Asphalt Mixtures," *ASCE, Journal of Materials in Civil Engineering,* pp. 131-137.

APPENDIX-A: Plots for Master Curves and Shift Factors

MIX-1 (S3 64-22)

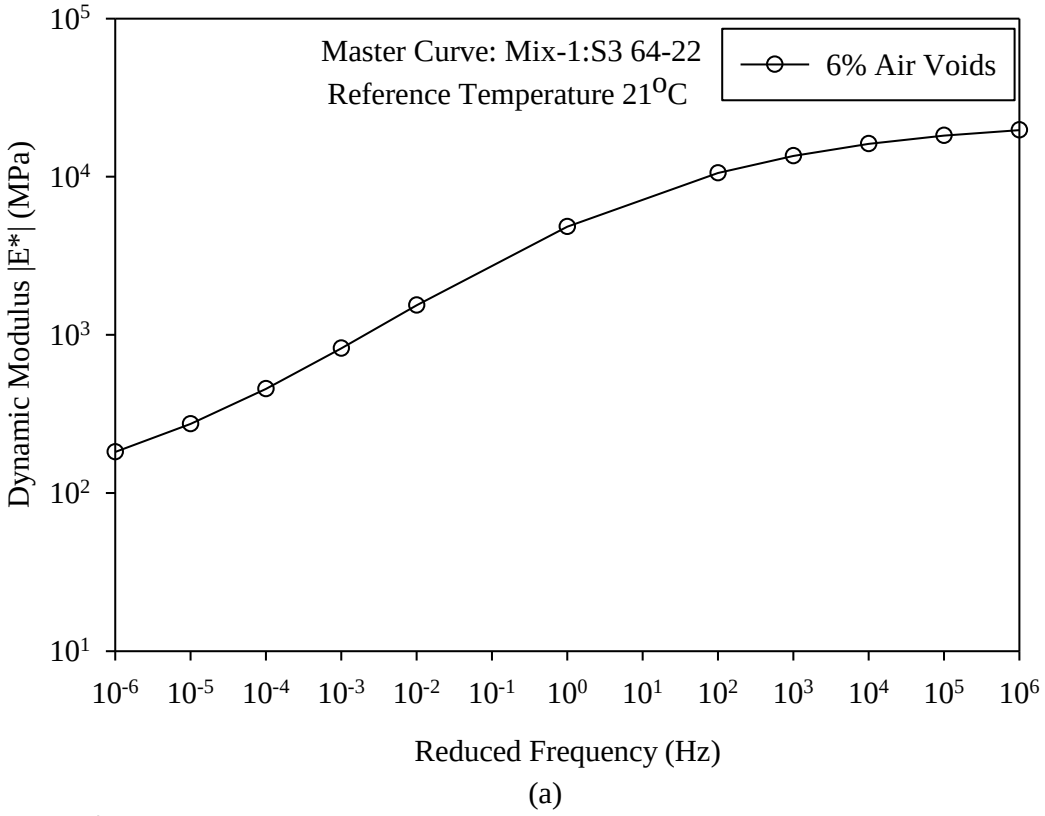

(a)

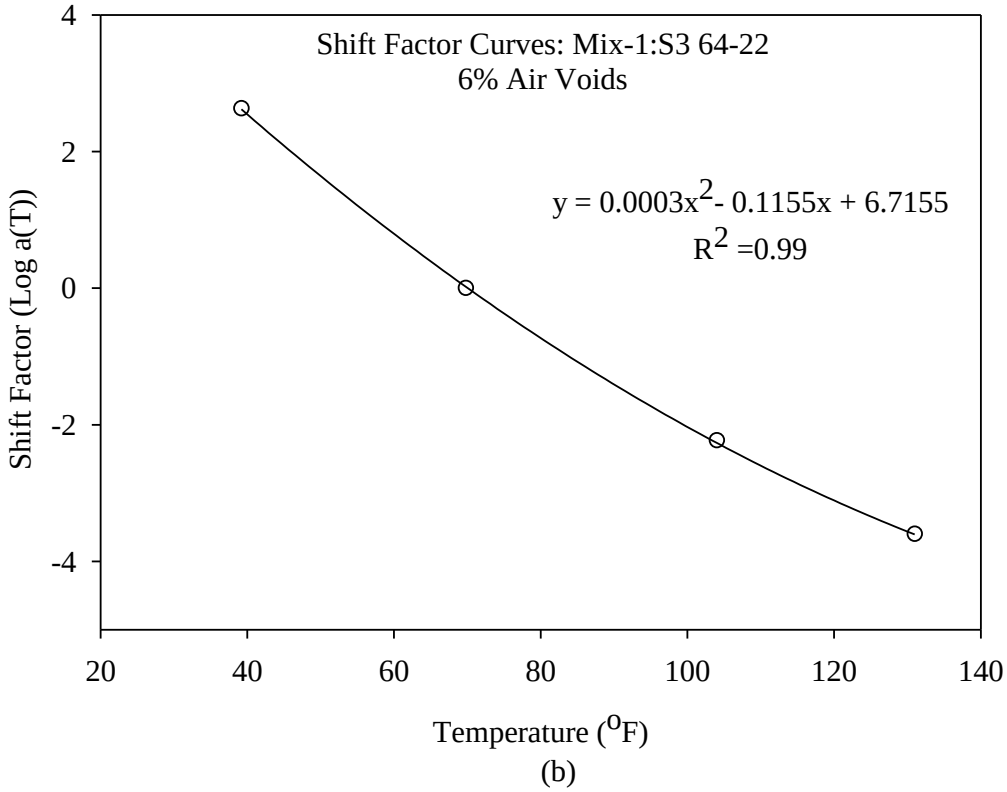

(b)

Figure A-1 (a) Master Curve (b) Shift Factor for Mix-1 at 6% Air Voids

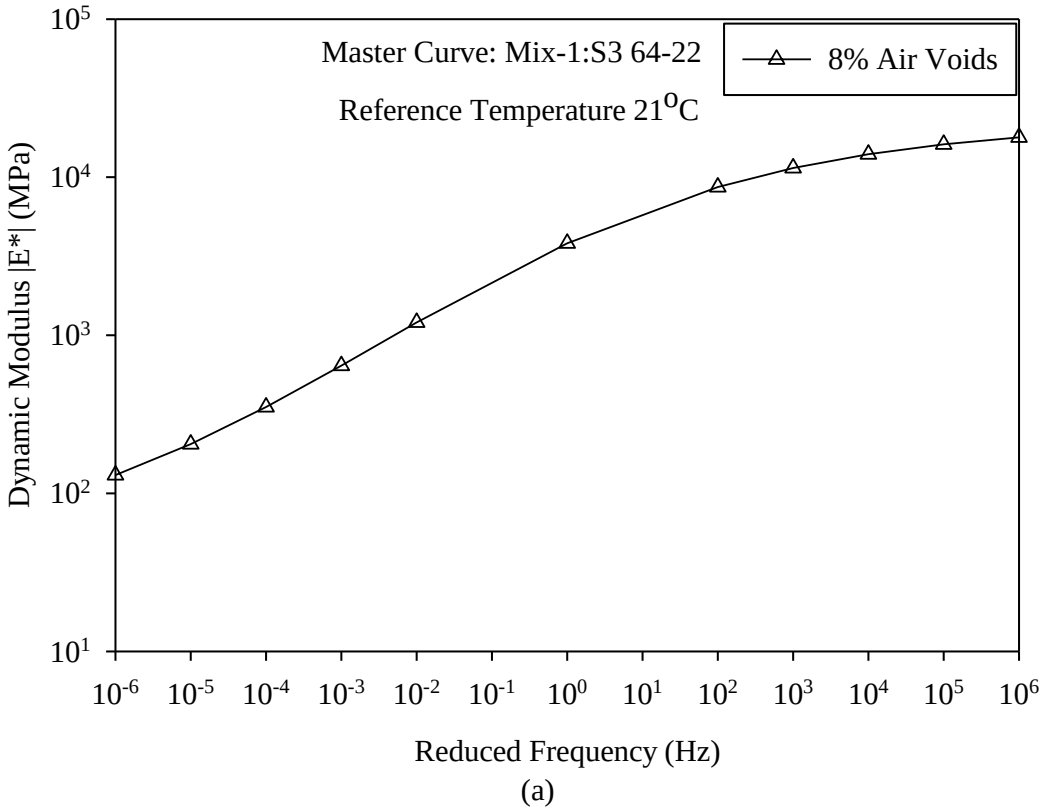

(a)

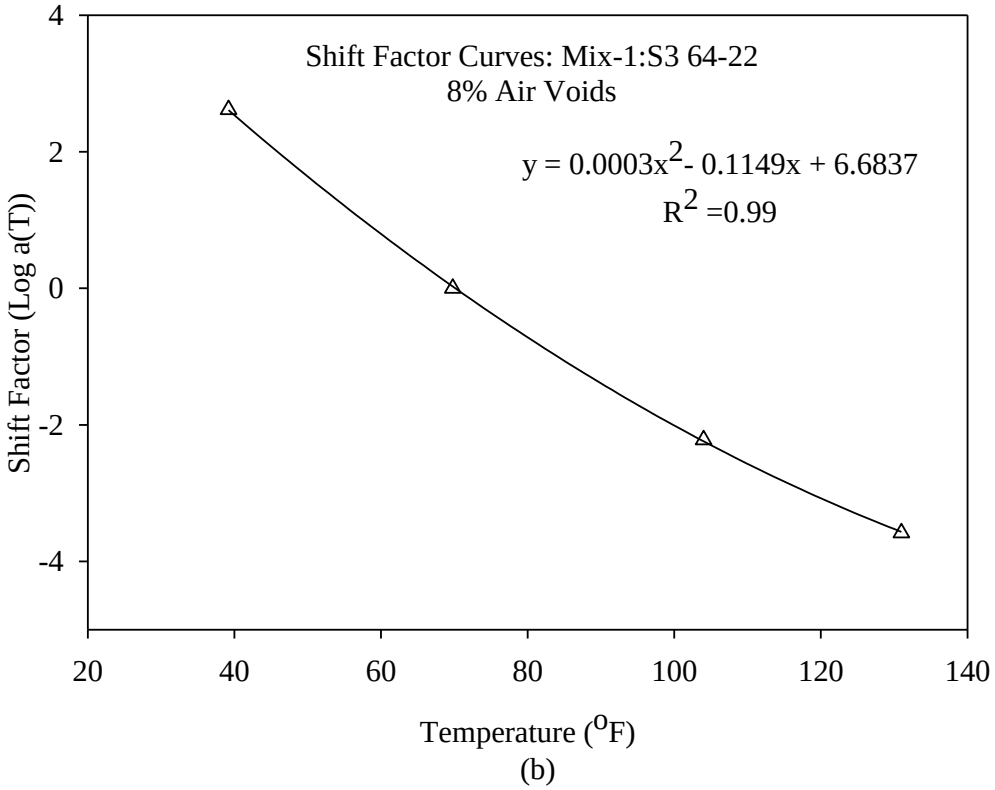

(b)

Figure A-2 (a) Master Curve (b) Shift Factor for Mix-1 at 8% Air Voids

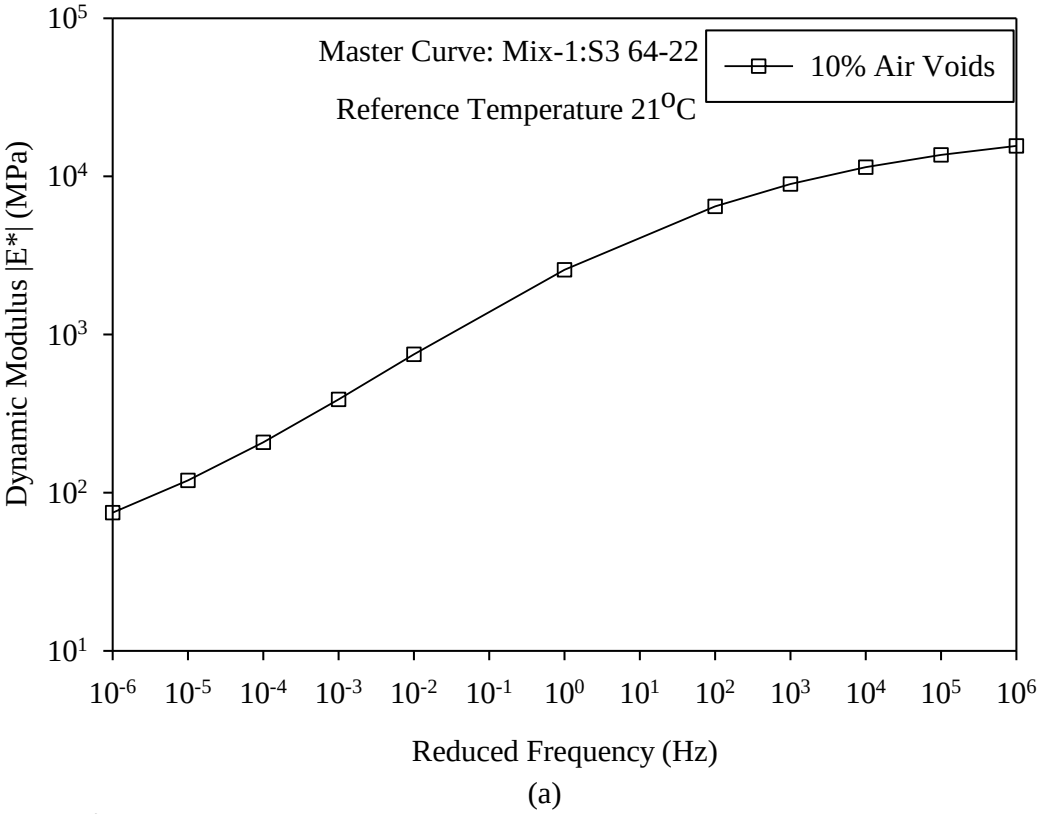

(a)

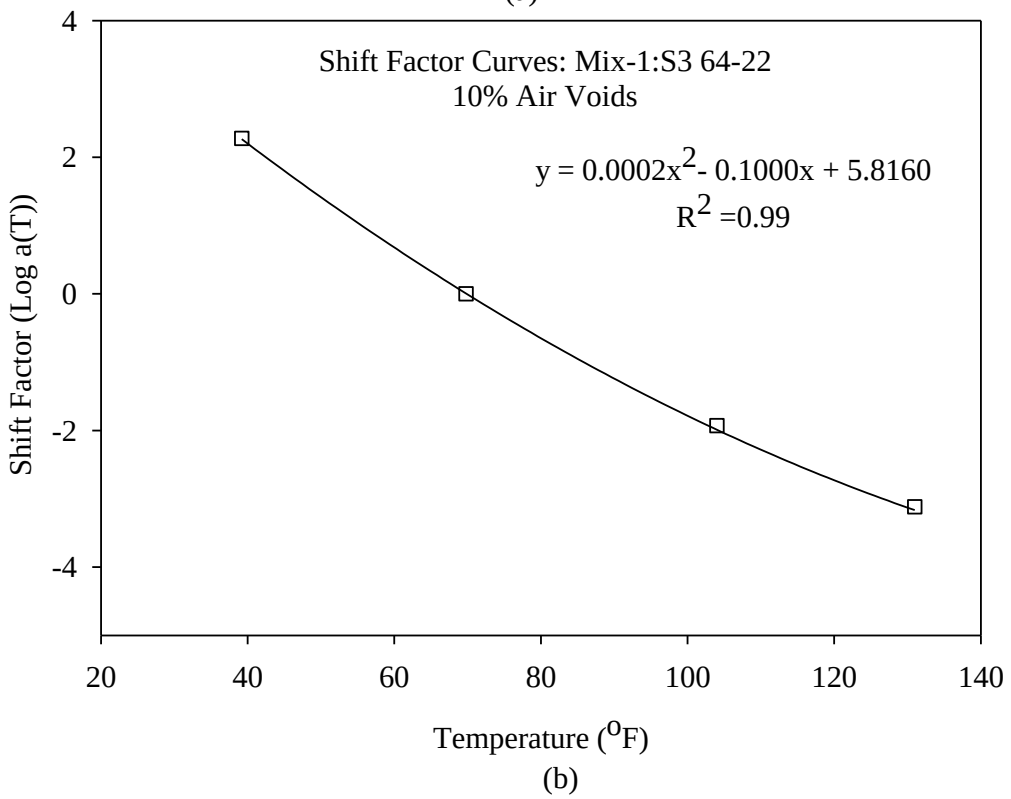

(b)

Figure A-3 (a) Master Curve (b) Shift Factor for Mix-1 at 10% Air Voids

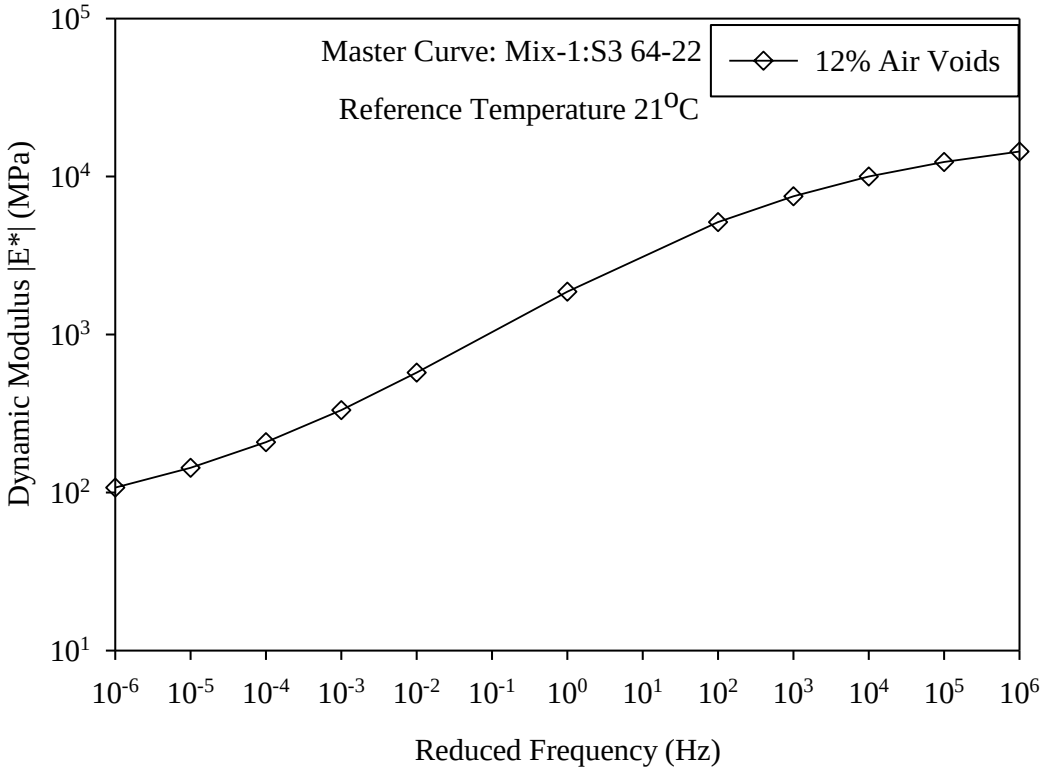

(a)

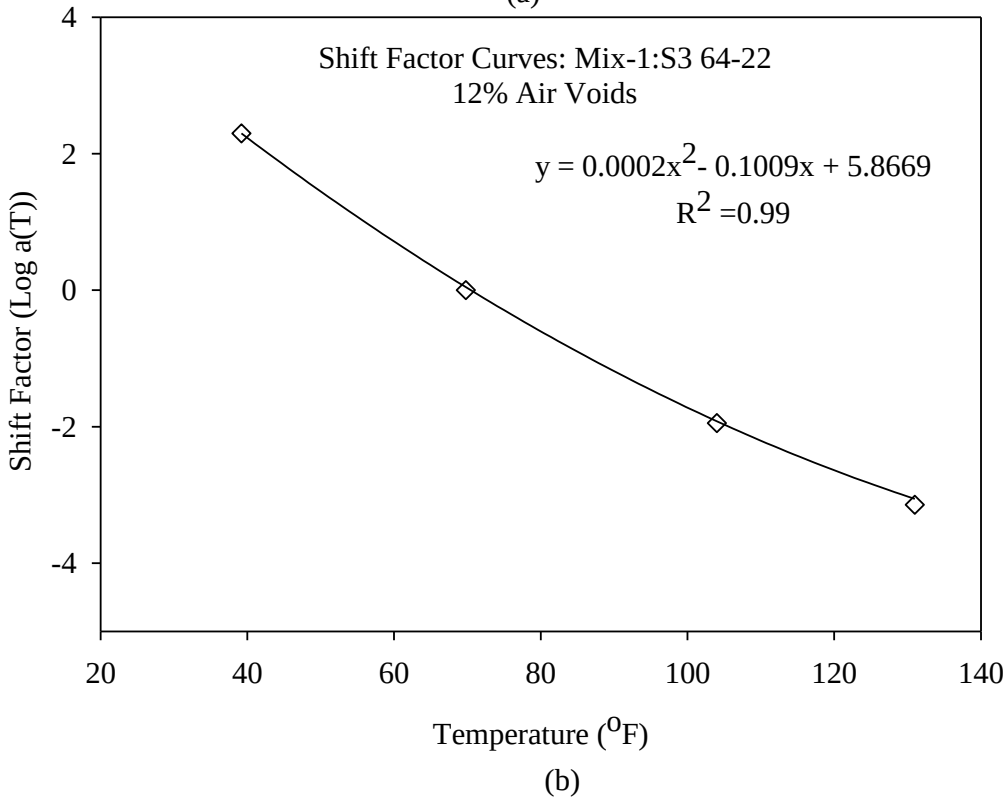

(b)

Figure A-4 (a) Master Curve (b) Shift Factor for Mix-1 at 12% Air Voids

MIX-2 (S3 76-28)

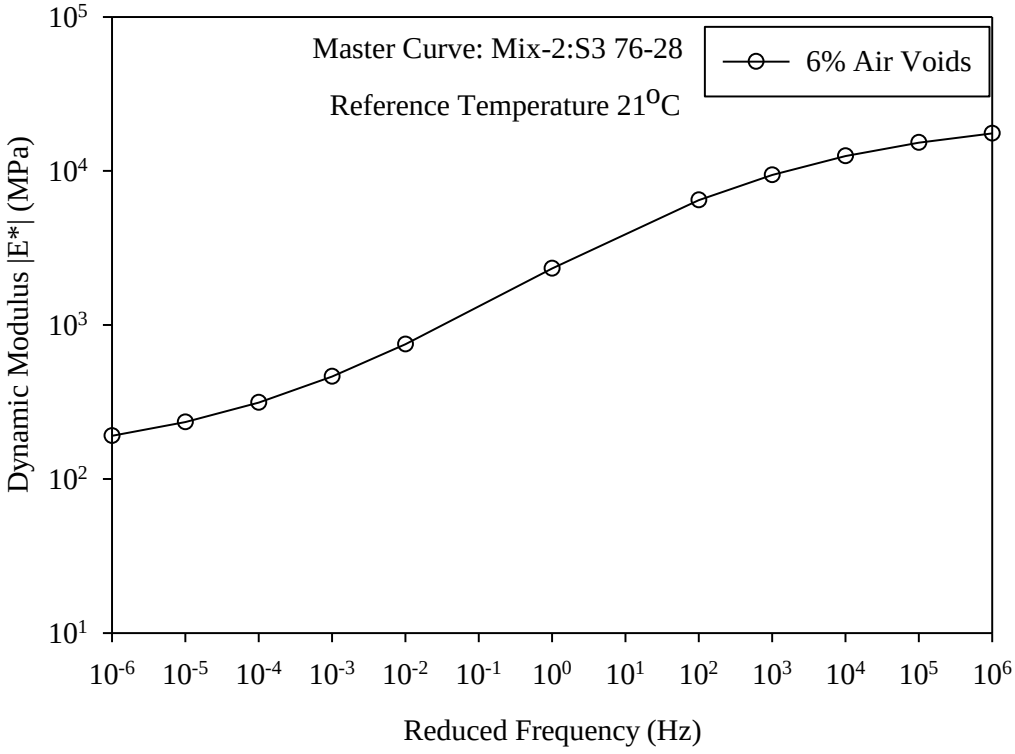

(a)

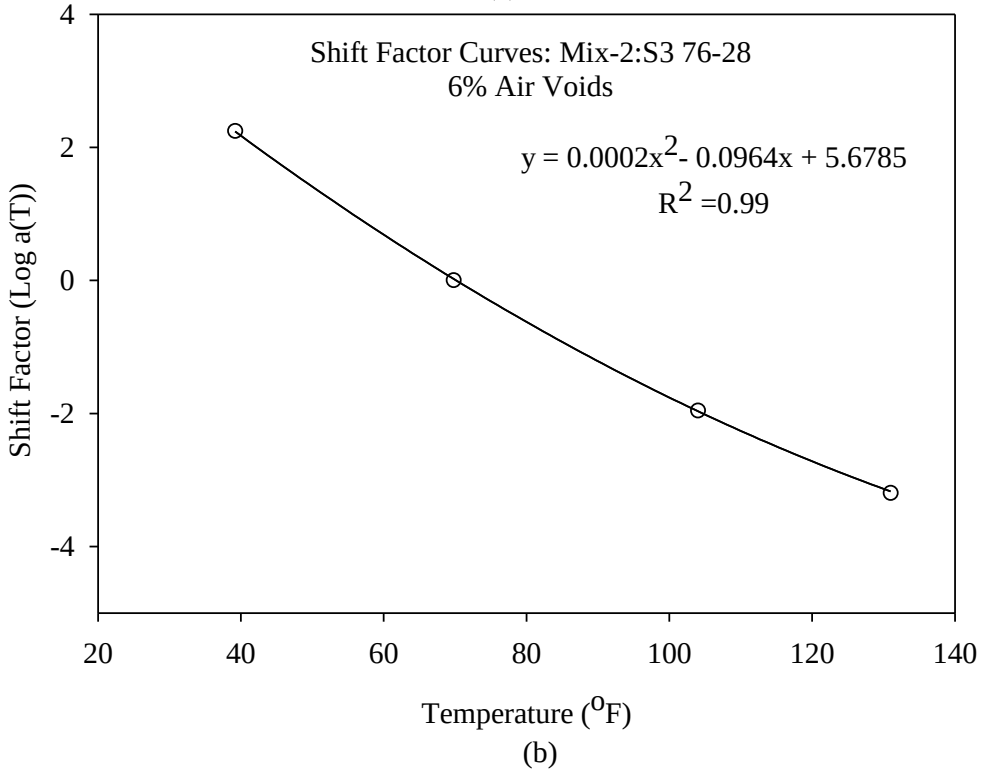

(b)

Figure A-5 (a) Master Curve (b) Shift Factor for Mix-2 at 6% Air Voids

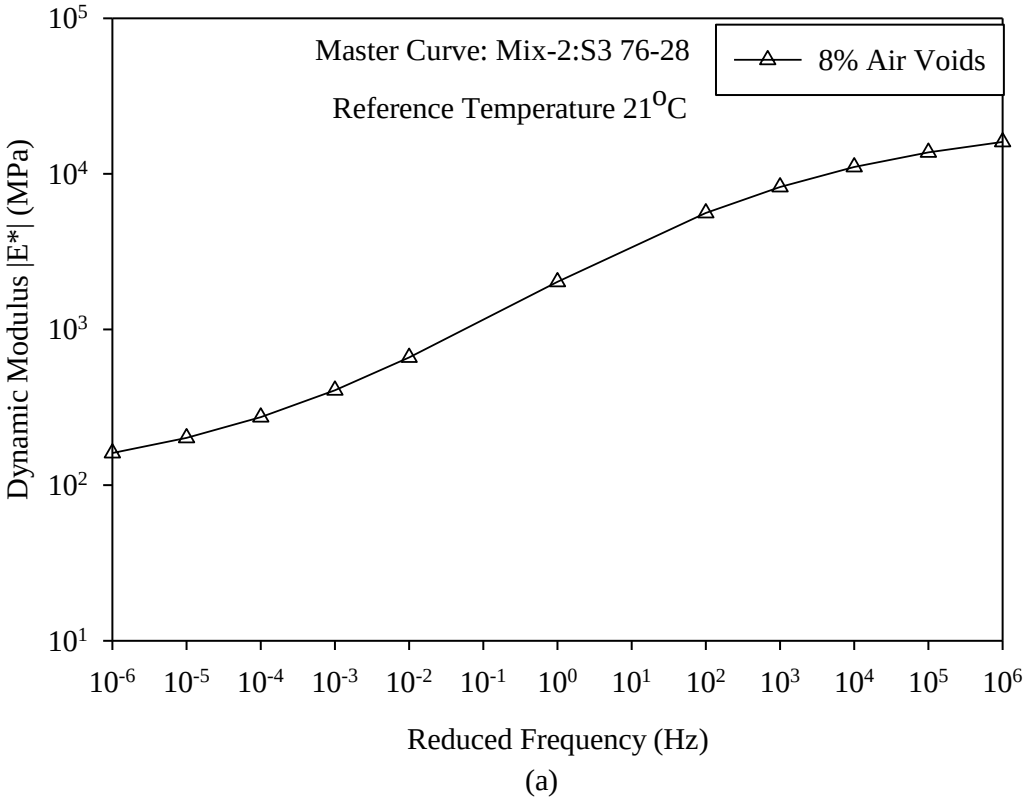

(a)

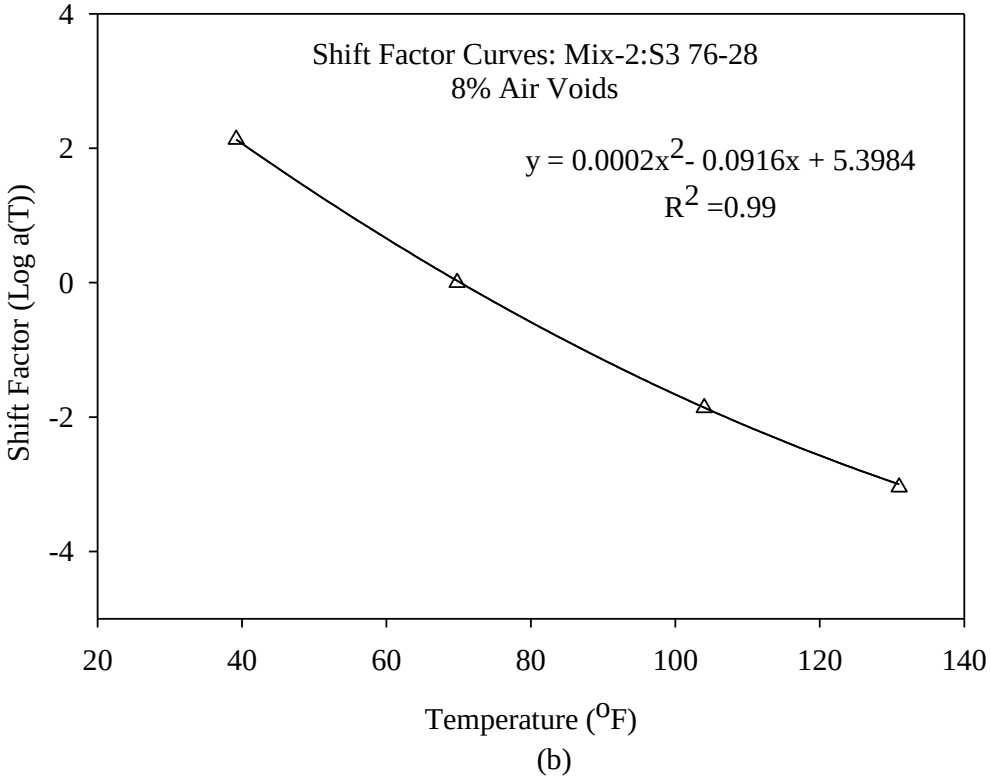

(b)

Figure A-6 (a) Master Curve (b) Shift Factor for Mix-2 at 8% Air Voids

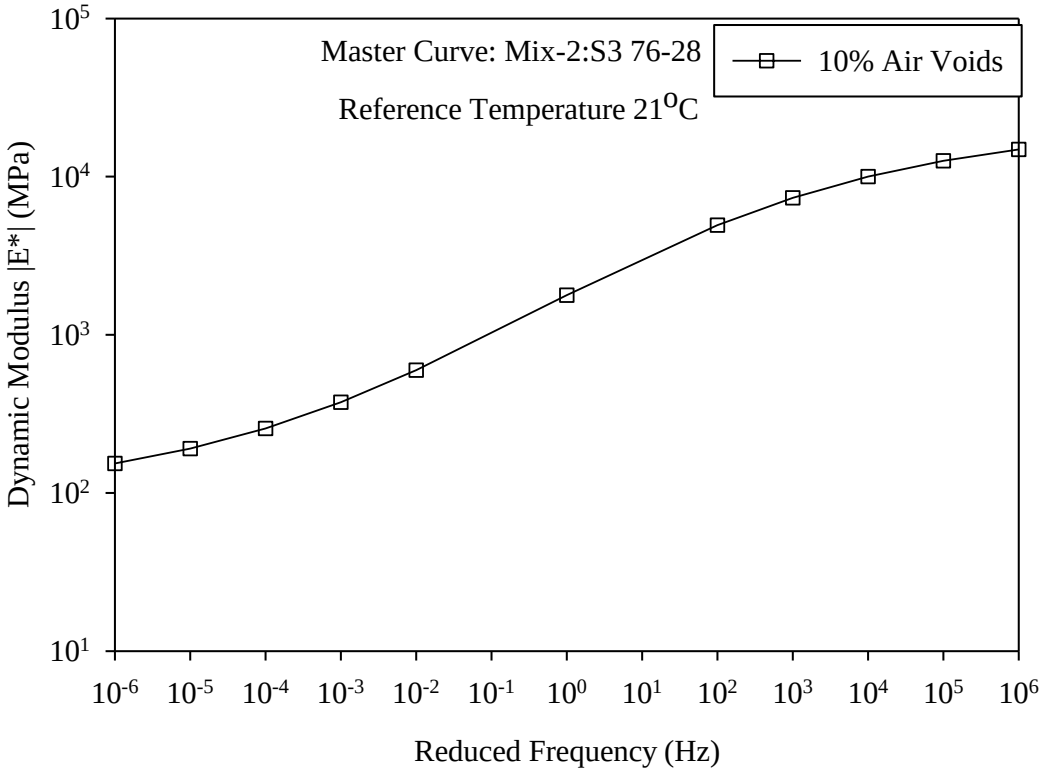

(a)

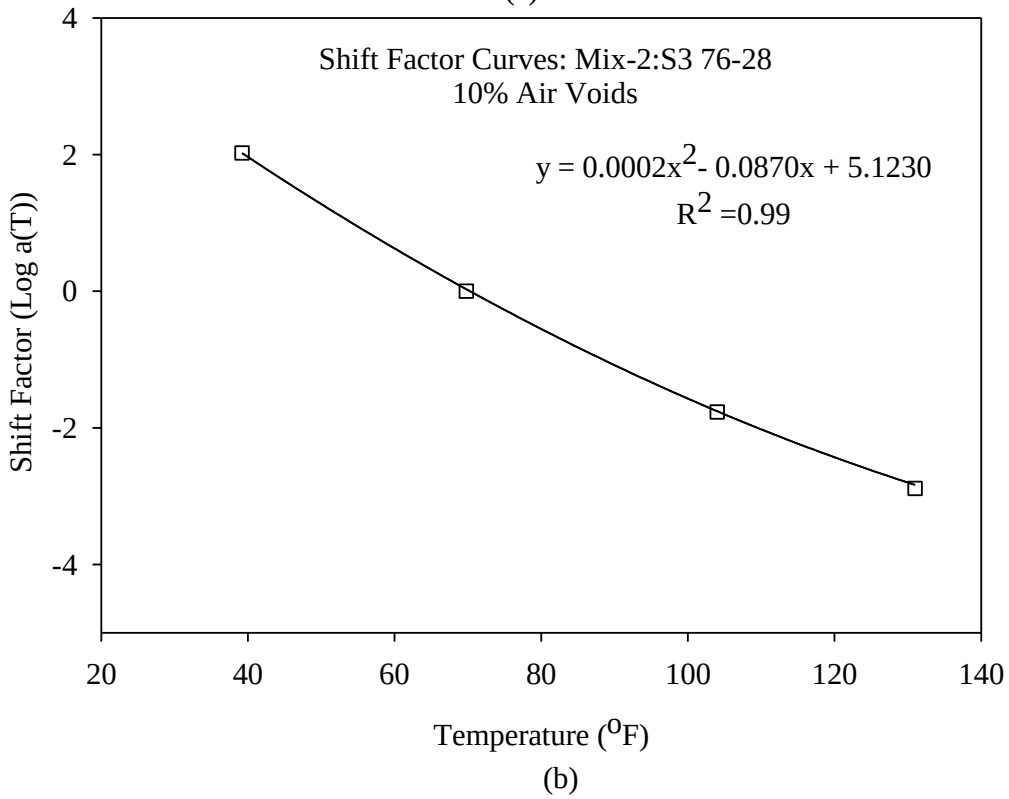

(b)

Figure A-7 (a) Master Curve (b) Shift Factor for Mix-2 at 10% Air Voids

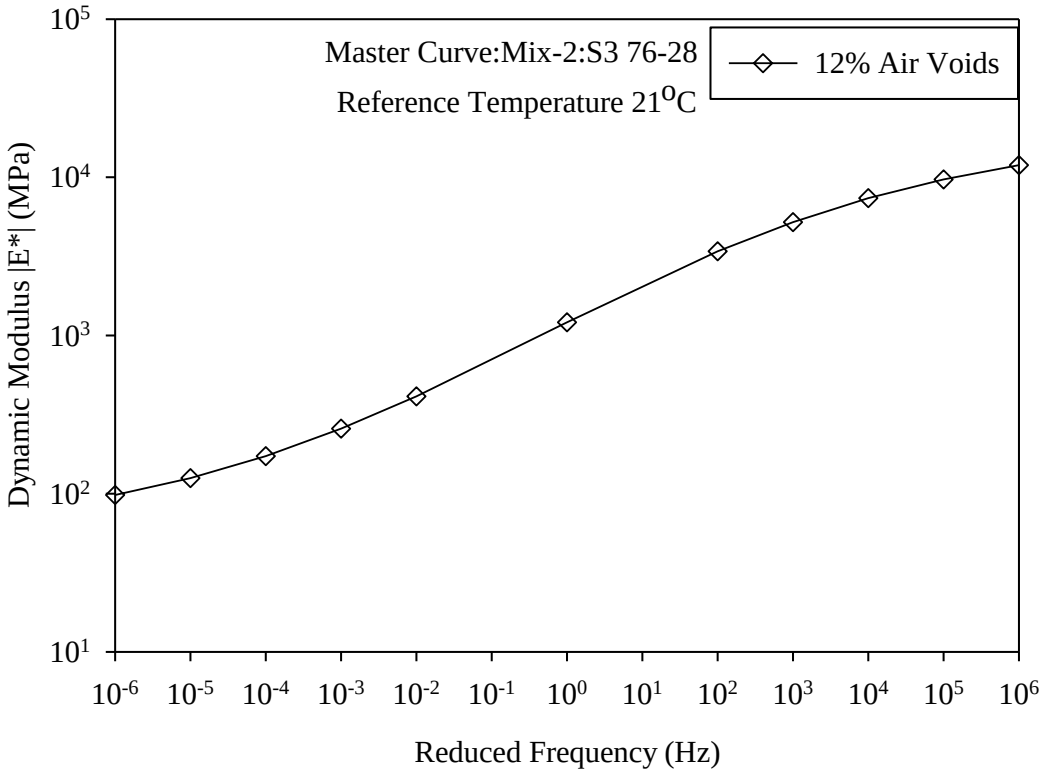

(a)

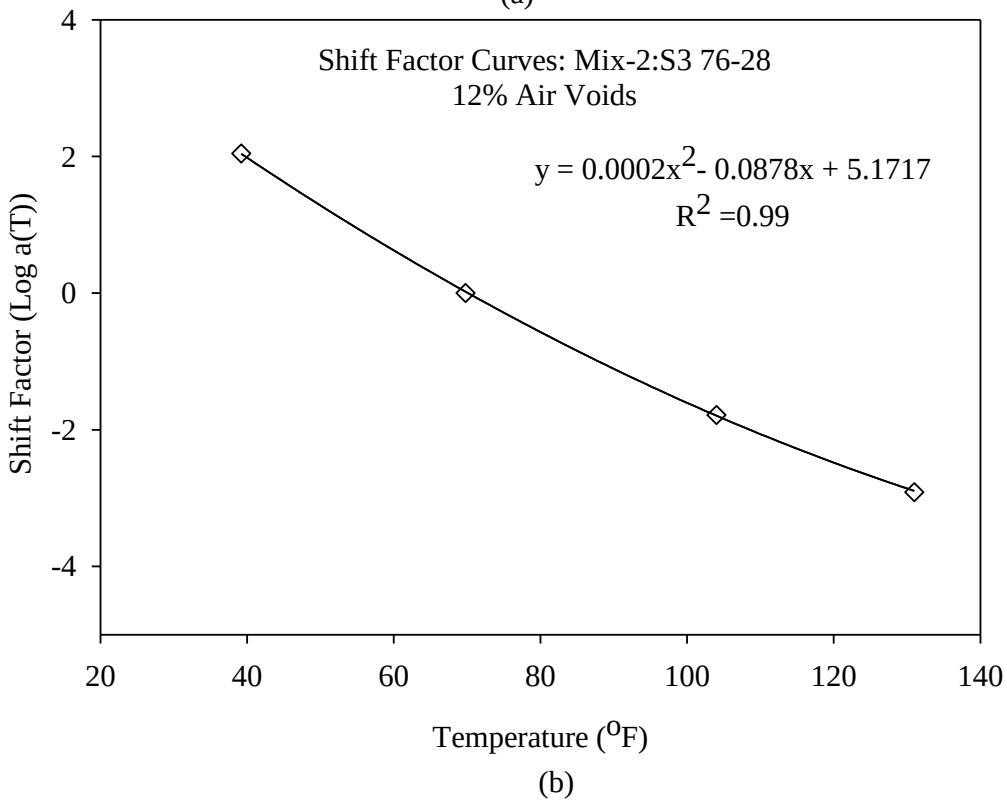

(b)

Figure A-8 (a) Master Curve (b) Shift Factor for Mix-2 at 12% Air Voids

MIX-3 (S4 70-28)

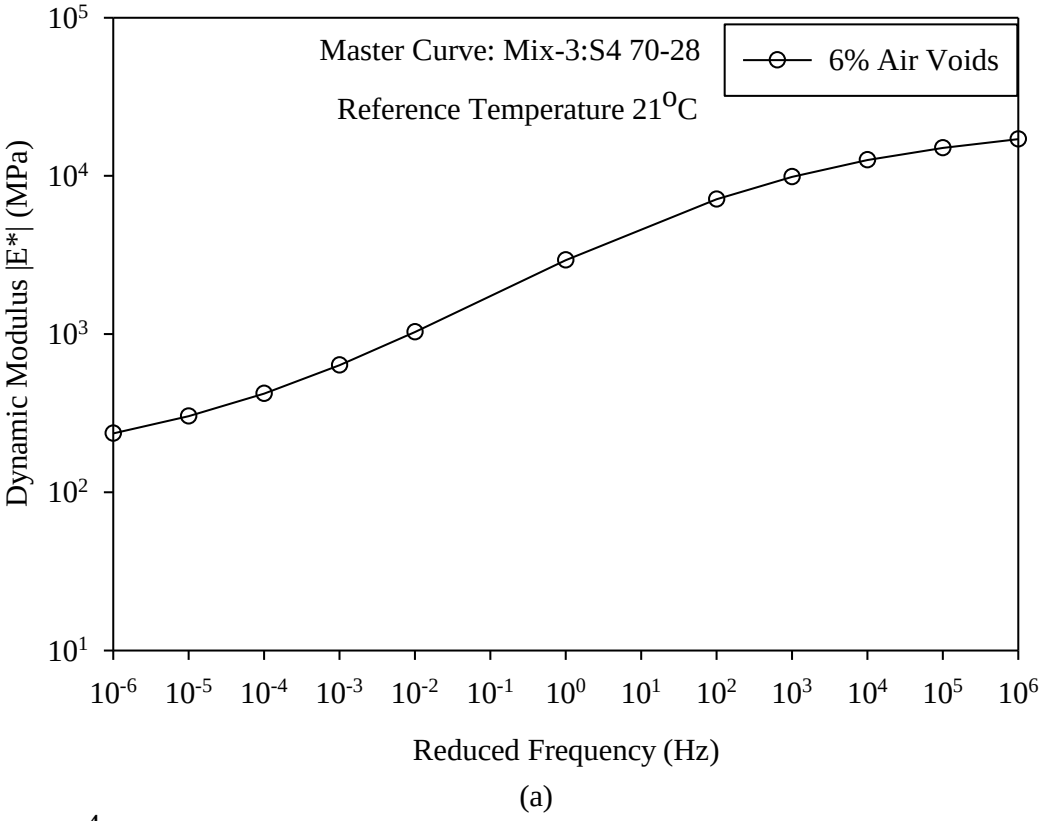

(a)

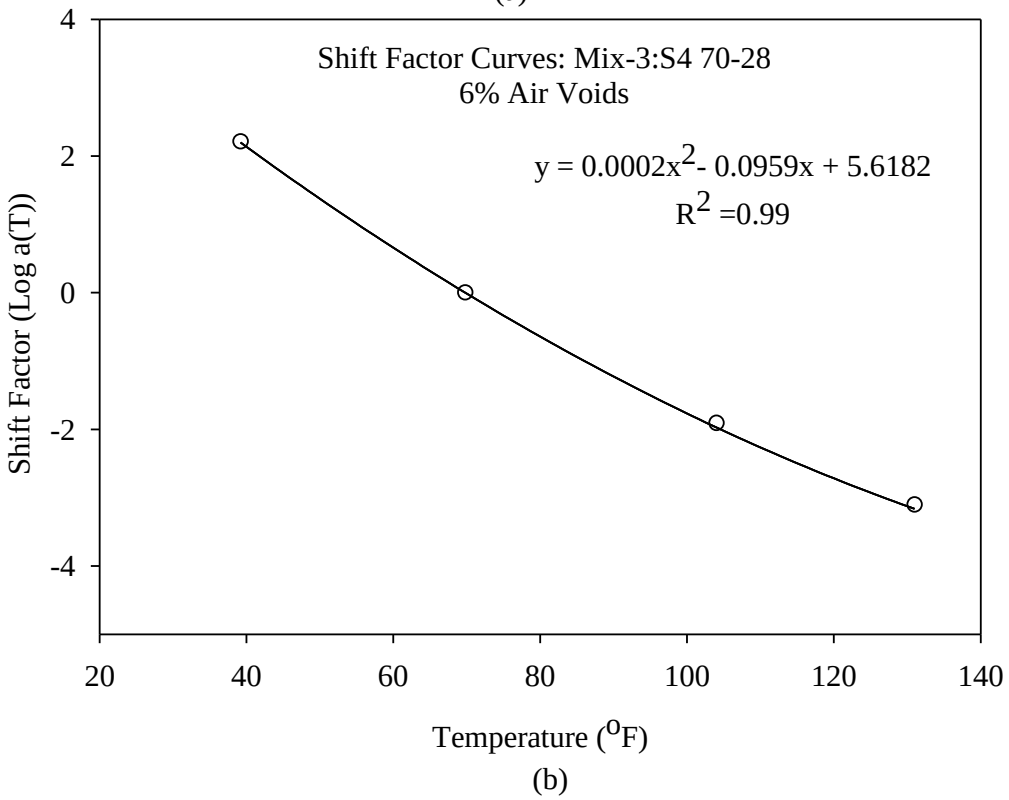

(b)

Figure A-9 (a) Master Curve (b) Shift Factor for Mix-3 at 6% Air Voids

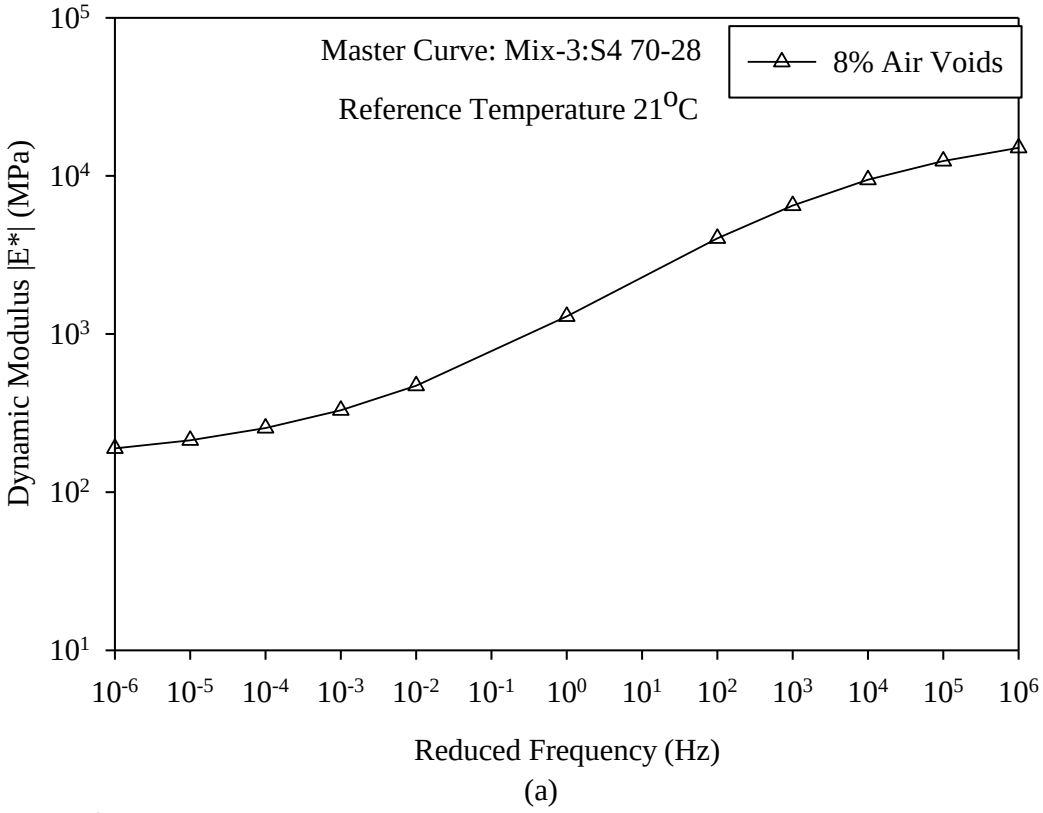

(a)

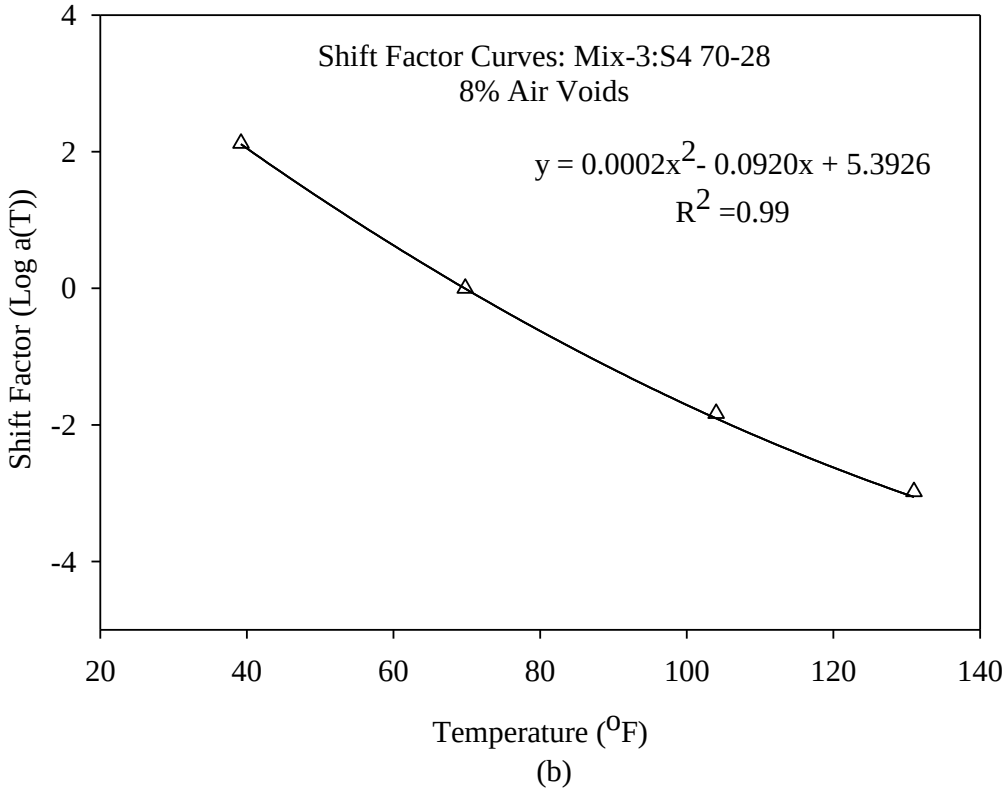

(b)

Figure A-10 (a) Master Curve (b) Shift Factor for Mix-3 at 8% Air Voids

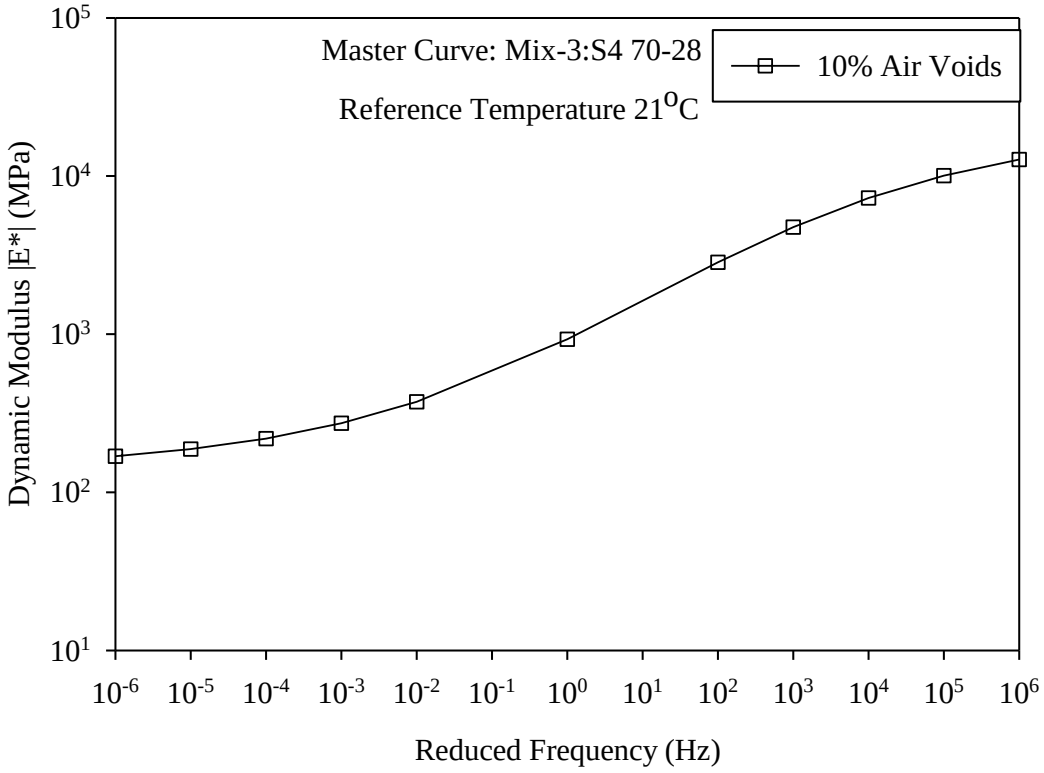

(a)

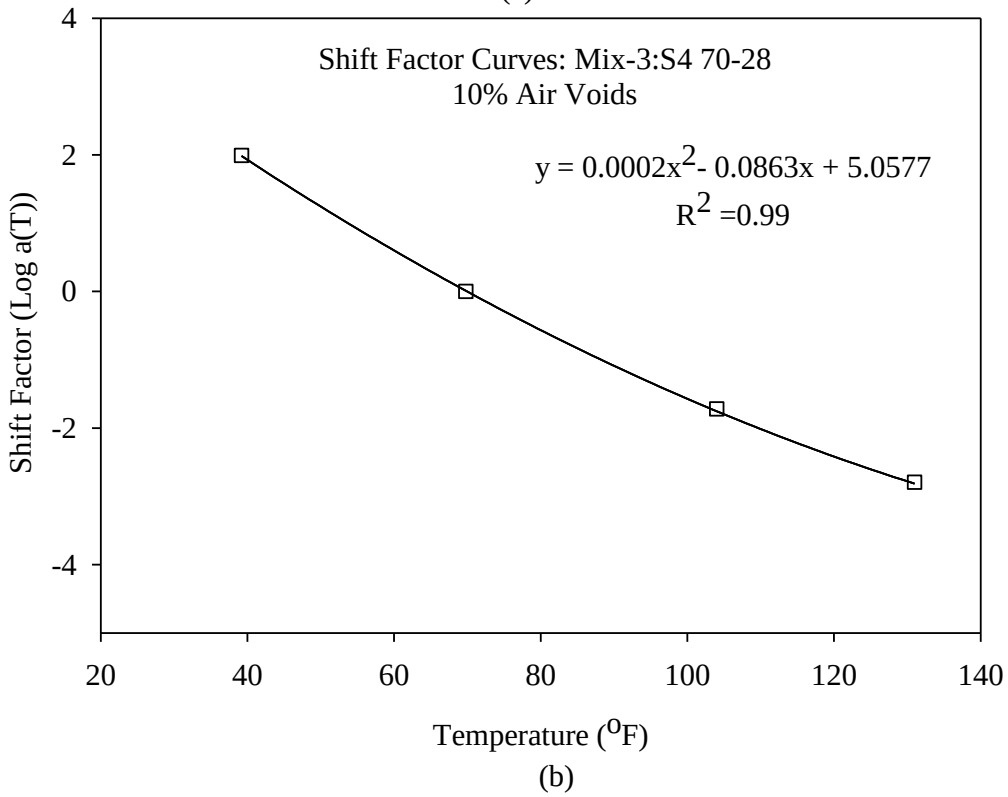

(b)

Figure A-11 (a) Master Curve (b) Shift Factor for Mix-3 at 10% Air Voids

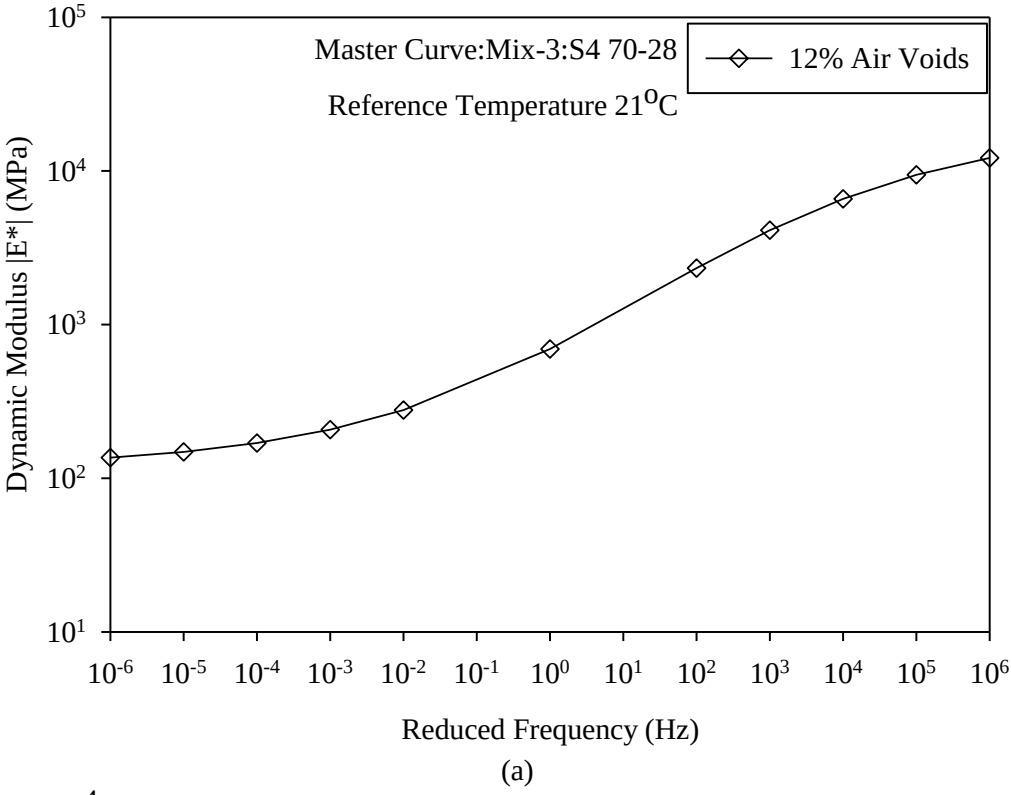

(a)

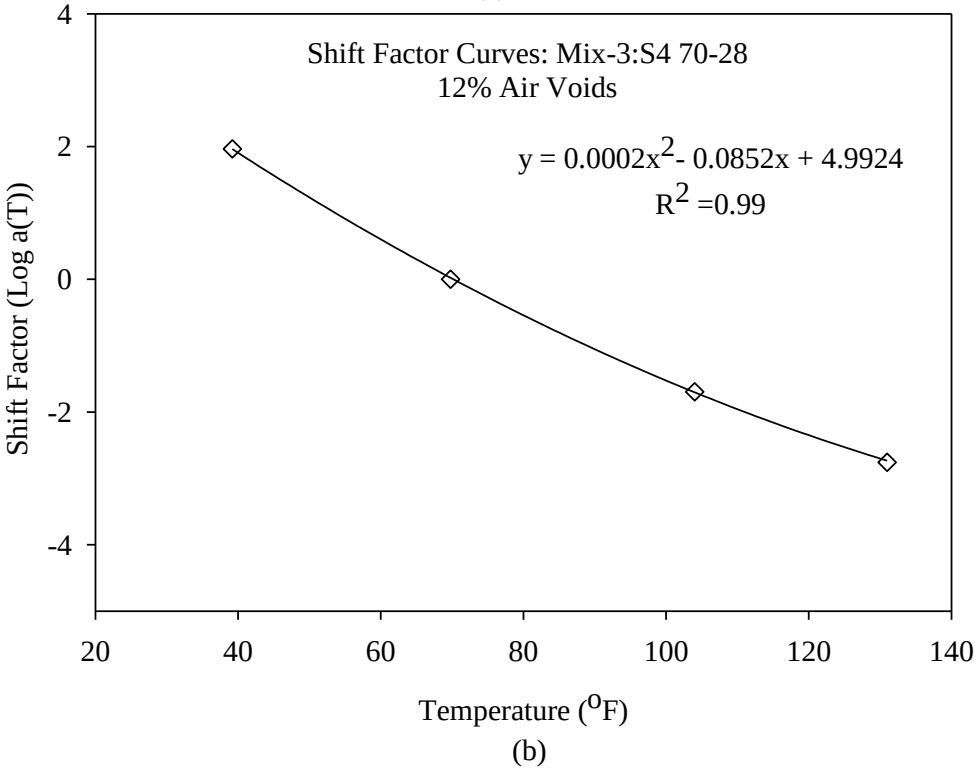

(b)

Figure A-12 (a) Master Curve (b) Shift Factor for Mix-3 at 12% Air Voids

MIX-4 (S4 64-22)

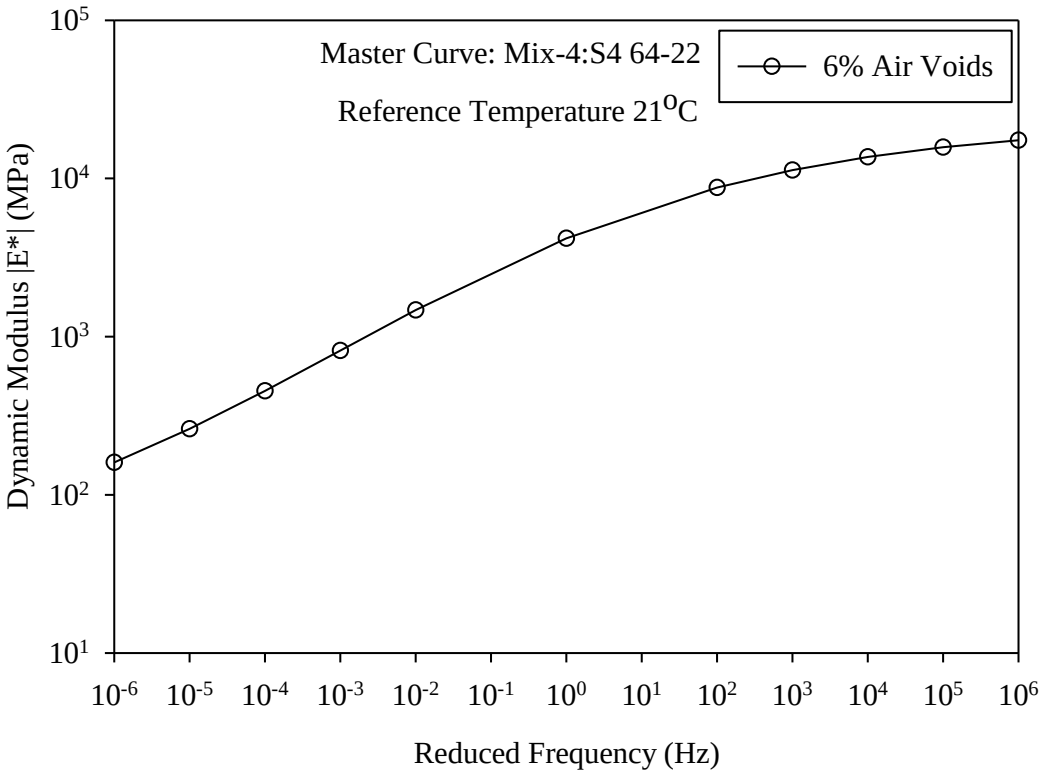

(a)

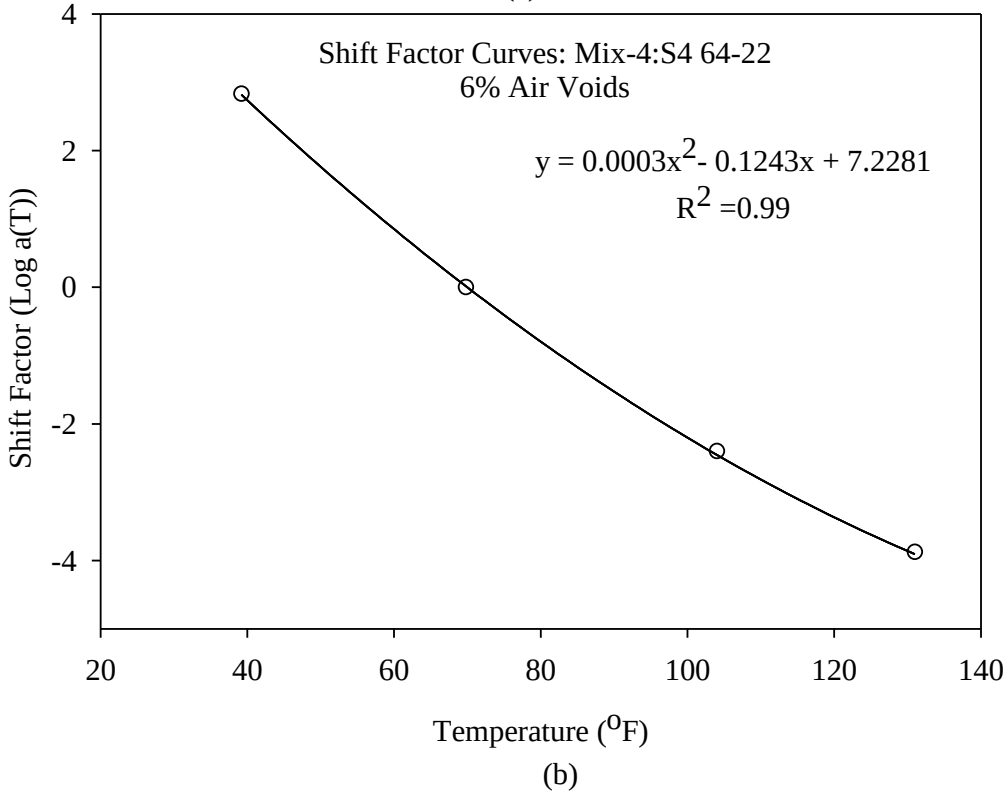

(b)

Figure A-13 (a) Master Curve (b) Shift Factor for Mix-4 at 6% Air Voids

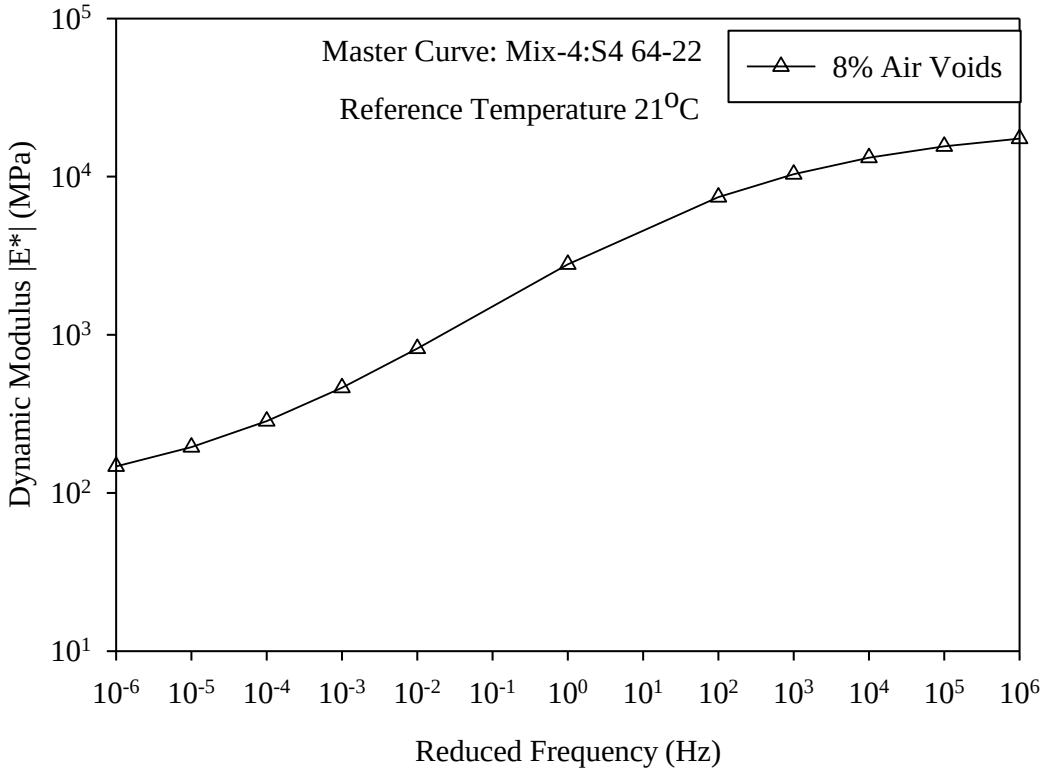

(a)

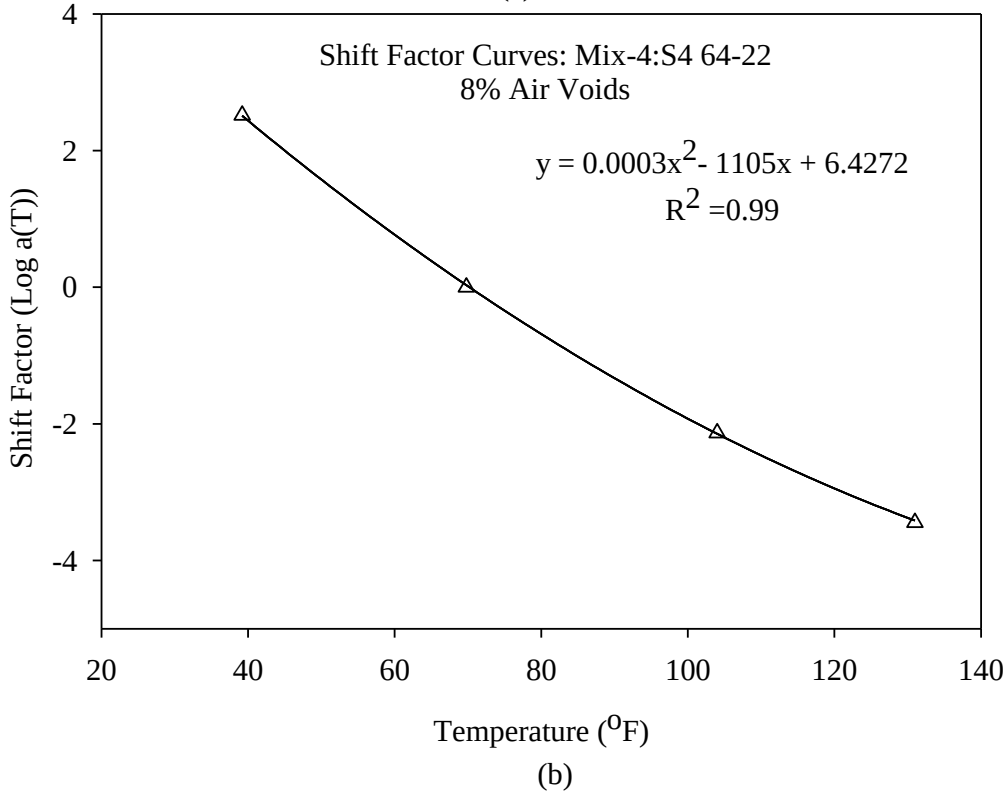

(b)

Figure A-14 (a) Master Curve (b) Shift Factor for Mix-4 at 8% Air Voids

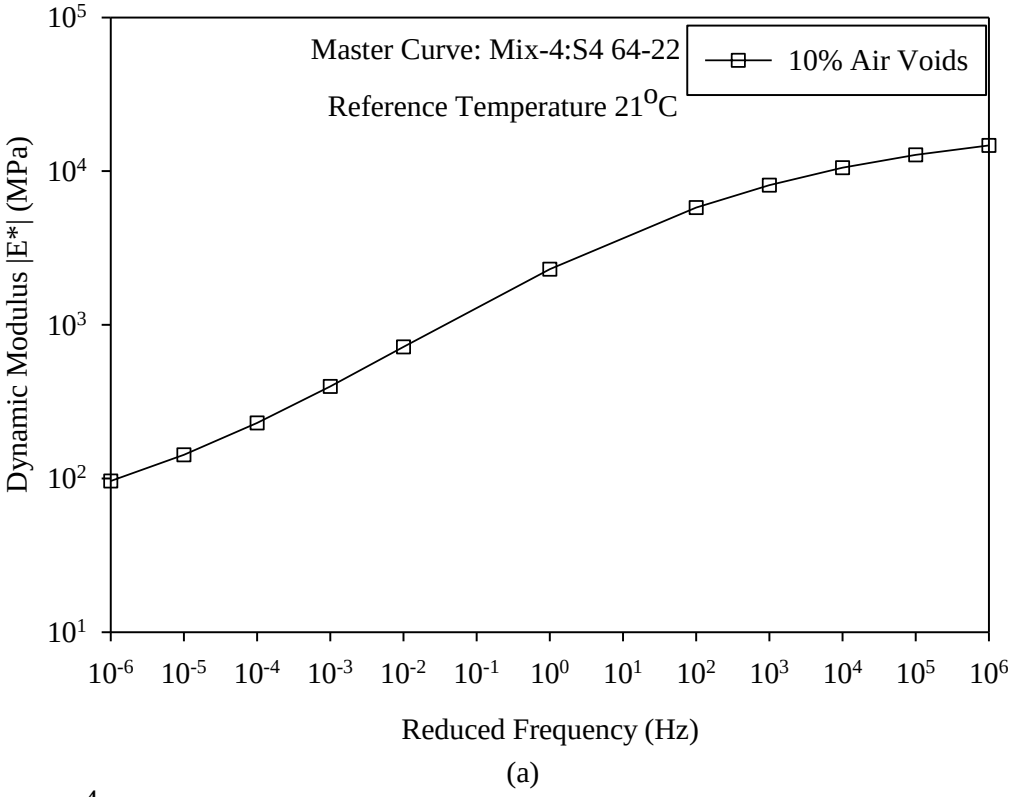

(a)

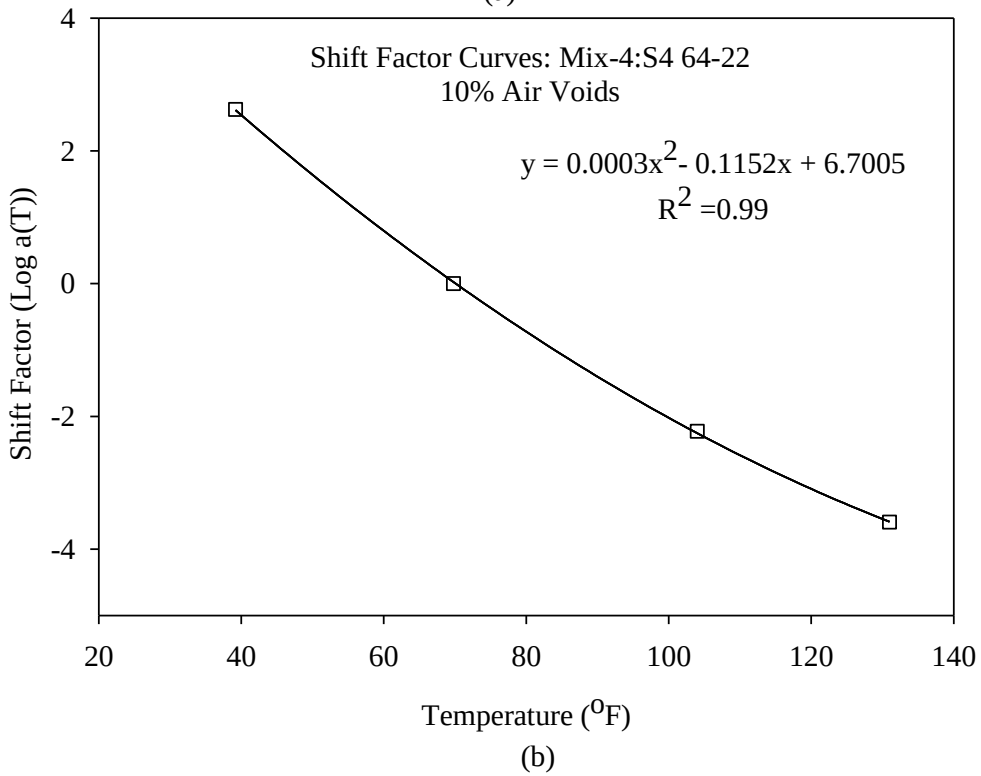

(b)

Figure A-15 (a) Master Curve (b) Shift Factor for Mix-4 at 10% Air Voids

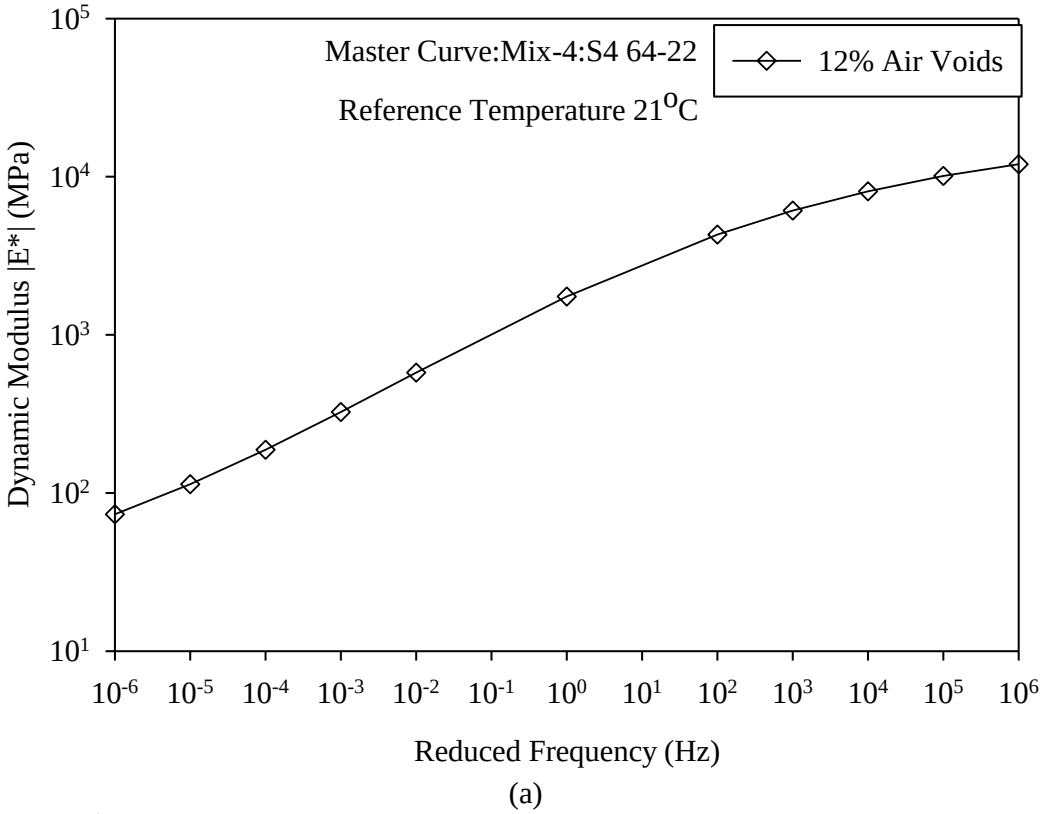

(a)

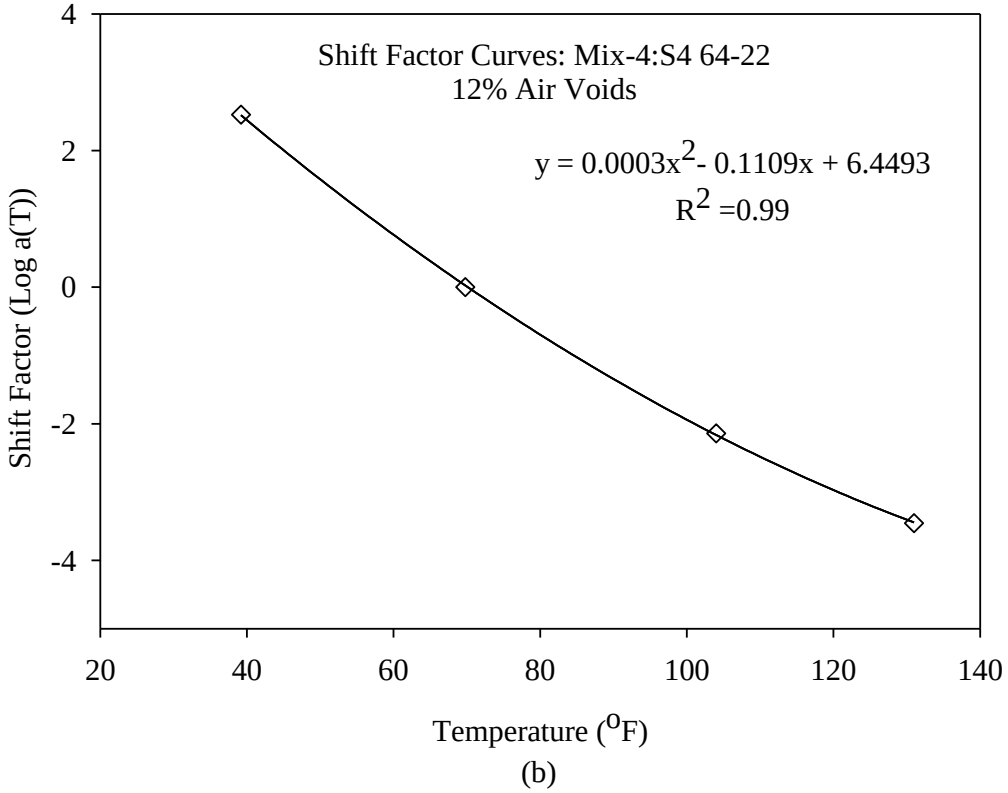

(b)

Figure A-16 (a) Master Curve (b) Shift Factor for Mix-4 at 12% Air Voids

MIX-5 (S4 76-28)

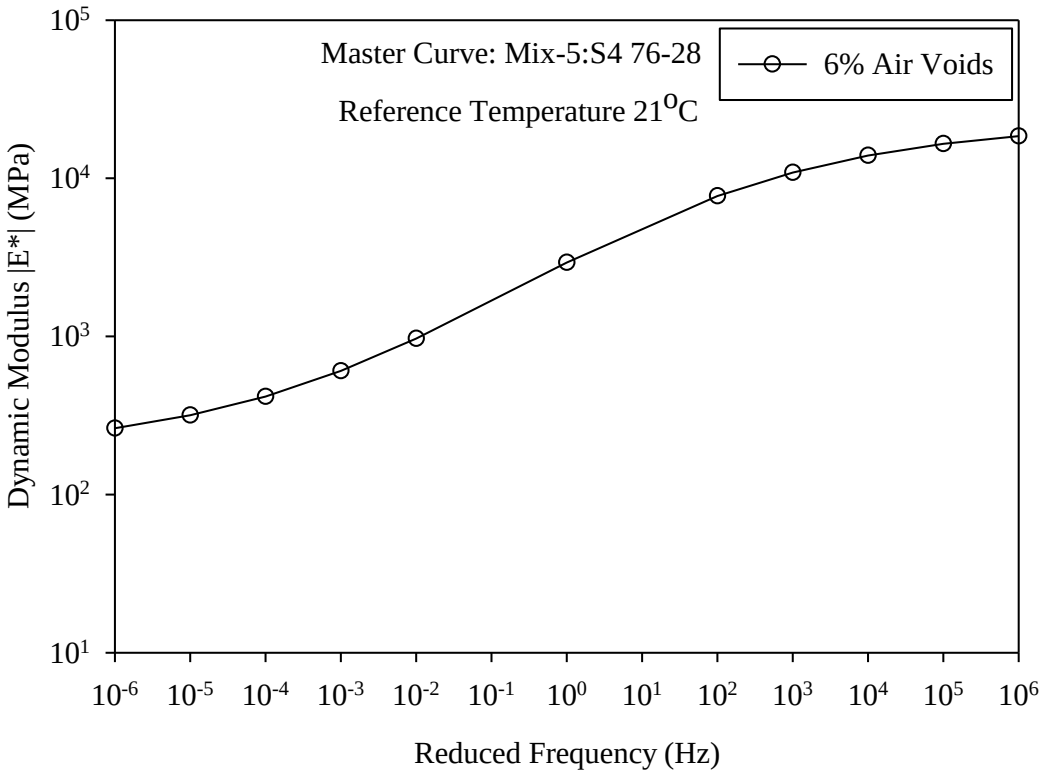

(a)

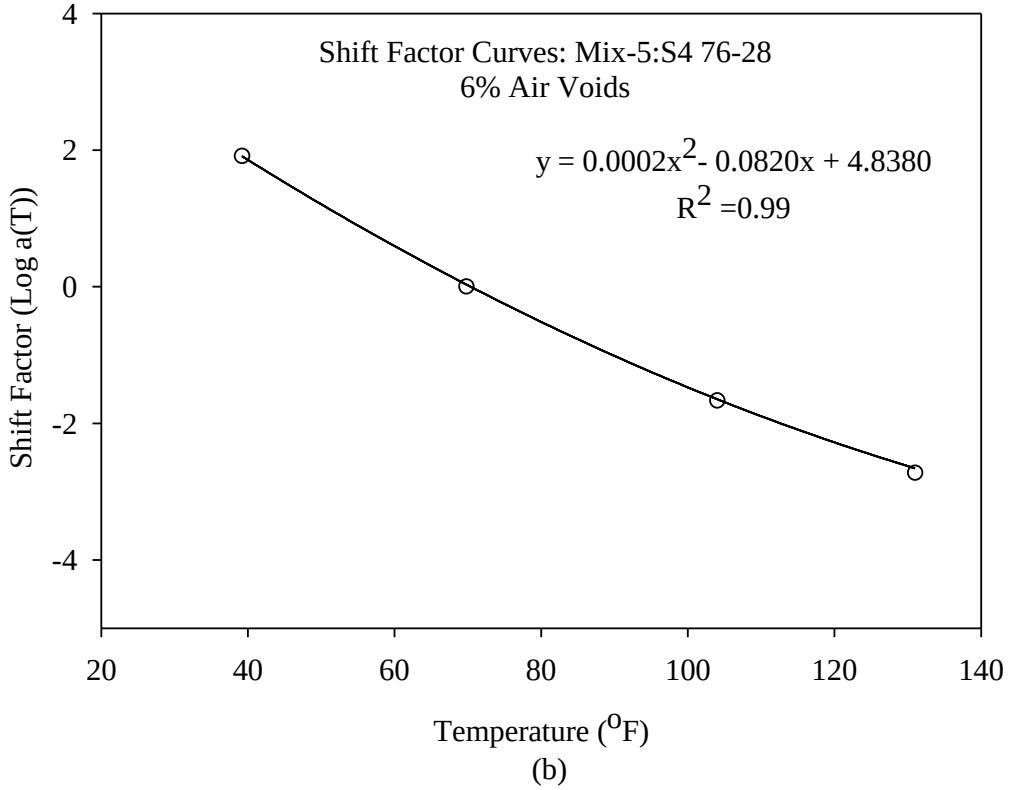

(b)

Figure A-17 (a) Master Curve (b) Shift Factor for Mix-5 at 6% Air Voids

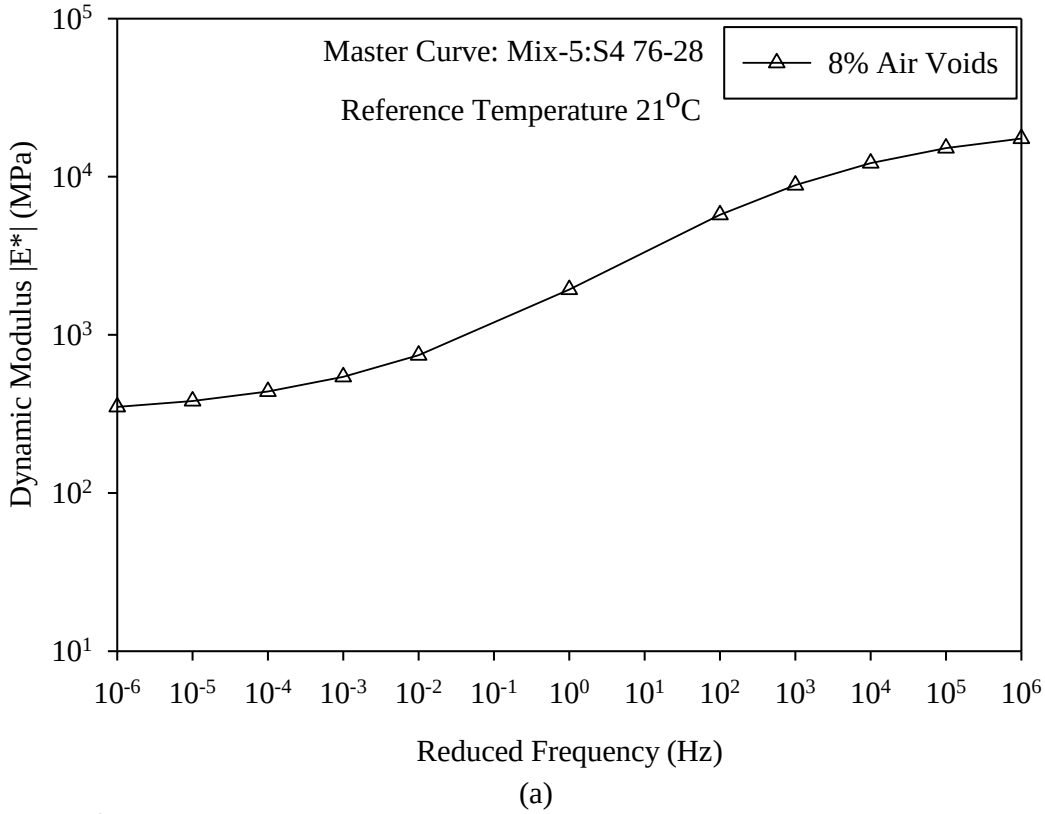

(a)

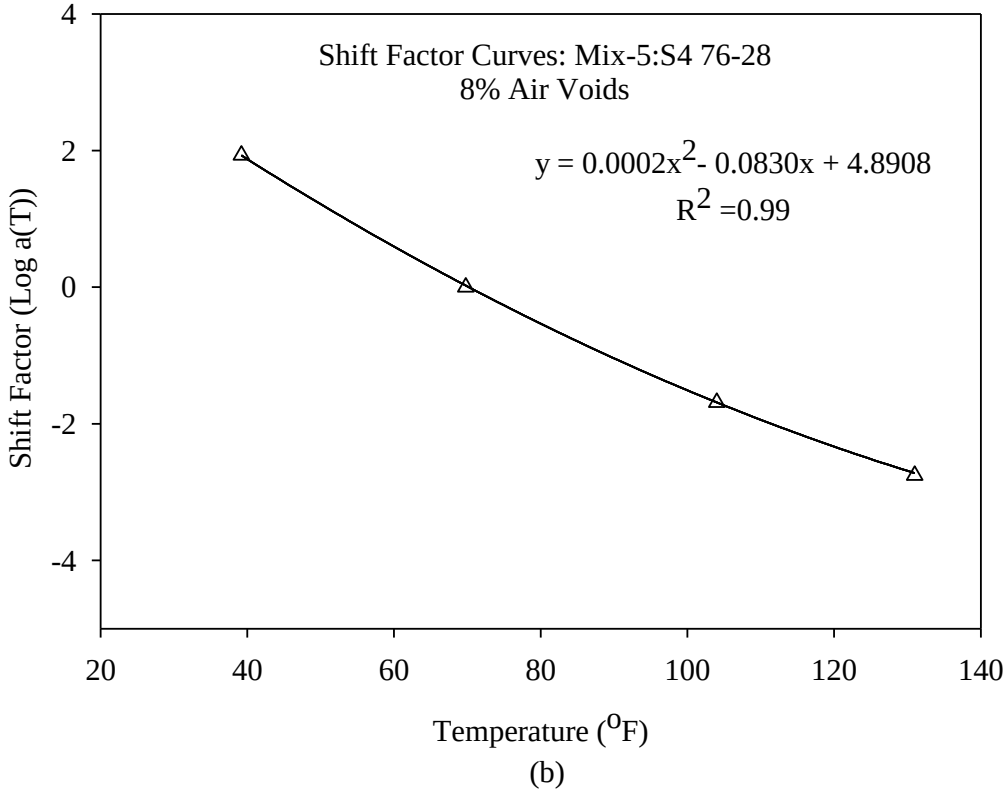

(b)

Figure A-18 (a) Master Curve (b) Shift Factor for Mix-5 at 8% Air Voids

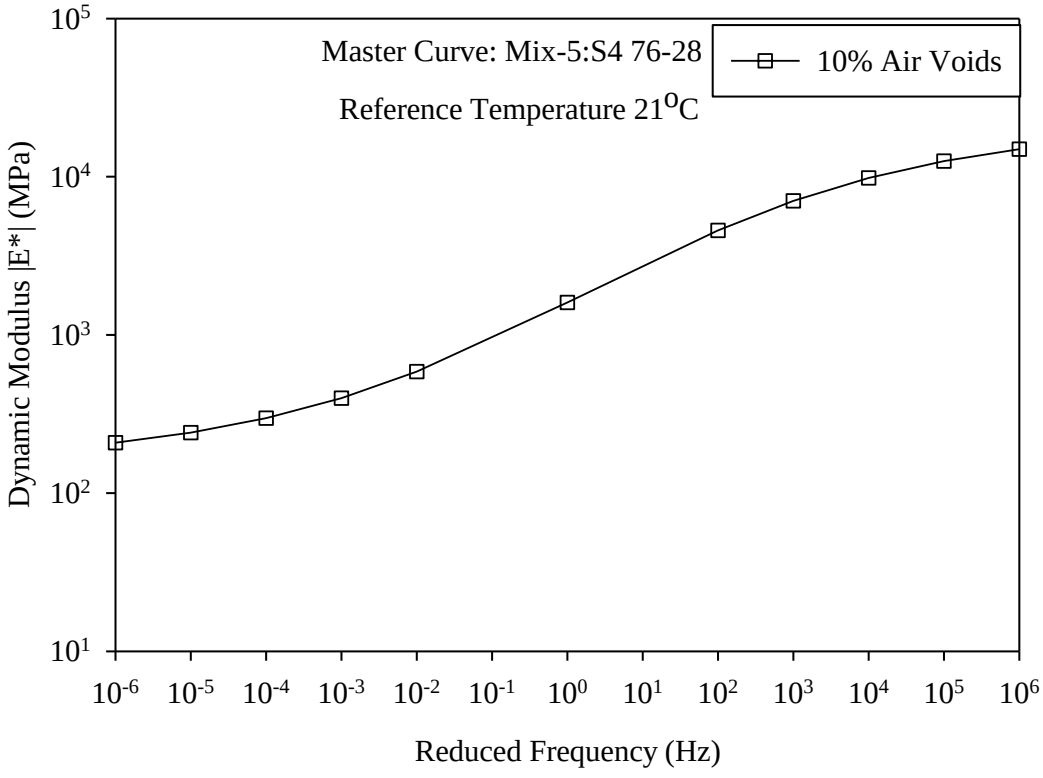

(a)

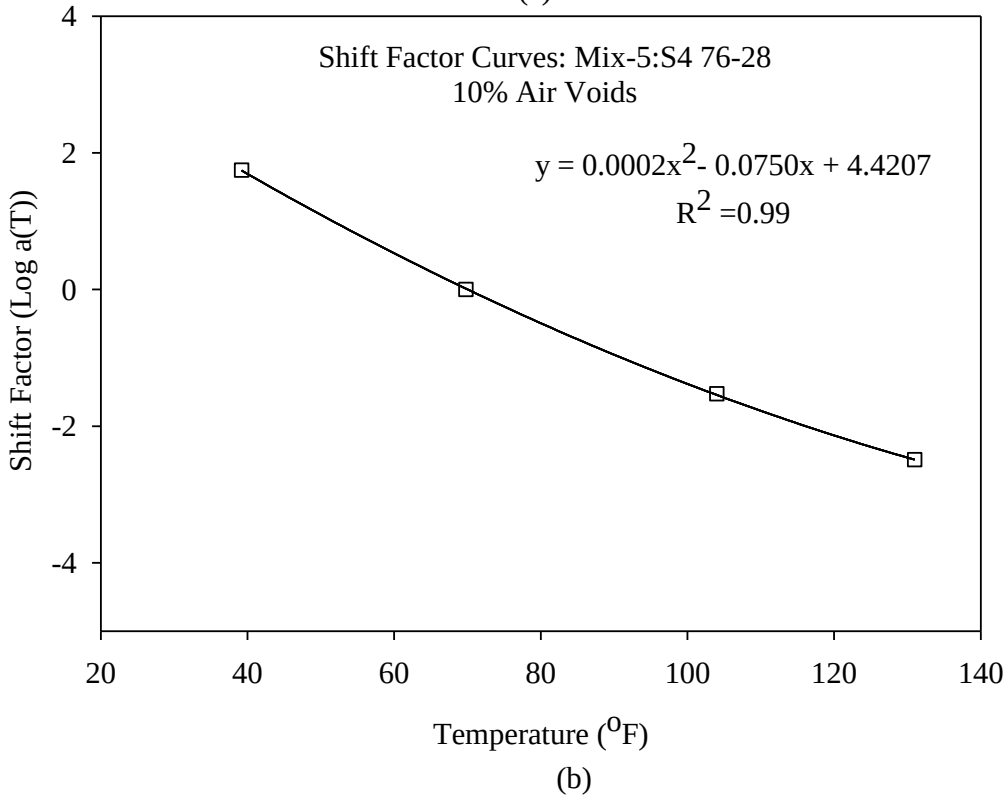

(b)

Figure A-19 (a) Master Curve (b) Shift Factor for Mix-5 at 10% Air Voids

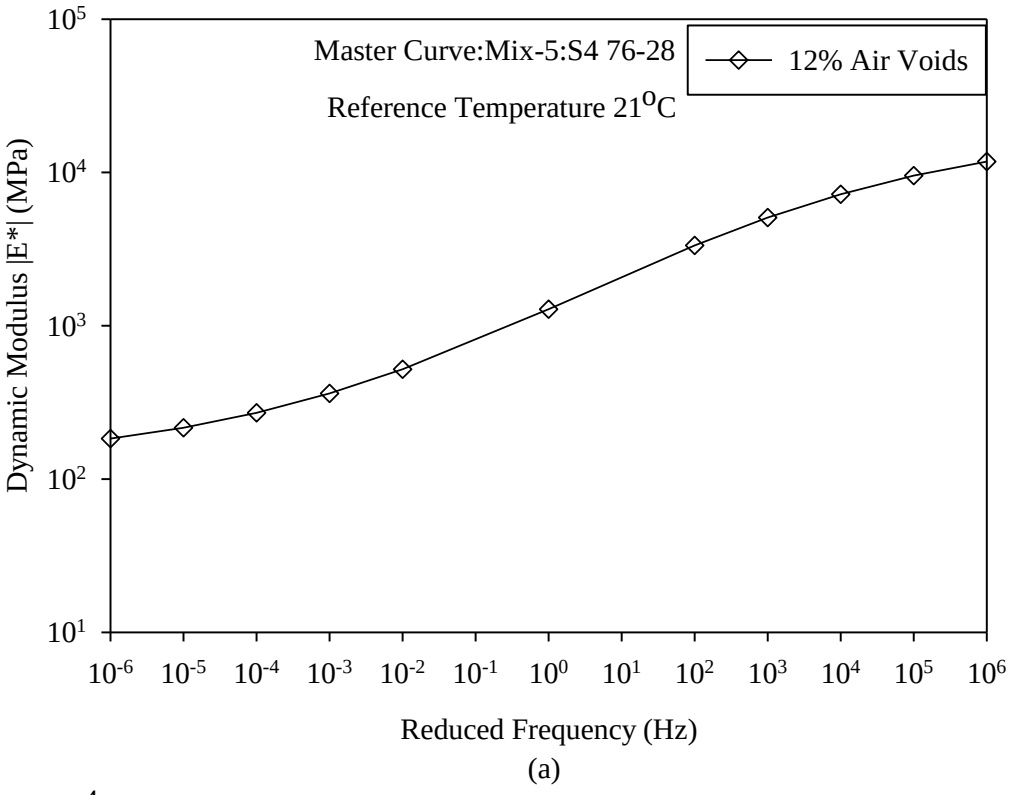

(a)

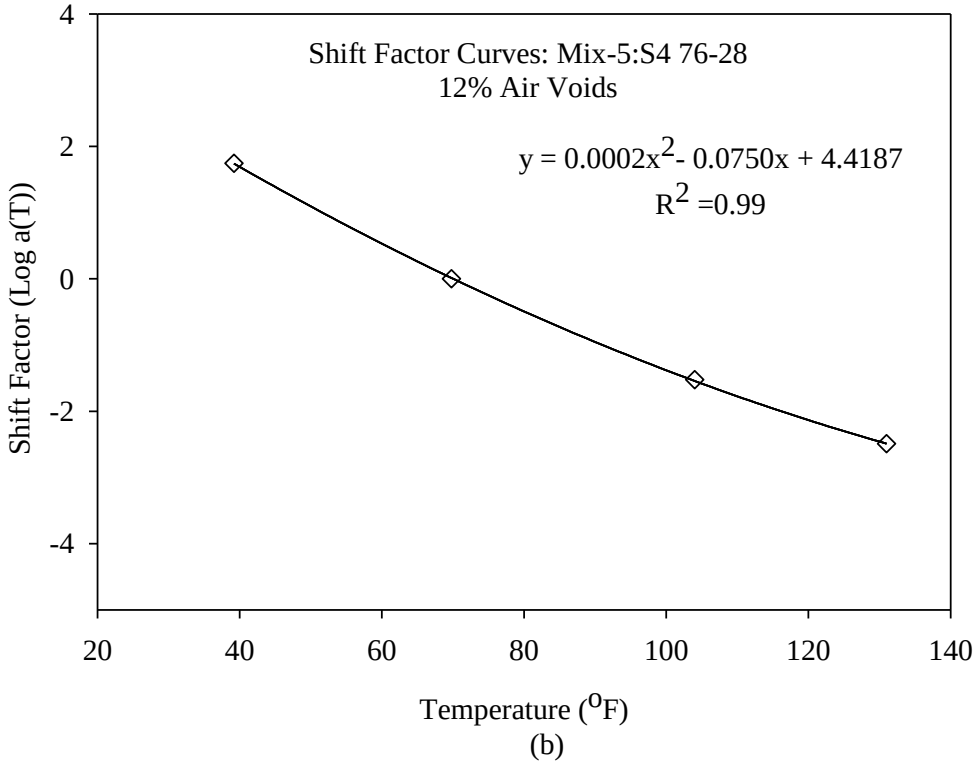

(b)

Figure A-20 (a) Master Curve (b) Shift Factor for Mix-5 at 12% Air Voids

APPENDIX-B: Parameters for Master Curves and Shift Factors

Table B-1: Master Curve and Shift Factor Parameter for Mix-1

Mix-1:S3 64-22									
Master Curve Parameters									
Air Voids (%)	Max |E*| (MPa)	α	δ	β	γ	c	R^2	S_e/S_y	Fit
6	23084	2.54	1.82	-1.01	-0.43	1.24	0.99	0.07	Excellent
8	22256	2.78	1.56	-0.97	-0.39	1.24	0.99	0.05	Excellent
10	21232	3.07	1.26	-0.85	-0.37	1.08	0.99	0.06	Excellent
12	19942	2.57	1.73	-0.40	-0.41	1.09	0.99	0.08	Excellent

Air Voids (%)	Shift Factors Parameters		
	m	n	p
6	0.0003	-0.1155	6.7155
8	0.0003	-0.1149	6.6837
10	0.0002	-0.1000	5.8160
12	0.0002	-0.1009	5.8669

Table B-2: Master Curve and Shift Factor Parameter for Mix-2

Mix-2:S3 76-28									
Master Curve Parameters									
Air Voids (%)	Max |E*| (MPa)	α	δ	β	γ	c	R^2	S_e/S_y	Fit
6	22826	2.26	2.10	-0.25	-0.45	1.18	1.00	0.04	Excellent
8	22027	2.35	1.99	-0.24	-0.42	1.12	0.99	0.05	Excellent
10	21157	2.35	1.98	-0.17	-0.42	1.07	1.00	0.04	Excellent
12	20182	2.60	1.71	-0.12	-0.37	1.08	1.00	0.05	Excellent

Air Voids (%)	Shift Factors Parameters		
	m	n	p
6	0.0002	-0.0964	5.6785
8	0.0002	-0.0916	5.3984
10	0.0002	-0.0870	5.1230
12	0.0002	-0.0878	5.1717

Table B-3: Master Curve and Shift Factor Parameter for Mix-3

Mix-3:S4 70-28									
Master Curve Parameters									
Air Voids (%)	Max |E*| (MPa)	α	δ	β	γ	c	R^2	S_e/S_y	Fit
6	22224	2.23	2.12	-0.43	-0.41	1.11	1.00	0.07	Excellent
8	21401	2.14	2.19	0.28	-0.47	1.06	0.99	0.09	Excellent
10	20367	2.16	2.15	0.49	-0.46	1.00	1.00	0.05	Excellent
12	19562	2.22	2.07	0.63	-0.49	0.98	0.99	0.06	Excellent

Air Voids (%)	Shift Factors Parameters		
	m	n	p
6	0.0002	-0.0959	5.6182
8	0.0002	-0.0920	5.3926
10	0.0002	-0.0863	5.0577
12	0.0002	-0.0852	4.9924

Table B-4: Master Curve and Shift Factor Parameter for Mix-4

Mix-4:S4 64-22									
Master Curve Parameters									
Air Voids (%)	Max |E*| (MPa)	α	δ	β	γ	c	R^2	S_e/S_y	Fit
6	22367	2.87	1.48	-1.08	-0.36	1.34	1.00	0.05	Excellent
8	21481	2.42	1.91	-0.55	-0.45	1.19	1.00	0.04	Excellent
10	20715	2.83	1.48	-0.68	-0.37	1.24	1.00	0.04	Excellent
12	19851	3.14	1.15	-0.68	-0.32	1.19	0.99	0.07	Excellent

Air Voids (%)	Shift Factors Parameters		
	m	n	p
6	0.0003	-0.1243	7.2281
8	0.0003	-0.1105	6.4272
10	0.0003	-0.1152	6.7005
12	0.0003	-0.1109	6.4493

Table B-5: Master Curve and Shift Factor Parameter for Mix-5

Mix-5:S4 70-28									
Master Curve Parameters									
Air Voids (%)	Max |E*| (MPa)	α	δ	β	γ	c	R^2	S_e/S_y	Fit
6	22632	2.09	2.26	-0.30	-0.47	1.01	0.99	0.05	Excellent
8	21675	1.85	2.49	0.28	-0.53	1.02	1.00	0.04	Excellent
10	21020	2.13	2.20	0.10	-0.45	0.92	1.00	0.06	Excellent
12	19842	2.20	2.09	0.16	-0.39	0.92	1.00	0.08	Excellent

Air Voids (%)	Shift Factors Parameters		
	m	n	p
6	0.0002	-0.0820	4.8380
8	0.0002	-0.0830	4.8908
10	0.0002	-0.0750	4.4207
12	0.0002	-0.0750	4.4187

DISCLAIMER

Neither the developers of this work nor the University of Oklahoma assume any legal liability or responsibility for the accuracy, completeness, or usefulness of any information, product or process disclosed in this dissertation.

LIST OF SYMBOLS

ϕ	Phase Angle
$\|E^*\|_m$	Absolute Value of Asphalt Mix Dynamic Modulus
$\|G^*\|_g$	Complex Shear Modulus of Asphalt Binder in Glassy State
$\|G_b{}^*\|$	Dynamic Shear Modulus of Asphalt Binder
δ_b	Phase Angle of Asphalt Binder
ε_o	Measured Strain Amplitude
ρ_{200}	% Passing # 200 (0.075 mm) sieve
ρ_{34}	Cumulative % retained on 3/4 inch (19 mm) sieve
ρ_{38}	Cumulative % retained on 3/8 inch (9.5 mm) sieve
ρ_4	Cumulative % retained on # 4 (4.75 mm) sieve
σ_o	Applied Stress Amplitude
|E*|	Dynamic Modulus
A	Regression Intercept of the Viscosity Temperature Susceptibility
a (T)	Shift Factor as a Function of Temperature and Age
E*	Complex Modulus
E_1	Storage or Elastic Modulus
E_2	Loss or Viscous Modulus
f	Loading frequency (Hz)
f_r	Reduced Frequency at Reference Temperature
M_R	Resilient Modulus
R^2	Correlation Coefficient
S_e/S_y	Standard Error of the Estimated/Standard Deviation
t	Loading Time in Seconds
V_a	Air Voids (% by Volume)
V_{beff}	Effective Binder Content (% by Volume)
VTS	Slope of the Viscosity-Temperature Line
A	Intercept of the Viscosity-Temperature Line
δ, β, γ, c	Fitting Parameters of Master Curves
η	Viscosity of binder

T_R	Temperature in Rankine
T	Temperature in ^oF
R_θ	Radius of the Particle at an Angle of θ
REE_θ	Radius of the Equivalent Ellipse at an Angle of θ
d_L	Longest Dimension of a Particle
d_I	Intermediate Dimension of a Particle
d_s	Shortest Dimension of a Particle
a_i	Mean shape parameter for a selected sieve size
x_i	Percentage retained aggregates on selected sieve sizes
$\|E^*\|_p$	Predicted Dynamic Modulus in MPa
$\|E^*\|_m$	Laboratory Measured Dynamic Modulus
i	Subscript for input layer
j	Subscript for first hidden layer
k	Subscript for second hidden layer
m	Number of input parameters
n	Number of nodes in first hidden layer
q	Number of nodes in second hidden layer
f_h	Transfer function for hidden layers
f_o	Transfer function for output layer
$W^{1h}{}_{ij}$	Weight factors for first hidden layer
$W^{2h}{}_{jk}$	Weight factors for second hidden layer
$W^{o}{}_{k}$	Weight factors for output layer
$b^{1h}{}_{j}$	Bias factors for first hidden layer
$b^{2h}{}_{k}$	Bias factors for second hidden layer
b_o	Bias factor for output layer
P_i	Input variables
O	Output value
n	Sample Size
k	Number of Independent Variables in the Model
ω	Angular Velocity

LIST OF ABBREVIATIONS

AASHTO	American Association of State Highway Transportation and Officials
AI	Asphalt Institute
AIMS	Aggregate Image Measurement System
ANOVA	Analysis of Variance
APA	Asphalt Pavement Analyzer
ARE	Average Relative Error
ASTM	American Society for Testing and Materials
AV	Air Voids
CA	Coarse Aggregates
CAI	Composite Angularity Index
CFI	Composite Form Index
CI	Composite Shape Index Factor
COAI	Composite Angularity Index for Coarse Aggregates
COFI	Composite Form Index for Coarse Aggregates
COTI	Composite Texture Index for Coarse Aggregates
CSI	Composite Sphericity Index
CTI	Composite Texture Index
DEM	Discrete Element Method
DOT	Department of Transportation
DSR	Dynamic Shear Rheometer
F&E	Flat and Elongated Particles
FA	Fine Aggregates
FAA	Fine Aggregate Angularity
FAI	Composite Angularity Index for Fine Aggregates
FEM	Finite Element Method
FHWA	Federal Highways Administration
LOE	Line of Equality
LTO	Long -Term Oven

LVDT	Linear Variable Differential Transducer
MARE	Mean Absolute Relative Error
MEPDG	Mechanistic Empirical Pavement Design Guide
MM	Modified Mix
MTS	Material Testing System
NCAT	National Center for Asphalt Technology
NCHRP	National Cooperative Highway Research Program
NMAS	Nominal Maximum Aggregate Size
NN	Neural Network
OA	Original Aggregates
ODOT	Oklahoma Department of Transportation
PG	Performance Grade
PM	Plant Mix Aggregates
QA	Quality Assurance
QC	Quality Control
RAP	Reclaimed Asphalt Pavement
RE	Relative Error
RTFO	Rolling Thin Film Oven
SBS	Styrene-Butadiene-Styrene
SEK	Standard Error of Kurtosis
SES	Standard Error of Skewness
SGC	Superpave Gyratory Compactor
SPSS	Statistical Package for the Social Sciences
SPT	Simple Performance Test
TRB	Transportation Research Board
UM	Unmodified Mix
VFA	Voids Filled with Asphalt
VMA	Voids in Mineral Aggregate

SI (METRIC) CONVERSION FACTORS									
Approximate Conversions to SI Units					*Approximate Conversions from SI Units*				
Symbol	*When you know*	*Multiply by*	*To Find*	*Symbol*	*Symbol*	*When you know*	*Multiply by*	*To Find*	*Symbol*
		LENGTH					***LENGTH***		
in	*inches*	*25.40*	*millimeters*	*mm*	*mm*	*millimeters*	*0.0394*	*inches*	*in*
ft	*feet*	*0.3048*	*meters*	*m*	*m*	*meters*	*3.281*	*feet*	*ft*
yd	*yards*	*0.9144*	*meters*	*m*	*m*	*meters*	*1.094*	*yards*	*yd*
mi	*miles*	*1.609*	*kilometers*	*km*	*km*	*kilometers*	*0.6214*	*miles*	*mi*
		AREA					***AREA***		
in²	*square inches*	*645.2*	*square millimeters*	*mm²*	*mm²*	*square millimeters*	*0.00155*	*square inches*	*in²*
ft²	*square feet*	*0.0929*	*square meters*	*m²*	*m²*	*square meters*	*10.764*	*square feet*	*ft²*
yd²	*square yards*	*0.8361*	*square meters*	*m²*	*m²*	*square meters*	*1.196*	*square yards*	*yd²*
ac	*acres*	*0.4047*	*hectares*	*ha*	*ha*	*hectares*	*2.471*	*acres*	*ac*
mi²	*square miles*	*2.590*	*square kilometers*	*km²*	*km²*	*square kilometers*	*0.3861*	*square miles*	*mi²*
		VOLUME					***VOLUME***		
fl oz	*fluid ounces*	*29.57*	*milliliters*	*mL*	*mL*	*milliliters*	*0.0338*	*fluid ounces*	*fl oz*
gal	*gallons*	*3.785*	*liters*	*L*	*L*	*liters*	*0.2642*	*gallons*	*gal*
ft³	*cubic feet*	*0.0283*	*cubic meters*	*m³*	*m³*	*cubic meters*	*35.315*	*cubic feet*	*ft³*
yd³	*cubic yards*	*0.7645*	*cubic meters*	*m³*	*m³*	*cubic meters*	*1.308*	*cubic yards*	*yd³*
		MASS					***MASS***		
oz	*ounces*	*28.35*	*grams*	*g*	*g*	*grams*	*0.0353*	*ounces*	*oz*
lb	*pounds*	*0.4536*	*kilograms*	*kg*	*kg*	*kilograms*	*2.205*	*pounds*	*lb*
T	*short tons (2000 lb)*	*0.907*	*megagrams*	*Mg*	*Mg*	*megagrams*	*1.1023*	*short tons (2000 lb)*	*T*
		TEMPERATURE (exact)					***TEMPERATURE (exact)***		
ºF	*degrees Fahrenheit*	*(ºF-32)/1.8*	*degrees Celsius*	*ºC*	*ºC*	*degrees Celsius*	*9/5+32*	*degrees Fahrenheit*	*ºF*
		FORCE and PRESSURE or STRESS					***FORCE and PRESSURE or STRESS***		
lbf	*poundforce*	*4.448*	*Newtons*	*N*	*N*	*Newtons*	*0.2248*	*poundforce*	*lbf*
lbf/in²	*poundforce per square inch*	*6.895*	*kilopascals*	*kPa*	*kPa*	*kilopascals*	*0.1450*	*poundforce per square inch*	*lbf/in²*